Inertial instability in two-layer flows

Sarah Elizabeth O'Mahony

Submitted in accordance with the requirements for the degree of
Doctor of Philosophy

The University of Leeds
Department of Applied Mathematics

July 2018

Abstract

Inertial instability occurs in rotating fluid systems when the absolute vorticity takes the opposite sign to the Coriolis parameter f. It has been observed in atmospheres and oceans, particularly near the equator where the latitudinal shear of the zonal winds can exceed f. Most previous studies of inertial instability adopt a continuously stratified fluid, for which the instability takes the form of overturning cells in the meridional plane. Here we instead study the instability using the zonally symmetric two-layer shallow water equations. We use a momentum-conserving interfacial friction, and show that the linear instability problem is then directly analogous to that of the continuously stratified system in the limit of infinite Prandtl number. Solutions for linear instabilities for a uniform shear flow on the equatorial beta plane are given in detail.

We then study frictionless nonlinear instabilities, using both weakly nonlinear theory and numerical solutions. On the equatorial β-plane, a third-order system of amplitude equations is derived, and their behaviour is verified and then extended into a moderately nonlinear regime numerically. On the f-plane, the nonlinear instability of a hyperbolic tangent shear flow is studied. Here the weakly nonlinear analysis requires a different scaling to the equatorial case, and the resulting system of amplitude equations is also different. The properties of this system are studied in depth, and the periodic oscillations that result are interpreted in terms of the evolving linear stability of the mean flow. The results are extended into a moderately nonlinear regime numerically.

Acknowledgements

First and foremost, I would like thank my supervisors Dr. Stephen Griffiths and Prof. Steve Tobias for their guidance and support and for sharing with me their vast mathematical knowledge in fluid dynamics. Without their unrelenting encouragement this thesis would not have been written.

I would like to express my gratitude to the Engineering and Physical Science Research Council for funding the research in this thesis.

My parents have always been there to offer words of encouragement whenever I doubted my ability to progress my research. Being mathematically minded himself my Father has always expressed a keen interest in my research and has even taken it upon himself to study a course in fluid dynamics in the hope of one day understanding my research. I'd also like to thank my Husband for appreciating how important this research has been to me and for being patient particularly in the final few months.

Contents

List of figures

List of tables

Chapter 1

Introduction

1.1 Introduction to instability in fluid flows

For a mechanical system to be stable, it must be stable to small disturbances, hence introducing an infinitesimally small disturbance to the system these disturbances must not amplify. A simple example of instability is that of a ball on a concave surface: if it is imagined a ball resting on the maximum of a surface that is concave downwards (figure 1.1(a)), the ball will be unstable to an infinitesimally small force: any infinitesimally small force applied to the ball in any direction will cause the ball to roll down the surface and oscillate around a minimum or alternatively in the case where there is friction settle into a new final state. On the other hand if the surface was concave upwards (figure 1.1(b)) with the ball resting at the bottom of the concave surface, any small force applied to the ball will not be enough to allow the ball to roll out of the dip. The final resting state will be the state the ball was in before any force was applied. This is the basic idea of linear instability theory.

Instability theory is fundamental to a range of phenomena in fluid dynamics, from laboratory scale flows, through to global scale (geophysical) flows and flows on other

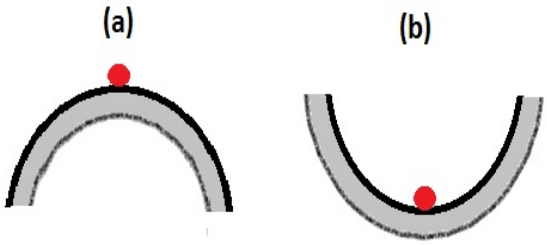

Figure 1.1: *An illustration of instability of a ball on a concave surface.*

planets and/or stars (astrophysical flows). All linear instability analysis starts with a prescribed basic state (a flow, along with density, pressure and perhaps temperature) and determines whether or not infinitesimally small disturbances to this state amplify in time. Perhaps the most famous example of a fluid instability is that of *thermal convection*, which may arise when a layer of fluid is heated from below, as exemplified by Bénard's work on the heating of a thin layer of viscous fluid and the resulting hexagonal pattern of motion that develops (Bénard, 1900). Another famous instability is that of *centrifugal instability*, which may arise in a circular vortex when the angular momentum decreases moving outwards (away from the rotation axis). Rayleigh (1916) derived the relevant inviscid criterion, assuming axisymmetric disturbances. Taylor (1923) performed corresponding experimental and analytical work for a viscous fluid between two rotating cylinders, a configuration now known as Taylor–Couette flow. He found that the instability caused vertically stacked cells to form between the two rotating cylinders. Taylor's results showed convergence between experiment and theory that helped confirm the accuracy of the Navier-Stokes equations.

Here instabilities in geophysical and astrophysical flows are of interest, where viscosity is often negligible, but rotation and stratification are often both important. For example, observations of the Earth's atmosphere show it to be full of complex and chaotic

phenomenon, many of which arise from instabilities of simpler underlying flows. There are corresponding instabilities in the atmosphere and ocean of other planets, although these are harder to observe.

One of the most important and most commonly occurring types of instability in geophysical and astrophysical flows is shear instability, which can arise when the basic state is sheared in one or more directions. On rotating planets, large scale zonal flows (i.e., east-west) are usually formed (Gill, 1982); for example, the Earth's atmosphere has strong mid-latitude jets (sheared both latitudinally and vertically), whilst the thin weather layer of Jupiter has an ordered set of alternating jets with regions of strong latitudinal shear. Such flows may be liable to a barotropic instability (due to the horizontal shear, when the appropriate extension of Rayleigh's inflection point criterion is satisfied) or baroclinic instability (due to the vertical shear), (e.g., Drazin and Reid (2004)).

For flows with horizontal shear, there is also the possibility of a geophysical analogue of the centrifugal instability of a circular vortex. The phrase *inertial instability* has now been adopted to describe such instabilities, which occur as a zonally symmetric motion (i.e., independent of longitude) in their simplest form. Using a local planar coordinate system, with y measuring distance northwards, a basic zonal flow $U(y)$ may be unstable when

$$fQ = f(f - dU/dy) < 0, \tag{1.1}$$

somewhere in the flow. The origin of this result can be traced back to the 1940s as discussed by Sawyer (1949), specifically a derivation of the result in Cartesian coordinates traces back to the 1950s (Arakawa, 1951). Here f is the Coriolis parameter, and Q is the absolute vorticity. In rapidly rotating flows, Q will often be dominated by f, so that $fQ > 0$. However, if the horizontal shears are sufficiently strong (and anticyclonic), then the absolute vorticity can take the opposite sign to f, and inertial instability may occur. This will be most easily achieved near the equator, where f becomes small.

1.2 Overview of equatorial inertial instability

Moving on to the development of instability theory in the atmosphere and ocean, Dunkerton (1981) performed linear analysis on a symmetrical rotating system on the equatorial β-plane taking an inviscid fluid with a uniform shear flow basic state. He then perturbed this shear flow and found the flow to be inertially unstable. However, such an instability was found to prefer structures with vanishingly small length scales rendering the instability unobservable. To obtain a finite vertical scale selection, Dunkerton considered a viscous flow of Prandtl number unity, where $Pr = \nu/\kappa$, where ν is the kinematic viscosity and κ is the thermal diffusivity. Dunkerton specifically looked at the specific case with $Pr = 1$. Choosing a viscous fluid was found to induce a lower bound on the length scales of these structures. There are then parallels with the structures found in unstable Taylor-Couette flow with those found by Dunkerton as a result of inertial instability. Dunkerton found flat pancake like structures of alternating sign stacked either side of the unstable region like those stacking structures of Taylor-Couette flow as shown in figure 1.2. Dunkerton found a dispersion relation given by

$$s = (\Lambda^2/4 - (2n+1)\beta N/|m|)^{1/2} - \nu|m|^2, \tag{1.2}$$

where s is the growth rate, Λ is the (constant) horizontal shear, N is the (constant) buoyancy frequency and m is the vertical wavenumber. The most unstable wavenumber is found by solving $ds/dm = 0$ and is given by the solution to

$$\left(\frac{4\nu m^6}{(2n+1)}\right) - 4\nu m^5 - 1 = 0. \tag{1.3}$$

The critical vertical wavenumber where there is a transition from stability to instability is given by

$$|m|_c^5 = \frac{(2n+1)\beta N}{4\nu^2}, \tag{1.4}$$

In figure 1.2 an example of pancake structures are shown as observed by Dunkerton: stacks of alternating warm and cold air appear either side of the unstable region. There are also circulations that form inside the unstable region which are accompanied by alternating western and eastern jets.

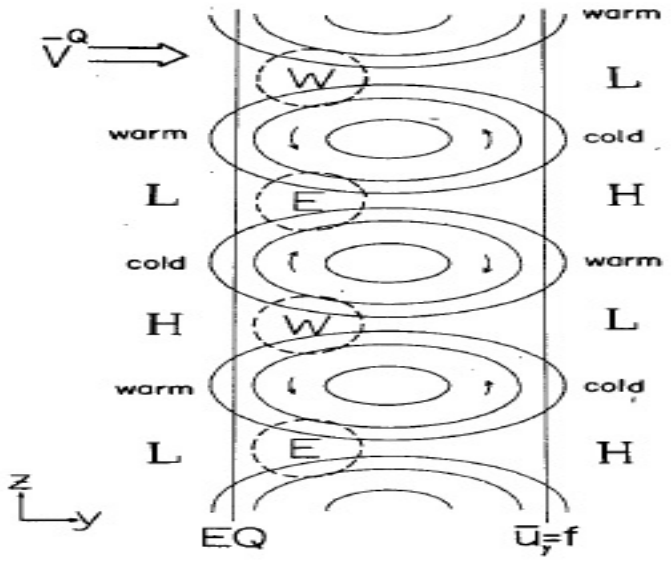

Figure 1.2: *Inertial Instability as pictured by Dunkerton (1981) on the equatorial β-plane. Stacks of alternating warm and cold air appear either side of the unstable region. Circulations form inside the unstable region which are accompanied by alternating western and eastern jets.*

Structures similar to those found by Dunkerton (figure 1.2) have been observed in the atmosphere through satellite data by Hayashi and Shiotani (1998). Such disturbances have been given the name "pancake" structures due to their large horizontal to vertical length scale ratio. Hayashi and Shiotani reported observations of structures with a vertical scale of approximately 10 km in the upper stratosphere and lower mesosphere during the southern winter. Figure 1.3 shows an example of the pancake like structures that were observed by Hayashi and Shiotani, these were shown through temperature perturbations between the upper stratosphere and lower mesosphere during the southern winter. There is persistent cross-equatorial shear in the upper stratosphere / lower mesosphere near the solstice, so inertial instability is expected; such shear was estimated by Hayashi and

Shiotani to be 2-4 $\times 10^{-5}$ s^{-1}.

An example of similar structures observed in the ocean was given by Richards and Edwards (2003) as in figure 1.4, which show observational data of salinity. The structures consisted of interleaving fresher and saltier water and a vertical height of approximately 10 m and horizontal length of approximately 100 km. These structures had a much thinner appearance than those observed in the atmosphere. Richards and Edwards (2003) however note that inertial instability may not be acting alone to produce these structures but is a contributing factor.

1.3 Related theoretical work: Linear and nonlinear

Another major strand of linear theory has looked at inertial instability for zonally asymmetric disturbances. Boyd and Christidis (1982) looked at disturbances with non-zero zonal wavenumber and showed that for sufficiently small vertical scales the fastest growing disturbances were zonally symmetric. Dunkerton (1983) noted that the disturbances of inertial instability may take a zonally non-symmetric form and found a reduction in the marginally stable shear; such results were obtained numerically. Clark and Haynes (1996) performed numerical calculations on a shear flow that varied slowly with longitude; they also looked at the interaction between planetary wave breaking and inertial instability. Griffiths (2008) also looked at the case where the zonal wavenumber is non-zero, deriving a linear dispersion relation involving both the vertical wavenumber and zonal wavenumber.

A natural progression from linear theory is to look at the weakly nonlinear regime as has been done in the analysis of many other instabilities such as convection and shear instabilities. One weakly nonlinear analysis of inertial instability in a continuously stratified flow was done by Griffiths (2003a) on the equatorial β-plane with viscosity. Through the weakly nonlinear analysis an amplitude equation was formed; through

looking at its evolution the dynamics of the flow can be understood. Growth was implied until the flow was neutralized and then was found to decay to a steady stable state. Another example of a viscous weakly nonlinear analysis on the equatorial β-plane was made by Griffiths (2000). Weakly nonlinear analysis on inertial instability has been performed in a two-layer model by Zhao and Ghil (1991) on the equatorial β-plane for a horizontal and vertical shear flow basic state. Their amplitude behaviour was different from that found by Griffiths (2003a); rather the system flips between stability and instability with the mean flow constantly evolving. These are the only weakly nonlinear analysis on inertial instability that we are aware of and it is worth noting that both of these are performed on the equatorial β-plane.

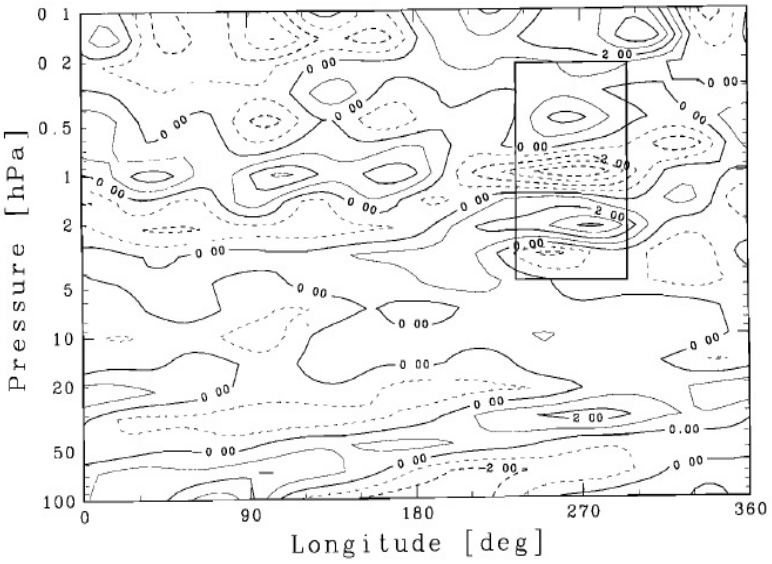

Figure 1.3: *Temperature perturbations in the southern winter around the stratopause, averaged between 29 July and 4 August 1992 with a contour interval of 1K (Hayashi and Shiotani, 1998). Similar structures are also observed in the northern winter, both cases typically lasting for a week.*

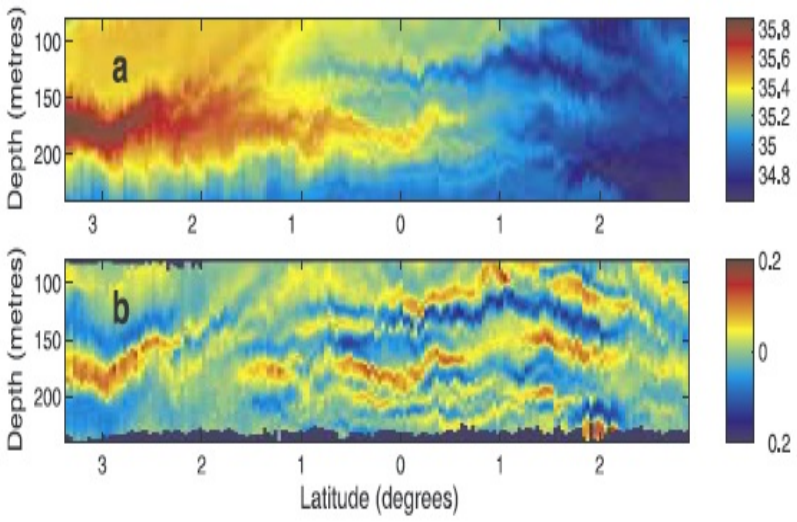

Figure 1.4: *Meridional sections of salinity (a), and salinity anomaly (b), taken along* $165^{o}E$*; showing interleaving structures of alternating fresher and saltier water as observed by Richards and Edwards (2003). The horizontal scale is approximately* 100 *km and vertical scale of approximately* 10 *m.*

1.4 Numerical simulations of inertial instability

There has been extensive nonlinear analysis on inertially unstable continuously stratified flows. For example, Griffiths (2003b) performed numerical simulations of a continuously stratified system on the equatorial β-plane. He found there exists a secondary Kelvin-Helmholtz instability arising from the inertial instability. This in turn creates an upscaling in the length scales to approximately $10\,$km, more consistent with the observable structures attributed to inertial instability. Zeitlin and Plougonven (2009) looked at a barotropic shear on the f-plane in a continuously stratified system noting Kloosterziel et al's (2007) previous work on predicting the final state flow linearly. Zeitlin and Plougonven (2009) extended this analysis numerically to learn what the baroclinic component of the final state might take. Moreover they found inertial instability to be a source of inertia-gravity waves.

With the ocean in mind, Hua et al. (1997) have shown numerically on the equatorial β-plane that a strong horizontal shear with vertical variation is unstable to inertial instability and creates structures akin to Dunkerton's. These structures are found to skew upwards away from the equator. D'Orgeville and Hua (2005) looked at numerical simulation in the deep ocean, they noted the lack of constant shear present in the deep ocean but note the presence of periodic signals known as equatorial free waves which can create a periodic shear. They investigated numerically the case for these periodic shears being a mechanism for producing the layering structures observed in the ocean below the thermocline.

More recent work has analysed inertial instability on the f-plane noting that there exists a competition between inertial instability and barotropic instability. For example, Kloosterziel et al. (2013) looked at the interaction between inertial instability and barotropic instability on the f-plane for a Gaussian jet basic state. As they did on the equatorial β-plane they used the conservation of linear angular momentum to predict the final state flow. Moreover it is found that for a wide range of Rossby number, inertial instability is the fastest growing instability over other instabilities. Natarov and Richards (2015) discussed numerical analysis of inertial instability with the ocean in mind. They did this on the equatorial β-plane, first allowing the symmetric inertial instability to stabilise before analysing the secondary instabilities of the modified zonal mean flow which favour zonally non-symmetric modes. They observe the secondary instability to be a dominant inflection point-type barotropic instability that favours disturbances with a large vertical scale.

The idea of inertial instability being stabilised through the mixing of potential vorticity was first discussed by Dunkerton (1981). Areas of negative potential vorticity mix with the positive potential vorticity outside the unstable region until the flow is stabilised. Nonlinear simulations by Griffiths (2003a,b) have shown that mixing of positive potential vorticity with negative potential vorticity results in a stable flow on the equatorial β-plane. Kloosterziel et al. (2007) looked at a continuously stratified system on the f-plane

using the conservation of linear angular momentum to predict the final state of flow after the instability has been resolved. They did this for various shear flow basic states and showed the robustness of their theory through nonlinear simulations. Kloosterziel et al. (2015) discussed inertial instability in a continuously stratified system; however, now they compare the equatorial β-plane with the f-plane approximation. Again they found predictions from the conservation of absolute linear momentum to agree with nonlinear simulations.

1.5 Inertial instability in two-layer models

The continuously stratified model of the atmosphere and ocean can be simplified by using various layered models, some examples of which are a one-layer or two-layer (or even three-layer) model with a rigid lid or free surface. The models are derived using the shallow water assumptions which result in no z-dependence within each layer as found in Vallis (2006), Salmon (1998) and Gill (1982). This has the advantage of eliminating one dimension in the governing equations making nonlinear simulations simpler to perform. One idea is to think of the atmosphere and ocean as consisting of infinite layered models of small vertical scale stacked one over the other; the disadvantages of such a model however are there is no allowance for vertical mixing or over turning. Having said this, there has been a large history of using such models in the analysis of instability, proving useful in the study of baroclinic instability, modeling turbulence in rotating flows and the analysis of jet formation.

The majority of work on inertial instability has concentrated on the nonlinear analysis of a continuously stratified system. However, the two-layer model should be appreciated for its simplicity but also for its ability to predict the behaviour in a continuously stratified system, something which will be looked at in Chapter 3. The limited work on inertial instability in two-layer flows includes Zhao and Ghil (1991) who performed a weakly

nonlinear analysis of inertial instability on the equatorial β-plane in a two-layer model. They use a basic state with a horizontal and vertical shear. Bouchut et al. (2011) and Zeitlin et al. (2014) have looked at one and two-layer models on both the f-plane and equatorial β-plane respectively. They use an upper free surface with a Bickley jet basic state flow. As in Griffiths (2003b), Bouchut et al. (2011) find a secondary Kelvin-Helmholtz instability observed in the fully nonlinear simulations.

There is a need to understand the fundamental nature of nonlinearity in layered models. In particular, more analysis can be done in the weakly nonlinear regime, which is the simplest way to achieve this. This will give more of an understanding of the transition between the linear and nonlinear dynamics. It can also offer an understanding of the mean flow evolution, which, as previously discussed, is key to understanding the nature of the instability.

1.6 Summary of thesis

We begin our analysis of inertial instability in Chapter 2 by reviewing some fundamental properties of zonally symmetric equatorial inertial instability. We first give the governing Boussinesq equations of motion and then recap the fundamental work of Dunkerton (1981) when Pr=1; reproducing Dunkerton's dispersion relation and critical shear at which the flow turns from unstable to stable. The case of infinite Prandtl number is examined ($Pr \to \infty$); however Dunkerton's analysis is advanced by deriving the critical conditions for instability analytically rather than as Dunkerton did numerically.

A common alternative approach in geophysical fluid dynamics is to instead use a model consisting of one or more layers of constant fluid density. Our choice here is to use a two-layer model which is derived in Chapter 3. The main benefits of a two-layer system are the mathematical simplifications and, as we shall see, there exists an analogy between the two-layer model with interface friction and the continuously stratified system with

$Pr \to \infty$. Hereafter our analysis will be focused on a two-layer system.

In Chapter 4 we study equatorial inertial instabilities with uniform shear in the two-layer model developed in Chapter 3. We start by deriving the (nondimensional) linear dispersion relation for instabilities on a flow with uniform shear, and perform asymptotic analysis for weak friction. We turn to looking at nonlinear effects by performing a weakly nonlinear analysis for the frictionless system, leading to an amplitude equation for the growth and subsequent oscillations of the unstable modes. A comparison with numerical solutions of the full nonlinear two-layer PDEs is then given.

In Chapter 5 we focus our analysis of the two-layer system on the f-plane with a localised shear flow basic state. The case for inertial instability at mid-latitudes has been made by Stevens and Ciesielski (1986) and Shen and Evans (2002) amongst others and therefore an f-plane analysis cannot be ignored. After a (nondimensional) linear dispersion is found we perform weakly nonlinear analysis deriving an amplitude equation. The weakly nonlinear results are then compared with a numerical solution to the full nonlinear PDEs. Here, we also make an analysis of the changes that take place to the mean flow as the instability develops.

We recap the work covered in this thesis and conclude our findings in Chapter 6. We discuss its relevance and agreement with similar work. A final conclusion is made on improvements that could be made as well as extensions to this work.

Chapter 2

Continuously stratified inertial instability

2.1 Introduction

The bulk of this thesis is concerned with models of linear and nonlinear inertial instabilities in two-layer flows. However, as will be discussed in detail in Chapter 3, we are using two-layer flows as simple representations of continuously stratified atmospheres and oceans. So, before considering inertial instabilities in two-layer flows, it is important to set out some fundamental properties of inertial instability in continuously stratified flows. Specifically, we consider a zonal flow with latitudinal shear and uniform buoyancy frequency, and its stability to zonally symmetric perturbations (i.e., no along-stream variations). We consider some properties of the eigenvalue problem determining linear instability, some simple exact solutions for linear instabilities, the role of viscous and thermal diffusion, and some issues relating to numerical solutions of linear eigenvalue problems.

Much of this work is related to two pioneering papers of Dunkerton (1981,1982), who

was concerned with applications to the equatorial atmosphere, although the same theory also applies to some oceanic flows. Dunkerton considered the linear instability of a zonal flow with uniform latitudinal shear on the equatorial β-plane. This configuration is always prone to inertial instability, since the vertical component of the absolute vorticity Q takes the opposite sign to the Coriolis parameter f on one side or other of the equator. In his first paper (Dunkerton 1981), he derived an exact dispersion relation describing instability with Prandtl number unity (i.e., equal kinematic viscosity and thermal diffusion). Without diffusion, there is always instability, which preferentially occurs with vanishingly small length scales (both vertically and latitudinally). With diffusion, Dunkerton derived the critical diffusivity at which the flow is stabilised, along with the corresponding vertical wavenumber. In the second paper (Dunkerton 1982), these results were extended to the case with arbitrary Prandtl number, mainly relying upon numerical results.

Here we start, in section 2.2, by giving the equations of motion to be used in this chapter – the hydrostatic, Boussinesq equations. The Boussinesq approximation is widely used in geophysical fluid dynamics, but it is particularly appropriate for studies of inertial instability, which occurs on the preferentially small vertical scales that are required for the Boussinesq approximation to be valid; a result of the Boussinesq approximation is the fluid has a small vertical scale and as Dunkerton (1982) has shown, inertial instability also selects small vertical length scales. In section 2.7, we derive the eigenvalue problem governing linear instabilities in a fluid with arbitrary Prandtl number, along with some general conditions for (inertial) instability. In section 2.8, we consider simple solutions for inviscid inertial instabilities on the f-plane and equatorial β-plane, both of which show the preference for the instability to select vanishingly small vertical scales. For the remaining sections, we consider solutions on the equatorial β-plane. In section 2.9, we review Dunkerton's solutions with Prandtl number unity. In section 2.10, we focus on the case with infinite Prandtl number, and explicitly derive expressions for the critical diffusivity at which the flow is stabilised, along with the corresponding vertical wavenumber, thus extending the numerical results of Dunkerton (1982). Finally, in

section 2.11, and thinking ahead to later chapters where numerical solutions are necessary, we consider numerical solutions of the linear eigenvalue problem on the equatorial β-plane, and how they depend upon resolution and domain size.

At the outset, we also note that instabilities with infinite Prandtl number are of special interest, since we shall see (in chapter 3) that there is an analogy between these and inertial instabilities in two-layer flows. Specifically, with an interfacial friction (or drag) in a two-layer flow, the dispersion relation for inertial instability is equivalent to that for a continuously stratified fluid with infinite Prandtl number. This fundamental equivalence will be key to our justification for using simple two-layer flows to model inertial instabilities in continuously stratified fluids.

2.2 Governing equations

2.3 The Boussinesq approximation

Throughout this study we use Boussinesq equations of motion, which are widely used to model atmospheric and oceanic flows. The Boussinesq approximation requires the flow to be confined to a sufficiently small layer depth, so that density variations remain small compared to the average density ρ_s. A derivation from the full compressible equations of motion for an ideal gas is given in Appendix A, although they apply for more general equations of state (e.g., for oceanic flows). The equations of motion are then

$$\frac{D\mathbf{u}}{Dt} + 2\boldsymbol{\Omega}\times\mathbf{u} = -\nabla\phi + b\mathbf{k} + \nu\nabla^2\mathbf{u}, \tag{2.1a}$$

$$\nabla\cdot\mathbf{u} = 0, \tag{2.1b}$$

$$\frac{Db}{Dt} + N^2(z)w = \kappa\nabla^2 b, \tag{2.1c}$$

The corresponding three dimensional flow is $\mathbf{u} = (u, v, w)$ with $\phi = p'/\rho_s$ (here, p' is the pressure perturbation as a result of motion and ρ_s is the density averaged over the fluid layer). An additional variable is the buoyancy $b = g\rho'/\rho_s$ where ρ' is the density perturbation as a result of motion. Also, g is the gravitational acceleration, $\mathbf{\Omega} = (0, \Omega\cos\theta, \Omega\sin\theta)$ is the rotation vector ($\Omega = 7.2921 \times 10^{-5}$ radians per second), ν and κ are the kinematic viscosity and the thermal diffusivity respectively (typically $\nu = 3 - 4 \times 10^{-5}\mathrm{m}^2\,\mathrm{s}^{-1}$ and $\kappa = 2 \times 10^{-5}\mathrm{m}^2\,\mathrm{s}^{-1}$ for dry air) and z is the height coordinate. Finally we also have the buoyancy frequency $N^2(z)$ which is related to the vertical gradient of the background density and temperature.

2.4 The f-plane and β-plane approximations

The Coriolis force represented by $2\mathbf{\Omega} \times \mathbf{u}$ is the force felt as a result of the Earth's rotation. Since the earth rotates along an axis that is not in-line with any of the coordinate directions, x, y and z there is a force felt in the y and z plane. The Coriolis force in full can be written

$$2\mathbf{\Omega} \times \mathbf{u} = (-fv + \gamma w, fu, -\gamma u), \tag{2.2}$$

where $f = 2\Omega\sin\theta$, $\gamma = 2\Omega\cos\theta$, and θ is latitude (which varies with y). It is normal to use either the

(i) f-plane approximation: $f = 2\Omega\sin\theta_0$ for some reference latitude θ_0,
(ii) β-plane approximation: $y \approx R_e\,(\theta - \theta_0)$ (with Earth radius R_e), and write $f = 2\Omega\sin(\theta_0 + y/R_e) \approx 2\Omega\sin\theta_0 + 2\Omega\cos\theta_0(y/Re) = f_0 + \beta y$, where $f_0 = 2\Omega\sin\theta_0$ and $\beta = 2\Omega\cos\theta_0/Re$.
(iii) Equatorial β-plane approximation: This is (ii) with $\theta_0 = 0$, so that $\beta = 2\Omega/R_e$ (for Earth $\beta \approx 2.3 \times 10^{-11}\mathrm{m}^{-1}\,\mathrm{s}^{-1}$).

Equations (2.1a) - (2.1c) then become

$$Du/Dt - fv + \gamma w = -\phi_x + \nu\nabla^2 u, \tag{2.3a}$$

$$Dv/Dt + fu = -\phi_y + \nu\nabla^2 v, \tag{2.3b}$$

$$Dw/Dt - \gamma u = -\phi_z + b + \nu\nabla^2 w, \tag{2.3c}$$

$$Db/Dt + N^2 w = \kappa\nabla^2 b, \tag{2.3d}$$

$$u_x + v_y + w_z = 0. \tag{2.3e}$$

2.5 Hydrostatic and traditional approximations

When we have the atmosphere and ocean in mind, we are studying horizontal flows of a few hundred or possibly thousands of kilometers compared to a vertical scale of a few kilometers; with this in mind, to keep the scaling of the continuity equation in balance, i.e.

$$\frac{W}{H} \sim \frac{U}{L},$$

we must have $w\cos\theta \ll v\sin\theta$, here W and U represent the vertical and horizontal velocity scales respectively and H and L represent the vertical and horizontal length scales respectively. That is the vertical velocities are much smaller than horizontal velocities. Finally, in order to maintain the conservation of energy, we neglect the Coriolis force in the vertical direction and the Coriolis force can be approximated by

$$2\mathbf{\Omega} \times \mathbf{u} \approx (-fu, fv, 0).$$

For motions with timescale T in which advection of the background stratification is important, we estimate $b/T \sim N^2 w$. Then $Dw/Dt/b \sim (w/T)/(TN^2 w) = 1/(N^2T^2)$.

So Dw/Dt can be neglected relative to b for any motions with $T \gg 1/N$. In particular, this is a good approximation for motions on inertial timescales (i.e., $T \sim 1/f$), since $1/f \gg 1/N$ or equivalently $f/N \ll 1$ for most atmospheric and oceanic flows. For example, with $f < 2\Omega = 1.4 \times 10^{-4}\,\mathrm{s}^{-1}$ and $N = 0.01\,\mathrm{s}^{-1}$ (a typical stratospheric value), we have $f/N < 1.4 \times 10^{-2} \ll 1$. The diffusive terms can be neglected on the same basis provided $|\nu\nabla^2 w| < |Dw/Dt|$, which is to be expected for large-scale flows. Thus the vertical momentum equation reduces to

$$b = \phi_z. \tag{2.4}$$

This is the well-known hydrostatic approximation.

2.6 Our governing equations

We make two further simplifications to the Boussinesq and hydrostatic equations of motion. First, we note that inertial instability is symmetric i.e. it occurs with no along-stream variations. Although there are extensions of the instability to modes with along-stream variations (e.g., Dunkerton (1983), Griffiths (2008)), the most unstable mode is usually symmetric. So we take $\partial/\partial x = 0$ in (2.1a) - (2.1c), which also eliminates the possibility of any competing barotropic (Kelvin–Helmholtz) instabilities in the (x, y) plane. Second, Dunkerton (1981) found inertial instability preferred structures with vanishingly small vertical length scales, that is, structures with $L_z \ll L_y$ hence, $1/L_z^2 \gg 1/L_y^2 \sim \partial^2/\partial y^2$. Therefore we approximate the Laplacian (diffusion) operators by $\partial^2/\partial z^2$. The resulting equations of motion are thus

$$Du/Dt - fv = \nu u_{zz}, \tag{2.5a}$$

$$Dv/Dt + fu = -\phi_y + \nu v_{zz}, \tag{2.5b}$$

$$\phi_z = b, \tag{2.5c}$$

$$Db/Dt + N^2 w = \kappa b_{zz}, \tag{2.5d}$$

$$v_y + w_z = 0, \tag{2.5e}$$

where $D/Dt = \partial/\partial t + v\partial/\partial y + w\partial/\partial z$. These equations are the basis for the rest of this chapter.

2.7 The governing eigenvalue problem for linear inertial instability

In this section we perform linear stability analysis of a basic flow $u = U(y)$ using equations (2.5a - 2.5e). We derive an eigenvalue problem for the growth rate (or frequency) in the form of an ordinary differential equation for the cross-stream flow v, and then discuss its properties. Special cases (equatorial β-plane, inviscid flow, $Pr = 1$, etc.) will be examined in later sections.

We consider the linear stability of a basic state $u = U(y)$, $v = w = 0$, $\phi = \Phi(y)$, $b = 0$, and with constant N, which satisfies $fU = -d\Phi/dy$. Introducing perturbations $u = U + u'$, $v = v'$, $w = w'$, $\phi = \Phi + \phi'$ and $b = b'$ we have

$$\frac{\partial u'}{\partial t} - Q(y)v' = \nu\frac{\partial^2 u'}{\partial z^2}, \tag{2.6a}$$

$$\frac{\partial v'}{\partial t} + f(y)u' = -\frac{\partial \phi'}{\partial y} + \nu\frac{\partial^2 v'}{\partial z^2}, \tag{2.6b}$$

$$\frac{\partial \phi'}{\partial z} = b', \tag{2.6c}$$

$$\frac{\partial v'}{\partial y} + \frac{\partial w'}{\partial z} = 0, \tag{2.6d}$$

$$\frac{\partial b'}{\partial t} + N^2 w' = \kappa \frac{\partial^2 b'}{\partial z^2}, \tag{2.6e}$$

where $Q(y) = f(y) - dU(y)/dy$. Now we look for wave like disturbances of the form

$$(u', v', w', \phi', b') = \mathbb{R}e\Big((\hat{u}(y), \hat{v}(y), \hat{w}(y), \hat{\phi}(y), \hat{b}(y)) \exp(imz + st) \Big),$$

where m is the chosen vertical wavenumber, and that the growth rate s is to be found in terms of m. Substituting into (2.6a) - (2.6e)

$$(s + \nu m^2)\hat{u} - Q\hat{v} = 0, \qquad (s + \nu m^2)\hat{v} + f\hat{u} = -\frac{d\hat{\phi}}{dy}, \qquad \frac{d\hat{v}}{dy} + im\hat{w} = 0, \tag{2.7}$$

$$(s + \kappa m^2)\hat{b} + N^2\hat{w} = 0, \qquad im\hat{\phi} = \hat{b}. \tag{2.8}$$

We reduce these to a single differential equation for $\hat{v}$. First we multiply (2.7b) by $(s + \nu m^2)$ and then substitute for $\hat{u}$ from (2.7a)

$$((s + \nu m^2)^2 + fQ)\hat{v} = (s + \nu m^2)\frac{d\hat{\phi}}{dy}. \tag{2.9}$$

Next we substitute (2.8b) into (2.8a) to eliminate $\hat{b}$, then eliminate $\hat{w}$ using (2.7c)

$$-im(s + \kappa m^2)\hat{\phi} = \frac{N^2}{im}\frac{d\hat{v}}{dy}. \tag{2.10}$$

To finally eliminate $\hat{\phi}$ we differentiate (2.10) and multiply by $(s + \nu m^2)$ then finally substitute for $d\hat{\phi}/dy$ from (2.9). After rearranging we have

$$\frac{d^2\hat{v}}{dy^2} - \frac{m^2(s + \kappa m^2)}{N^2(s + \nu m^2)}\Big((s + \nu m^2)^2 + fQ \Big)\hat{v} = 0. \tag{2.11}$$

Equation (2.11) is the desired equation for $\hat{v}$ and was first derived by Dunkerton (1982). We solve it subject to

$$\hat{v} = 0 \quad \text{at} \quad y = \pm L, \tag{2.12}$$

corresponding to the presence of rigid walls, where L may alternatively be taken to be infinite (corresponding to vanishing disturbances in the far field). Equation (2.11) is then an eigenvalue problem for the unknown growth rate s, in terms of the prescribed vertical wavenumber m, the buoyancy frequency N, the diffusivities ν and κ, and the function fQ, which varies with y.

2.7.1 Necessary conditions for instability

Multiplying (2.11) by the complex conjugate, $\hat{v}^*$, and integrating over the domain $[-L, L]$ we have

$$-\frac{N^2}{m^2}\int_{-L}^{L}\left|\frac{d\hat{v}}{dy}\right|^2 dy - (s+\kappa m^2)(s+\nu m^2)\int_{-L}^{L}|\hat{v}|^2 dy = \left(\frac{s+\kappa m^2}{s+\nu m^2}\right)\int_{-L}^{L} fQ|\hat{v}|^2 dy, \tag{2.13}$$

where we have applied both integration by parts and the boundary condition (2.12) on the first term. We consider three special cases of (2.13), each of which imply that $fQ < 0$ is a necessary condition for instability.

Firstly, when $\nu = \kappa = 0$ we have

$$-\frac{N^2}{m^2}\int_{-L}^{L}\left|\frac{d\hat{v}}{dy}\right|^2 dy - s^2\int_{-L}^{L}|\hat{v}|^2 dy = \int_{-L}^{L} fQ|\hat{v}|^2 dy. \tag{2.14}$$

Rearranging (2.14) to find s we have

$$s^2 = \left(\int_{-L}^{L}|\hat{v}|^2 dy\right)^{-1}\left(-\frac{N^2}{m^2}\int_{-L}^{L}\left|\frac{d\hat{v}}{dy}\right|^2 dy - \int_{-L}^{L} fQ|\hat{v}|^2 dy\right). \tag{2.15}$$

So, for instability, ($s^2 > 0$) we require $fQ < 0$ somewhere in the domain.

Secondly, when $\nu = \kappa$, (2.13) becomes

$$-\frac{N^2}{m^2}\int_{-L}^{L}\left|\frac{d\hat{v}}{dy}\right|^2 dy - (s+\nu m^2)^2\int_{-L}^{L}|\hat{v}|^2 dy = \int_{-L}^{L} fQ|\hat{v}|^2 dy, \tag{2.16}$$

and we find

$$s = \left(-\frac{N^2}{m^2}\int_{-L}^{L}\left|\frac{d\hat{v}}{dy}\right|^2 dy - \int_{-L}^{L} fQ|\hat{v}|^2 dy\right)^{1/2}\left(\int_{-L}^{L}|\hat{v}|^2 dy\right)^{-1/2} - \nu m^2. \tag{2.17}$$

Since we require $s > 0$ for instability, the first term of (2.17) must be positive; so we require the contents of the first bracketed term to be positive, implying that fQ must be somewhere negative.

Finally, when $\kappa = 0$,

$$-\frac{N^2}{m^2}\int_{-L}^{L}\left|\frac{d\hat{v}}{dy}\right|^2 dy - s(s+\nu m^2)\int_{-L}^{L}|\hat{v}|^2 dy = \left(\frac{s}{s+\nu m^2}\right)\int_{-L}^{L} fQ|\hat{v}|^2 dy. \tag{2.18}$$

Rearranging (2.18) produces a cubic polynomial $As^3 + Bs^2 + Cs + D = 0$, where

$$A = \int_{-L}^{L}|\hat{v}|^2 dy, \quad B = 2\nu m^2\int_{-L}^{L}|\hat{v}|^2 dy, \quad D = \nu N^2\int_{-L}^{L}\left|\frac{d\hat{v}}{dy}\right|^2 dy \tag{2.19}$$

$$C = \frac{N^2}{m^2}\int_{-L}^{L}\left|\frac{d\hat{v}}{dy}\right|^2 dy + \nu^2 m^4\int_{-L}^{L}|\hat{v}|^2 dy + \int_{-L}^{L} fQ|\hat{v}|^2 dy. \tag{2.20}$$

We are interested in conditions which guarantee instability (at least one root where $s < 0$) or stability (all roots positive $s \geq 0$). By the Routh-Hurwitz stability criterion (Hurwitz, 1895), for the cubic to have all stable roots, where for purely real roots they are zero or negative and for complex roots the real parts are either zero or negative, we must have

$$A, B, C, D > 0 \qquad \text{and} \qquad BC > AD. \tag{2.21}$$

Note that the Routh-Hurwitz criteria also holds for the case where $A, B, C, D < 0$ however, A, B and D cannot be negative so we have excluded this case. It is easy to see that A, B and D are positive, and C will also be positive if $fQ > 0$. So, $fQ > 0$ implies stability, and a necessary (but not sufficient) condition for instability is that $fQ < 0$ somewhere in the flow.

So, we can see that for inertial instability to occur we must have $fQ < 0$ somewhere in the flow. This condition has been derived in various ways for various flow configurations in the past (Sawyer (1949), Hua et al. (1997), Griffiths (2008)).

2.8 Simple inviscid solutions with constant shear

We now look at two inviscid solutions for inertial instability: one on a bounded f-plane, and the other on an unbounded equatorial β-plane. In both cases, we take a basic flow with constant shear:

$$U = \Lambda y, \tag{2.22}$$

which is the simplest possible shear flow that could give inertial instability. We use (2.11) with $\nu = \kappa = 0$:

$$\frac{d^2\hat{v}}{dy^2} - \frac{m^2}{N^2}\left(s^2 + fQ\right)\hat{v} = 0, \tag{2.23}$$

where $Q = f - \Lambda$.

2.8.1 A bounded f-plane

We set $f = f_0 =$ constant in (2.23), so that $Q = f_0 - \Lambda$ is also constant. We consider a laterally bounded domain such that $v = 0$ at $y = \pm L$. Then the general solution is given by

$$\hat{v} = A\cos\left(Gy\right), \tag{2.24}$$

where $G^2 = -(m^2(s^2 + f_0 Q)/N^2)$ and the boundary conditions imply

$$G = \frac{(2n+1)\pi}{2L}, \tag{2.25}$$

where n is a non-negative integer. Hence, we obtain a dispersion relation which gives us information about how the wavenumber m and growth rate s are related,

$$s^2 = -\frac{(2n+1)^2\pi^2 N^2}{4L^2 m^2} - f_0 Q. \tag{2.26}$$

There is the possibility of instability when $f_0 Q < 0$, but there is a stabilising effect due to stratification. The most unstable disturbances have $m \to \infty$ showing that the instability prefers vanishingly small length scales in the vertical. It should also be noted that the $n = 0$ mode is the most unstable and by setting $n = 0$ in (2.26),

$$s^2 = -\frac{\pi^2 N^2}{4L^2 m^2} - f_0 Q. \tag{2.27}$$

By setting $s = 0$ we can see that marginal stability is reached when $m_c^2 = -\pi^2 N^2/4L^2 f_0 Q$, where m_c denotes the critical wavenumber. We have instability occurring if $m > m_c$. So, the growth rate and marginal stability depend on the domain size with larger domains being more unstable.

2.8.2 An unbounded equatorial β-plane

Next we turn our attention to the inviscid case on an unbounded equatorial β-plane and re-visit previous work by Dunkerton (1981). We carry on from (2.11), however now with $f = \beta y$:

$$\frac{d^2\hat{v}}{dy^2} - \frac{m^2}{N^2}\Big(s^2 + \beta y(\beta y - \Lambda)\Big)\hat{v} = 0, \quad \text{where} \quad \hat{v} \to 0 \quad \text{as} \quad |y| \to \infty. \tag{2.28}$$

After completing the square (2.28) becomes

$$\frac{d^2\hat{v}}{dy^2} - \frac{m^2}{N^2}\left(s^2 - \frac{\Lambda^2}{4} + \beta^2(y - \Lambda/2\beta)^2\right)\hat{v} = 0. \tag{2.29}$$

Introducing a nondimensional coordinate Y defined via

$$Y = \frac{y - \Lambda/2\beta}{L}, \text{ with } L = \left(\frac{N}{2\beta|m|}\right)^{1/2}, \tag{2.30}$$

equation (2.29) becomes

$$\frac{d^2v}{dY^2} + \left(\mu + \frac{1}{2} - \frac{Y^2}{4}\right)v = 0, \text{ where } \mu + \frac{1}{2} = -\frac{|m|}{2N\beta}\left(s^2 - \frac{\Lambda^2}{4}\right), \tag{2.31}$$

where $\hat{v} \to 0$ as $|Y| \to \infty$. Note that the wavenumber m is now written as $|m|$, this is to keep the Y real in (2.30). It can be shown that μ must be a non-negative integer to satisfy $\hat{v} \to 0$ as $|Y| \to \infty$ (Bender and Orszag, 1999), in which case $\hat{v}$ is a Hermite polynomial in Y multiplied by $\exp(-Y^2/4)$. This yields the dispersion relation

$$s^2 = \frac{\Lambda^2}{4} - \frac{\beta N(2n+1)}{|m|}, \tag{2.32}$$

where n is a non-negative integer. As $m \to \infty$ the dispersion relation (2.32) can be approximated by $s \approx \pm\Lambda/2$ and hence there is an unstable mode, whatever the sign of Λ. On the other hand, as $m \to 0$ we have $s^2 \approx -(2n+1)(N\beta/|m|)$ and the solution is stable. The critical wavenumber m_c giving marginal stability is given by $s = 0$ and hence with $n = 0$ which corresponds to the most unstable mode,

$$m_c = \frac{4N\beta}{\Lambda^2},$$

with instability when $m > m_c$.

2.9 Equatorial β-plane: $Pr = 1$

Here we re-derive the conditions that Dunkerton (1981) gave for marginal stability, in part because he gave so few details, and in part because understanding this method is key to the more complicated calculation with $Pr \neq 1$ (to be performed in section 2.10). We start from (2.11) with $\nu = \kappa$,

$$\frac{d^2\hat{v}}{dy^2} - \frac{m^2}{N^2}\Big((s+\nu m^2)^2 + \beta y(\beta y - \Lambda)\Big)\hat{v} = 0. \tag{2.33}$$

Using the same transformation of variables used in section 2.8.2 and completing the square, (2.33) becomes

$$\frac{d^2v}{dY^2} + \left(\mu + \frac{1}{2} - \frac{Y^2}{4}\right)v = 0, \text{ where } \mu + \frac{1}{2} = -\frac{|m|}{2N\beta}\left((s+\nu m^2)^2 - \frac{\Lambda^2}{4}\right). \tag{2.34}$$

As with the inviscid case, equation (2.34) is of the form of a parabolic cylinder function and we therefore find eigenvalues to be a positive integer n. Hence

$$s = \left(\Lambda^2/4 - \frac{(2n+1)\beta N}{|m|}\right)^{1/2} - \nu|m|^2, \tag{2.35}$$

where we have taken the positive square root to allow for the possibility of an unstable mode. Since we require $Re(s) > 0$ for instability, dispersion relation (2.35) shows that we are guaranteed stability if

$$\frac{\Lambda^2}{4} - \frac{(2n+1)\beta N}{|m|} < 0. \tag{2.36}$$

In this viscous case the growth rate decreases for sufficiently large $|m|$. Thus the maximum growth rate occurs for some finite value of m. To analyse this, it is easier

to work with a nondimensional dispersion relation. We write

$$s = (\Lambda/2)s_*, \quad |m| = (4\beta N/\Lambda^2)|m|_* \quad \text{and} \quad \nu = ((\Lambda/2) \times (\Lambda^2/4\beta N)^2)\nu_* \tag{2.37}$$

in equation (2.35) to get

$$s_* = \sqrt{1 - \frac{2n+1}{|m|^*}} - \nu_*|m|_*^2. \tag{2.38}$$

As m_* increases from zero, the roots are complex but with all real parts negative, implying stability. There is a transition when $m_* \approx 1$, at which both roots become real and the larger one quickly becomes positive. For yet larger m_*, this larger (real) root again becomes negative, so that there is a single band of m_* corresponding to instability. Thus, the instability no longer prefers vanishingly small length scales. Figure 2.1 illustrates the dispersion relation in the case where $n = 0$ and $\nu_* = 5 \times 10^{-3}$.

2.9.1 Critical viscosity and shear flow

It is of interest to find the linear shear flow at which stability is guaranteed as shown by Dunkerton (1981), i.e. the shear flow that ensures s_* is negative for all wavenumbers m. We can see from figure 2.1 that the curve has a maximum, and hence in order to ensure this curve is below the m_*-axis we require $s_* = 0$ and $ds_*/d|m_*| = 0$ for some value of $|m_*|$. Note that where the maximum of s_* occurs, s_* itself is purely real. Firstly allowing $s_* = 0$ in equation (2.38)

$$0 = \sqrt{1 - \frac{(2n+1)}{|m_*|}} - \nu_*|m_*|^2 \qquad \Rightarrow \left(1 - \frac{(2n+1)}{|m_*|}\right)^{-1/2} = \frac{1}{\nu_*|m_*|^2} \tag{2.39}$$

then from $ds_*/d|m_*| = 0$ we have

$$\frac{ds_*}{d|m_*|} = \frac{(2n+1)}{2|m_*|^2}\left(1 - \frac{(2n+1)}{|m_*|}\right)^{-1/2} - 2\nu_*|m_*| = 0. \tag{2.40}$$

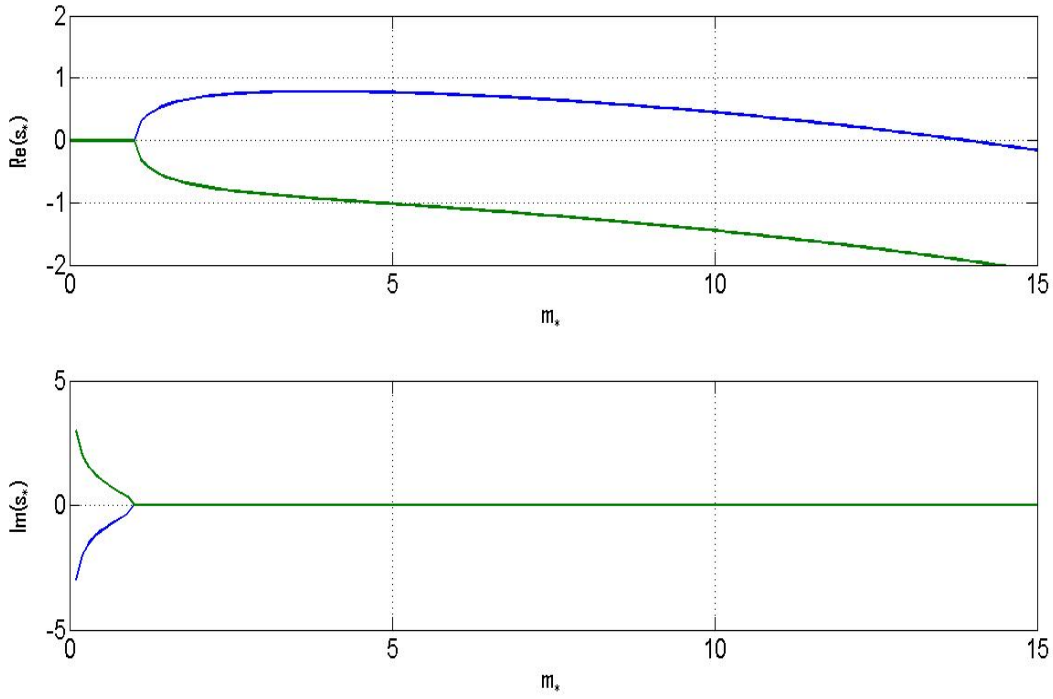

Figure 2.1: *The viscous nondimensional dispersion relation (2.38) on the equatorial β-plane, where $Pr = 1$ and the viscosity is fixed at $\nu_* = 5 \times 10^{-3}$ with $n = 0$.*

Substituting (2.39) into (2.40)

$$\frac{(2n+1)}{2|m_*|^4\nu_*} = 2\nu_*|m_*| \qquad \Rightarrow |m_*|_c^5 = \frac{(2n+1)}{4\nu_*^2}. \tag{2.41}$$

Substituting $|m_*|_c$ into equation (2.39) gives the critical viscosity

$$\nu_{c*} = \left(\frac{1}{4(1/4+(2n+1))^5}\right)^{1/2}. \tag{2.42}$$

For $n = 0$ we have specific values of $\nu_c = 0.026258$ & $m_c = 1.955059$. Finally, using the nondimensional variable $\nu = ((\Lambda/2) \times (\Lambda^2/4\beta N)^2)\nu_*$ we can then find a critical shear

Λ_c given by

$$\Lambda_c = 2(1/4 + (2n+1))^{1/2}\nu^{1/5}\left(\frac{\beta N}{4}\right)^{2/5}, \tag{2.43}$$

where we have used "$_c$" to denote the critical shear. This is the result of Dunkerton (1981) and implies greater stratification or greater diffusivity stabilizes the flow as a stronger shear is needed for instability. An illustration of a critical case if given in figure 2.2.

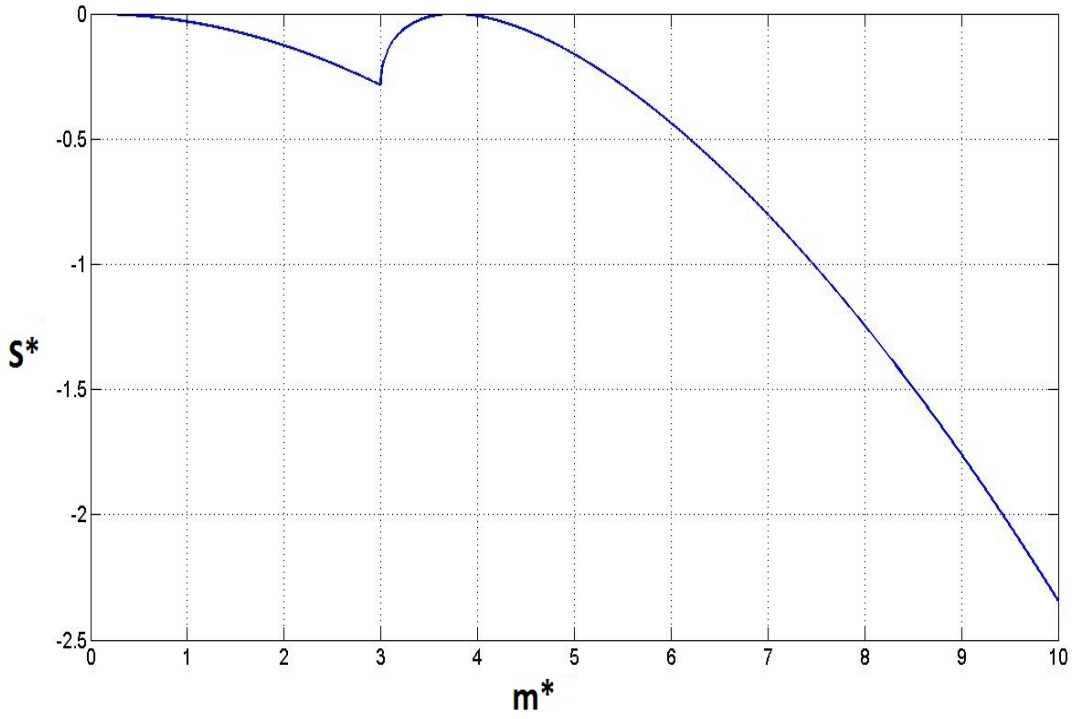

Figure 2.2: *The real part of the viscous nondimensional dispersion relation, (2.38) on the equatorial β-plane with $Pr = 1$. Here the viscosity is equal to the critical value (2.41) and the flow never becomes unstable.*

2.10 Equatorial β-plane: $Pr = \infty$

Here we now examine the case with no thermal diffusion (i.e., $\kappa = 0$), but retaining viscosity (i.e., $\nu \neq 0$), which corresponds to infinite Prandtl number, $Pr = \infty$. This

choice of Prandtl number provides a good leading order model especially for the ocean; however the main motivation for choosing such a parameter will become clearer when we discuss the two-layer model in chapter 3.

We again use a shear flow basic state $U(y) = \Lambda y$ and use the eigenvalue problem (2.31). However, now with $\kappa \to 0$ we have

$$\frac{d^2\hat{v}}{dy^2} - \frac{m^2}{N^2}\left(\frac{s}{s+\nu m^2}\right)\left((s+\nu m^2)^2 - \frac{\Lambda^2}{4} + \beta^2\left(y - \frac{\Lambda}{2\beta}\right)^2\right)\hat{v} = 0. \tag{2.44}$$

Setting $(y - \Lambda/2\beta) = LY$ equation (2.44) transforms to the parabolic cylinder equation

$$\frac{d^2\hat{v}}{dy^2} + \left(\hat{\mu} + \frac{1}{2} - \frac{Y^2}{4}\right)\hat{v} = 0, \tag{2.45}$$

where

$$L^4 = (4|m|^2\beta^2/N^2)^{-1}(s/(s+\nu|m|^2))^{-1} \tag{2.46}$$

and

$$\hat{\mu} = -(|m|^2/N^2)(s/(s+\nu|m|^2))((s+\nu|m|^2)^2 - \Lambda^2/4) - 1/2. \tag{2.47}$$

Note that we require L to be real to satisfy the boundary conditions and it can be shown that there always exists a real positive root of L^4 regardless of s being real or complex (appendix B). Also note that (2.46) reduces to (2.30) when $\nu = 0$. Now, applying the boundary conditions $\hat{v} = 0$ as $Y \to \pm\infty$, ($\hat{v} = 0$ as $y \to \pm\infty$), the eigenvalue $\hat{\mu}$ is equal to a non-negative integer n (Bender & Orszag 1978) and hence

$$\frac{(2n+1)N\beta}{|m|} = -\left(\frac{s}{s+\nu|m|^2}\right)^{1/2}\left((s+\nu|m|^2)^2 - \frac{\Lambda^2}{4}\right), \tag{2.48}$$

which is the dispersion relation describing the relationship between the growth rate s, viscosity ν and wavenumber m.

In order to analyse the dispersion relation (2.48) further it is easier to nondimensionalise.

We again use the nondimensionalisation (2.37), in which case (2.48) becomes

$$\frac{(2n+1)}{|m_*|} = -\left(\frac{s_*}{s_* + \nu_*|m_*|^2}\right)^{1/2}\left((s_* + \nu_*|m_*|^2)^2 - 1\right). \tag{2.49}$$

Dispersion relation (2.49) is shown in figure 2.3, where the viscosity is fixed at $\nu = 5 \times 10^{-3}$ and $n = 0$. The roots were found by squaring the dispersion relation to form a quintic polynomial which was solved for a fixed m using a MATLAB roots finder. Any spurious roots were discarded by re-substituting back into the dispersion relation and checking the residual is sufficiently small, this always left three true roots of the dispersion relation. The roots start purely imaginary before branching off into complex pairs with one purely real root. Through inspection the flow appears to become unstable when $m \approx 2.25$, which is less than the $Pr = 1$ case for the same viscosity.

2.10.1 Critical viscosity and shear flow

We will now look for the critical viscosity. Dunkerton (1982) discussed the critical viscosity for $Pr = \infty$, however no explicit solution for the critical viscosity was given; his numerical solutions are shown in figure 2.4. We aim to find an analytical and numerical solution for the critical shear and compare this to Dunkerton's results. Analytically, my method was as follows, dropping the "*", we first squared dispersion relation (2.49) producing a fifth order polynomial in s

$$as^5 + 4a^2s^4 + (6a^3 - 2a)s^3 + (4a^4 - 4a^2)s^2 + (a^5 - 2a^3 + a - T^4)s - aT^4 = 0, \tag{2.50}$$

where $a = \nu m^2$ and $T^4 = \nu(2n+1)^2$. We will now solve for a and T under marginal conditions which in turn can be used to deduce m and ν.

We write the growth rate in the form $s = s_r + is_i$ which was substituted into (2.50). We look for the point where the flow turns from unstable $s_r > 0$ to stable $s_r < 0$ and

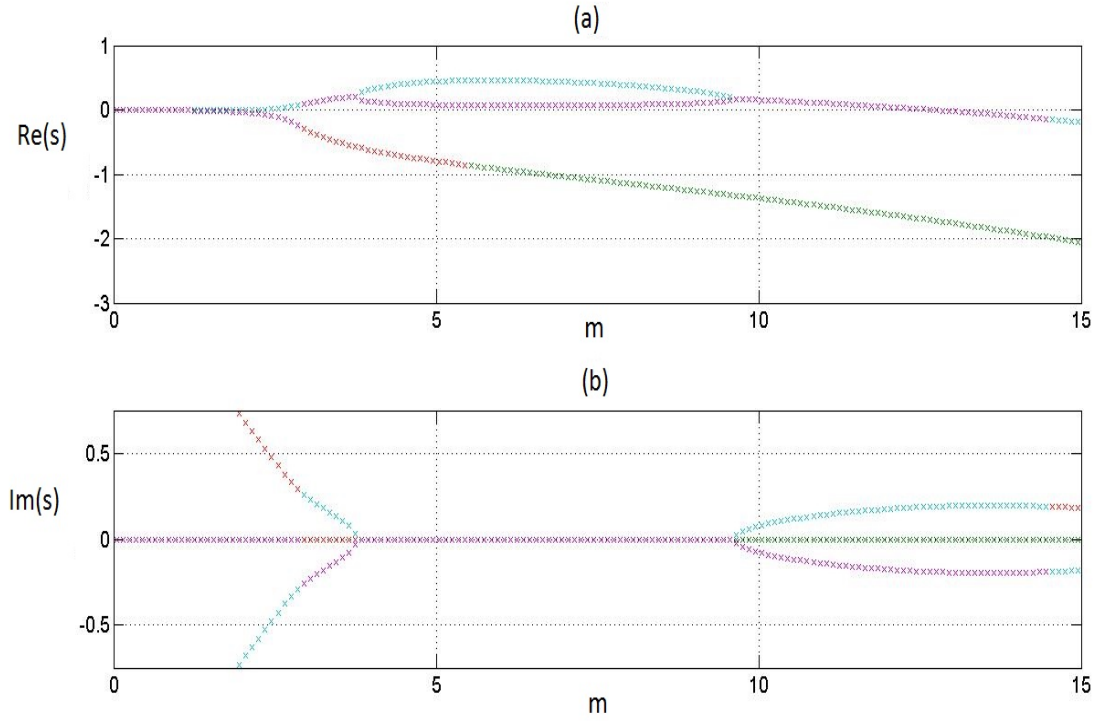

Figure 2.3: *The nondimensional viscous dispersion relation (2.49) on the equatorial β-plane with $\nu = 5 \times 10^{-3}$ and $n = 0$. Although the scale of the graph does not make this clear for very small m there are three purely imaginary roots, as m increases the flow becomes unstable as the real part of the roots is no longer zero, these roots then become purely real before two of them merge into complex conjugate pairs. As m increases further the flow becomes stable again.*

take $s_r = 0$. If this point is also the maximum growth rate, then simultaneously we have $ds_r/da = 0$, since $a = \nu m^2$ is now our variable expressing changes in m. Equating real and imaginary parts in (2.50) we have

$$4a_c s_i^4 - (4a_c^3 - 4a_c)s_i^2 - T^4 = 0, \qquad a_c s_i^4 - (6a_c^3 - 2a_c)s_i^2 + a_c^5 - 2a_c^3 + a_c - T^4 = 0, \quad (2.51)$$

where a_c denotes the critical value of a when $s_r = 0$. Two more equations can then be formed by differentiating (2.50) then setting both $\partial s_r/\partial a(a_c, T_c) = 0$ and $s_r = 0$ and

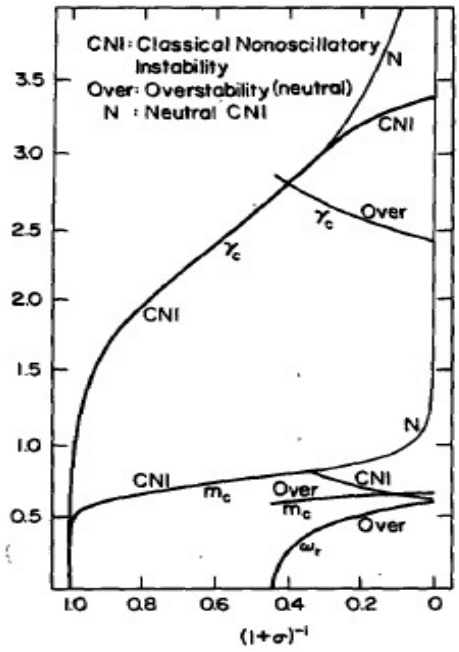

Figure 2.4: *The numerical solution to dispersion relation (2.48) as solved by (Dunkerton, 1982)* $\sigma = \nu/\kappa$.

again taking real and imaginary parts gives

$$\left(16a_c^2 s_i^3 - 2(4a_c^4 - 4a_c^2)s_i\right)\frac{ds_i}{da}(a_c, T_c) + \left(8a_c s_i^4 - (16a_c^3 - 8a_c)s_i^2 - T_c^4\right) = 0, \quad (2.52)$$

$$\left(5a_c s_i^4 - 3(6a_c^3 - 2a_c)s_i^2 + a_c^5 - 2a_c^3 + a_c - T_c^4\right)\frac{ds_i}{da}(a_c, T_c) +$$

$$\left(s_i^5 - (18a_c^2 - 2)s_i^3 + (5a_c^4 - 6a_c^2 + 1)s_i\right) = 0. \quad (2.53)$$

We can eliminate $ds_i/da(a_c, T_c)$ from (2.52) and (2.53) to get a single equation

$$\left(5a_c s_i^4 - 3(6a_c^3 - 2a_c)s_i^2 + a_c^5 - 2a_c^3 + a_c - T_c^4\right)\left(8a_c s_i^4 - (16a_c^3 - 8a_c)s_i^2 - T^4\right) -$$
$$\left(16a_c^2 s_i^3 - 2(4a_c^4 - 4a_c^2)s_i\right)\left(s_i^5 - (18a_c^2 - 2)s_i^3 + (5a_c^4 - 6a_c^2 + 1)s_i\right) = 0. \quad (2.54)$$

We have three equations and three unknowns, s_i, a_c and T_c^4. We choose to eliminate a_c and T_c to find a single equation for s_i. First we eliminate T_c^4 between both equations of (2.51) by writing

$$T_c^4 = 4a_c s_i^4 - (4a_c^3 - 4a_c)s_i^2. \tag{2.55}$$

Substituting into (2.54) we have

$$\begin{aligned}\Big(a_c s_i^4 - (14a_c^3 - 2a_c)s_i^2 + a_c^5 - 2a_c^3 + a_c\Big)\Big(4a_c s_i^4 - (12a_c^3 - 4a_c)s_i^2\Big) - \\ \Big(16a_c^2 s_i^3 - 2(4a_c^4 - 4a_c^2)s_i\Big)\Big(s_i^5 - (18a_c^2 - 2)s_i^3 + (5a_c^4 - 6a_c^2 + 1)s_i\Big) = 0.\end{aligned} \tag{2.56}$$

The next step is to eliminate T^4 from (2.51) by subtracting one equation from the other

$$a_c^4 - 2(s_i^2 + 1)a_c^2 - 2s_i^2 - 3s_i^4 + 1 = 0, \tag{2.57}$$

and solve for a_c^2 to obtain

$$a_c^2 = s_i^2 + 1 \pm 2s_i\sqrt{s_i^2 + 1}. \tag{2.58}$$

Note, it was found that taking either root in (2.58) produces the same critical values for ν, m and only results in a change in sign of s_i. We will therefore take the "$\pm$" to be a "$+$" without losing any information about the critical case. We now have two equations (2.56) and (2.58) for two unknowns a_c and s_i. We substitute (2.58) into (2.56) which gives us a single equation for s_i. We then used the MAPLE solve command to find s_i. Any spurious roots that arise from the squaring of the dispersion relation were discarded by re-substituting into (2.49) and checking the residual was suitably negligible. The values for s_i we were left with were substituted into (2.58) to find a_c^2 and then (2.55) was used to find T_c. Finally this resulted in the following critical values

$$s_i = \pm 0.500235 \qquad \nu_c = 0.4061 \qquad m_c = 0.9451. \tag{2.59}$$

To compare these critical values to the numerical values found by Dunkerton shown in figure 2.4 we note that Dunkerton's nondimensional variables are as follows

$$\omega_d = \frac{\omega}{\nu^{1/5}(N\beta)^{2/5}}, \quad m_d = \frac{m}{m_0}, \tag{2.60}$$

where the subscript "d" denotes Dunkerton's nondimensional variables. Using (2.37), these critical values relate to Dunkerton's in the following way

$$\omega_d = \frac{(s_i)_s}{\nu_s^{1/5}} = 0.5987, \qquad m_d = m_s \nu_s^{2/5}, \tag{2.61}$$

where the "s" subscript represents the nondimensional variables from (2.37). The relationship between the two nondimensional shears is more difficult to differentiate. We can persevere by noting from (2.37) that

$$\Lambda^5 = \frac{32\nu N^2 \beta^2}{\nu_s}. \tag{2.62}$$

Then nondimensionalising the shear as per Dunkerton we have

$$\Lambda_d = \frac{\Lambda}{\gamma_0} = \frac{32}{\nu_s}, \tag{2.63}$$

where $\gamma_0 = \nu^{1/5}(N\beta)^{2/5}$. Hence using the variables from (2.59) we find the critical values in terms of Dunkerton's variables are as follows

$$(\Lambda_d)_c = 2.3950, \qquad (m_d)_c = 0.6591, \quad \text{and} \quad (\omega_d)_c = 0.5990. \tag{2.64}$$

Comparing (2.64) to figure 2.4 from Dunkerton's 1982 paper we conclude that our result is in agreement with Dunkerton's numerical results. We can compare this to the $Pr = 1$ case which where $\nu_c = 0.026258$ and $m_c = 1.955059$ and find that $Pr \to \infty$ requires a larger viscosity to stabilize the flow. The $Pr = \infty$ is unstable to larger ranges of viscosity and is therefore more unstable. This is not unreasonable since we have taken out one

component of friction.

MATLAB was used to also solve the dispersion relation numerically; this was done by squaring (2.49) to find a polynomial in s. We then fixed ν and solved the polynomial as m was varied. We then gradually increased ν until all roots became stable across the range of m giving us the value for critical ν. Clearly some of these roots would be fictitious and have come about through the squaring of the dispersion relation; however these were discarded through substituting into the dispersion relation and checking the residual is sufficiently small. The critical diffusion solved numerically was as follows

$$\nu_c = 0.4061 \qquad m_c = 0.9451. \tag{2.65}$$

Since the polynomial was solved using increments in m and ν of order 10^{-5} there can only be accuracy of up to 4 decimal places. We can see that the analytical result and numerical result using MATLAB are consistent to within numerical error. A plot of the critical case is shown in figure 2.5 which uses the results of the critical viscosity from (2.65).

2.11 Numerical solutions on the equatorial β-plane

In each of the last three sections, the equatorial inertial instability has been governed by a parabolic cylinder equation of the form

$$\frac{d^2\hat{v}}{dy^2} + \left(\mu + \frac{1}{2} - \frac{Y^2}{4}\right)\hat{v} = 0, \tag{2.66}$$

where μ varied between cases according to our choice of ν and κ. We used the analytical solution $\mu = 0, 1, 2, \cdots$ for the eigenvalue when $\hat{v} \to 0$ as $|Y| \to \infty$. However, later in the thesis we will turn to numerical solutions which are necessarily calculated on a finite domain with $\hat{v} = 0$ at $y = \pm L$ and it is interesting to know the relationship

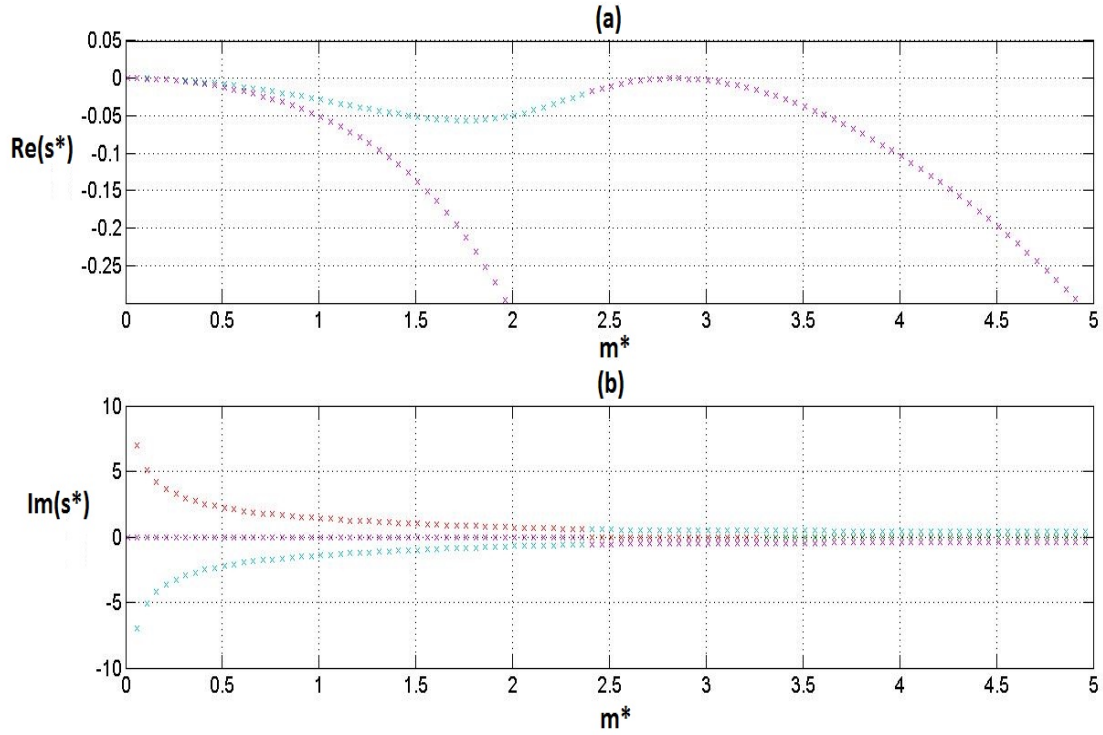

Figure 2.5: *The dispersion relation (2.49) for symmetric disturbances with diffusion ($Pr \to \infty$) on the equatorial β-plane with critical viscosity ν_* given by(2.65).*

between previously discussed infinite domain linear solutions and numerical solutions on a bounded domain. We are considering localised flows around the equator, hence provided we have sufficiently large enough L solutions relating to a bounded domain can be a good estimate of infinite domain solutions in the atmosphere and ocean. Since we are restricted numerically to bounded domains these boundaries would impose effects on the solution which would be regarded as being unphysical. It is therefore necessary to gauge how large L is required to be to achieve the level of accuracy we require when using it as an estimate to the true physical system of an infinite domain.

When considering equations of the form (2.66) we can obtain an analytic solution (Bender and Orszag, 1999) when the boundary conditions $\hat{v} = 0$ as $y \to \infty$ are applied. Our approach in this chapter is to solve an ODE of the form (2.66) using the infinite domain

solution as a guide for finding an asymptotic solution for ν in the limit of large L. We then compare the accuracy of this asymptotic solution with solutions found using numerical method BVP4C. The BVP4C code implements a collocation formula and was adapted to use continuation, that is using previous numerical results as the initial guess for the solution. The eigenvalues of the asymptotic and numerical results were compared for various values of L (domain size) to see how the length of the domain affected the accuracy of the numerics. Various other factors were investigated for their effects on the accuracy of the eigenvalues such as mesh spacing and tolerance levels.

2.11.1 Asymptotic results

We cannot solve the parabolic cylinder equation asymptotically for the case where rigid boundary conditions are applied, but we can find an asymptotic solution as $L \to \infty$. First note that the general solution of (2.66) is

$$v(Y) = AD_{\mu}(-Y) + BD_{-\mu-1}(-iY), \tag{2.67}$$

where $D_{\mu}(Y)$ is the parabolic cylinder function. Then setting $V(\pm L) = 0$, non-trivial solutions (i.e., $AB \neq 0$) are obtained when

$$D_{-\mu-1}(-iL)D_{\mu}(-L) - D_{\mu}(L)D_{-\mu-1}(iL) = 0. \tag{2.68}$$

This implicit relation for μ can be examined for large L, using expressions from Bender and Orszag (1999) for the behaviour of D_{μ} for large arguments:

$$v(Y) = D_{\mu}(Y) = (Y)^{\mu} \exp{(Y^2/L)}\omega_{\mu}(Y), \qquad |\arg(Y)| < \frac{3\pi}{4} \tag{2.69}$$

where ω is the asymptotic expansion

$$\omega_\mu(Y) = 1 - \frac{\mu(\mu-1)}{2Y^2} + \frac{\mu(\mu-1)(\mu-2)(\mu-3)}{2\cdot 4Y^4} - \ldots, \tag{2.70}$$

valid when $Y = L, iL$ and $-iL$ and $L \to \infty$. For $Y = -L$ we have

$$\begin{aligned} v(Y) = D_\mu(Y) &= (Y)^\mu \exp(Y^2/4)\omega_\mu(Y) \\ &- \frac{(2\pi)^{1/2}}{\Gamma(-\mu)} \exp(i\pi\mu)(Y)^{-\mu-1} \exp(Y^2/4)\omega_{-\mu-1}(Y), \qquad \frac{\pi}{4} < arg(Y) < \frac{5\pi}{4}, \end{aligned} \tag{2.71}$$

again valid for when $L \to \infty$. Substituting (2.69) and (2.71) into (2.68) then gives

$$\begin{aligned} (-iL)^{-\mu-1} \exp(L^2/4)\omega_{-\mu-1}(-iL)\Bigg(&(-L)^\mu \exp(-L^2/4)\omega_\mu(-L) \\ &- \frac{(2\pi)^{1/2}}{\Gamma(-\mu)} \exp(i\pi\mu)(-L)^{-\mu-1} \exp(L^2/4)\omega_{-\mu-1}(-L)\Bigg) \\ - \Bigg((L)^\mu \exp(-L^2/4)\omega_\mu(L)\Bigg)&\Bigg((iL)^{-\mu-1} \exp(L^2/4)\omega_{-\mu-1}(iL)\Bigg) = 0, \end{aligned} \tag{2.72}$$

which simplifies to

$$\begin{aligned} \Bigg((L)^\mu \exp(-L^2/4)\omega_\mu(L)\Bigg) - (-1)^{-\mu-1}\Bigg(&(-L)^\mu \exp(-L^2/4)\omega_\mu(-L) \\ &- \frac{(2\pi)^{1/2}}{\Gamma(-\mu)} \exp(i\pi\mu)(-L)^{-\mu-1} \exp(L^2/4)\omega_{-\mu-1}(-L)\Bigg) = 0 \end{aligned} \tag{2.73}$$

If we assume L to be large considering (2.70) we can make the approximation $\omega_\mu(-L) = \omega_{-\mu-1}(-L) = \omega_\mu(L) \approx 1$ and hence (2.73) becomes

$$\begin{aligned} ((-1)^{-\mu-1})^2\Bigg((-1)^{2\mu+1}(L)^\mu \exp(-L^2/2) - \frac{(2\pi)^{1/2}}{\Gamma(-\mu)} \exp(i\pi\mu)(L)^{-\mu-1}\Bigg) \\ - \Bigg((L)^\mu \exp(-L^2/2)\Bigg) = 0, \end{aligned} \tag{2.74}$$

which simplifies to

$$\frac{2\exp\left(-L^2/2\right)(L)^{2\mu+1}}{(2\pi)^{1/2}} = -\frac{\exp\left(i\pi\mu\right)}{\Gamma(-\mu)}. \tag{2.75}$$

The is an implicit relation for μ involving L. We know that $\mu \approx n + \delta$ for large L, where the non-negative integer n is the exact eigenvalue in the limit $L \to \infty$, and δ is a small correction. Substituting into (2.75) and solving for δ

$$\frac{2\exp\left(-L^2/2\right)(L)^{2(n+\delta)+1}}{(2\pi)^{1/2}} = -\frac{\exp\left(i\pi(n+\delta)\right)}{\Gamma(-n-\delta)}. \tag{2.76}$$

Since $\delta \ll 1$ we make the approximation $\exp\left(i\pi(n+\delta)\right) \approx (-1)^n$ and $L^{2(n+\delta)+1} \approx L^{2n+1}$. However note that the effect of δ within the Gamma function is large meaning it cannot be neglected,

$$\frac{2\exp\left(-L^2/2\right)(L)^{2n+1}}{(2\pi)^{1/2}} = -\frac{(-1)^n}{\Gamma(-n-\delta)}. \tag{2.77}$$

To manipulate the Gamma functions we have the following relations, for $0 < \delta < 1$

$$\Gamma(-\delta) = \frac{\Gamma(-\delta+1)}{-\delta}. \tag{2.78}$$

Using the transform $-\delta \to -\delta - 1$ we find

$$\Gamma(-\delta-1) = \frac{\Gamma(-\delta)}{-\delta-1}. \tag{2.79}$$

Combining (2.79) with (2.78) gives

$$\Gamma(-\delta-1) = -\frac{\Gamma(-\delta+1)}{(-\delta-1)\delta}. \tag{2.80}$$

Repeating this step gives

$$\Gamma(-\delta-n) = -\frac{\Gamma(-\delta+1)}{\delta(-\delta-1)\ldots(-\delta-n)}, \tag{2.81}$$

which as $\delta \to 0$ can be approximated by

$$\Gamma(\delta - n) = -\frac{(-1)^n}{n!\delta}. \tag{2.82}$$

Finally, substituting this into (2.77) gives

$$\delta \approx \frac{2\exp(-L^2/2)(L)^{2n+1}}{(2\pi)^{1/2}n!}, \tag{2.83}$$

which now gives us a new approximation,

$$\mu = n + \delta = n + \frac{2\exp(-L^2/2)(L)^{2n+1}}{(2\pi)^{1/2}n!} \tag{2.84}$$

for the eigenvalues of the parabolic cylinder equation (2.66) with boundary conditions $v = 0$ at $Y = \pm L$ applied.

2.11.2 Numerical results for a finite domain

In section 2.11.1 we added a correctional term to the eigenvalues representing a shift from an infinite domain to a bounded domain. But our correction is an asymptotic expression as $L \to \infty$, so how good is it for large (but finite) L? In this section we will show for different mode values n how the accuracy of the solution changes and the effect this has on our requirement for L. We do this though a comparison of the asymptotic eigenvalues found in (2.84) with eigenvalues found using the numerical scheme BVP4C to solve the eigenvalue problem. We strengthen our findings by looking at various factors which may affect the outcomes of the numerical method itself. These factors include the initial mesh size of the numerical scheme and the tolerance level to which is works.

2.11.3 Example of numerical solutions for various values of L

Figure 2.6 shows the relative error of δ. This is a test to see how small the domain has to be before the effects of the finite domain are felt. The relative error was calculated as follows; the asymptotic correction term was taken from the numerical correction term $(\delta_a - \delta n)$, then this was divided by the maximum value of either δa or δn. The subscripts "a" and "n" have been used to represent the asymptotic values and the numerical values respectively. It is easy to see that when $n = 0$ the numerical results and the asymptotic results are very similar for domain size $L > 5$, with the more accurate results being obtained with $L = 10$. The result for other values of n is unclear as the relative error is much larger and seem to increase again in the $n = 4$ case after an initial improvement in the relative error. However, it should be noted that the $n = 0$ case is of more interest as this is the most unstable mode.

Figure 2.7 shows examples of the BVP4C solution to (2.66) solved with different domain sizes L and mode values n. We find that as the domain size L gets smaller the discrepancy between the numerical solution and the asymptotic solution increases. We also find that as the mode value n is increased we require larger domains to achieve the same accuracy. The reason behind this may be because increasing the mode increases the number of turning points in the solution. BVP4C will be competing to fit all turning points into the domain while at the same time satisfying the boundary conditions; as a result accuracy may be compromised.

2.11.4 Differences between the eigenvalues of the asymptotic and numerical results

In figure 2.8 we can see a complete picture of how the eigenvalues vary with L for values of $n = 0$ to $n = 6$. It is evident that the larger the value of n, the larger the domain size L is required for the numerics to give a reasonable approximation of the eigenvalue. This

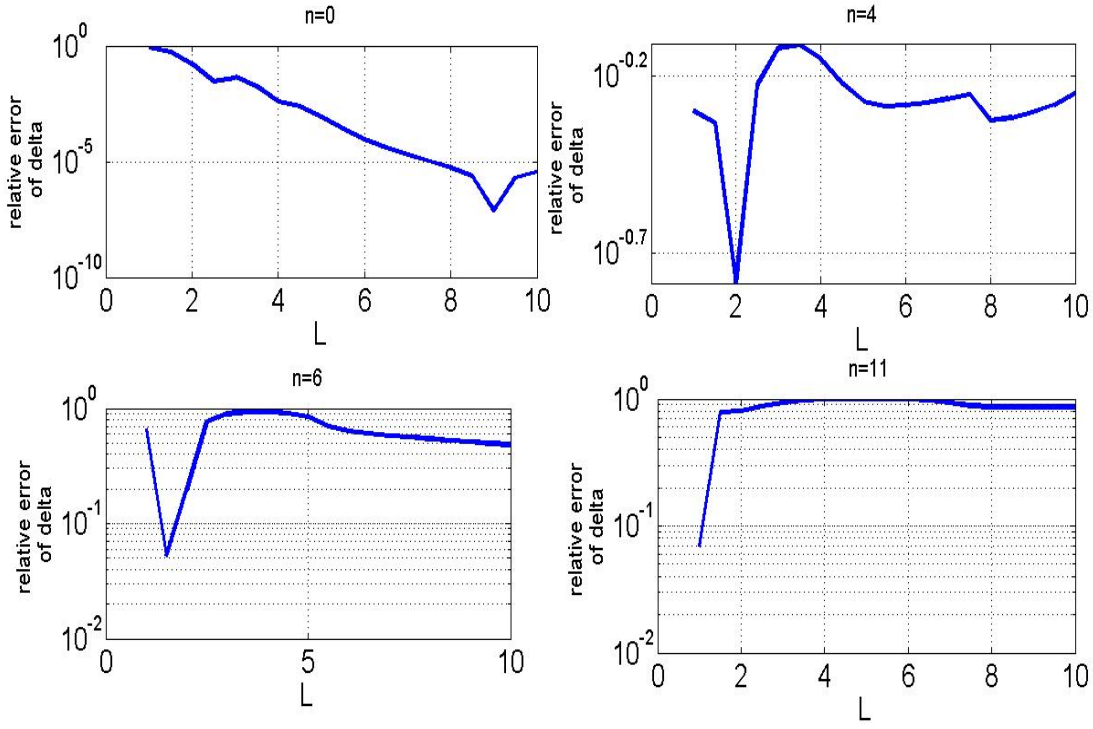

Figure 2.6: *The relative error of the correction term δ when boundary conditions are applied at $Y = \pm L$ as opposed to $Y = \pm\infty$ for the cases where (a) $n = 0$, (b) $n = 4$, (c) $n = 6$ and (d) $n = 11$.*

should not impact our instability analysis as the mode of most interest is the most unstable mode which is $n = 0$.

2.11.5 Effect of the mesh size on the solution

When using BVP4C an option can be made in order to vary the mesh size. Therefore figure 2.9 shows how the mesh size might affect the relative error of δ. It is clear we will encounter an error with small mesh sizes, with the eigenvalue tending towards a limit as mesh size is increased. Provided we start with a large enough mesh size we should reach satisfactory accuracy. How large this mesh needs to be will depend on the accuracy levels required.

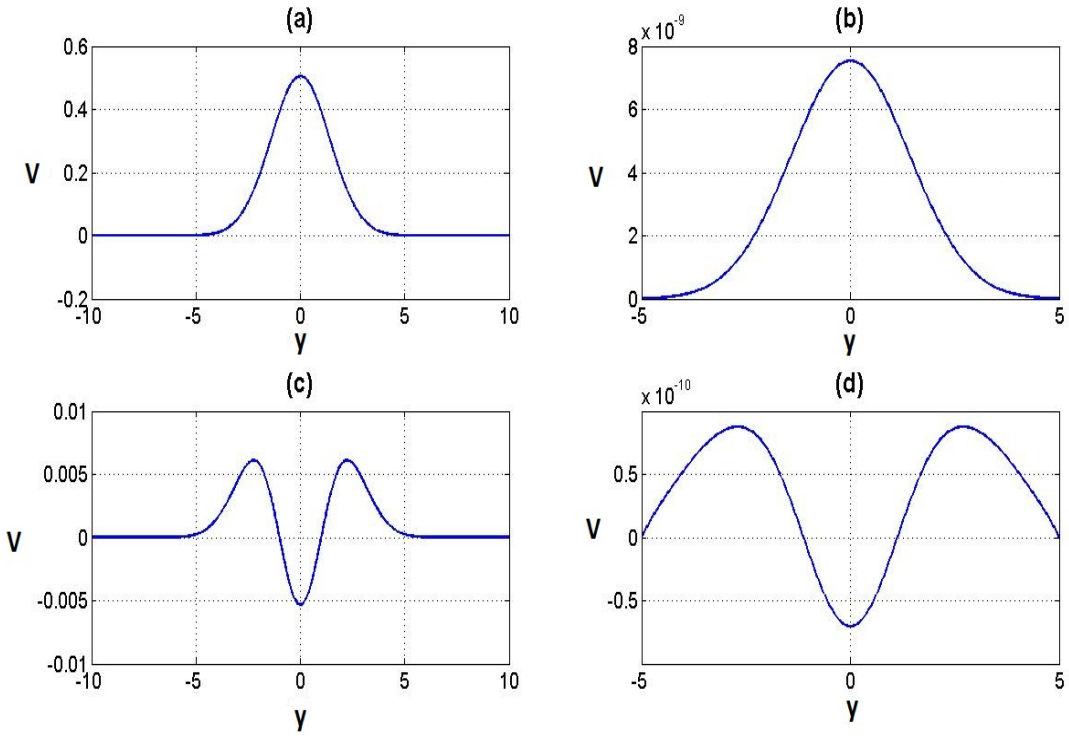

Figure 2.7: *BVP4C solution v for (a) eigen-mode $n = 0$, domain length $L = 10$, (b) $n = 0$, $L = 5$, (c) $n = 2$, $L = 10$ and (d) $n = 2$, $L = 5$. The corresponding differences between the asymptotic and BVP4C eigenvalues were as follows, (a) 3.8×10^{-11}, (b) 6.6×10^{-7}, (c) 5.4×10^{-9} and (d) 1.4×10^{-3} ∋.*

2.11.6 Effect of the tolerance levels on the solution

As with the initial mesh size, BVP4C also allows for a change in the tolerance level. Figure 2.10 shows how the relative error varies as the tolerance level is increased. A tolerance level below 10^{-6} shows very little variation in the eigenvalue solution; however when increasing the tolerance level further the eigenvalue begins to increase. It is therefore necessary when using BVP4C to use a tolerance level below 10^{-6}.

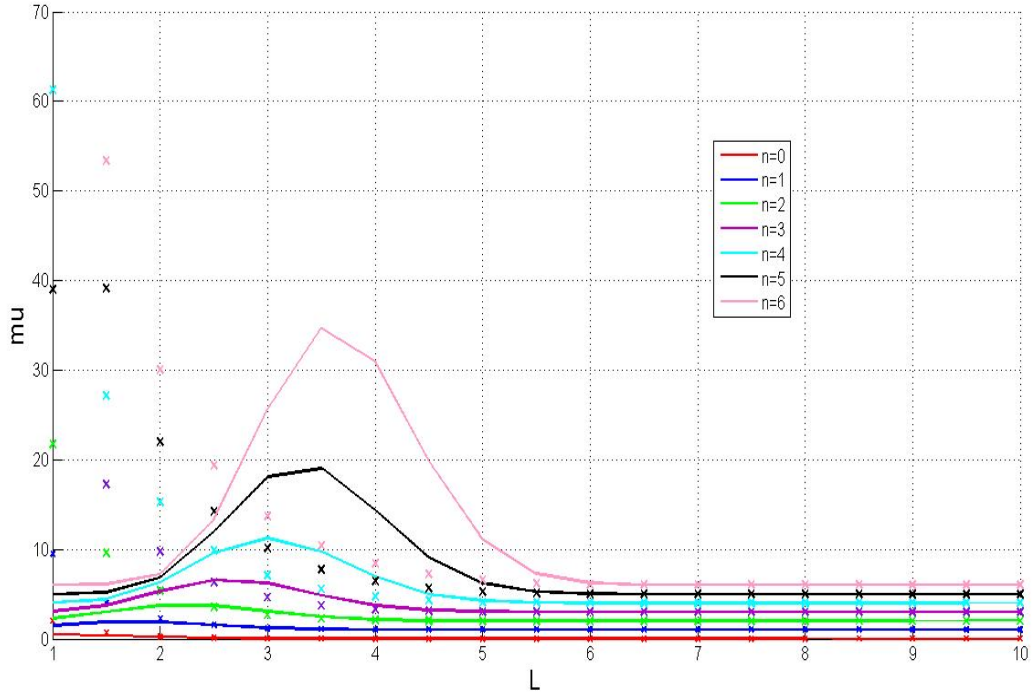

Figure 2.8: *The numerical and asymptotic eigenvalues for various values of n. Again it is clear that for higher mode values of n we require a larger domain size L to achieve the same accuracy as smaller mode values.*

2.12 Summary

In this chapter we have examined various models and aspects of linear inertial instability in continuously stratified fluids. Throughout we have used the Boussinesq approximation in the equations of motion, which is only valid for sufficiently thin fluid layers. However, this is perfectly appropriate for inertial instability, which naturally selects small vertical scales. Indeed, as noted by Dunkerton (1981), in the inviscid case the instability occurs on vanishingly small vertical scales, although such an instability cannot be realised in a real fluid with finite viscosity.

Temperature observations of the stratosphere from the Limb Infrared Monitor revealed

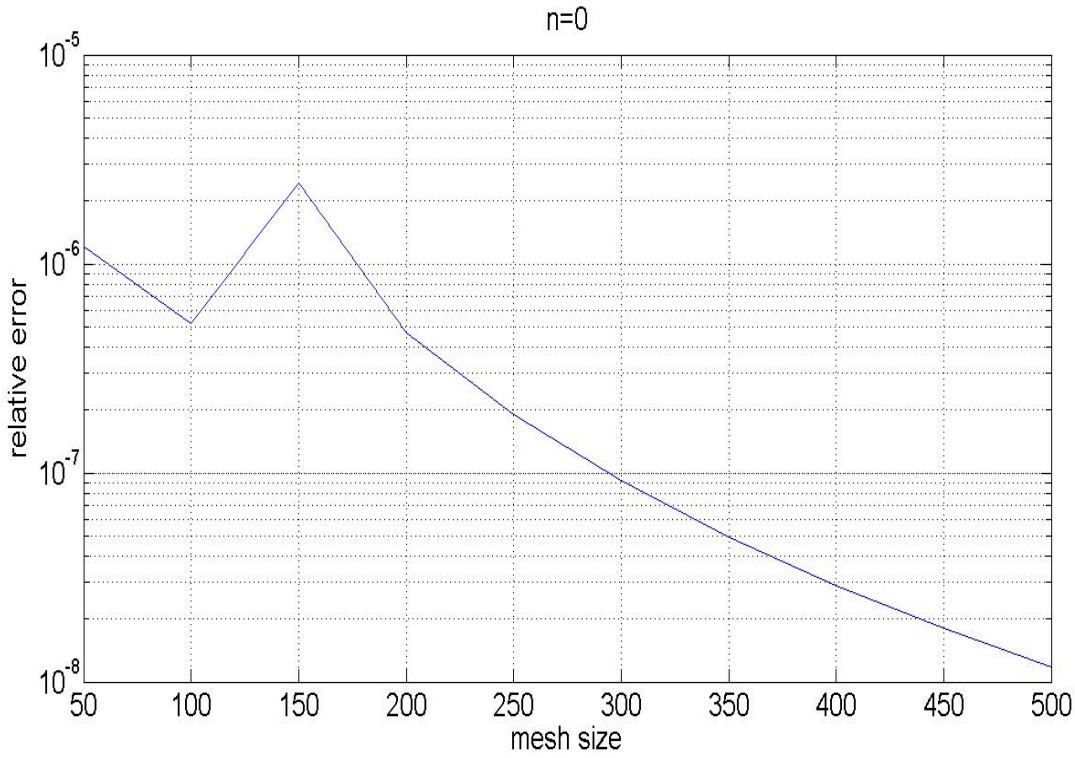

Figure 2.9: *The relative error of δ with varying mesh size when $n = 0$ and $L = 10$. It can clearly be seen the eigenvalue solution is tending towards some limit, a reasonable mesh size to choose would be* 400.

that in the northern winter of 1978/79, vertically layered large scale temperature perturbations appeared (Hitchman et al 1987). Such structures resemble the "pancake structure" produced by inertial instability as discussed by Dunkerton (1981). Pancake structures was a term coined to best describe these structures because of their vertical length scale being much smaller than the horizontal, giving it a pancake appearance. If inertial instability prefers such structures we can clearly see how the Boussinesq approximation is appropriate to any analysis.

In section 2.7 we derived the eigenvalue problem (2.11) for inertial instability for an arbitrary shear flow with arbitrary f, and with arbitrary ν and κ. We examined general criteria for instability, and recovered the well-known result that $fQ < 0$ somewhere in

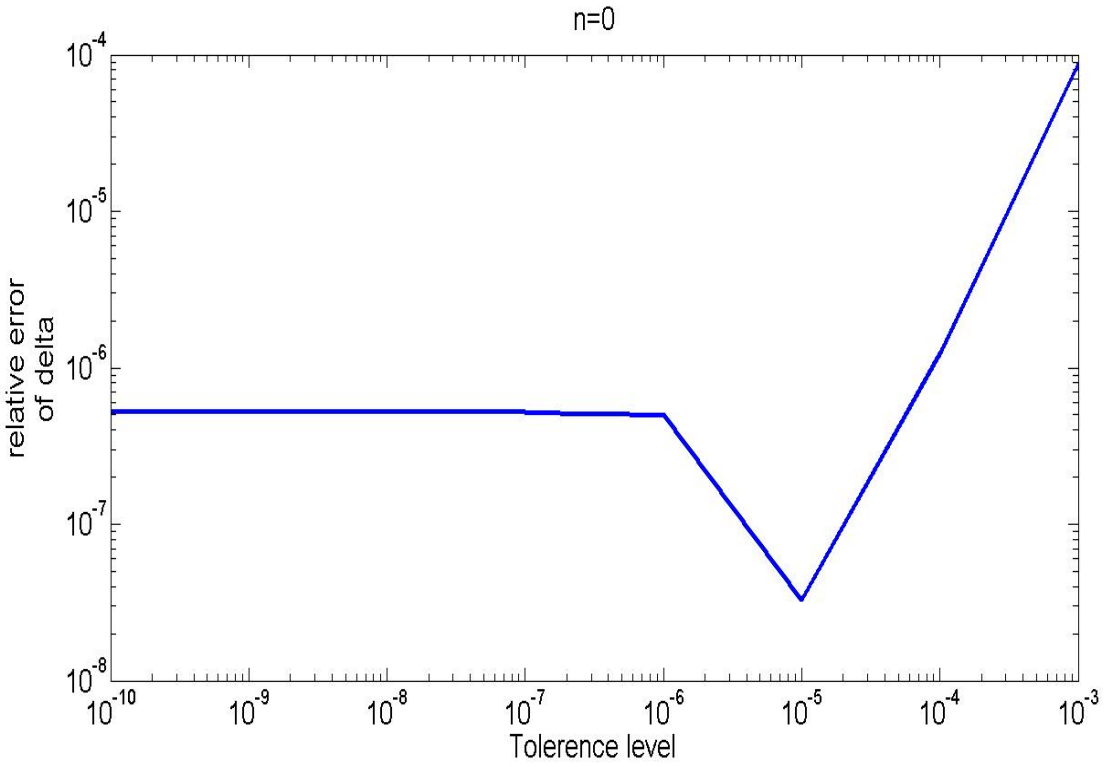

Figure 2.10: *The BVP4C solution of the eigenvalue plotted against tolerance level. It would appear a tolerance level smaller than* 1×10^{-6} *has no noticeable improvement on the eigenvalue solution.*

the flow is a necessary condition for instability, where Q is the vertical component of the absolute vorticity. We then looked at two models of inviscid inertial instability, both with uniform shear, but with one on the f-plane and one on the equatorial β-plane. For both models, the eigenvalue problem can be solved exactly and in both cases, the growth rate increases monotonically with vertical wavenumber m, so that the instability prefers vanishingly small vertical scales, where the maximum possible growth rate of $\Lambda/2$ is achieved.

It is theorized that there is some underlying mechanism for turning the structures most desired by linear inertial instability (vanishingly small) into the observable structures of finite depth. Since the atmosphere and ocean is viscous such a mechanism could

be viscosity, which diffuses the very small scale structures, producing a bound that the vertical wavenumber cannot exceed. We looked at introducing viscosity into the system by adding a kinematic viscosity term, ν, and also a thermal diffusivity κ. This introduces the well known Prandtl number ν/κ into our equations. If we are suggesting that viscosity be the underlying cause of bounding the wavenumber we would probably only look at the case where $\kappa = 0$. However analysis of $\nu = \kappa$ ($Pr = 1$) is more representative of the atmosphere, whilst the case with infinite Pr is more representative of the ocean. We find, as to be expected, there is now a bound on the vertical wavenumber and the overturning structures have a finite length scale, more in line with the observations by Hitchman (1987). It should be noted however, as in Griffiths (2003a), the vertical scales found in the analysis are still at a mismatch with those observed, which suggests there is something else at play in the dynamics.

We began by looking at the viscous equatorial β-plane. First we recapped the work of Dunkerton (1982) where $Pr = 1$, which was a good approximation for the atmosphere. For sufficiently large ν the flow is unstable in the following way: it is stable at small m before becoming unstable at a fixed m and then returning to stability again. For sufficiently small ν the flow is unstable to the following effect; it is stable at small m (stratification dominates), then there is a band of unstable m before becoming stable again at large m (viscosity dominates). In this case, there is a single maximum in the growth rate at some value of m. There is a critical condition that can be derived, that is the point at which the flow is stable to all wavenumbers m. We found that this is dependent on shear, viscosity, stratification and β.

Since viscosity is adding a bound to the vertical wavenumber we should also look at $\kappa = 0$. The analysis however is more complicated, the dispersion relation can only be solved numerically. The numerical solution to the dispersion relation tells us that for small wavenumber the flow is stable with one negative real root and two complex conjugate pairs. The flow turns unstable as m increases and as we would hope is bounded at a

finite wavenumber m. We therefore find that although the analysis is less straightforward than the $Pr = 1$ case, viscosity ν alone is all that is needed to add a bound to the most unstable wavenumber. Dunkerton (1982) discussed the nature of the instability; when the flow initially turned unstable the roots are complex and he refers to this as over-stability, the disturbance is growing but oscillating at the same time. When the roots become purely real this is a classic non-oscillatory instability.

We finally considered the appropriateness of using a bounded numerical solution as an estimate to the solution in a unbounded domain. We looked at how small the domain size L need be before it had an effect on the solution. The results were quite remarkable: the domain size had to become rather small before their effects were felt, approximately $L < 5$. However this was when considering the smallest mode $n = 0$ which was convenient since this is also the most interesting unstable case. Other factors were looked at such as tolerance level and mesh size and it was found the restrictions on these were reasonable in order to maintain accuracy.

Chapter 3

A two-layer model: The governing equations and conservation laws

3.1 Introduction

With very rare exceptions where there are rapid changes in density over short vertical length scales, most parts of the atmosphere and ocean are best modeled as a continuously stratified fluid. This was the approach taken in the previous chapter, where we looked at linear inertial instability in various settings. However, a common alternative approach in geophysical fluid dynamics is to instead use a model consisting of one or more layers of constant fluid density. This approach for a single layer dates back to Laplace (1776), but perhaps it is most extensively used with two-layers. Typically the approach is to consider an inviscid fluid, and to assume hydrostatic dynamics in each layer, leading to the so-called shallow-water approximation. The resulting equations then only depend upon (x, y, t); the explicit vertical dependence is removed, and only remains in the coupling between the layers. In such models, generally one is not regarding the fluid as being composed of two or more distinct layers, but rather one is using the layers as a simple representation of a thin layer of continuously stratified fluid. We can think of the

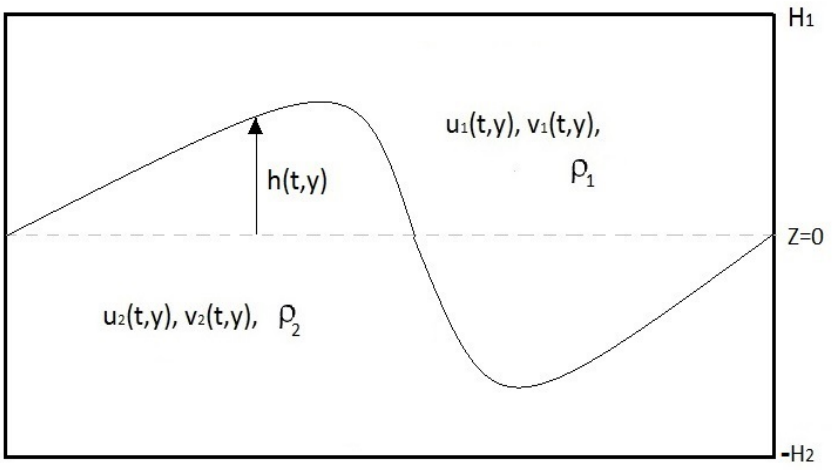

Figure 3.1: *An illustration of the two-layer model.*

stratification in the atmosphere as being made up of an infinite stack of infinitesimally thin layers, where the vertical length scale is much smaller than the horizontal. The main benefits are the mathematical simplifications and, as we shall see, there exists an analogy between the two-layer model with interfacial friction and the continuously stratified system with $Pr \to \infty$. An illustration of the two-layer model is found in figure 3.1.

We consider the configuration shown in figure 3.1 with two layers separated by an interface and with rigid surfaces above and below. We do not use a free surface as we are interested in internal dynamics which are readily represented in the rigid lid model. A free surface model would permit both a fast free surface mode and a slow internal mode; we are interested in the latter. In previous studies of inertial instability in layered systems to be discussed, Zhao and Ghil (1991) also used a rigid lid model, whilst Zeitlin and Plougonven (2009) used a free surface model, although the basis for this is not clear unless one is really interested in entire oceanic flows. The layer of fluid has a rigid base and rigid lid at $z = -H_2$ and $z = H_1$. As we shall see, the use of a rigid base and lid

produces an analogy between the two-layer and the continuously stratified models which is the reasoning behind the use of this setup. The interface of the fluid at rest lies at $z = 0$ and there is assumed to be a friction force acting at the interface between the two-layers. The derivation of the two-layer shallow water equations is shown in section 3.2 where one set of shallow water equations for each layer are combined into a set of shallow water equations for the whole system, plus an additional equation for the evolution of the depth-averaged mean flow. In section 3.3 we derive a set of conservation laws which will help in understanding the evolving flow. These conserved quantities include mass, energy, absolute momentum and potential vorticity.

Although linear friction is often applied at the bottom of a single layer model it is less commonly used at the interface between two-layers. It has an important role to play in the consideration of inertial instability: Griffiths (2003a) and Dunkerton (1982) discussed the role of viscosity in the atmosphere playing an important role in the vertical mixing of momentum, which helps to neutralise the instability. This concept is applied to the two-layer system through the introduction of friction. In fact, as we shall see, this leads to a direct analogy with the continuously stratified $Pr \to \infty$ case. We leave the detailed analysis of this model on the equatorial β-plane and f-plane to later in chapters 4 and 5 respectively.

3.2 Governing equations

The shallow-water approximation for an inviscid two-layer fluid confined between rigid upper and lower surfaces is well established in geophysical fluid dynamics (Gill, 1982; Salmon, 1998; Vallis, 2006). In the shallow-water approximation, the pressure is assumed to be hydrostatic, a discussion of which can be found in Gill (1982), but the approximation can be used as the horizontal length scale is much large than the vertical length scale. The

upper layer pressure is

$$p_1 = p(x, y, t) - \rho_1 g(z - H_1), \tag{3.1}$$

where p is the (unknown) pressure at the upper lid, and the lower layer pressure is

$$p_2 = -\rho_2 g(z - h) - \rho_1 g(h - H_1) + p(x, y, t), \tag{3.2}$$

applying continuity of p at the displaced interface $z = h$. The horizontal pressure gradients in each layer are independent of height z, so, provided any body forces in the horizontal momentum equations are also independent of z, the horizontal flow in each layer may be taken to be independent of z. In the special case of along stream symmetry $(\partial/\partial x = 0)$, we thus obtain

$$\frac{\partial u_1}{\partial t} + v_1 \frac{\partial u_1}{\partial y} - f v_1 = F_1, \tag{3.3}$$

$$\frac{\partial u_2}{\partial t} + v_2 \frac{\partial u_2}{\partial y} - f v_2 = F_2, \tag{3.4}$$

$$\frac{\partial v_1}{\partial t} + v_1 \frac{\partial v_1}{\partial y} + f u_1 = -\frac{1}{\rho_0} \frac{\partial p}{\partial y} + G_1, \tag{3.5}$$

$$\frac{\partial v_2}{\partial t} + v_2 \frac{\partial v_2}{\partial y} + f u_2 = -\frac{1}{\rho_0} \frac{\partial p}{\partial y} - g' \frac{\partial h}{\partial y} + G_2. \tag{3.6}$$

Here, h is the lift or depression of the top layer, i.e. h is positive when the bottom layer is lifted upwards from rest ($h = 0$). The horizontal velocities are given by u_1, v_1 in the x and y directions respectively in the upper layer, with u_2 and v_2 representing velocities in the bottom layer. The Coriolis parameter is represented by f and g' is the reduced gravity given by $g' = g(\rho_2 - \rho_1)/\rho_2$. Body forces are represented by G and F; for example, these might include frictional forces.

Integrating $\nabla \cdot \mathbf{u} = 0$ over each fluid layer separately yields two further equations:

$$-\frac{\partial h}{\partial t} + \frac{\partial}{\partial y}\Big((H_1 - h)v_1\Big) = 0, \tag{3.7}$$

$$\frac{\partial h}{\partial t} + \frac{\partial}{\partial y}\Big((H_2 + h)v_2\Big) = 0. \tag{3.8}$$

Along with (3.3) - (3.6) we have six equations for six unknowns. These are to be solved subject to $v_1, v_2 = 0$ at $y = \pm L$, or $v_1, v_2 \to 0$ as $y \to \pm\infty$.

3.2.1 Momentum transfer between the fluid layers

In a continuously stratified fluid inertial instability saturates in the nonlinear regime via the mixing of absolute momentum or equivalently potential vorticity. In a weakly nonlinear instability this mixing is realised through vertical diffusion acting on the thin pancake structures generated by the linear instability. In a strongly nonlinear instability this mixing could be enhanced through turbulence. In a two-layer flow with $\partial/\partial x = 0$ neither of these processes can act and so we need a term that transfers horizontal momentum between the two fluid layers, in such a way that the total horizontal momentum of the flow is conserved. The easiest way to do this is via linear frictional terms of the form,

$$F_1 = -\frac{\epsilon(u_1 - u_2)}{(H_1 - h)}, \quad F_2 = -\frac{\epsilon(u_2 - u_1)}{(H_2 + h)}, \tag{3.9}$$

$$G_1 = -\frac{\epsilon(v_1 - v_2)}{(H_1 - h)}, \quad G_2 = -\frac{\epsilon(v_1 - v_2)}{(H_1 - h)}. \tag{3.10}$$

The factors of $H_1 - h$ and $H_2 + h$ in the denominators guarantee that the depth integrated momentum is conserved, as in the continuously stratified system.

3.2.2 Evolution of h

We have two equations describing the evolution of h; we can replace (3.7) and (3.8) by their difference and sum:

$$\frac{\partial}{\partial y}\Big((H_1 - h)v_1 + (H_2 + h)v_2\Big) = 0, \tag{3.11}$$

$$\frac{\partial h}{\partial t} + \frac{1}{2}\frac{\partial}{\partial y}\Big((H_2 + h)v_2 - (H_1 - h)v_1\Big) = 0. \tag{3.12}$$

Since $v_1 = 0$ and $v_2 = 0$ at the boundaries for all time we can conclude that

$$(H_1 - h)v_1 + (H_2 + h)v_2 = 0. \tag{3.13}$$

Thus, knowledge of any two of v_1, v_2 and h implies the third.

It proves convenient to use $\hat{v} = v_2 - v_1$ as our main working variable, in which case (3.13) implies

$$v_1 = -\frac{(H_2 + h)\hat{v}}{H} \quad \text{and} \quad v_2 = \frac{(H_1 - h)\hat{v}}{H}, \tag{3.14}$$

where $H = H_1 + H_2$. Then (3.12) can be rewritten in terms of h and $\hat{v}$ as

$$\frac{\partial h}{\partial t} + \frac{\partial}{\partial y}\left(\frac{(H_2 + h)(H_1 - h)\hat{v}}{H}\right) = 0; \tag{3.15}$$

3.2.3 Evolution of v

Another weakness of (3.3) - (3.8) is that there is no prognostic equation for $p(x, y, t)$, the unknown pressure at the upper lid. This issue is circumvented by subtracting (3.6) from (3.5), giving

$$\frac{\partial \hat{v}}{\partial t} + v_2\frac{\partial v_2}{\partial y} - v_1\frac{\partial v_1}{\partial y} + f\hat{u} = -g'\frac{\partial h}{\partial y} - \frac{\epsilon\hat{v}H}{(H_1 - h)(H_2 + h)}, \tag{3.16}$$

where $\hat{u} = u_2 - u_1$. Note how $\hat{v} = v_2 - v_1$ thus emerges naturally. We now eliminate v_1 and v_2 from (3.16) in favour of $\hat{v}$, using (3.14), to obtain

$$\frac{\partial \hat{v}}{\partial t} + \frac{1}{2}\frac{\partial}{\partial y}\left(\frac{(H_1 - h)\hat{v}}{H}\right)^2 - \frac{1}{2}\frac{\partial}{\partial y}\left(\frac{(H_2 + h)\hat{v}}{H}\right)^2 + f\hat{u} = -g'\frac{\partial h}{\partial y} - \frac{\epsilon \hat{v} H}{(H_1 - h)(H_2 + h)}, \quad (3.17)$$

3.2.4 Evolution of u

We could continue to work in terms of u_1 and u_2, but we instead choose to work in terms of $\hat{u} = u_2 - u_1$, and the mean flow, $\bar{u}$ given by

$$\bar{u} = \frac{1}{H}\int_{-H_2}^{H_1} u dz = \frac{1}{H}\int_{-H_2}^{h} u_2 dz + \frac{1}{H}\int_{h}^{H_1} u_1 dz = \frac{1}{H}\Big((H_1 - h)u_1 + (H_2 + h)u_2\Big). \quad (3.18)$$

Together these relations imply

$$u_1 = \bar{u} - \frac{(H_2 + h)\hat{u}}{H} \qquad u_2 = \bar{u} + \frac{(H_1 - h)\hat{u}}{H}. \quad (3.19)$$

We can form an evolution equation for $\hat{u}$ by taking (3.4) − (3.3)

$$\frac{\partial \hat{u}}{\partial t} + v_2\frac{\partial u_2}{\partial y} - v_1\frac{\partial u_1}{\partial y} - f\hat{v} = \frac{\epsilon H \hat{u}}{(H_2 + h)(H_1 - h)}. \quad (3.20)$$

Substituting from (3.14) and (3.19) for u_1, u_2, v_1 and v_2 gives

$$\frac{\partial \hat{u}}{\partial t} + \frac{(H_1 - h)}{H}\hat{v}\frac{\partial}{\partial y}\left(\bar{u} + \frac{(H_1 - h)\hat{u}}{H}\right) + \frac{(H_2 + h)\hat{v}}{H}\frac{\partial}{\partial y}\left(\bar{u} - \frac{(H_2 + h)\hat{u}}{H}\right) - f\hat{v} = -\frac{\epsilon H \hat{u}}{(H_2 + h)(H_1 - h)}. \quad (3.21)$$

We can form an evolution equation for $\bar{u}$ by taking $\partial/\partial t$ of (3.18)

$$\frac{\partial \bar{u}}{\partial t} = \frac{1}{H}\bigg((H_1 - h)\frac{\partial u_1}{\partial t} + (H_2 + h)\frac{\partial u_2}{\partial t} + u_2\frac{\partial h}{\partial t} - u_1\frac{\partial h}{\partial t}\bigg). \tag{3.22}$$

Substituting from (3.3) and (3.4) into (3.22) and using $\hat{u} = u_2 - u_1$

$$\frac{\partial \bar{u}}{\partial t} = \frac{1}{H}\bigg((H_2+h)\bigg(-v_2\frac{\partial v_2}{\partial y}+fv_2-\frac{\epsilon\hat{u}}{(H_2+h)}\bigg)+(H_1-h)\bigg(-v_1\frac{\partial v_1}{\partial y}+fv_1+\frac{\epsilon\hat{u}}{(H_1-h)}\bigg) - u_2\frac{\partial}{\partial y}\bigg((H_2+h)v_2\bigg) - u_1\frac{\partial}{\partial y}\bigg((H_1-h)v_1\bigg)\bigg). \tag{3.23}$$

After some cancelling of terms

$$\frac{\partial \bar{u}}{\partial t} = -\frac{1}{H}\frac{\partial}{\partial y}\bigg((H_2 + h)v_2u_2 + (H_1 - h)u_1v_1\bigg), \tag{3.24}$$

the Coriolis terms in the above being cancelled due to equation (3.13). Substituting for u_1, u_2, v_1 and v_2 from (3.19) and (3.14) respectively we have

$$\frac{\partial \bar{u}}{\partial t} = -\frac{1}{H^2}\frac{\partial}{\partial y}\bigg((H_2 + h)(H_1 - h)\hat{u}\hat{v}\bigg). \tag{3.25}$$

3.2.5 Summary of reduced equations

We have now a reduced set of equations for four unknowns, with $p(y, t)$ eliminated from the formulation, and the constraint (3.13) respected. These governing equations are

$$\frac{\partial \hat{u}}{\partial t} + \frac{(H_1 - h)}{H}\hat{v}\frac{\partial}{\partial y}\bigg(\bar{u} + \frac{(H_1 - h)\hat{u}}{H}\bigg) + \frac{(H_2 + h)\hat{v}}{H}\frac{\partial}{\partial y}\bigg(\bar{u} - \frac{(H_2 + h)\hat{u}}{H}\bigg) - f\hat{v} = -\frac{\epsilon H\hat{u}}{(H_2 + h)(H_1 - h)}, \tag{3.26}$$

$$\frac{\partial \hat{v}}{\partial t} + \frac{1}{2}\frac{\partial}{\partial y}\left(\frac{(H_1 - h)\hat{v}}{H}\right)^2 - \frac{1}{2}\frac{\partial}{\partial y}\left(\frac{(H_2 + h)\hat{v}}{H}\right)^2 + f\hat{u} = -g'\frac{\partial h}{\partial y} - \frac{\epsilon \hat{v} H}{(H_1 - h)(H_2 + h)}, \quad (3.27)$$

$$\frac{\partial h}{\partial t} + \frac{\partial}{\partial y}\left(\frac{(H_2 + h)(H_1 - h)\hat{v}}{H}\right) = 0 \quad (3.28)$$

$$\frac{\partial \bar{u}}{\partial t} = -\frac{1}{H^2}\frac{\partial}{\partial y}\Big((H_2 + h)(H_1 - h)\hat{u}\hat{v}\Big). \quad (3.29)$$

Note that our original variables v_1, v_2, u_1 and u_2 can be calculated from (3.13) and (3.19). From now on we will write $g = g'$.

3.3 Conservation Laws

It is possible to derive a set of conservation laws, where each conservation law is a relationship between u, v, h and $\bar{u}$ that does not change as the flow evolves.

3.3.1 Conservation of mass

Conservation of mass is guaranteed because of the way the shallow water equations are derived. This conservation can be demonstrated by evaluating

$$\frac{d}{dt}\int_{-L}^{L} h dy = \int_{-L}^{L} \frac{\partial h}{\partial t} dy. \quad (3.30)$$

Substituting for $\partial h/\partial t$ from (3.7) we have

$$\frac{d}{dt}\int_{-L}^{L} h dy = \int_{-L}^{L} \frac{\partial}{\partial y}\Big((H_1 - h)v_1\Big) dy = 0, \quad (3.31)$$

where since we have $v_1 = 0$ as $|y| = L$ the integral is zero.

3.3.2 Conservation of momentum

Here we shall derive the conservation of momentum. We start by integrating the horizontal velocity u over the z and y domain. Firstly integrating over the z domain we have

$$\begin{aligned}\frac{d}{dt}\int_{-L}^{L}\int_{-H_2}^{H_1} u dz dy &= \frac{d}{dt}\int_{-L}^{L} H\bar{u} dy = H\int_{-L}^{L}\frac{\partial \bar{u}}{\partial t} dy \\ &= -\int_{-L}^{L}\frac{\partial}{\partial y}\Big(H_2+h)(H_1-h)\hat{u}\hat{v}\Big) dy = -\left[(H_2+h)(H_1-h)\hat{u}\hat{v}\right]_{-L}^{L} = 0, \quad (3.32)\end{aligned}$$

since $\hat{v} = 0$ at $y = \pm L$.

3.3.3 Conservation of energy

First we will derive an energy equation showing that it is only conserved in the fricitonless case, $\epsilon = 0$. With the introduction of friction $\epsilon \neq 0$ we find that energy is no longer conserved. However, we find that the decay of energy is proportional to ϵ. To see this we will first note that the kinetic energy of both the lower and upper layers is proportional to

$$E_k = (H_2+h)(u_2^2+v_2^2) + (H_1-h)(u_1^2+v_1^2). \quad (3.33)$$

We integrate (3.33) over the domain and take the time derivative

$$\begin{aligned}\frac{\rho}{2}\frac{d}{dt}\int_{-L}^{L} E_k dy = \rho\int_{-L}^{L}\Bigg((H_2+h)\Big(u_2\frac{\partial u_2}{\partial t}+v_2\frac{\partial v_2}{\partial t}\Big) + (H_2-h)\Big(u_1\frac{\partial u_1}{\partial t}+v_1\frac{\partial v_1}{\partial t}\Big) \\ + \frac{(u_2^2+v_2^2)}{2}\frac{\partial h}{\partial t} - \frac{(u_1^2+v_1^2)}{2}\frac{\partial h}{\partial t}\Bigg) dy. \quad (3.34)\end{aligned}$$

Next substituting for $\partial u_1/\partial t$, $\partial u_2/\partial t$, $\partial v_1/\partial t$, $\partial v_2/\partial t$ and $\partial h/\partial t$ from (3.3) - (3.7) we

have

$$\frac{\rho}{2}\frac{d}{dt}\int_{-L}^{L} E_k dy = \rho\int_{-L}^{L}\Bigg((H_2+h)\bigg(u_2\bigg(-v_2\frac{\partial u_2}{\partial y}+fv_2-\frac{\epsilon(u_2-u_1)}{(H_2+h)}\bigg)+ v_2\bigg(-v_2\frac{\partial v_2}{\partial y}-fu_2-\frac{1}{\rho}\frac{\partial p}{\partial y}-g\frac{\partial h}{\partial y}-\frac{\epsilon(v_2-v_1)}{(H_2+h)}\bigg)\bigg)+ (H_1-h)\bigg(u_1\bigg(-v_1\frac{\partial u_1}{\partial y}+fv_1-\frac{\epsilon(u_1-u_1)}{(H_1-h)}\bigg)+ v_1\bigg(-v_1\frac{\partial v_1}{\partial y}-fu_1-\frac{1}{\rho}\frac{\partial p}{\partial y}-\frac{\epsilon(v_1-v_2)}{(H_1-h)}\bigg)\bigg)- \frac{(u_2^2+v_2^2)}{2}\frac{\partial}{\partial y}\bigg((H_2+h)v_2\bigg)-\frac{(u_1^2+v_1^2)}{2}\frac{\partial}{\partial y}\bigg((H_1-h)v_1\bigg)\Bigg)dy. \quad (3.35)$$

The Coriolis terms involving f cancel and we re-write the first, fourth, ninth and twelfth terms in the above by splitting into two differentials such as

$$(H_2+h)u_2v_2\frac{\partial u_2}{\partial y}=\frac{1}{2}\frac{\partial}{\partial y}\bigg((H_2+h)v_2u_2^2\bigg)-\frac{u_2}{2}\frac{\partial}{\partial y}\bigg((H_2+h)v_2\bigg). \quad (3.36)$$

Many terms cancel and we are left with

$$\frac{\rho}{2}\frac{d}{dt}\int_{-L}^{L} E_k dy = \rho\int_{L}^{L}\Bigg(-\frac{1}{2}\frac{\partial}{\partial y}\bigg((H_2+h)v_2(u_2^2+v_2^2)+(H_1-h)v_1(u_1^2+v_1^2)+2g(H_2+h)hv_2\bigg) -\epsilon(u_2-u_1)^2-\epsilon(v_2-v_1)^2-\frac{1}{\rho}\bigg((H_2+h)v_2+(H_1-h)v_1\bigg)\frac{\partial p}{\partial y}+hg\frac{\partial}{\partial y}\bigg((H_2+h)v_2\bigg)\Bigg)dy. \quad (3.37)$$

Note that the first derivative term cancels since at the boundary we have $v_1 = 0$ and $v_2 = 0$. Also for the same reason the pressure term cancels due to (3.13). The final term using (3.8) can be replaced with $-\frac{g}{2}\frac{\partial h^2}{\partial t}$. Hence we can re-write (3.37) by taking the final

term to the other side, $E = E_k + gh^2$

$$\frac{\rho}{2}\frac{d}{dt}\int_{-L}^{L} E dy = \frac{\rho}{2}\frac{\partial}{\partial t}\int_{-L}^{L}\Big((H_2+h)(u_2^2+v_2^2)+(H_1-h)(u_1^2+v_1^2)+gh^2\Big)dy = \\ -\epsilon\rho\int_{-L}^{L}\Big((u_2-u_1)^2+(v_2-v_1)^2\Big)dy. \quad (3.38)$$

Substituting for u_1, u_2, v_1, v_2 from (3.14) and (3.19) and also using $\hat{u} = u_2 - u_1$ and $\hat{v} = v_2 - v_1$ we can re-write (3.38) as

$$\frac{\rho}{2}\frac{d}{dt}\int_{-L}^{L}\Big(H\bar{u}^2+\frac{(H_2+h)(H_1-h)}{H}(\hat{v}^2+\hat{u}^2)+gh^2\Big)dy = \\ -\rho\epsilon\int_{-L}^{L}(\hat{u}^2+\hat{v}^2)dy. \quad (3.39)$$

We can therefore see that energy is conserved when $\epsilon = 0$, with energy decaying when $\epsilon \neq 0$.

3.3.4 A two-layer equivalent of the conservation of potential vorticity

In a single fluid layer there is a famous conservation law for potential vorticity; we now derive a two-layer equivalent. We start by deriving the conservation of potential vorticity separately for each layer. Firstly for the first layer we take $-\partial/\partial y$ of (3.3)

$$\frac{\partial}{\partial t}\Big(-\frac{\partial u_1}{\partial y}\Big)-\frac{\partial}{\partial y}\Big(v_1\frac{\partial u_1}{\partial y}\Big)+f\frac{\partial v_1}{\partial y}+v_1\frac{\partial f}{\partial y}=0, \quad (3.40)$$

which can alternatively be written as

$$\frac{\partial}{\partial t}\Big(f-\frac{\partial u_1}{\partial y}\Big)+v_1\frac{\partial}{\partial y}\Big(f-\frac{\partial u_1}{\partial y}\Big)+\Big(f-\frac{\partial u_1}{\partial y}\Big)\frac{\partial v_1}{\partial y}=0. \quad (3.41)$$

Letting the relative vorticity in the upper layer be noted as $-\partial u_1/\partial y = \xi_1$ we have

$$\frac{\partial(\xi_1 + f)}{\partial t} + v_1 \frac{\partial(\xi_1 + f)}{\partial y} + (\xi_1 + f)\frac{\partial v_1}{\partial y} = 0. \tag{3.42}$$

Note that the term in the relative vorticity dv_1/dx here is zero due to the symmetry of the flow in the x direction. Next from equation (3.7) we have

$$\frac{\partial v_1}{\partial y} = \frac{1}{(H_1 - h)}\left(\frac{\partial h}{\partial t} + v_1 \frac{\partial h}{\partial y}\right) \tag{3.43}$$

and substituting this into (3.42) we have

$$\frac{\partial(\xi_1 + f)}{\partial t} + v_1 \frac{\partial(\xi_1 + f)}{\partial y} + \frac{(f + \xi_1)}{(H_1 - h)}\left(\frac{\partial h}{\partial t} + v_1 \frac{\partial h}{\partial y}\right) = 0. \tag{3.44}$$

This can be written as

$$\frac{D_1}{Dt}\left(\frac{\xi_1 + f}{H_1 - h}\right) = 0, \tag{3.45}$$

where $D_1/Dt = \partial/\partial t + v_1\partial/\partial y$. Here $(\xi_1 + f)/(H_1 - h)$ is known as the potential vorticity in the upper layer. Note that an analogous equation also exists for the bottom layer given by

$$\frac{D_2}{Dt}\left(\frac{\xi_2 + f}{H_2 + h}\right), \tag{3.46}$$

where $D_2 = \partial/\partial t + v_2\partial/\partial y$ and $\xi_2 = -\partial u_2/\partial y$. Equation (3.42) can be written as

$$\frac{d(\xi_1 + f)}{dt} + \frac{d}{dy}(v_1(\xi_1 + f)) = 0. \tag{3.47}$$

Integrating this across the domain gives

$$\frac{d}{dt}\int_{-L}^{L}(f + \xi_1)dy = 0, \tag{3.48}$$

so there is conservation of upper layer vorticity.

3.4 Linear instability

Here we perform linear analysis on the two-layer system, with a basic state shear flow $\bar{u} = U(y)$, $\hat{u} = 0$ and $\hat{v} = 0$. From equation (3.27) we therefore have $-g\partial h/\partial y = 0$ and hence h must be constant; we therefore take $h = 0$. We perturb to $\bar{u} = U(y) + \bar{u}'$, $\hat{v} = v'$, $h = h'$ and $\hat{u} = \hat{u}'$; substituting this into equations (3.26) - (3.29) and linearising we have

$$\frac{\partial u'}{\partial t} - Qv' = -\frac{\epsilon H u'}{H_1 H_2}, \tag{3.49a}$$

$$\frac{\partial v'}{\partial t} + fu' = -g\frac{\partial h'}{\partial y} - \frac{\epsilon H v'}{H_1 H_2}, \tag{3.49b}$$

$$\frac{\partial h'}{\partial t} + \frac{H_1 H_2}{H}\frac{\partial v'}{\partial y} = 0, \tag{3.49c}$$

where $Q = f - dU/dy$. Note that (3.29) becomes $\partial\bar{u}/\partial t = 0$ in the linear regime approximation and is therefore not needed for the stability analysis. Recall here $Q = f - dU(y)/dy$. Next we take disturbances of the form

$$(u', v', h') = Re\left(\tilde{u}(y), \tilde{v}(y), \tilde{h}(y)\right)\exp(st) \tag{3.50}$$

and substitute into (3.48a) - (3.48c), to give

$$\left(s + \frac{\epsilon H}{H_1 H_2}\right)\tilde{u} = Q\tilde{v}, \tag{3.51a}$$

$$\left(s + \frac{\epsilon H}{H_1 H_2}\right)\tilde{v} = -g\frac{d\tilde{h}}{dy} - f\tilde{u}, \tag{3.51b}$$

$$s\tilde{h} = -\frac{H_1 H_2}{H}\frac{d\tilde{v}}{dy}. \tag{3.51c}$$

We re-derive the inertial instability condition $fQ < 0$: Multiplying (3.50b) by s and using (3.50c) to eliminate $\tilde{h}$ we have

$$\left(s + \frac{\epsilon H}{H_1 H_2}\right) s\tilde{v} = \frac{gH_1H_2}{H}\frac{d^2\tilde{v}}{dy^2} - sf\tilde{u}. \tag{3.52}$$

Finally multiplying (3.52) by $(s + \epsilon H/H_1H_2)$ and substituting for $\tilde{u}$ from (3.58a), after rearranging we have

$$\frac{d^2\tilde{v}}{dy^2} - \frac{H}{gH_1H_2}\left(\frac{s}{s + \epsilon H/H_1H_2}\right)\Big((s + \epsilon H/H_1H_2)^2 + fQ\Big)\tilde{v} = 0. \tag{3.53}$$

With the addition of boundary conditions $\tilde{v} = 0$ at $y = \pm L$, this is the eigenvalue problem for the growth rate s of linear inertial instability in the two-layer system. We re-derive the inertial instability condition $fQ < 0$. To do this we follow a similar procedure as in section 2.7. We multiply (3.53) by the complex conjugate $\tilde{v}^*$ and integrate over the domain $y = [-L, L]$,

$$-\frac{gH_1H_2}{H}\int_{-L}^{L}\left|\frac{d\tilde{v}}{dy}\right|^2 dy - s\left(s + \frac{\epsilon H}{H_1H_2}\right)\int_{-L}^{L}|\tilde{v}|^2 dy = \frac{s}{(s + \epsilon H/H_1H_2)}\int_{-L}^{L} fQ|\tilde{v}|^2 dy, \tag{3.54}$$

where we have used integration by parts and applied boundary conditions $\tilde{v} = 0$ at $y = \pm L$ on the first term. We now rearrange the polynomial in the form $As^3 + Bs^2 + Cs + D = 0$, where

$$A = \int_{-L}^{L}|\tilde{v}|^2 dy, \quad B = 2\frac{\epsilon H}{H_1H_2}\int_{-L}^{L}|\tilde{v}|^2 dy, \quad D = g\epsilon\int_{-L}^{L}\left|\frac{d\tilde{v}}{dy}\right|^2 dy, \tag{3.55}$$

$$C = \frac{gH_1H_2}{H}\int_{-L}^{L}\left|\frac{d\tilde{v}}{dy}\right|^2 dy + \frac{\epsilon^2H^2}{H_1^2H_2^2}\int_{-L}^{L}|\tilde{v}|^2 dy + \int_{-L}^{L} fQ|\tilde{v}|^2 dy. \tag{3.56}$$

By the Routh Hurwitz stability criterion, a necessary and sufficient condition for the cubic to have three stable roots is

$$A, B, C, D > 0 \qquad \text{and} \qquad BC > AD. \tag{3.57}$$

We can see that A, B and D are always positive for non-trivial solutions. If fQ is everywhere positive, then C is also positive, and we are thus guaranteed stability. So $fQ < 0$ somewhere in the flow is a necessary (but not sufficient) condition for instability.

$$2AD + 2\frac{\epsilon H}{H_1 H_2} A \left(\frac{\epsilon^2 H^2}{H_1^2 H_2^2} A + \int_{-L}^{L} fQ|\tilde{v}|^2 dy \right) > AD. \tag{3.58}$$

The only way either condition can be broken is therefore if C becomes negative or equivalently $fQ < 0$ somewhere in the flow.

3.4.1 Formal analogy with continuously stratified system

We show there exists a mathematical analogy between the two-layer system and the continuously stratified system with infinite Prandtl number. It should however be noted that there is also a physical analogy since infinite Prandtl number implied no mixing of density which is also the case in the two-layer model. It is sufficient to compare the linear eigenvalue problems in the continuously stratified case (2.44),

$$\frac{d^2\hat{v}}{dy^2} - \frac{m^2(s + \kappa m^2)}{N^2(s + \nu m^2)} \left((s + \nu m^2)^2 + fQ \right) \hat{v} = 0, \tag{3.59}$$

and (3.53) in a two-layer flow,

$$\frac{d^2\tilde{v}}{dy^2} - \frac{H}{gH_1H_2} \left(\frac{s}{s + \epsilon H/H_1H_2} \right) \left((s + \epsilon H/H_1H_2)^2 + fQ \right) \tilde{v} = 0. \tag{3.60}$$

The analogy is established using the equivalence

$$gH_e = \frac{N^2}{m^2}, \quad \nu m^2 = \frac{\epsilon}{H_e}, \tag{3.61}$$

where $H_e = H_1 H_2 / H$. The analogy however is not that simple; in the two-layer system gravity, g is fixed as is the combined layer depth H and individual layer depths H_1 and H_2, with only ϵ varying. In the continuously stratified system we kept N^2 fixed while varying both viscosity, ν, and wavenumber m. We can therefore see that the continuously stratified system has an extra degree of freedom in the wavenumber m; this can make comparison between the two systems more complicated. For example we found in the continuously stratified system that increasing viscosity made the flow more stable; however, we still might find wavenumbers for which the flow is unstable. Increasing viscosity effectively increases the range of wavenumbers for which the flow is stable. In the two-layer case however, at a particular friction, the flow can either be stable or unstable; it cannot be stable to disturbances of certain length-scales and unstable to others.

3.5 Summary

We have derived the two-layer model with a rigid lid approximation, scarcely used so far in the analysis of inertial instability but used extensively in the study of other geophysical flows. A non-standard interface friction was applied. Other work with interfacial friction that should be mentioned is that by Zeitlin et al (2014); here the friction is more complex and only comes into effect when the vertical shear is sufficiently large.

The factors of $H_1 - h$ and $H_2 + h$ in the denominators of the frictional terms guarantee that the depth integrated momentum is conserved, as it is in the continuously stratified system. We identified four conserved quantities, those being energy, mass, absolute momentum and potential vorticity.

As we have done for the continuously stratified system we performed linear analysis for a shear flow basic state $\bar{u} = U(y)$ and again find stability is guaranteed for $fQ > 0$ regardless of friction. The key message of this chapter is the importance of the analogy between the linear instability of the continuously stratified system with $Pr \to \infty$ as seen in section 2.10 and the two-layer system with interfacial friction. Given the importance of vertical diffusion of momentum in inertial instability this makes the two-layer system particularly suitable for studying this type of instability.

Chapter 4

Nonlinear instabilities on the equatorial β plane

4.1 Introduction

A zonal flow $U(y)$ with absolute vorticity $Q = f - dU/dy$ is inertially unstable if $fQ < 0$, in the inviscid or frictionless limit. On an equatorial β-plane with $f = \beta y$, any non-zero shear at the equator necessarily leads to inertial instability. The simplest model of such a flow is one with uniform shear, i.e., $U(y) = \Lambda y$, in which case $fQ < 0$ between $y = 0$ and $y = \Lambda/\beta$, and the maximum possible growth rate is $\Lambda/2$. So the stronger the shear, the larger is the unstable region and the strength of the instability.

Near solstice (i.e. June and December), the zonal flows in the Earth's equatorial upper stratosphere and mesosphere can be regarded as having approximately uniform cross-equatorial shear. There is a strong mid-latitude eastward jet in the winter hemisphere and a strong mid-latitude westward jet in the summer hemisphere (as illustrated by Hobbs and Wallace (1977)). As discussed in detail in section 3 of Dunkerton (1981), these zonal flows are driven by a strong cross-equatorial flow from the summer to winter hemisphere,

that is part of the mean meridional circulation. Typical horizontal shears are of the order of 2–4 $\times 10^{-5}$ s^{-1} (Hayashi and Shiotani, 1998) and since the unstable region is bound between $y = 0$ and Λ/β we find the inertially unstable band of air extends from the equator to 10–20 degrees.

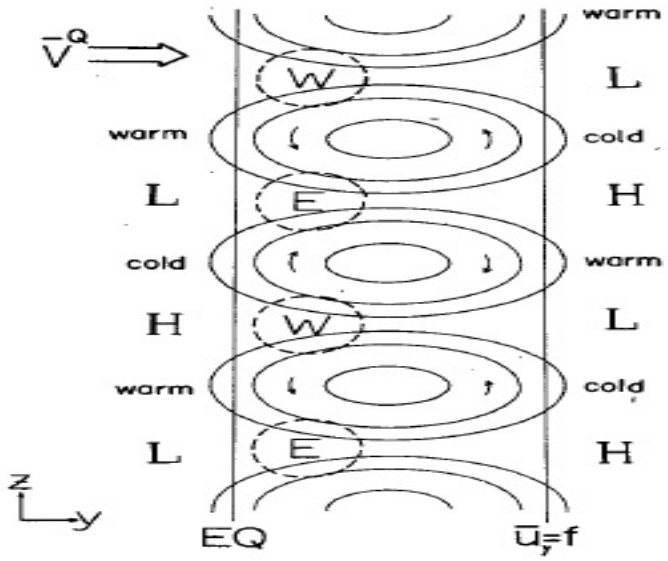

Figure 4.1: Inertial instability as pictured by Dunkerton (1981) on the equatorial β-plane. Stacks of alternating warm and cold air appear either side of the unstable region. There are circulations inside the unstable region which aim to mix the negative potential vorticity with positive potential vorticity outside of the unstable region. This also creates alternating western and eastern jets.

Since inertial instabilities can develop in a symmetric system (i.e., $\partial/\partial x = 0$), analysis is undertaken in the (y, z) plane. There is a large collection of such work on inertial instability; the early work by Dunkerton (1981) looked at inertial instability on the equatorial β-plane in a continuously stratified system. Dunkerton first looked at a basic state with uniform shear, $U = \Lambda y$, and found a transition from stability to instability with increasing vertical wavenumber. He found these instabilities displayed physically as stacked overturning motions developing on the edges of the initially unstable region, as illustrated in Figure 4.1. Dunkerton (1982) later extended his linear analysis further to look at a diffusive system with $Pr \neq 1$ and again found that diffusion set the vertical scale

for inertial instability. Griffiths (2003a,b) looked at a similar system also with $U = \Lambda y$ however with $Pr = 1$. Griffiths (2003a) applied weakly nonlinear theory, the analysis of which showed exponential growth of the linear perturbation before weakly nonlinear effects take hold which stabilise the flow by neutralising the mean flow before decaying. A numerical simulation of the nonlinear system was also looked at in Griffiths (2003b), who also confirmed the presence of stacked overturning structures. Kloosterziel et al (2015) also looked at inertial instability in an unstratified system on the equatorial β-plane; however they adopted the approach of using the conservation of linear momentum to predict the change in the mean flow as a result of changes made by the instability. Their prediction and theory were strengthened by numerical simulations.

Here we study these equatorial inertial instabilities with uniform shear in the two-layer model developed in Chapter 3. We start, in section 4.2, by nondimensionalising the full set of nonlinear PDEs with interfacial friction. In section 4.3, we derive the (nondimensional) linear dispersion relation for instabilities on a flow with uniform shear, and perform asymptotic analysis for weak friction. Then we turn to nonlinear effects. We start, in section 4.4, by performing a weakly nonlinear analysis for the frictionless system, leading to an amplitude equation for the growth and subsequent oscillations of the unstable modes. Numerical solutions of the amplitude equation are given in section 4.5, and a comparison with numerical solutions of the full nonlinear two-layer PDEs is given in section 4.6. Here we restrict our nonlinear investigations to the frictionless case, since in the atmosphere and ocean we have a high Reynolds number $Re = UL/\nu$, where U and L are characteristic velocity and length scale respectively. Since we have made an analogy between viscosity and friction at the end of the previous chapter we deduce that a high Reynolds number manifests itself through small friction.

This sort of approach (i.e., studying amplitude equations derived from a weakly nonlinear analysis) is common in various branches of fluid mechanics. It can be contrasted to the approach of Ribstein et al. (2014) who used numerical simulations to attack the strongly

nonlinear two-layer inertial instability problem directly. In the context of equatorial inertial instability in two-layer flows, there is some closely related work by Zhao and Ghil (1991). We will discuss this and how it is related to our work in section 4.6.2. However, at the outset, it is worth noting that the Zhao and Ghil (1991) analysis actually corresponds to a special case of the more general analysis we give.

4.2 Nondimensionalisation of the governing equations

Before analysing the two-layer system it is convenient for us to use a nondimensional form of equations (3.26) - (3.29). We define new variables as follows

$$\tilde{u} = \hat{u}/U, \quad \tilde{v} = \hat{v}/U, \quad \tilde{\bar{u}} = \bar{u}/U, \quad \tilde{h} = h/H_e, \quad \tilde{t} = t/T, \quad \tilde{y} = y/L, \tag{4.1}$$

where U, L, T are characteristic velocity, length and time scales respectively, and $H_e = H_1H_2/H$, with $H = H_1 + H_2$. If we write $H_1 = \alpha H$ and $H_2 = (1-\alpha)H$ where α is the fractional depth of the upper layer, then $H_e = \alpha(1-\alpha)$. Also recall that on the equatorial-β plane we have $f = \beta y = \beta L\tilde{y}$. Substituting into equations (3.26) - (3.29) we have

$$\begin{aligned}\frac{\partial\tilde{u}}{\partial\tilde{t}} + \left(\frac{UT}{L}\right)(\alpha - \alpha(1-\alpha)\tilde{h})\tilde{v}\frac{\partial}{\partial\tilde{y}}\left(\tilde{\bar{u}} + (\alpha - \alpha(1-\alpha)\tilde{h})\tilde{u}\right) + \\ \left(\frac{UT}{L}\right)((1-\alpha) + \alpha(1-\alpha)\tilde{h})\tilde{v}\frac{\partial}{\partial\tilde{y}}\left(\tilde{\bar{u}} - (((1-\alpha) + \alpha(1-\alpha)\tilde{h}))\tilde{u}\right) \\ - \beta(LT)\tilde{y}\tilde{v} = -\frac{T\epsilon\tilde{u}}{H(1-\alpha)\alpha(1+\alpha\tilde{h})(1-(1-\alpha)\tilde{h})},\end{aligned} \tag{4.2}$$

$$\frac{\partial\tilde{v}}{\partial\tilde{t}}+\left(\frac{UT}{2L}\right)\frac{\partial}{\partial\tilde{y}}\left((\alpha-\alpha(1-\alpha)\tilde{h})\tilde{v}\right)^2-\left(\frac{UT}{2L}\right)\frac{\partial}{\partial\tilde{y}}\left(((1-\alpha)+\alpha(1-\alpha)\tilde{h}))\tilde{v}\right)^2$$
$$+\beta(LT)\tilde{y}\tilde{u}=-g'\frac{\alpha(1-\alpha)HT}{LU}\frac{\partial\tilde{h}}{\partial\tilde{y}}-\frac{T\epsilon\tilde{v}}{H(1-\alpha)\alpha(1+\alpha\tilde{h})(1-(1-\alpha)\tilde{h})}, \quad (4.3)$$

$$\frac{\partial\tilde{h}}{\partial\tilde{t}}+\left(\frac{UT}{L\alpha(1-\alpha)}\right)\frac{\partial}{\partial\tilde{y}}\left(\alpha(1-\alpha)(1+\alpha\tilde{h})(1-(1-\alpha)\tilde{h})\tilde{v}\right)=0, \quad (4.4)$$

$$\frac{\partial\tilde{\tilde{u}}}{\partial\tilde{t}}=-\left(\frac{UT}{L}\right)\frac{\partial}{\partial\tilde{y}}\left(\alpha(1-\alpha)(1+\alpha\tilde{h})(1-(1-\alpha)\tilde{h})\tilde{u}\tilde{v}\right). \quad (4.5)$$

We choose $L=\Lambda/\beta$ and $T=\Lambda^{-1}$ since this is the timescale of the inviscid instability, and hence $U=\Lambda^2/\beta$. We also define a nondimensional friction $\tilde{\epsilon}=H\epsilon/T$. The final nondimensional, nonlinear two-layer equations on the equatorial β-plane are

$$\frac{\partial\tilde{u}}{\partial\tilde{t}}+\tilde{v}\frac{\partial}{\partial\tilde{y}}(\tilde{\bar{u}}-\tilde{u})+2D_1\tilde{v}\frac{\partial}{\partial\tilde{y}}\tilde{u}+\tilde{v}\tilde{u}\frac{\partial}{\partial\tilde{y}}D_1-\tilde{y}\tilde{v}=-\frac{\tilde{\epsilon}\tilde{u}}{D_1D_2}, \quad (4.6)$$

$$\frac{\partial\tilde{v}}{\partial\tilde{t}}-\tilde{v}\frac{\partial}{\partial\tilde{y}}\tilde{v}+2D_1\tilde{v}\frac{\partial}{\partial\tilde{y}}\tilde{v}+\tilde{v}^2\frac{\partial}{\partial\tilde{y}}D_1+\tilde{y}\tilde{u}=-\tilde{g}\frac{\partial\tilde{h}}{\partial\tilde{y}}-\frac{\tilde{\epsilon}\tilde{v}}{D_1D_2}, \quad (4.7)$$

$$\frac{\partial\tilde{h}}{\partial\tilde{t}}+\frac{1}{\alpha(1-\alpha)}\frac{\partial}{\partial\tilde{y}}\left(D_1D_2\tilde{v}\right)=0, \quad (4.8)$$

$$\frac{\partial\tilde{\tilde{u}}}{\partial\tilde{t}}=-\frac{\partial}{\partial\tilde{y}}\left(D_1D_2\tilde{u}\tilde{v}\right), \quad (4.9)$$

where

$$D_1=\alpha-\alpha(1-\alpha)\tilde{h}, \qquad D_2=1-\alpha+\alpha(1-\alpha)\tilde{h},$$

and

$$\tilde{g}=\alpha(1-\alpha)(g'H)\beta^2/\Lambda^4.$$

This system is characterised by three nondimensional parameters: α (the fractional depth of the lower layer), $\tilde{g}$ (nondimensional parameter of the reduced gravity) and $\tilde{\epsilon}$ (the nondimensional friction coefficient). As we expect, and as we will see from the linear analysis, gravity has a stabilising effect. We find in the linear analysis to come that the

flow is stable for large $\tilde{g}$ and unstable at small $\tilde{g}$ with a critical value in between. We can achieve large $\tilde{g}$ by considering layers of equal depth $\alpha = 0.5$ or a small shear Λ. Recall that $g' = (\rho_2 - \rho_1)/\rho_2$, which becomes large as the density difference between the two densities becomes large. To achieve small $\tilde{g}$ we can deduce that the opposite is true.

The nondimensionalisation can also be applied to the conservation laws. Firstly we find the conservation of energy is given by

$$\frac{\partial}{\partial t}\int_{-\infty}^{\infty}\left(\tilde{\bar{u}}^2 + D_1 D_2(\tilde{u}^2+\tilde{v}^2) + \tilde{g}\alpha(1-\alpha)\tilde{h}^2\right)dy = -\int_{\infty}^{\infty}\tilde{\epsilon}(\tilde{u}^2+\tilde{v}^2)dy. \tag{4.10}$$

Next we have conservation of momentum: after nondimensionalising and using (3.19) we have

$$\frac{\partial}{\partial t}\int_{-\infty}^{\infty}\tilde{\bar{u}}dy = 0. \tag{4.11}$$

For the conservation of mass we have

$$\frac{d}{dt}\int_{-\infty}^{\infty}\tilde{h}dy = 0. \tag{4.12}$$

Lastly we have

$$\frac{d}{dt}P_1 - D_2\tilde{v}\frac{\partial}{\partial y}P_1 = 0 \tag{4.13}$$

where

$$P_1 = \frac{y + \frac{\partial}{\partial y}\left(D_2\tilde{u} - \tilde{\bar{u}}\right)}{D_1}, \tag{4.14}$$

giving the conservation of potential vorticity. Following this same derivation as the top layer we have

$$\frac{\partial}{\partial t}P_2 + D_1\tilde{v}\frac{\partial}{\partial y}P_2 = 0 \tag{4.15}$$

where

$$P_2 = \frac{y - \frac{\partial}{\partial y}\left(D_1\tilde{u} + \tilde{\bar{u}}\right)}{D_2}. \tag{4.16}$$

4.3 Linear instability

Before performing a weakly nonlinear analysis, a thorough understanding of the linear instability must be obtained. The relevant distribution equations were derived in dimensional form for an arbitrary flow in section 3.4; it therefore only remains to find the nondimensional form of the governing equation (3.53). Given the analogy noted in section 3.4.1 and the linear instability analysis already performed for the continuously stratified system in section 2.10, we could already anticipate the general nature of linear instabilities. However, here we explicitly derive and analyse the growth rate as a function of α, $\tilde{\epsilon}$ and $\tilde{g}$. The nondimensionalised equation for the perturbation meridional velocity $\tilde{v}'$ is

$$\frac{d^2\tilde{v}'}{d\tilde{y}^2} - \frac{1}{\tilde{g}}\left(\frac{\tilde{s}}{\tilde{s}+\tilde{\epsilon}/\alpha(1-\alpha)}\right)\left(\left(\tilde{s}+\frac{\tilde{\epsilon}}{\alpha(1-\alpha)}\right)^2 + \tilde{y}(\tilde{y}-1)\right)\tilde{v}' = 0. \tag{4.17}$$

After completing the square

$$\frac{d^2\tilde{v}'}{d\tilde{y}^2} - \frac{1}{\tilde{g}}\left(\frac{\tilde{s}}{\tilde{s}+\tilde{\epsilon}/\alpha(1-\alpha)}\right)\left(\left(\tilde{s}+\frac{\tilde{\epsilon}}{\alpha(1-\alpha)}\right)^2 + \left(\tilde{y}-\frac{1}{2}\right)^2 - \frac{1}{4}\right)v' = 0. \tag{4.18}$$

We define a new variable $Y/M = (\tilde{y} - 1/2)$; substituting into (4.18) we have

$$\frac{d^2\tilde{v}'}{dY^2} + \frac{1}{\tilde{g}M^2}\left(\frac{\tilde{s}}{\tilde{s}+\tilde{\epsilon}/\alpha(1-\alpha)}\right)\left(-\left(\tilde{s}+\frac{\tilde{\epsilon}}{\alpha(1-\alpha)}\right)^2 - \left(\frac{Y}{M}\right)^2 + \frac{1}{4}\right)\tilde{v}' = 0. \tag{4.19}$$

Then with

$$M^4 = \frac{4\tilde{s}}{\tilde{g}\left(\tilde{s}+\tilde{\epsilon}/\alpha(1-\alpha)\right)},$$

equation (4.19) becomes

$$\frac{d^2\tilde{v}'}{dY^2} + \left\{\frac{1}{2}\left(\frac{\tilde{s}}{\tilde{g}(\tilde{s}+\tilde{\epsilon}/\alpha(1-\alpha))}\right)^{1/2}\left(-\left(\tilde{s}+\frac{\tilde{\epsilon}}{\alpha(1-\alpha)}\right)^2 + \frac{1}{4}\right) - \frac{Y^2}{4}\right\}\tilde{v}' = 0. \tag{4.20}$$

With boundary conditions $\tilde{v}' \to 0$ applied at $Y \to \pm\infty$, equation (4.20) forms the parabolic cylinder equation whose solutions are given by Bender and Orszag (1999). It is found that the eigenvalues must equal a non-negative integer and hence leads to the dispersion relation

$$(2n+1)\tilde{g}^{1/2} = -\left(\frac{\tilde{s}}{(\tilde{s}+\tilde{\epsilon}/\alpha(1-\alpha))}\right)^{1/2}\left(\left(\tilde{s}+\frac{\tilde{\epsilon}}{\alpha(1-\alpha)}\right)^2 - \frac{1}{4}\right). \tag{4.21}$$

4.3.1 The frictionless case

With no friction, $\epsilon = 0$, the linear growth rate from (4.21) is

$$\tilde{s}^2 = \frac{1}{4} - (2n+1)\tilde{g}^{1/2}, \tag{4.22}$$

which has zero growth rate when $\tilde{g}^{1/2} = \tilde{g}_c^{1/2} = 1/(4(2n+1))$. This growth rate is shown in figure 4.2. For instability we require small $\tilde{g}$. This implies a small reduced gravity, a strong shear, a large ratio between the two-layer depths or a small overall layer depth. This is consistent with the physical system, as a weak gravity may not be strong enough to inhibit any uplift in the interface, a strong shear is less stable (since the shear drives the instability) and layer depths of a similar size allows for a maximum lift in the interface (since h is conserved).

4.3.2 Asymptotic solutions for weak friction

It is impossible to solve (4.21) exactly when $\tilde{\epsilon} \neq 0$. However, we can investigate the frictional behaviour by considering the limit $\tilde{\epsilon} \to 0$. It is convenient to work in terms of $\hat{s} = 2\tilde{s}$, $\hat{\epsilon} = 2\tilde{\epsilon}/(\alpha(1-\alpha))$ and T defined by $T^2 = 4(2n+1)\tilde{g}^{1/2}$, in which case (4.21) becomes

$$T^2 = -\left(\frac{\hat{s}}{\hat{s}+\hat{\epsilon}}\right)^{1/2}\left(\left(\hat{s}+\hat{\epsilon}\right)^2 - 1\right). \tag{4.23}$$

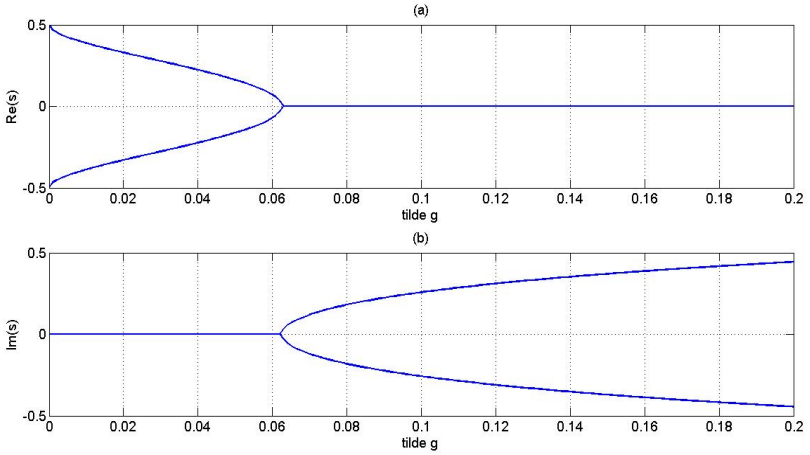

Figure 4.2: *A plot of the dispersion relation (4.22) showing the growth rate (a) and the frequency (b) with* $n = 0$*. The flow becomes stable at* $\tilde{g}_c = 0.0625$.

Note that the inviscid limit gives $\hat{s} = 1 - T^2$. The dispersion relation was then solved for $\hat{s}$ by expanding $\hat{s}$ as a power series of $\hat{\epsilon}$. We can expand (4.23) using the Taylor series expansion

$$(\hat{s}^2 + 2\hat{\epsilon}\hat{s} + \hat{\epsilon}^2 - 1)\left(1 - \frac{\hat{\epsilon}}{2\hat{s}} + \frac{3\hat{\epsilon}^2}{8\hat{s}^2} - \frac{15\hat{\epsilon}^3}{48\hat{s}^3} + \cdots\right) + T^2 = 0. \tag{4.24}$$

Expanding this gives

$$\hat{s}^2 + \frac{3}{2}\epsilon\hat{s} + \left(T^2 - 1 + \frac{3}{8}\hat{\epsilon}^2\right) + \left(\frac{\hat{\epsilon}}{2} - \frac{3}{48}\hat{\epsilon}^3\right)\hat{s}^{-1} - \frac{3}{8}\hat{\epsilon}^2\hat{s}^{-2} + \frac{15}{48}\hat{\epsilon}^3\hat{s}^{-3} = 0. \tag{4.25}$$

Case 1 $1 - T^2 = O(1)$**:**

Here we assume $1 - T^2$ does not become small enough to interfere with the expansion of s which is assumed to be $O(1)$. After using a dominant balance approach it is found that $\hat{s}$ can be written

$$\hat{s} = \hat{s}_0 + \hat{\epsilon}\hat{s}_1 + \hat{\epsilon}^2\hat{s}_2 + O(\hat{\epsilon}^3). \tag{4.26}$$

Hence (4.25) becomes

$$\hat{s}_0^2 + 2\hat{\epsilon}\hat{s}_0\hat{s}_1 + 2\hat{\epsilon}^2\hat{s}_0\hat{s}_2 + \hat{\epsilon}^2\hat{s}_1^2 + \frac{3}{2}\hat{\epsilon}\hat{s}_0 + \frac{3}{2}\hat{\epsilon}^2\hat{s}_1 + T^2 - 1 + \frac{3}{8}\hat{\epsilon}^2 + \frac{1}{2\hat{s}_0}\hat{\epsilon}\left(1 - \hat{\epsilon}\frac{\hat{s}_1}{\hat{s}_0} + \dots\right) - \frac{3}{8\hat{s}_0^2}\hat{\epsilon}^2\left(1 - \dots\right) + O(\epsilon^3) = 0, \quad (4.27)$$

where we have used a Taylor series expansion on the last two terms. Comparing like powers of $\hat{\epsilon}$

$$O(1): \qquad \hat{s}_0^2 = 1 - T^2, \quad (4.28)$$

$$O(\hat{\epsilon}): \qquad \hat{s}_1 = -\left(\frac{1}{2} + \frac{3}{2}\hat{s}_0^2\right)/2\hat{s}_0^2. \quad (4.29)$$

The first equation in (4.28) is the equivalent of the frictionless dispersion relation given by (4.22). Two approximations for the roots of the dispersion relation (4.23) are therefore given by (4.26), where $\hat{s}_0$ and $\hat{s}_1$ are given by (4.28) and (4.29) respectively.

If $T < 1$, then there is a root for $\hat{s}_0$ that is real and positive and thus there is instability at leading order. However, if $T \geq 1$, then $\hat{s}_0$ is imaginary and we need to go to the next order in $\hat{\epsilon}$ to determine whether or not the flow is stable. From (4.29), we find

$$\hat{s}_1 = -\frac{4 - 3T^2}{4(1 - T^2)}. \quad (4.30)$$

So, for $1 < T^2 < 4/3$, $\hat{s}_1$ is real and positive and hence we have instability. So the friction has the surprising effect of destabilizing the flow in this regime. However, for $T^2 > 4/3$, $\hat{s}_1$ is real and negative and hence we have stability.

It is possible to verify these roots satisfy (4.23). However numerical results show that there exists a third admissible root of (4.23) when $\hat{\epsilon} \ll 1$. To find this, it is necessary to seek a different leading order balance in (4.23). We seek a solution where $\hat{s}$ is $O(\hat{\epsilon})$, and

thus write $\hat{s} = \hat{\epsilon}\bar{s}$. Substituting in (4.23) gives

$$T^2 = -\left(\frac{\bar{s}}{\bar{s}+1}\right)^{1/2}\left(\hat{\epsilon}^2(\bar{s}+1)^2 - 1\right). \tag{4.31}$$

To solve this, we first square to obtain,

$$T^4(1+\bar{s}) = \bar{s}\left(\hat{\epsilon}^4 - 2\hat{\epsilon}^2(1+\bar{s})^2 + 1\right).$$

Substituting $\bar{s} = \bar{s}_0 + \hat{\epsilon}^2\bar{s}_1 + \cdots$, at leading order we have $T^4(1+\tilde{s}_0) = \bar{s}_0$, so that

$$\bar{s}_0 = \frac{T^4}{1-T^4}. \tag{4.32}$$

At $O(\hat{\epsilon}^2)$. we have $T^4\bar{s}_1 = \bar{s}_1 - 2\bar{s}_0(1+\bar{s}_0)^2$, so that

$$\bar{s}_1 = \frac{2\bar{s}_0(1+\bar{s}_0)^2}{1-T^4} = \frac{2T^4}{(1-T^4)^2}. \tag{4.33}$$

Hence we have

$$\hat{s} = \frac{\epsilon\hat{T}^4}{1-T^4} + \frac{2\hat{\epsilon}^3T^4}{(1-T^4)^2} + \cdots. \tag{4.34}$$

When $T > 1$, this corresponds to a weakly decaying mode. However, when $T < 1$, there is a weak instability, the existence of which depends upon friction. Again, it is interesting that the addition of friction leads to an additional unstable mode, but this mode is generally irrelevant because of the much stronger primary mode already discussed with $\hat{s}^2 \approx 1-T^2$.

Case 2: $T^2 - 1 \ll 1$

When $\hat{\epsilon} \ll 1$, the obvious leading-order balance comes from assuming that $\hat{s}$ and T are order-unity. Then $\hat{s}/(\hat{s}+\hat{\epsilon}) \approx \hat{s}/\hat{s} = 1$, and we have from (4.23)

$$T^2 \approx 1 - \hat{s}^2 \;\Rightarrow\; \hat{s}^2 \approx 1 - T^2. \tag{4.35}$$

This is self-consistent provided $1 - T^2 = O(1)$. However, there is third root with $\hat{s} =$

$O(\epsilon)$, in which case the $(\hat{s}+\epsilon)^2$ term in (4.23) is negligible and we have

$$T^2 \approx \left(\frac{\hat{s}}{\hat{s}+\epsilon}\right)^{1/2} \;\Rightarrow\; T^4 \approx \frac{\hat{s}}{\hat{s}+\epsilon} \;\Rightarrow\; \hat{s} \approx \frac{\epsilon T^4}{1-T^4}, \tag{4.36}$$

which, since $1-T^4 = (1-T^2)(1+T^2)$, thus again implicitly requires that $1-T^2 = O(1)$.

We thus have three approximate roots of (4.31) when $1 - T^2 = O(1)$. However, as $T^2 \to 1$, the two roots (4.35) with $\hat{s} \propto \sqrt{1-T^2}$ become small, whilst the single root (4.36) with $hats \propto hat\epsilon/(1-T^2)$ becomes large. We expect that a new asymptotic regime, which simultaneously describes all three roots when $T^2 \approx 1$, will occur when $\sqrt{1-T^2} \sim \hat{\epsilon}/(1-T^2)$, i.e., when $1 - T^2 = O(\hat{\epsilon}^{2/3})$, implying $\hat{s} = O(\hat{\epsilon}^{1/3})$. We thus write

$$T^2 = 1 + \tau\hat{\epsilon}^{2/3} \text{ and } \hat{s} = \hat{\epsilon}^{1/3}S. \tag{4.37}$$

Substituting in (4.23), we note that $\hat{s}/(\hat{s}+\hat{\epsilon}) = (1+\hat{\epsilon}/\hat{s})^{-1} \approx 1-\hat{\epsilon}/\hat{s} = 1-\hat{\epsilon}^{2/3}/S$, and that $(\hat{s}+\hat{\epsilon})^2 \approx \hat{s}^2 = \hat{\epsilon}^{2/3}S^2$, so we have

$$1+\tau\hat{\epsilon}^{2/3} \approx \left(1-\frac{\hat{\epsilon}^{2/3}}{2S}\right)\left(1-\hat{\epsilon}^{2/3}S^2\right) \approx 1-\hat{\epsilon}^{2/3}\left(\frac{1}{2S}+S^2\right) \;\Rightarrow\; S^3+\tau S+\frac{1}{2} \approx 0. \tag{4.38}$$

The roots of this cubic equation describe the transition from $T < 1$ (negative τ) to $T > 1$ (positive τ), through the point $T = 1$ ($\tau = 0$). Through this transition we go from three real roots to one real root (given by (4.36) for large τ) plus two complex conjugate roots (given by $\hat{s}^2 \approx \pm i\sqrt{T^2-1}$ for large τ, from (4.35)). The complex roots first appear when the discriminant of (4.38), i.e., $\Delta = -4\tau^3 - 27/4$, changes from positive to negative. There are thus three real roots only when

$$\tau < -\frac{3}{2\cdot 2^{1/3}} \;\Leftrightarrow\; T^2 < 1 - \frac{3\epsilon^{2/3}}{2\cdot 2^{1/3}}.$$

Finally, note that the roots (4.35) and (4.36) are fully consistent with (4.38), as can be

seen by considering the limit $|\tau| \gg 1$. Then one distinguished limit of (4.38) is

$$S^3 + \tau S \approx 0 \;\Rightarrow\; S^2 \approx -\tau \;\Rightarrow\; \frac{s^2}{\hat{\epsilon}^{2/3}} \approx -\frac{T^2-1}{\hat{\epsilon}^{2/3}} \;\Rightarrow\; s^2 \approx 1 - T^2,$$

i.e., (4.35), whilst the other distinguished limit is

$$\tau S + \frac{1}{2} \approx 0 \;\Rightarrow\; S \approx -\frac{1}{2\tau} \;\Rightarrow\; \frac{s}{\hat{\epsilon}^{1/3}} \approx -\frac{1}{2(T^2-1)/\hat{\epsilon}^{2/3}} \;\Rightarrow\; \hat{s} \approx \frac{\hat{\epsilon}}{2(1-T^2)}, \quad (4.39)$$

which is just (4.36) with the additional factor of $T^4/(1+T^2)$ set to its value at $T = 1$ of $1/2$.

The asymptotic results are displayed in figures 4.3 - 4.5 where the real and imaginary solution for $\hat{s}$ is plotted against T; each figure represents a fixed value of $\hat{\epsilon}$. In each case we have three solutions for $\hat{s}$ (apart from the case where $T = 1$), the solutions are plotted such that the expansions for $\hat{s}$ are substituted into (4.23) and discarded when the residual is too high. This ensures the transition from case 1 to case 2 is picked up and only the relevant roots are displayed.

4.3.3 Numerical solutions

The solutions were also found numerically using a roots finder in MATLAB. To do this we start by squaring the dispersion relation (4.23) and rearranging,

$$\hat{s}^5 + 4\hat{\epsilon}\hat{s}^4 + (6\hat{\epsilon}^2 - 2)\hat{s}^3 + (4\hat{\epsilon}^3 - 4\hat{\epsilon})\hat{s}^2 + (\hat{\epsilon}^4 - T^4 - 2\hat{\epsilon}^2 + 1)\hat{s} - T^4\hat{\epsilon} = 0. \quad (4.40)$$

The above is then solved for fixed values of $\hat{\epsilon}$ and as will be discussed various values of $\hat{\epsilon}$ have been looked at. The solution to this equation yields five roots, not all of which will be solutions to the original dispersion relation. The roots were 'checked' by substituting back into (4.23) and calculating their residual, discarding any roots with a residual greater than 10^{-4}.

The solution $\hat{s}$ plotted against T for various values of $\hat{\epsilon}$ can be seen in figures 4.3 - 4.5 with the growth rate and frequency being displayed separately. Both the numerical results (crossed) and asymptotic roots (solid line) are shown. Away from $T = 1$ the red line shows the two roots given by (4.28) at leading order, the blue line shows (4.32). As $T \to 1$ we find asymptotic results are described by the solution to (4.38), what we see plotted is consistent as two real roots merge into two complex conjugate pairs.

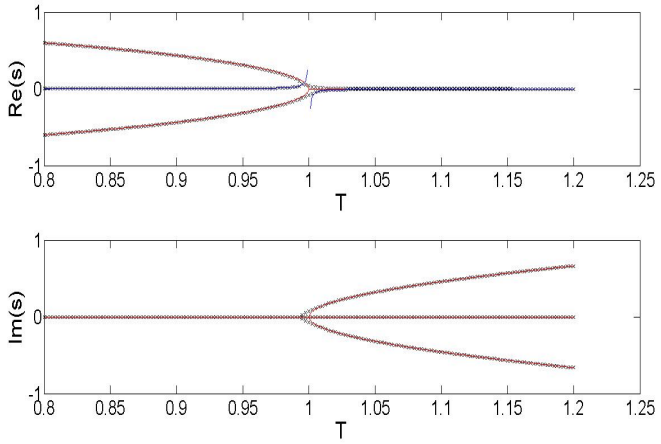

Figure 4.3: *A plot of the asymptotic (solid lines) and numerical solutions (crosses) of the dispersion relation (4.23). Plotted is the growth rate (a) and frequency (b) where* $\hat{\epsilon} = 0.001$.

Probably one of the most important results from this analysis is how the stability is affected by the drag coefficient $\hat{\epsilon}$. To show this, figure 4.6 plots the friction at which all roots become stable. This figure was produced by solving (4.23) numerically across a range of $\hat{\epsilon}$. Therefore we have an area of instability below the curve and an area of stability above the curve. When $T^2 > 4/3$ the flow is stable for all friction: Between $1 < T^2 < 4/3$ the frictionless flow is unstable; however we found that the flow is actually destabilized with the introduction of weak friction, which is the cause of the discontinuity in the curve.

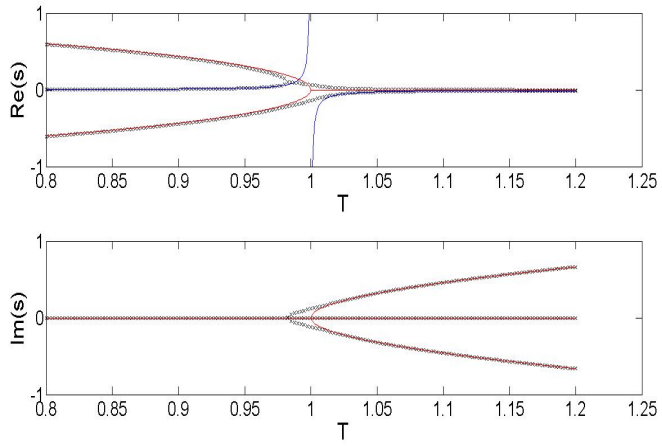

Figure 4.4: *A plot of the asymptotic (solid lines) and numerical solutions (crosses) of the dispersion relation (4.23). Plotted is the growth rate (a) and frequency (b) where* $\hat{\epsilon} = 0.005$.

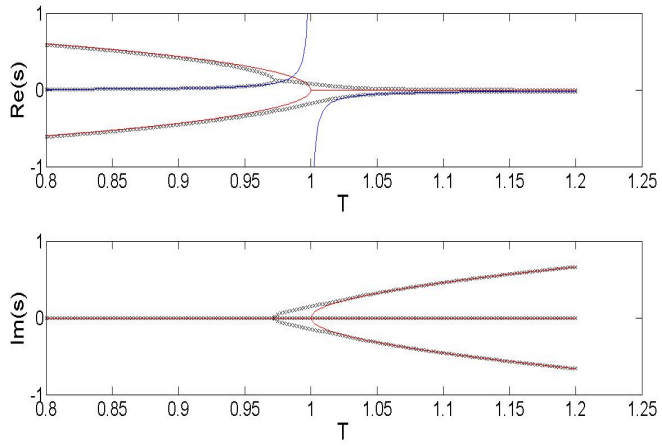

Figure 4.5: *A plot of the asymptotic (solid lines) and numerical solutions (crosses) of the dispersion relation (4.23). Plotted is the growth rate (a) and frequency (b) where* $\hat{\epsilon} = 0.01$.

4.4 Weakly nonlinear analysis

We now move beyond linear dynamics to weakly nonlinear dynamics. Although we have argued that it is desirable to include interfacial friction in our equations of motion (as an

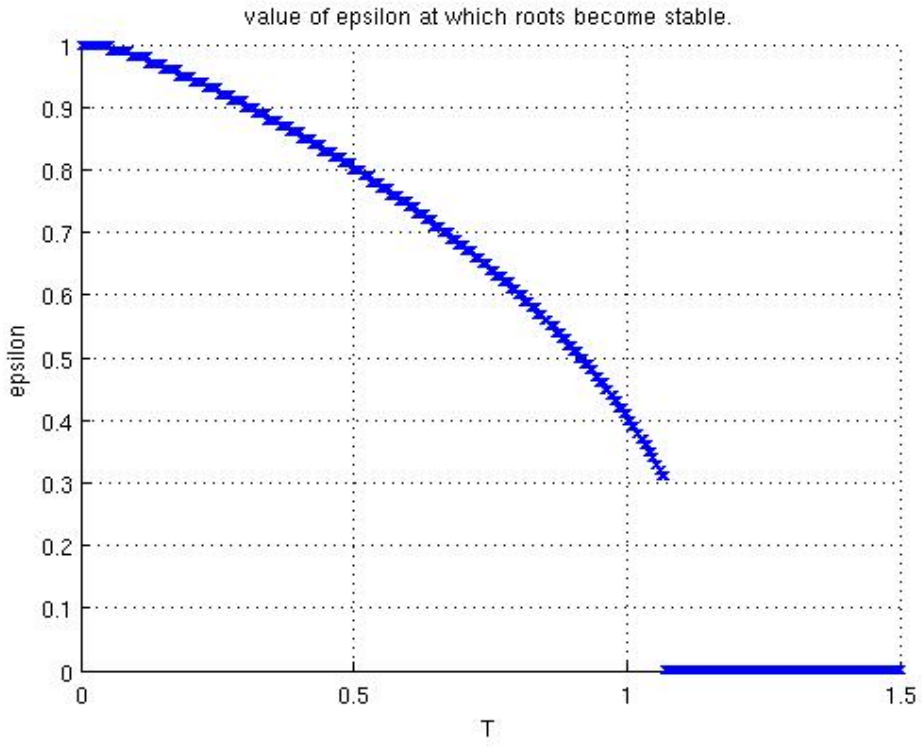

Figure 4.6: *Stability as a function of $\hat{\epsilon}$, the stable region is shown above the curve. There is a discontinuity since between $1 < T^2 < 4/3$ the friction is actually found to destabilize the flow.*

analog of vertical diffusivity in the continuously stratified system), the frictionless case ($\epsilon = 0$) already leads to interesting dynamics; we focus on this. Our aim is to use standard multiple-scale asymptotic analysis to derive an amplitude equation, which will show how the instability stops growing, and reveal the nature of the subsequent dynamics. We will be able to compare this with the amplitude equations of Zhao and Ghil (1991) and Griffiths (2003b) for other types of weakly nonlinear inertial instabilities.

As before, we take a basic shear flow $\bar{u} = y$, and rewrite (4.6) - (4.9) with the linear terms

on the left hand side and the nonlinear terms on the right hand side.

$$\frac{\partial u}{\partial t} + (1-y)v = v\bigg(- \frac{\partial \bar{u}_{non}}{\partial y} + (1-2\alpha)\frac{\partial u}{\partial y} + 2\alpha(1-\alpha)h\frac{\partial u}{\partial y} + \alpha(1-\alpha)u\frac{\partial h}{\partial y}\bigg) = \mathcal{N}_1, \quad (4.41)$$

$$\frac{\partial v}{\partial t} + yu + g\frac{\partial h}{\partial y} = v\bigg((1-2\alpha)\frac{\partial v}{\partial y} + 2\alpha(1-\alpha)h\frac{\partial v}{\partial y} + \alpha(1-\alpha)v\frac{\partial h}{\partial y}\bigg) = \mathcal{N}_2, \quad (4.42)$$

$$\frac{\partial h}{\partial t} + \frac{\partial v}{\partial y} = \frac{\partial}{\partial y}\bigg((1-2\alpha)hv + \alpha(1-\alpha)h^2 v\bigg) = \mathcal{N}_3, \quad (4.43)$$

$$\frac{\partial \bar{u}_{non}}{\partial t} = -\frac{\partial}{\partial y}\bigg(D_1 D_2 uv\bigg) = \mathcal{N}_4, \quad (4.44)$$

where we take $\bar{u} = y + \bar{u}_{non}$ and where we have dropped the "$\sim$" notation. We can form a single equation for v by taking $\partial/\partial t$ of (4.42) and substituting for $\partial u/\partial t$ and $\partial h/\partial t$ from (4.41) and (4.43) respectively to obtain

$$\frac{\partial^2 v}{\partial t^2} + y(y-1)v - g\frac{\partial^2 v}{\partial y^2} = -g\frac{\partial \mathcal{N}_3}{\partial y} - y\mathcal{N}_1 + \frac{\partial \mathcal{N}_2}{\partial t}. \quad (4.45)$$

The linear analysis of (4.45) was performed after a rescaling of coordinates. We will therefore use the same rescaling here, $y - 1/2 = Y/L$ where $L = (4/g)^{1/4}$. Transforming equations (4.41) and (4.43) - (4.45) into the new variable Y we have

$$\frac{\partial u}{\partial t} + \left(\frac{1}{2} - Y\left(\frac{g}{4}\right)^{1/4}\right)v = v\left(\frac{4}{g}\right)^{1/4}\bigg(- \frac{\partial \bar{u}_{non}}{\partial Y} + (1-2\alpha)\frac{\partial u}{\partial Y} + 2\alpha(1-\alpha)h\frac{\partial u}{\partial Y} + \alpha(1-\alpha)u\frac{\partial h}{\partial Y}\bigg) = \tilde{\mathcal{N}}_1, \quad (4.46)$$

$$\frac{\partial h}{\partial t} + \left(\frac{4}{g}\right)^{1/4}\frac{\partial v}{\partial Y} = \left(\frac{4}{g}\right)^{1/4}\frac{\partial}{\partial Y}\bigg((1-2\alpha)hv + \alpha(1-\alpha)h^2 v\bigg) = \tilde{\mathcal{N}}_3, \quad (4.47)$$

$$\frac{\partial \bar{u}_{non}}{\partial t} = -\left(\frac{4}{g}\right)^{1/4} \frac{\partial}{\partial Y}\left(D_1 D_2 uv\right) = \tilde{\mathcal{N}}_4, \tag{4.48}$$

$$2g^{1/2}\frac{\partial^2 v}{\partial Y^2} - \frac{\partial^2 v}{\partial t^2} - \left(Y^2\left(\frac{g}{4}\right)^{1/2} - \frac{1}{4}\right)v = \left(Y\left(\frac{g}{4}\right)^{1/4} + \frac{1}{2}\right)\tilde{\mathcal{N}}_1 + g\left(\frac{4}{g}\right)^{1/4}\frac{\partial \tilde{\mathcal{N}}_3}{\partial Y} - \frac{\partial \tilde{\mathcal{N}}_2}{\partial t}. \tag{4.49}$$

4.4.1 Weakly nonlinear scaling

Now since the strength of the instability is determined by the growth rate, to look at the weakly nonlinear regime we look at a region of small growth rate. Recall the linear dispersion relation with the most unstable mode $n = 0$ is given by

$$s^2 = \frac{1}{4} - g^{1/2}, \tag{4.50}$$

which has marginal stability when $g^{1/2} = g_c^{1/2} = 1/4$. To obtain weak instability we therefore set $g^{1/2} = 1/4 - \delta^2$ (a small deviation of g away from the critical value g_c). We have $s^2 = \delta^2$. Then provided $\delta \ll 1$ we are weakly unstable. We also introduce a rescaled (long) time $\tau = \delta t$ and use a Taylor series expansion of $(4/g)^{1/4}$ and $(g/4)^{1/4}$. It is also necessary to introduce scalings for $\hat{u}$, $\hat{v}$, $\hat{h}$ and $\bar{u}_{non}$. Presumably they will all remain small, and thus each scale like some power of δ. However, it is not clear what those powers should be. In (4.45) and (4.49) the leading order balance will be linear, with $\partial u/\partial t \sim v$ and $\partial h/\partial t \sim v$, implying $\delta u \sim v$ and $\delta h \sim v$. So, if $v \sim \delta^n$, we know $u \sim h \sim \delta^{(n-1)}$. Then, from (4.47), we have $\delta \bar{u}_{non} \sim uv \sim \delta^{(2n-1)}$, so $\bar{u}_{non} \sim \delta^{(2n-2)}$. However, this process does not determine n uniquely. We find from consideration of the nonlinear terms (below) that we should take $n = 3$ to get interesting dynamics. So $v \sim \delta^3$,

$u \sim h \sim \delta^2$ and $\bar{u}_{non} \sim \delta^4$. We thus introduce asymptotic expansions

$$v = \delta^3 v_1 + \delta^5 v_2 + \ldots, \qquad u = \delta^2 u_1 + \delta^4 u_2 + \ldots, \tag{4.51}$$

$$h = \delta^2 h_1 + \delta^4 h_2 + \ldots, \qquad \bar{u}_{non} = \delta^4 \bar{u}_1 + \delta^6 \bar{u}_2 + \ldots. \tag{4.52}$$

These scalings show a meridional flow weaker than the zonal flow, which reflects what is found in observations of the atmosphere and ocean (Zhao and Ghil, 1991). With these scalings, equations (4.46) - (4.49) become

$$\begin{aligned}\delta\frac{\partial}{\partial\tau}(\delta^2 u_1 + \delta^4 u_2 + \ldots) + \left(\frac{1}{2} - \left(\frac{Y}{2\sqrt{2}}(1-2\delta^2)\right)(\delta^3 v_1 + \delta^5 v_2 + \ldots) = \\ 2\sqrt{2}(1+2\delta^2)(\delta^3 v_1 + \delta^5 v_2 + \ldots)\Bigg(- \frac{\partial}{\partial Y}(\delta^4\bar{u}_1 + \delta^6\bar{u}_2 + \ldots) \\ + (1-2\alpha)\frac{\partial}{\partial Y}(\delta^2 u_1 + \delta^4 u_2 + \ldots) + 2\alpha(1-\alpha)(\delta^2 h_1 + \delta^4 h_2 + \ldots)\frac{\partial}{\partial Y}(\delta^2 u_1 + \delta^4 u_2 + \ldots) \\ + \alpha(1-\alpha)(\delta^2 u_1 + \delta^4 u_2 + \ldots)\frac{\partial}{\partial Y}(\delta^2 h_1 + \delta^4 h_2 + \ldots)\Bigg),\end{aligned} \tag{4.53}$$

$$\begin{aligned}\delta\frac{\partial}{\partial\tau}(\delta^2 h_1 + \delta^4 h_2 + \ldots) + 2\sqrt{2}(1+2\delta^2)\frac{\partial}{\partial Y}(\delta^3 v_1 + \delta^5 v_2 + \ldots) = \\ 2\sqrt{2}(1+2\delta^2)\frac{\partial}{\partial Y}\Bigg((1-2\alpha)(\delta^2 h_1 + \delta^4 h_2 + \ldots)(\delta^3 v_1 + \delta^5 v_2 + \ldots) \\ + \alpha(1-\alpha)(\delta^2 h_1 + \delta^4 h_2 + \ldots)^2(\delta^3 v_1 + \delta^5 v_2 + \ldots)\Bigg),\end{aligned} \tag{4.54}$$

$$\delta\frac{\partial}{\partial\tau}(\delta^4\bar{u}_1 + \delta^6\bar{u}_2 + \ldots) = -2\sqrt{2}(1+2\delta^2)\frac{\partial}{\partial Y}\Bigg(D_1 D_2(\delta^2 u_1 + \delta^4 u_2 + \ldots)(\delta^3 v_1 + \delta^5 v_2 + \ldots)\Bigg) \tag{4.55}$$

and lastly,

$$\begin{aligned}
&\frac{1}{2}(1-4\delta^2)\frac{\partial^2}{\partial Y^2}(\delta^3 v_1+\delta^5 v_2+\ldots)-\delta^2\frac{\partial^2}{\partial \tau^2}(\delta^3 v_1+\delta^5 v_2+\ldots)\\
&\qquad -\left(\frac{Y^2}{8}(1-4\delta^2)-\frac{1}{4}\right)(\delta^3 v_1+\delta^5 v_2+\ldots)=\\
&(Y+\sqrt{2}(1+2\delta^2))(\delta^3 v_1+\delta^5 v_2+\ldots)\Bigg(-\frac{\partial}{\partial Y}(\delta^4\bar{u}_1+\delta^6\bar{u}_2+\ldots)+(1-2\alpha)\frac{\partial}{\partial Y}(\delta^2 u_1+\delta^4 u_2+\ldots)\\
&\qquad +2\alpha(1-\alpha)(\delta^2 h_1+\delta^4 h_2+\ldots)\frac{\partial}{\partial Y}(\delta^2 u_1+\delta^4 u_2+\ldots)\\
&\qquad +\alpha(1-\alpha)(\delta^2 u_1+\delta^4 u_2+\ldots)\frac{\partial}{\partial Y}(\delta^2 h_1+\delta^4 h_2+\ldots)\Bigg)\\
&\quad +2\left(\frac{1}{4}-\delta^2\right)\frac{\partial^2}{\partial Y^2}\Bigg((1-2\alpha)(\delta^2 h_1+\delta^4 h_2+\ldots)(\delta^3 v_1+\delta^5 v_2+\ldots)\\
&\qquad +\alpha(1-\alpha)(\delta^2 h_1+\delta^4 h_2+\ldots)^2((\delta^3 v_1+\delta^5 v_2+\ldots))\Bigg)\\
&-2\delta\sqrt{2}(1+2\delta^2)\frac{d}{d\tau}\Bigg((\delta^3 v_1+\delta^5 v_2+\ldots)\Bigg((1-2\alpha)\frac{\partial}{\partial Y}(\delta^3 v_1+\delta^5 v_2+\ldots)+\\
&\qquad 2\alpha(1-\alpha)(\delta^2 h_1+\delta^4 h_2+\ldots)\frac{\partial}{\partial Y}(\delta^3 v_1+\delta^5 v_2+\ldots)\\
&\qquad +\alpha(1-\alpha)(\delta^3 v_1+\delta^5 v_2+\ldots)\frac{\partial}{\partial Y}(\delta^2 h_1+\delta^4 h_2+\ldots)\Bigg)\Bigg)=0. \quad (4.56)
\end{aligned}$$

4.4.2 Leading-order terms

The next step is to equate powers of δ. We choose to start with (4.56) because it gives us a familiar differential equation in v which we have seen in previous analysis. At order δ^3 we have

$$\frac{\partial^2 v_1}{\partial Y^2}+\left(\frac{1}{2}-\frac{Y^2}{4}\right)v_1=0.$$

This is the familiar parabolic cylinder equation. However now it is not an eigenvalue problem and there is one specific solution bounded as $|Y|\to\infty$ given by

$$v_1=A(\tau)\exp\left(-Y^2/4\right). \quad (4.57)$$

From (4.53) and (4.55) at order δ^3 we then have

$$\frac{\partial u_1}{\partial \tau} + \left(\frac{1}{2} - \frac{Y}{2\sqrt{2}}\right) v_1 = 0 \quad \Rightarrow \quad u_1 = B(\tau)\left(\frac{Y}{2\sqrt{2}} - \frac{1}{2}\right) \exp\left(-Y^2/4\right), \tag{4.58}$$

$$\frac{\partial h_1}{\partial \tau} + 2\sqrt{2}\frac{\partial v_1}{\partial Y} = 0 \quad \Rightarrow \quad h_1 = B(\tau)\sqrt{2}Y \exp\left(-Y^2/4\right); \tag{4.59}$$

here $B_\tau = A$ and we have used (4.47). That completes the leading order analysis.

4.4.3 First-order terms

We now look at the next order terms, starting with the $O(\delta^5)$ terms of (4.56), which yield

$$\frac{\partial^2 v_2}{\partial Y^2} + \left(\frac{1}{2} - \frac{Y^2}{4}\right) v_2 = \\ 4\frac{\partial^2 v_1}{\partial Y^2} + 2\frac{\partial^2 v_1}{\partial \tau^2} - Y^2 v_1 + 2(Y + \sqrt{2})(1 - 2\alpha) v_1 \frac{\partial u_1}{\partial Y} + \frac{\partial^2}{\partial Y^2}\left((1 - 2\alpha) h_1 v_1\right).$$

We substitute for u_1, v_1, h_1, then multiplying by $\exp -Y^2/4$ and integrate over $-\infty \leq Y \leq \infty$. The left hand side then vanishes (using integration by parts), and, after considerable simplification, we are left with

$$0 = -A(\tau)\int_{-\infty}^{\infty} \exp\left(-Y^2/2\right) dY + \frac{d^2 A(\tau)}{d\tau^2}\int_{-\infty}^{\infty} \exp\left(-Y^2/2\right) dY + \\ \frac{(1 - 2\alpha)}{2} A(\tau) B(\tau) \int_{-\infty}^{\infty} \exp\left(-3Y^2/4\right) dY.$$

Since $\int_{-\infty}^{\infty} \exp\left(-aY^2\right) dY = \sqrt{\pi/a}$, evaluating the integrals gives

$$\frac{d^2 A(\tau)}{d\tau^2} = A(\tau) - R A(\tau) B(\tau), \tag{4.60}$$

where $R = (1 - 2\alpha)/\sqrt{6}$. We assume R to be of order unity (or, equivalently, that α is not close to $1/2$); otherwise, an alternative scaling will be needed (see section 4.6.1).

Along with $B_\tau = A$, (4.60) is the governing amplitude equation that we require. Introducing a further variable $C = A_\tau$, we can rewrite this as a third-order system of ODEs:

$$A_\tau = C, \tag{4.61}$$

$$B_\tau = A, \tag{4.62}$$

$$C_\tau = A(\tau) - RA(\tau)B(\tau). \tag{4.63}$$

These equations form the basis for the analysis of the rest of this section.

4.4.4 Properties of the ODE system

Although an explicit solution cannot be found, some progress can be made when trying to solve for A, B and C. Firstly substituting $C_\tau = B_{\tau\tau\tau}$ and $A = B_\tau$ into (4.63) and then integrating we have

$$B_{\tau\tau} = C(\tau) = B - R\frac{B^2}{2} + \kappa_1, \tag{4.64}$$

where $\kappa_1 = C(0) - B(0) + RB^2(0)/2$. Next multiplying (4.64) by B_τ and integrating we have

$$\frac{B_\tau^2}{2} = \frac{A^2}{2} = \frac{B^2}{2} - \frac{RB^3}{6} + \kappa_1 B + \kappa_2, \tag{4.65}$$

where $\kappa_2 = A^2(0)/2 - B^2(0)/2 + RB^3(0)/6 - \kappa_1 B(0)$. We can rewrite this equation as

$$A^2 = f(B), \quad \text{where} \quad f(B) = -\frac{RB^3}{3} + B^2 + 2\kappa_1 B + 2\kappa_2. \tag{4.66}$$

By sketching $A^2 = f(B)$, we can thus determine possible dynamics in the system, and how they depend upon κ_1 and κ_2 (i.e., the initial conditions $A(0)$, $B(0)$ and $C(0)$), and R. For example, regions where $A^2 < 0$ will be inaccessible, and could lead to closed orbits.

To help us to do this we make several observations:

1. To investigate all possible outcomes, we need only consider $R > 0$, (along with all combinations of κ_1 and κ_2). Since $f(B)$ is invariant under the transformation $R \to -R$, $B \to -B$ and $\kappa_1 \to -\kappa_1$, a case with $R < 0$ is equivalent (dynamically) to one with $R > 0$ but the opposite sign of κ_1.

2. With $R > 0$, $f(B) \to -\infty$ as $B \to \infty$, (i.e., there is a maximum possible value for B, where $A^2 = 0$). But $f(B) \to \infty$, as $B \to -\infty$, (i.e., there is no minimum possible value for B).

3. Close to $B = 0$, we have $A^2 \approx 2\kappa_2 B + 2\kappa_1$.

4. Equation (4.65) can be written as

$$A^2 = -\frac{R}{3}(B - a)(B - b)(B - c), \tag{4.67}$$

   where $abc = 6\kappa_2/R$. The nature of the roots of $f(B) = 0$ is thus determined by the sign of κ_2:

   (a) $\kappa_2 > 0$. Then $abc > 0$, and we either have

      i. 3 real roots, (all positive)

      ii. 3 real roots, (2 negative, 1 positive),

      iii. 1 complex conjugate pair, 1 positive real root.

   (b) $\kappa_2 < 0$. The $abc < 0$, and we either have

      i. 3 real roots, (all negative)

      ii. 3 real roots, (1 negative, 2 positive)

      iii. 1 complex conjugate pair, 1 negative real root.

5. $f'(B) = RB^2 + 2B + 2\kappa_1$, so $A^2 = f(B)$ has extrema where

$$B = \frac{1 \pm \sqrt{1 + 2\kappa_1 R}}{2}. \tag{4.68}$$

There are three cases (recalling that we have assumed $R > 0$):

(a) $\kappa_1 > 0$. There is one extremum with $B < 0$ and another with $B > 0$. Since $f''(B) = -2RB + 2$, the extremum in $B < 0$ is a minimum, and thus that in $B > 0$ is a maximum.

(b) $-1/2R \leq \kappa_1 \leq 0$. There are two extrema with $B > 0$. The smaller value of B gives a minimum, and the larger value of B gives a maximum (since $f(B) \to -\infty$ as $B \to \infty$).

(c) $\kappa_1 \leq -1/2R$. There are no extrema (for real B).

With this information we can then draw some conclusions about the solution. Firstly consider $\kappa_1 > 0$ and $\kappa_2 > 0$. We cannot have all roots positive with a positive gradient at the A^2-axis. The possible forms of the solution are therefore case 4(a) (ii) and (iii) and are shown in figure 4.7.

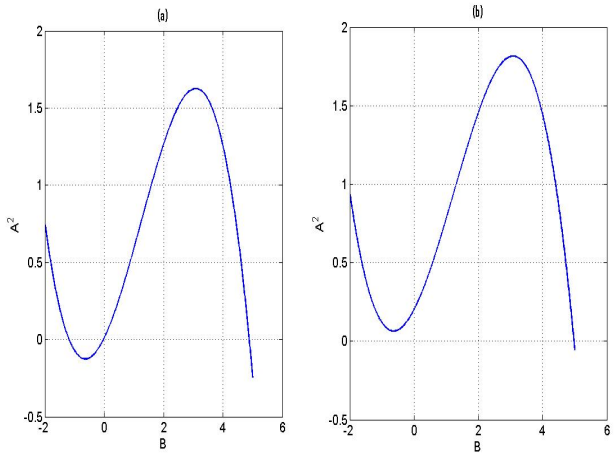

Figure 4.7: *Possible forms the solution of (4.65) could take in the case where $\kappa_1 > 0$ and $\kappa_2 > 0$, i.e. an illustration of case 4(a) (ii) and (iii) where $\kappa_1 > 0$.*

Next we consider $\kappa_2 > 0$ and $\kappa_1 < 0$. We can only have Case 4(a) (i) and (iii), which are shown in figure 4.8. Case 4(a) (ii) implies the maxima and minima occur when $B < 0$ and we can see from (4.68) this cannot be the case.

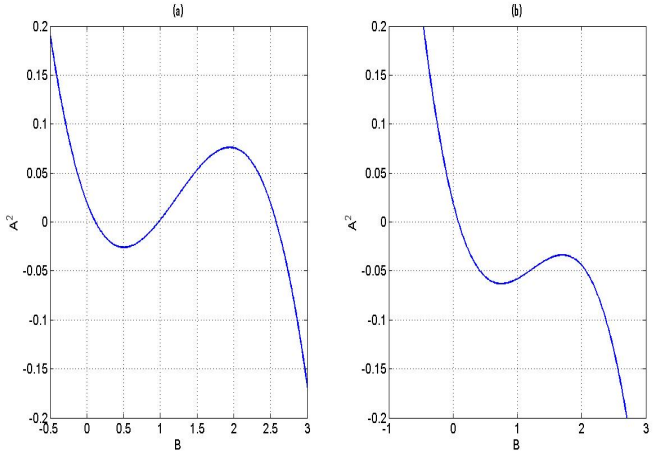

Figure 4.8: *Possible forms the solution of (4.65) could take in the case where $\kappa_1 < 0$ and $\kappa_2 > 0$, i.e. an illustration of case 4(a) (i) and (iii) where $\kappa_1 < 0$.*

Now changing the sign of κ_2 changes the intercept with the A^2-axis to be negative. Firstly consider $\kappa_2 < 0$ with $\kappa_1 > 0$; here we can only have case 4(b) (ii) and (iii), we cannot have all three roots negative with a positive gradient at the A^2-axis. The two possible solutions are shown in figure 4.9. It is important, however, to note that case 4(b) (iii) does not produce a cyclic orbit for A; only a solution that grows indefinitely is found here.

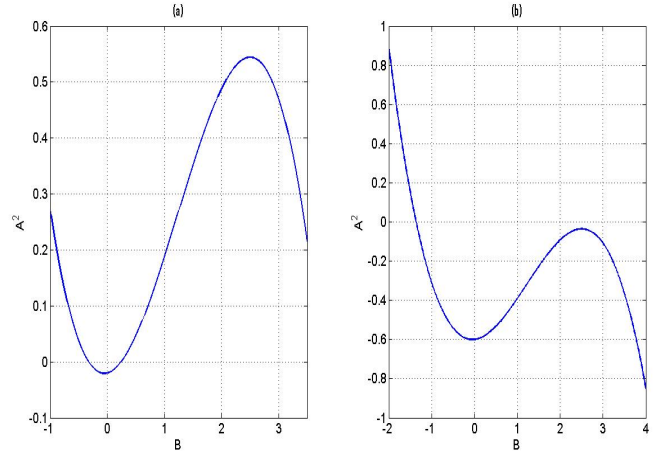

Figure 4.9: *Possible forms the solution of (4.65) could take in the case where $\kappa_1 > 0$ and $\kappa_2 < 0$, i.e. an illustration of case 4(b) (ii) and (iii) with $\kappa_1 > 0$.*

Lastly we consider $\kappa_2 < 0$ and $\kappa_1 < 0$; again we cannot have case 4(b) (i) since this implies both maxima and minima occur where $B < 0$ and from (4.68) this cannot be the case. We therefore can only have case 4(b) (ii) and (iii) as shown in figure 4.10. However again we note that case 4(b) produces no cyclic orbit, rather only producing a solution that grows indefinitely in A and B. It should be noted that like the dynamics found by

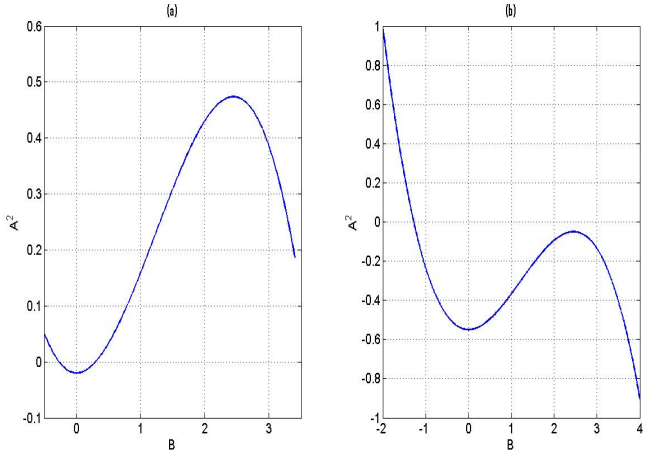

Figure 4.10: *Possible forms the solution of (4.65) could take in the case where $\kappa_1 < 0$ and $\kappa_2 < 0$, i.e. an illustration of case 4(b) (ii) and (iii) with $\kappa_1 < 0$.*

Zhao and Ghil (1991) produce two closed cyclic orbits; the system does not display the behaviour of A growing indefinitely to infinity as $B \to \pm\infty$. However, with the addition of vertical shear the cyclic orbit becomes a limit cycle with the amplitude of the horizontal velocities approaching some limit smaller than their initial amplitude.

Small amplitude

Now consider the case where the instability takes the form of a linear disturbance (i.e., the weakly nonlinear terms are initially negligible), in which case (4.61) becomes $A_{\tau\tau} = A$. Then the growing mode has $A = A(0)\exp(\tau)$ (with $A(0) \ll 1$ for consistency), with B and C following from (4.62) and (4.63): $B = C = A(0) = \exp(\tau)$. So $B(0) = C(0) =$

$A(0) \ll 1$. Then (4.64) and (4.65) imply κ_1 and κ_2, so that

$$C(\tau) = B - R\frac{B^2}{2} + \frac{RA^2(0)}{2} \tag{4.69}$$

and

$$\frac{A^2(\tau)}{2} = \frac{B^2}{2} - \frac{RB^3}{6} + \frac{RA^2(0)B(\tau)}{2} - \frac{RA^3(0)}{3}. \tag{4.70}$$

The interesting result comes from looking at the maximum of $A = A_{max}$. At the maximum of A we have $dA/d\tau = d^2B/d\tau^2 = C = 0$ and hence from (4.69)

$$0 = B_* - \frac{R}{2}B_*^2 + \frac{RA^2(0)}{2} \quad \Rightarrow \quad B_* = \frac{1 \pm \sqrt{1 + R^2A(0)^2}}{R}, \tag{4.71}$$

where B_* is the value of B when $A = A_{max}$. Since we have assumed $A(0) \ll 1$, it follows that $B_* = 2/R$. Substituting in (4.70) and ignoring terms involving $A^2(0)$ and $A^3(0)$ we have

$$A_{max} = \frac{2}{\sqrt{3}R}.$$

We can perform a similar analysis to find the maximum of B when $A(0)$ and $B(0)$ are small; at the maximum of B we have $dB/d\tau = 0$ and from (4.70) we find

$$B_{max} = \frac{3}{R}. \tag{4.72}$$

4.4.5 Numerical solutions of the amplitude equation

Having exhausted analytical methods for solving the amplitude equations (4.63)-(4.61), we now turn to numerical methods. We solve (4.63)-(4.61) using a 4th order Runge-Kutta scheme which is given in more detail in Appendix C. The main reasons for choosing such a scheme is the advantage of a large stability region compared to other schemes such as a 3rd order Runge-Kutta or Adams Bashforth method. We write the initial values of A, B

and C in the form

$$A(\tau) = A_0 \exp \tau, \quad B(\tau) = B_0 \exp \tau, \quad C(\tau) = C_0 \exp \tau, \tag{4.73}$$

where A_0, B_0 and C_0 sets the amplitude of the initial disturbance. We allow for variations in A_0, B_0 and C_0; this in turn will vary the initial conditions.

$\kappa_1, \kappa_2 > 0$

Our first example will be case 4(a) (ii) shown in figure 4.7 (a), where κ_1 and κ_2 are both positive. We manipulate κ_1 and κ_2 by changing A_0, B_0, and C_0; hence taking $A_0 = 0.7$ $B_0 = 0.4$, and $C_0 = 0.5$ we have $\kappa_1 = 0.4163$ and $\kappa_2 = 0.0606$. We find the solutions form a periodic orbit with B becoming negative, causing the cyclic orbit to cross the A-axis in figure 4.12. We find a solution which is in alignment with figure 4.7 (a). The solution of A and B with time is shown in Figure 4.11; we can see here that as A and B grows, A reaches a maximum before decaying, passing through zero as B reaches its maximum. As B then decays, A now grows negatively before reaching a negative maximum before decaying again with B. They both pass through zero to start the cycle again.

In the next example we show case 4(a) (iii) as shown in 4.8 (b), here we have an interesting case as the solution almost completes one cycle; however it then follows a path that takes the solution to infinity. We take $A_0 = 0.325$, $B_0 = 0.0125$ and $C_0 = 0.125$ and we have $\kappa_1 = 0.1219$ and $\kappa_2 = 0.0513$. The solution of A and B plotted against time is shown in figure 4.13 and we can clearly see the solution goes through one cycle before growing to negative infinity. It is clear why this is the case looking at figure 4.14, where we plot A against B with the cubic polynomial (4.65). This solution is found to be in alignment with figure 4.8 (b).

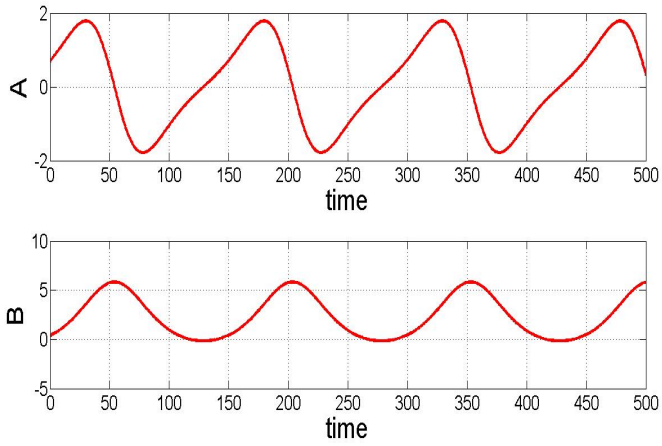

Figure 4.11: *The numerical solution to the ODE system (4.61) - (4.63) where $A_0 = 0.7$, $B_0 = 0.4$, and $C_0 = 0.5$. Here we have case 4(a) (ii) with $\kappa_1 > 0$ and $\kappa_2 > 0$, indicating the solution follows a cyclic orbit in A and B.*

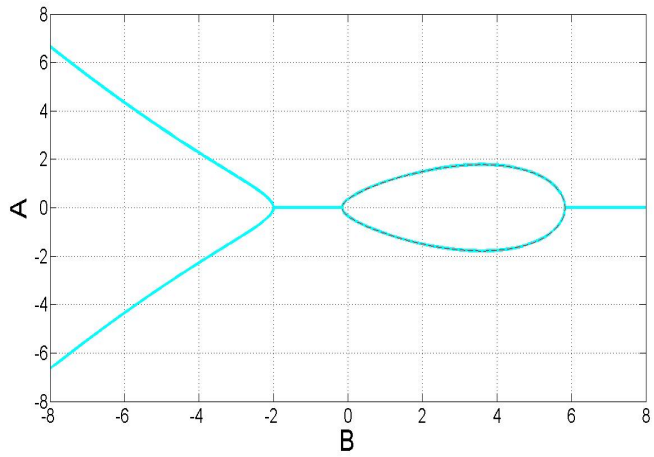

Figure 4.12: *The cyclic orbit numerical solution of (4.61) - (4.63) (dash line) showing A against B where $A_0 = 0.7$, $B_0 = 0.4$, and $C_0 = 0.5$. Here we have case 4(a) (ii) with $\kappa_1 > 0$ and $\kappa_2 > 0$, indicating the solution follows a cyclic orbit in A and B. Also plotted is the cubic function (4.66) (cyan).*

$\kappa_1 < 0$, $\kappa_2 > 0$

We now look at the case where $\kappa_1 < 0$ and $\kappa_2 > 0$. We do this by taking $A_0 = B_0 = -C_0 = 0.0012$; here we have $\kappa_1 = -0.1186$ and $\kappa_2 = 0.0302$ and we have case 4(a) (i)

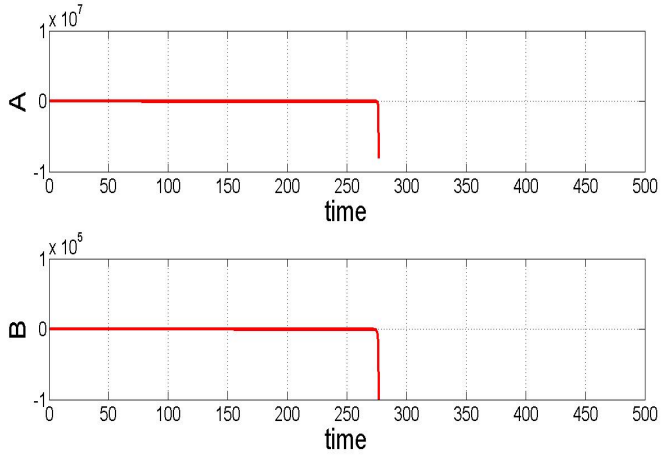

Figure 4.13: *The numerical solution to the ODE system (4.61) - (4.63) where $A_0 = 0.325$, $B_0 = 0.0125$ and $C_0 = 0.125$. Here we have case 4(a) (ii) with $\kappa_1 > 0$ and $\kappa_2 > 0$; the solution seems to follow a periodic orbit in A and B, however the orbit is not quite complete and the solution follows a trajectory to infinity.*

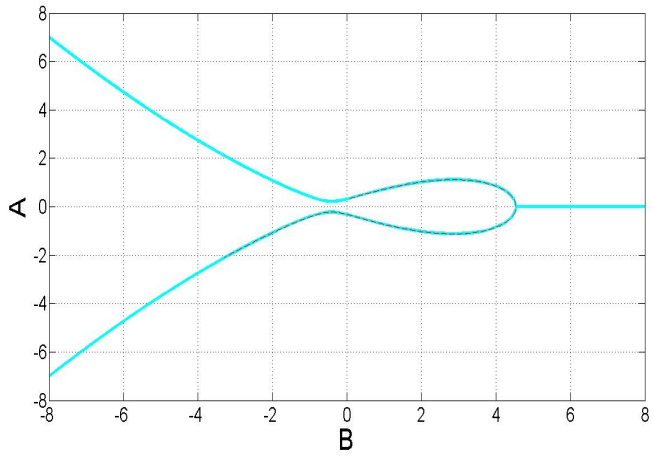

Figure 4.14: *The numerical ODE solution of (4.61) - (4.63) (dashed line) showing A against B where $A_0 = 0.325$, $B_0 = 0.0125$ and $C_0 = 0.125$. The solution seems to follow a periodic orbit in A and B, however the orbit is not quite complete and the solution follows a trajectory to infinity. Also plotted is the cubic function (4.66) (cyan).*

as shown in figure 4.8 (a). The solution of A and B is plotted in figure 4.15 with A plotted against B in figure 4.16. We can see that although there exists a cyclic orbit the solution

does not follow it, instead it falls on the path of the cubic which take A and B to negative infinity. This is in agreement with figure 4.8 (a). It was found that changing the initial condition to manipulate the solution into the cyclic orbit changed the values of κ_1 and κ_2 and therefore changed the cubic itself. A cyclic orbit of this form was not found although it may exist.

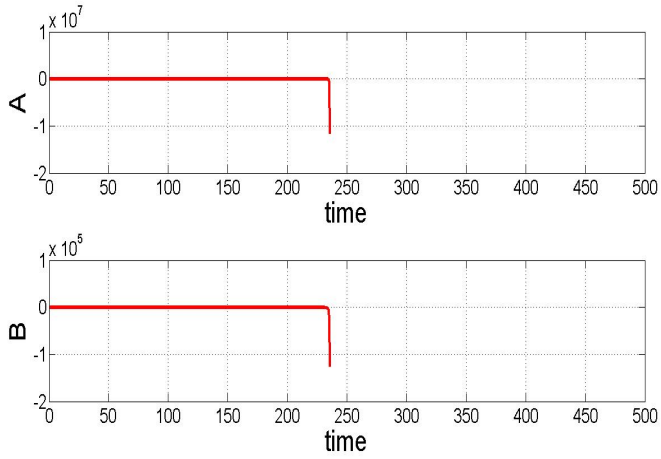

Figure 4.15: *The numerical solution to the ODE system (4.61) - (4.63), where* $A_0 = B_0 = -C_0 = 0.0012$. *Here we have case 4(a) (i) with* $\kappa_1 < 0$ *and* $\kappa_2 > 0$, *the solution does not follow a periodic orbit in* A *and* B.

There was one other form the solution could take when $\kappa_1 < 0$ and $\kappa_2 > 0$, which is case 4(a) (iii) shown in figure 4.8 (b), where there is only one real root. To do this we take $A_0 = 1.8750$, $C_0 = -1.25$ and $B_0 = 0.1250$ and we have $\kappa_1 = -0.6939$ and $\kappa_2 = 1.9208$. We can see from figure 4.17, where A is plotted against B, the cyclic orbit on the right hand side has disappeared as two of the roots to the cubic (4.65) have become complex. The solution has no choice but to land on a path that grows indefinitely negative.

$\kappa_1 > 0$, $\kappa_2 < 0$

We now move on to look at $\kappa_2 < 0$ starting with $\kappa_1 > 0$. We can either have three real roots (2 positive and 1 negative) or one negative root with a complex conjugate pair. To

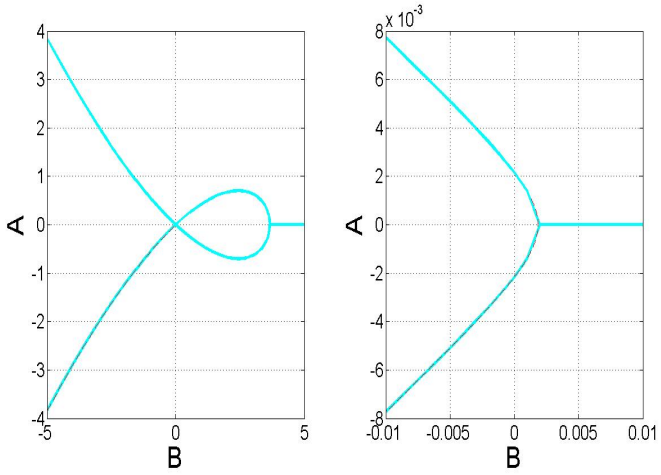

Figure 4.16: *The numerical solution to the ODE system (4.61) - (4.63) (dashed line), where $A_0 = B_0 = -C_0 = 0.0012$. Here we have case 4(a) (i) with $\kappa_1 < 0$ and $\kappa_2 > 0$, the solution does not follow a periodic orbit in A and B. Also plotted is the cubic function (4.66) (cyan).*

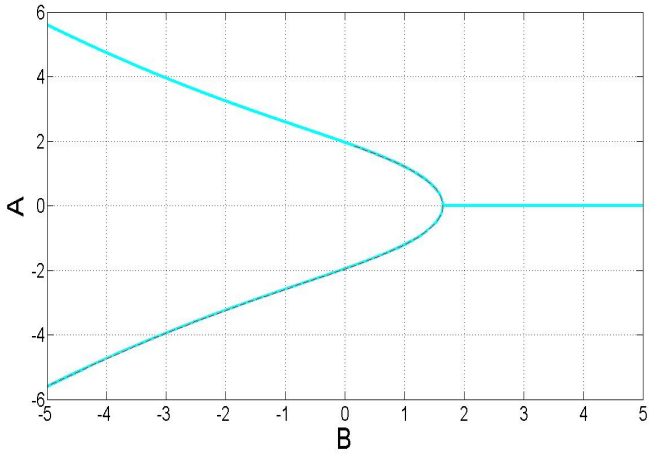

Figure 4.17: *The numerical solution of (4.61) - (4.63) (dashed line) showing A against B where $A_0 = 1.8750$, $C_0 = -1.25$ and $B_0 = 0.1250$. Here the solution illustrated case 4(a) (iii) with $\kappa_1 < 0$ and $\kappa_2 > 0$ The cubic function (4.66) is also shown (cyan).*

show the first we take $A_0 = -0.1250$, $C_0 = B_0 = 0.1250$ and have $\kappa_1 = 0.005$ and $\kappa_2 = -0.0011$ and we therefore have case 4(b) (ii) as shown in figure 4.9 (a). It was not possible from repeated trial and error to demonstrate case 4(b) (iii) where two of the roots turn complex.

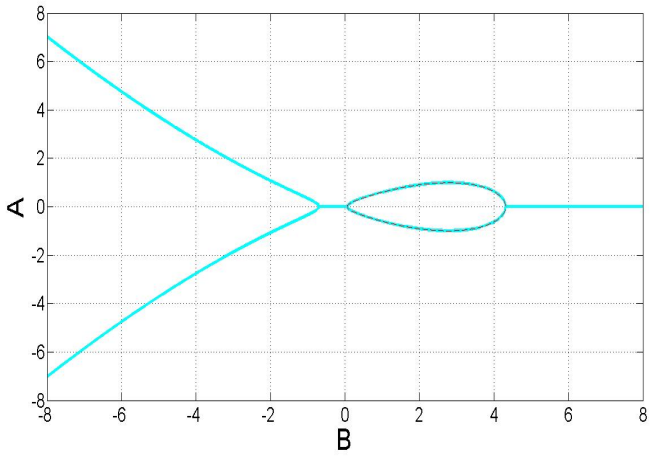

Figure 4.18: *The numerical solution of (4.61) - (4.63) (dashed line) showing A and B where $A_0 = -0.1250$ and $C_0 = B_0 = 0.1250$. Here we have case 4(b) (ii) where $\kappa_1 > 0$ and $\kappa_2 < 0$. The cubic function (4.66) is also shown (cyan).*

$\kappa_1 < 0$, $\kappa_2 < 0$

In figure 4.19 we show an example of the ODE solution with both κ_1 and κ_2 negative, here $A_0 = 1.25 \times 10^{-3}$, $B_0 = 0.5$ and $C_0 = 0.05$. It is worth noting here $\kappa_1 = -0.0495$ and $\kappa_2 = -0.0023$. We therefore have case 4(b) (ii) as shown in figure 4.10 (a), where there are three real roots: One negative and two positive. This tells us there exists one cyclic orbit in A and B. We also find that B cannot become negative. The cyclic orbit of A plotted against B is also shown in figure 4.20 and follows the cyclic orbit indicated by the solution to (4.66).

We could not demonstrate case 4(b) (iii) when κ_2 and κ_1 are both negative.

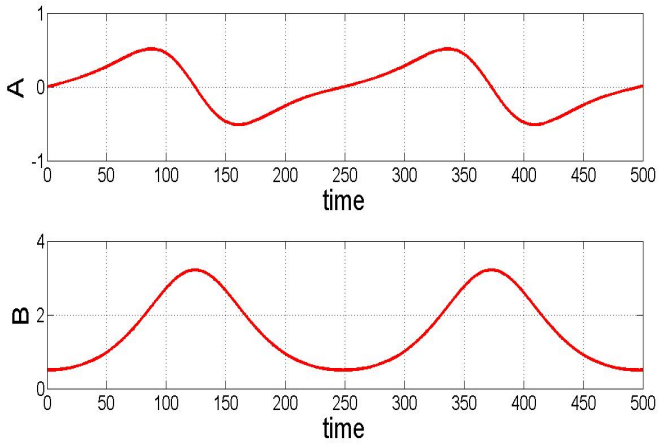

Figure 4.19: *The numerical solution to the ODE system (4.61) - (4.63) where* $A_0 = 1.25 \times 10^{-3}$, $B_0 = 0.5$ *and* $C_0 = 0.05$. *Here we have* $\kappa_1 < 0$ *and* $\kappa_2 < 0$ *indicating the solution follows a periodic orbit in* A *and* B.

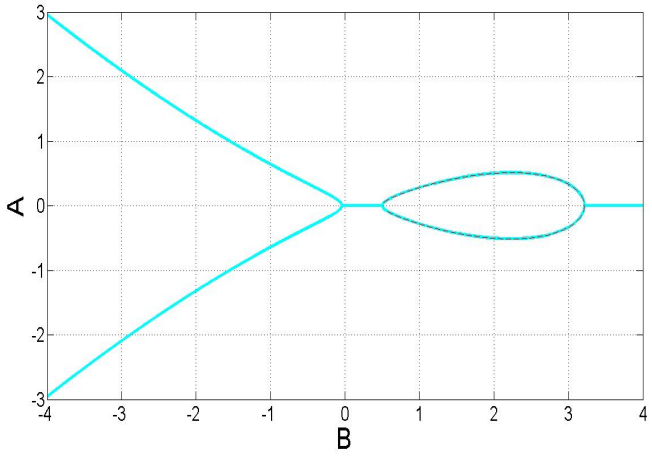

Figure 4.20: *The numerical solution of (4.61) - (4.63) showing* A *against* B *(dashed line), where* $A_0 = 1.25 \times 10^{-3}$, $B_0 = 0.5$ *and* $C_0 = 0.05$. *Here we have* $\kappa_1 < 0$ *and* $\kappa_2 < 0$. *The cubic function (4.66) is also plotted (cyan).*

4.5 Numerical solutions of the moderately nonlinear regime

We now present numerical solutions of the nonlinear PDEs (4.6) - (4.9). This allows us to verify the predictions of the weakly nonlinear analysis when $\delta \ll 1$, and then to

investigate somewhat more unstable regimes when δ is larger. The PDEs were solved using a 4th order Runge-Kutta scheme to step forward in time. The derivatives in the PDEs were evaluated via a Chebyshev differential matrix over an unevenly spaced discretization, outlined in more detail in Appendix C. The PDEs were solved over the domain $y = [-D, D]$ with the following boundary conditions applied at every time step, $v = 0$ at $y = \pm D$.

We also initialize the PDEs with the fastest growing mode which are the solutions to the linear form of equations (4.6) - (4.9) given by

$$v = v_m \exp\left(-L^2(y-1/2)^2/4\right), \quad u = \frac{(y-1)}{s} v_m \exp\left(-L^2(y-1/2)^2/4\right), \tag{4.74}$$

$$h = \frac{v_m L^2}{2s}\left(y - \frac{1}{2}\right) \exp\left(-L^2(y-1/2)^2/4\right), \tag{4.75}$$

where recall $L = (4/g)^{1/4}$. Here, v_m is the amplitude of the initial PDE disturbance. However, in order to compare the ODEs and PDEs we must have $v_m = A_0\delta^3$. Equations (4.6) - (4.9) contain two parameters α which is fixed and g which is variable. The PDEs are related to the ODEs through the relationship shown by (4.50) where $g^{1/2} = 1/4 - \delta^2$.

4.5.1 The moderately nonlinear regime

We first look at the case where $v_m = 1 \times 10^{-4}$, $\delta = 0.08$ and $\alpha = 0.25$. We set the domain length to be $D = 5$ and discretized with $N = 256$ grid points. Here $\kappa_1 = -0.0156$ and $\kappa_2 = -0.0041$. Figure 4.21 shows how both A and B vary with time; it is clear that both A and B enter a periodic orbit. Furthermore figure 4.22 shows A plotted against B, since both κ_1 and κ_2 are negative we have case 4(b) (ii).

We can see from figure 4.22 that as A increases B also increases; B continues to increase as A reaches its maximum before decaying. As A passes though zero, B reaches its maximum value before also decaying. As A reaches its maximum negative value B

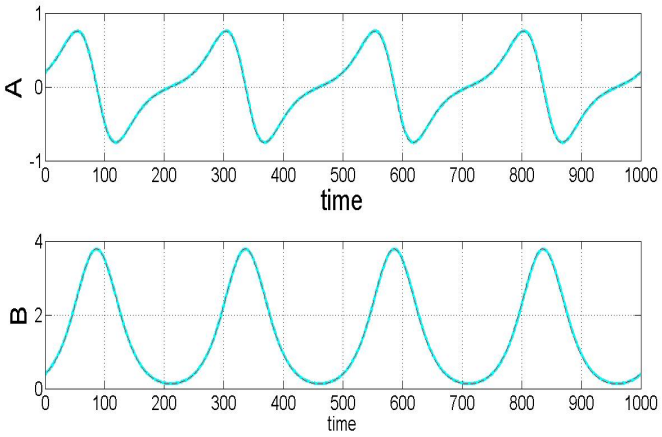

Figure 4.21: *The numerical solution of the PDEs (4.6) - (4.9) (cyan), and ODEs (4.61) - (4.63) (red-). Here $v_m = 1 \times 10^{-4}$ and $\delta = 0.08$ with $\alpha = 0.25$. We can see that the ODEs and PDEs enter a periodic orbit.*

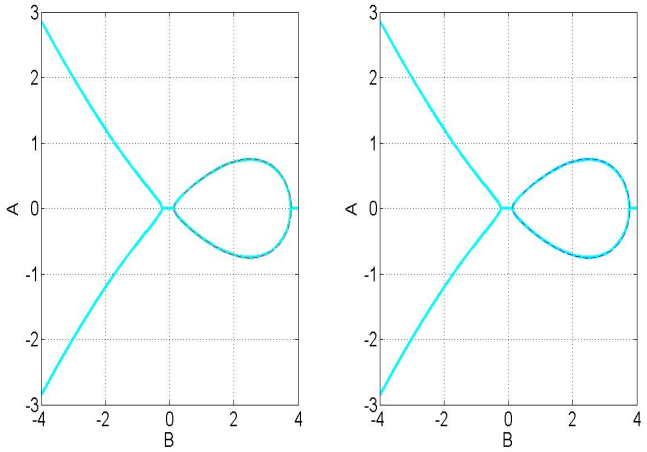

Figure 4.22: *The solution of A plotted against B when $v_m = 1 \times 10^{-4}$ and $\delta = 0.08$ with $\alpha = 0.25$. On the left is the ODE solution (red-) plotted with the solution to (4.66) (cyan). On the right is the PDE solution (blue-) plotted with the solution to (4.66) (cyan).*

continues to decay before both A and B have decayed to their initial amplitude.

The next example we will look at is as above $v_m = 1 \times 10^{-4}$, $\delta = 0.08$, however now with $\alpha = 0.75$, which changes the sign of R. The solution of A plotted against B is shown in

figure 4.23, we can see that the solution does not enter a periodic orbit. Here $\kappa_1 = 0.0156$ and $\kappa_2 = 0.0041$ and we have case 4(a) (iii). However note that the change in α changes the sign of R and we have a "flipped" version of plot 4.7 (b).

Thus, we have shown that in the moderately nonlinear regime the PDEs do behave in accordance with the ODEs derived from the weakly nonlinear analysis.

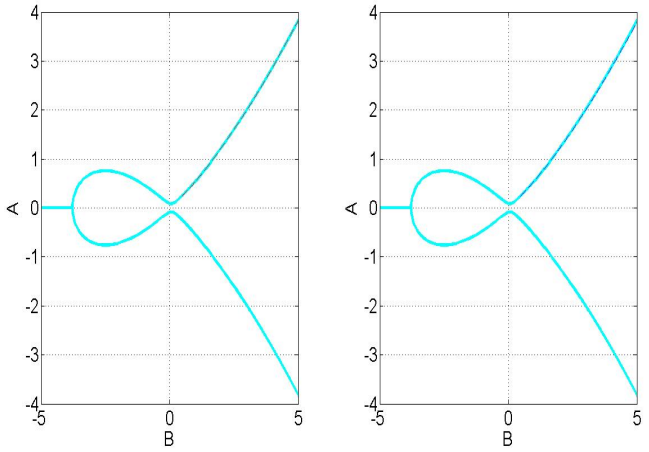

Figure 4.23: *The solution of A plotted against B when $v_m = 1 \times 10^{-4}$ and $\delta = 0.08$ with $\alpha = 0.75$. On the left is the ODE solution (red-) plotted with the solution to (4.66) (cyan). On the right is the PDE solution (blue-) plotted with the solution to (4.66) (cyan).*

4.5.2 The strongly nonlinear regime

In the previous sections we used weakly nonlinear theory to test the numerics used to solve the PDEs. We now push the numerics to achieve the maximum growth rate that is permissible by our model. We have seen during the previous simulations that the PDEs can form a cyclic orbit which puts a cap on the maximum amplitude of A, B and C, where at this point nonlinear terms become large enough to stop any further growth through nonlinear effects. When we push the numerics to their most unstable through an increase in the growth rate, we must consider the physical limitation in the growth of h; our layers

are of a finite depth and hence the disturbance of the interface must not be greater than the depth of either layer.

The strength of the nonlinearity can be adjusted through increasing δ which in turn decreases g and increases the growth rate. Small g is also achieved through small α. This would mean making one layer depth much smaller than the other. However there becomes a fine balancing act between reducing g through small α but not making α too small such that the interface becomes larger than one of the layer depths. Here we experiment with two choices of α: $\alpha = 0.25$ and $\alpha = 0.45$. We will push the PDE numerics to their most nonlinear behavior through increasing δ until the absolute minimum for h has been reached.

Firstly we look at $\alpha = 0.25$ and fix $v_m = 1 \times 10^{-4}$; we increased δ from 0.05 and noted the interface height for each run. The results are shown in figure 4.24; here, δ is plotted against the minimum interface displacement, h. Clearly the limits of the model have been reached when $min(h) \leq -0.25$ and this was where the experiment was stopped. A more accurate figure for δ can be obtained through linearly interpolating the results and it was found that $min(h) = -0.25$ when $\delta = 0.2340$. We also plotted the solutions in two cases when $\alpha = 0.25$, one when $\delta = 0.05$ when the layer depth is not a concern for the solution of the PDEs (figure 4.25) and another case when $\delta = 0.2$ where the limits of the model are closely met (figure 4.26).

Secondly we look at $\alpha = 0.45$ and fix $v_m = 1 \times 10^{-4}$; again we increased δ from 0.05 and noted the interface height h for each run. The results are shown in figure 4.27; as before δ is plotted against the minimum interface displacement h. This time the limit of the model has been reached when $min(h) \leq -0.45$. Through linear interpolation a more accurate figure for δ can be obtained and it was found that $min(h) = -0.45$ when $\delta = 0.1417$. We also plotted the solutions in two cases when $\alpha = 0.45$, one when $\delta = 0.05$ when the layer depth is not a concern for the solution of the PDEs (figure 4.28) and another case when $\delta = 0.14$ where the limits of the model are closely met (figure 4.29).

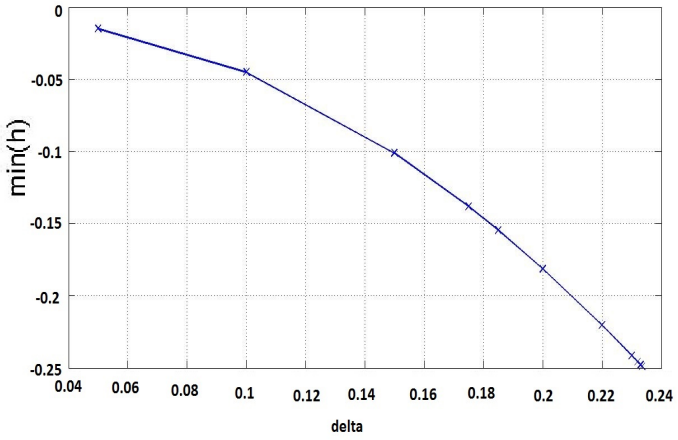

Figure 4.24: *The minimum interface displacement h plotted against δ. In this case $\alpha = 0.25$ and $v_m = 1 \times 10^{-4}$.*

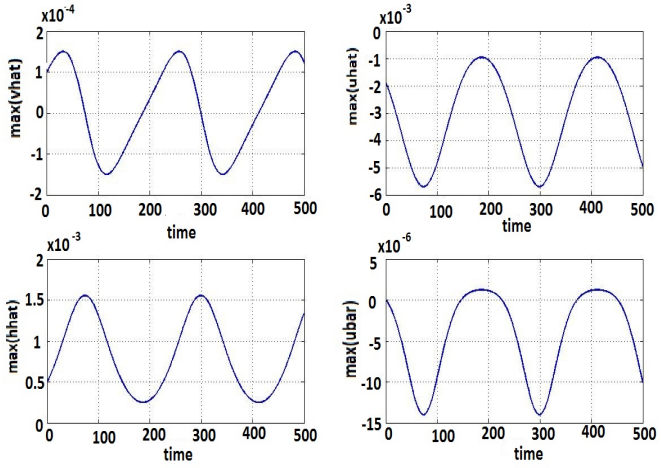

Figure 4.25: *The nonlinear solution of the PDEs when $\alpha = 0.25$, $\delta = 0.05$ and $v_m = 1 \times 10^{-4}$.*

4.5.3 Changes to the mean flow

We need to understand the dynamics of the two-layer system, in particular how are the periodic orbits related to the dynamics of the physical system. To do this we first consider the case where $v_m = 1 \times 10^{-4}$, $\delta = 0.08$ and $\alpha = 0.25$, the results of which are shown in figures 4.21 and 4.22; recall A, B and C entered a periodic orbit. The physical dynamics

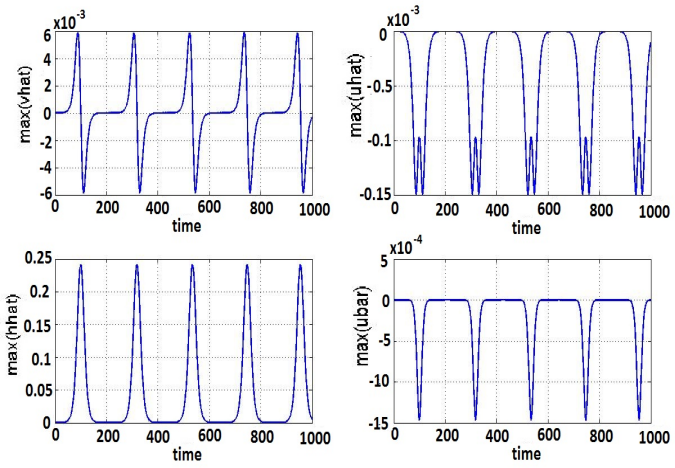

Figure 4.26: *The nonlinear solution of the PDEs when* $\alpha = 0.25$, $\delta = 0.2$ *and* $v_m = 1 \times 10^{-4}$.

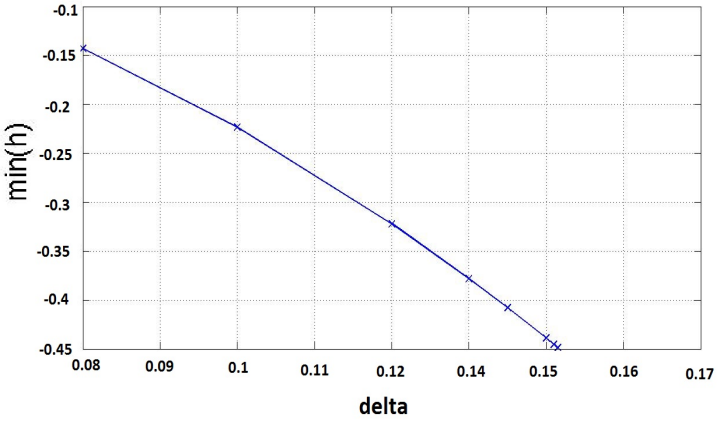

Figure 4.27: *The minimum interface displacement* h *plotted against* δ. *In this case* $\alpha = 0.45$ *and* $v_m = 1 \times 10^{-4}$.

of the flow are as follows: firstly figure 4.30 shows v, u, h and $\bar{u}$ at the point where A has reached its maximum. The shape of v indicates that the flow is strongest at $y = 0$, since $v = v_2 - v_1$. We will assume without loss of generality that, $v_2 > 0$, $v_1 < 0$. The top layer moves to the left and as a result the interface to the left of $y = 0$ dips down to accommodate the displaced fluid. The bottom layer moves to the right and the interface lifts upwards to the right of $y = 0$ to accommodate the displacement of fluid in the bottom

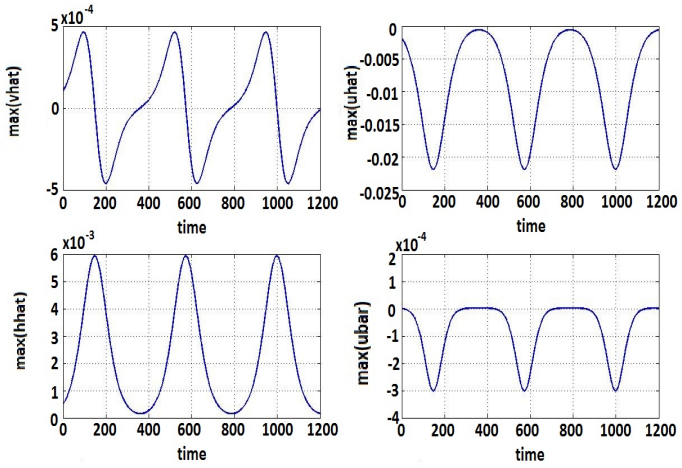

Figure 4.28: *The nonlinear solution of the PDEs when* $\alpha = 0.45$, $\delta = 0.05$ *and* $v_m = 1 \times 10^{-4}$.

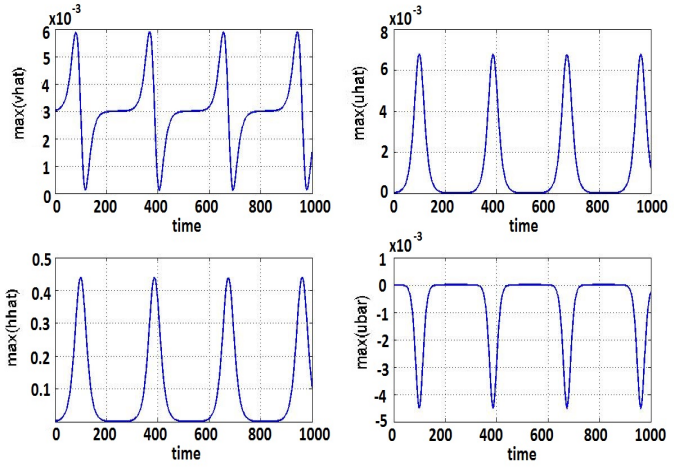

Figure 4.29: *The nonlinear solution of the PDEs when* $\alpha = 0.45$, $\delta = 0.14$ *and* $v_m = 1 \times 10^{-4}$.

layer. Next, as A passed through zero when B is at its maximum as shown in figure 4.31 we have the interface at its maximum displacement ($h \sim \delta^2 B$). Here A is passing through zero and will reverse sign, we therefore have flow in the opposite direction $v_2 < 0$, $v_1 > 0$ and the fluid starts to return, the return flow $v < 0$ reaches a peak as shown in figure 4.32 before reaching its minimum when the fluid has returned to its initial starting point; the cycle is then ready to repeat.

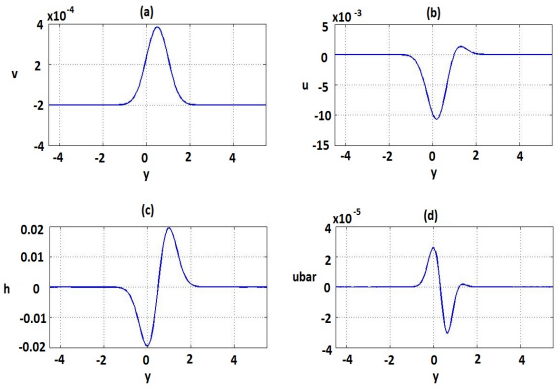

Figure 4.30: *The solution (a) v, (b) u, (c) h, (d) $\bar{u}$ when v has reached its maximum, the interface has lifted to the right of $y = 0$ to accommodate the displacement of fluid which is most predominately shifted to the left in the bottom layer. On the other hand to the left of the origin the interface has dipped down to fill the void of displaced fluid.*

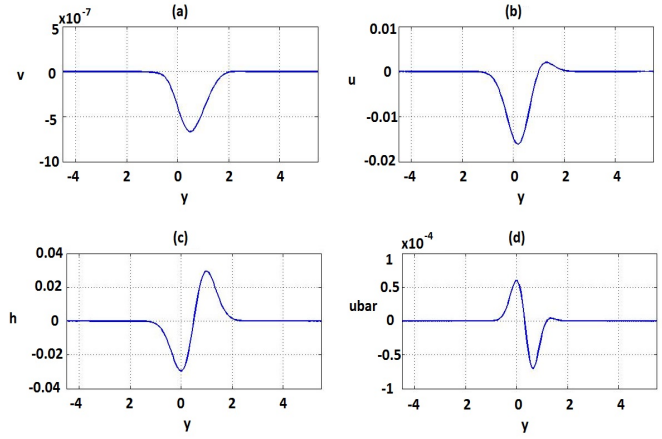

Figure 4.31: *The solution (a) v, (b) u, (c) h, (d) $\bar{u}$ when the interface is at its maximum displacement. Here fluid is just starting to return to its original starting place.*

Since it is the instability that is driving the dynamics of the flow we may wish to consider how the instability itself is altered by the change of flow. There are different ways to look at this; firstly we can look at how the growth rate s changes as the flow evolves and secondly we can look at how fQ evolves (recall we require $fQ < 0$ for instability).

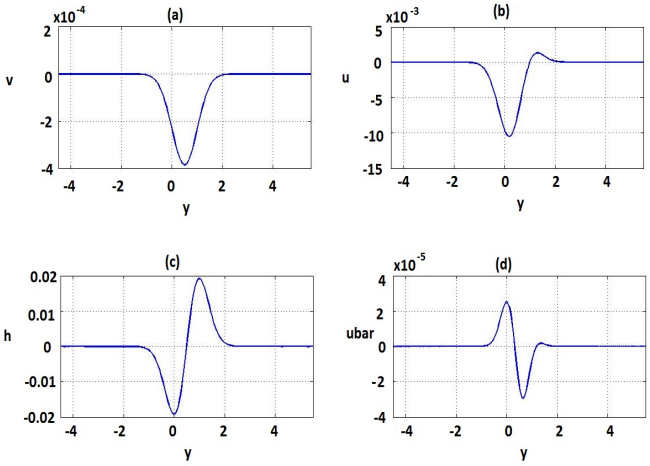

Figure 4.32: *The solution (a) v, (b) u, (c) h, (d) $\bar{u}$ when $v < 0$ is at its maximum strength in the opposite direction returning displaced fluid back to its starting position.*

To plot a continuously evolving growth rate s we would solve the original eigenvalue problem (4.17)

$$\frac{d^2\tilde{v}}{d\tilde{y}^2} - \frac{1}{\tilde{g}}\left(\tilde{s}^2 + fQ\right)\tilde{v} = 0, \tag{4.76}$$

however now we take $fQ = y(y - 1 - \partial\bar{u}/\partial y)$ which incorporates changes to the mean flow. Unfortunately although many methods were tried in order to solve (4.76) they were unsuccessful, this remains something to be investigated. This however was not the case when considering the f-plane as we shall see in section 5.8.

4.6 Special case: $\alpha = 0.5$

It is immediately evident from (4.60) that the amplitude equation is invalid when $\alpha = 0.5$ since $R = 0$ causes the nonlinear terms to disappear. This special case corresponds to our two-layer depths being equal. In fact we can anticipate the breakdown of the scalings we have used in the weakly nonlinear analysis by looking at the full nonlinear, nondimensional governing equations, (4.41) - (4.44). We can see that with $\alpha = 0.5$ some

nonlinear terms disappear. Here we will derive the weakly nonlinear amplitude equations for this special case as we have done previously when $\alpha \neq 0.5$.

First note that the frictionless equations of motion (4.41) - (4.44) with $\alpha = 0.5$ become

$$\frac{\partial u}{\partial t} + (1-y)v = v\bigg(- \frac{\partial \bar{u}_{non}}{\partial y} + \frac{1}{2}h\frac{\partial u}{\partial y} + \frac{1}{4}u\frac{\partial h}{\partial y}\bigg) = \mathcal{N}_1, \tag{4.77}$$

$$\frac{\partial v}{\partial t} + yu + g\frac{\partial h}{\partial y} = v\bigg(\frac{1}{2}h\frac{\partial v}{\partial y} + \frac{1}{4}v\frac{\partial h}{\partial y}\bigg) = \mathcal{N}_2, \tag{4.78}$$

$$\frac{\partial h}{\partial t} + \frac{\partial v}{\partial y} = \frac{\partial}{\partial y}\bigg(\frac{1}{4}h^2 v\bigg) = \mathcal{N}_3, \tag{4.79}$$

$$\frac{\partial \bar{u}_{non}}{\partial t} = -\frac{\partial}{\partial y}\bigg(\bigg(\frac{1}{4} - \frac{1}{16}h^2\bigg)uv\bigg) = \mathcal{N}_4. \tag{4.80}$$

Here we do two things: in section 4.6.1 we derive the weakly nonlinear equations for this special case, in section 4.6.2 we show how these equations correspond to those derived by Zhao and Ghil (1991) in a somewhat different context.

4.6.1 Modified weakly nonlinear analysis

We can form a single equation for v by taking $\partial/\partial t$ of (4.42) and substituting for $\partial u/\partial t$ and $\partial h/\partial t$ from (4.77) and (4.79) respectively to obtain

$$\frac{\partial^2 v}{\partial t^2} + y(y-1)v - g\frac{\partial^2 v}{\partial y^2} = -g\frac{\partial \mathcal{N}_3}{\partial y} - y\mathcal{N}_1 + \frac{\partial \mathcal{N}_2}{\partial t}. \tag{4.81}$$

Since α appears only in the nonlinear terms of the governing equations (4.46) - (4.49) we can conclude that the linear growth rate s remains unchanged.

$$s^2 = \frac{1}{4} - (2n+1)g^{1/2}, \tag{4.82}$$

with $n = 0$ giving the most unstable mode.

Since we have seen that some of the nonlinear terms in (4.46) - (4.49) disappear it will be necessary to calculate the scalings of u, v, h and $\bar{u}_{non}$ using a dominant balance. In (4.46) and (4.47) the leading order balance will be linear, with $\partial u/\partial t \sim v$ and $\partial h/\partial t \sim v$. As before we obtain a weakly nonlinear regime by taking $g^{1/2} = 1/4 - \delta^2$, hence $s^2 = \delta^2$ and we rescale (long) time $\tau = \delta t$, thus implying $\delta u \sim v$ and $\delta h \sim v$. So, if $v \sim \delta^n$, we know $u \sim h \sim \delta^{(n-1)}$. Then, from (4.80), we have $\delta \bar{u}_{non} \sim uv \sim \delta^{(2n-1)}$, so $\bar{u}_{non} \sim \delta^{(2n-2)}$. However, this process does not determine n uniquely. We find from consideration of the nonlinear terms that we should take $n = 2$ to get interesting dynamics. Note that this is different to the case where $\alpha \neq 0.5$ due to the fact that some nonlinear terms have disappeared: in the $\alpha = 0.5$ case v, u and h scale one order of δ less than the $\alpha \neq 0.5$ case, the mean flow, $\bar{u}$ scales two orders of δ less than in the $\alpha = 0.5$ case. In fact we should note here that when $\alpha = 0.5$, v and $\bar{u}$ scale to the same order of δ.

Before we apply these scalings as before we use a transformation of variables by taking $y - 1/2 = Y/L$ where $L = (4/g)^{1/4}$; hence (4.77) and (4.79) - (4.81) become

$$\frac{\partial u}{\partial t} + \left(\frac{1}{2} - Y\left(\frac{g}{4}\right)^{1/4}\right)v = v\left(\frac{4}{g}\right)^{1/4}\left(- \frac{\partial \bar{u}_{non}}{\partial Y} + \frac{1}{2}h\frac{\partial u}{\partial Y} + \frac{1}{4}u\frac{\partial h}{\partial Y}\right) = \tilde{\mathcal{N}}_1, \quad (4.83)$$

$$\frac{\partial h}{\partial t} + \left(\frac{4}{g}\right)^{1/4}\frac{\partial v}{\partial Y} = \left(\frac{4}{g}\right)^{1/4}\frac{\partial}{\partial Y}\left(\frac{1}{4}h^2 v\right) = \tilde{\mathcal{N}}_3, \quad (4.84)$$

$$\frac{\partial \bar{u}_{non}}{\partial t} = -\left(\frac{4}{g}\right)^{1/4}\frac{\partial}{\partial Y}\left(\left(\frac{1}{4} - \frac{1}{16}h^2\right)uv\right) = \tilde{\mathcal{N}}_4. \quad (4.85)$$

$$2g^{1/2}\frac{\partial^2 v}{\partial Y^2} - \frac{\partial^2 v}{\partial t^2} - \left(Y^2\left(\frac{g}{4}\right)^{1/2} - \frac{1}{4}\right)v = \left(Y\left(\frac{g}{4}\right)^{1/4} + \frac{1}{2}\right)\tilde{\mathcal{N}}_1 + g\left(\frac{4}{g}\right)^{1/4}\frac{\partial \tilde{\mathcal{N}}_3}{\partial Y} - \frac{\partial \tilde{\mathcal{N}}_2}{\partial t}. \quad (4.86)$$

Since we have marginal stability when $g^{1/2} = 1/4$, we set $g^{1/2} = 1/4 - \delta^2$, $t = \tau/\delta$ and use

$$\left(\frac{4}{g}\right)^{1/4} = 2\sqrt{2}(1 + 2\delta^2 + \ldots), \quad \text{and} \quad \left(\frac{g}{4}\right)^{1/4} = \frac{1}{2\sqrt{2}}(1 - 2\delta^2 + \ldots). \tag{4.87}$$

Next from using a dominant balance we found appropriate scalings to be

$$v = \delta^2 v_1 + \delta^4 v_2 + \ldots, \quad u = \delta u_1 + \delta^3 u_2 + \ldots, \quad h = \delta h_1 + \delta^3 h_2 + \ldots, \tag{4.88}$$

$$\bar{u}_{non} = \delta^2 \bar{u}_1 + \delta^3 \bar{u}_2 + \ldots. \tag{4.89}$$

After substituting (4.87), (4.88) and (4.89) into (4.83) - (4.86) we have

$$\begin{aligned}\delta\frac{\partial}{\partial\tau}(\delta u_1 + \delta^3 u_2 + \ldots) + \left(\frac{1}{2} - \frac{Y}{2\sqrt{2}}(1 - 2\delta^2 + \ldots)\right)(\delta^2 v_1 + \delta^4 v_2 + \ldots) \\ = (\delta^2 v_1 + \delta^4 v_2 + \ldots)2\sqrt{2}(1 + 2\delta^2 + \ldots)\bigg(- \frac{\partial}{\partial Y}(\delta^2 \bar{u}_1 + \delta^4 \bar{u}_2 + \ldots) + \\ \frac{1}{2}(\delta h_2 + \delta^3 h_2 + \ldots)\frac{\partial}{\partial Y}(\delta u_1 + \delta^3 u_2 + \ldots) + \\ \frac{1}{4}(\delta u_1 + \delta^3 u_2 + \ldots)\frac{\partial}{\partial Y}(\delta h_1 + \delta^3 h_2 + \ldots)\bigg),\end{aligned} \tag{4.90}$$

$$\begin{aligned}\delta\frac{\partial}{\partial\tau}(\delta h_1 + \delta^3 h_2 + \ldots) + 2\sqrt{2}(1 + 2\delta^2 + \ldots)\frac{\partial}{\partial Y}(\delta^2 v_1 + \delta^4 v_2 + \ldots) \\ = 2\sqrt{2}(1 + 2\delta^2 + \ldots)\frac{\partial}{\partial Y}\left(\frac{1}{4}(\delta h_1 + \delta^3 h_2 + \ldots)^2(\delta^2 v_1 + \delta^4 v_2 + \ldots)\right),\end{aligned} \tag{4.91}$$

$$\begin{aligned}\delta\frac{\partial}{\partial\tau}(\delta^2 \bar{u}_1 + \delta^4 \bar{u}_2 + \ldots) = -2\sqrt{2}(1 + 2\delta^2 + \ldots)\frac{\partial}{\partial Y}\bigg(\bigg(\frac{1}{4} - \\ \frac{1}{16}(\delta h_1 + \delta^3 h_2 + \ldots)\bigg)(\delta u_1 + \delta^3 u_2 + \ldots)(\delta^2 v_1 + \delta^4 v_2 + \ldots)\bigg),\end{aligned} \tag{4.92}$$

$$\frac{1}{2}(1-4\delta^2)\frac{\partial^2}{\partial Y^2}(\delta^2 v_1+\delta^4 v_2+\ldots)-\delta^2\frac{\partial^2}{\partial\tau^2}(\delta^2 v_1+\delta^4 v_2+\ldots)-$$
$$\left(\frac{Y^2}{2}\left(\frac{1}{4}-\delta^2\right)-\frac{1}{4}\right)(\delta^2 v_1+\delta^4 v_2+\ldots)=$$
$$\left(Y+\sqrt{2}(1+2\delta^2+\ldots)\right)(\delta^2 v_1+\delta^4 v_2+\ldots)\Big(-\frac{\partial}{\partial Y}(\delta^2\bar{u}_1+\delta^4\bar{u}_2+\ldots)+$$
$$\frac{1}{2}(\delta h_1+\delta^3 h_2+\ldots)\frac{\partial}{\partial Y}(\delta u_1+\delta^3 u_2+\ldots)+$$
$$\frac{1}{4}(\delta u_1+\delta^3 u_2+\ldots)\frac{\partial}{\partial Y}(\delta h_1+\delta^3 h_2+\ldots)\Big)+$$
$$\frac{1}{8}(1-4\delta^2)\frac{\partial^2}{\partial Y^2}\Big((\delta^2 h_1^2+2\delta^4 h_1 h_2)(\delta^2 v_1+\delta^4 v_2+\ldots)\Big)-$$
$$2\sqrt{2}(1+2\delta^2+\ldots)\delta\frac{\partial}{\partial\tau}\Big((\delta^2 v_1+\delta^4 v_2+\ldots)\Big(\frac{1}{2}(\delta h_1+\delta^3 h_2+\ldots)\frac{\partial}{\partial Y}(\delta^2 v_1+\delta^4 v_2+\ldots)+$$
$$\frac{1}{4}(\delta^2 v_1+\delta^4 v_2+\ldots)\frac{\partial}{\partial Y}(\delta h_1+\delta^3 h_2+\ldots)\Big)\Big). \quad (4.93)$$

Leading order terms

The next step is to equate powers of δ. Starting with δ^2 we have from (4.90) - (4.93)

$$\frac{\partial u_1}{\partial\tau}+\left(\frac{1}{2}-\frac{Y}{2\sqrt{2}}\right)v_1=0,\quad \frac{\partial h_1}{\partial\tau}+2\sqrt{2}\frac{\partial v_1}{\partial Y}=0, \quad (4.94)$$

$$\frac{\partial^2 v_1}{\partial Y^2}+\left(\frac{1}{2}-\frac{Y^2}{4}\right)v_1=0,\quad \frac{\partial\bar{u}_1}{\partial\tau}=-2\sqrt{2}\frac{\partial}{\partial Y}\left(\frac{1}{4}u_1 v_1\right). \quad (4.95)$$

The only bounded solution of the equation for v_1 is $v_1 = A(\tau)\exp(-Y^2/4)$, then the remaining equations imply

$$u_1=B(\tau)\left(\frac{Y}{2\sqrt{2}}-\frac{1}{2}\right)\exp(-Y^2/4),\quad h_1=C(\tau)\sqrt{2}Y\exp(-Y^2/4) \quad (4.96)$$

and

$$\bar{u}_1=\frac{B^2(\tau)}{8}(Y^2-\sqrt{2}Y-1)\exp(-Y^2/2), \quad (4.97)$$

where $dB(\tau)/d\tau = A(\tau)$. Note that here $B = C$ from the linear terms in equation (4.78).

Since the above have been obtained through an integration with respect to τ we incur a $+G(Y)$ term, but since we are starting from a state of rest we take $G(Y) = 0$.

First order term

The next order terms are of $O(\delta^3)$. We find from (4.93)

$$\frac{\partial^2 v_2}{\partial Y^2} - \left(\frac{Y^2}{4} - \frac{1}{2}\right)v_2 = 4\frac{\partial^2 v_1}{\partial Y} + 2\frac{\partial^2 v_1}{\partial \tau^2} - 2\frac{Y^2}{2} + 2(Y+\sqrt{2})v_1\left(-\frac{\partial \bar{u}_1}{\partial Y} + \frac{1}{2}h_1\frac{\partial u_1}{\partial Y} + \frac{1}{4}u_1\frac{\partial h_1}{\partial Y}\right). \quad (4.98)$$

Substituting v_1, u_1, h_1 and $\bar{u}_1$ from (4.96) and (4.97) we find

$$\frac{\partial^2 v_2}{\partial Y^2} - \left(\frac{Y^2}{4} - \frac{1}{2}\right)v_2 = 2\frac{d^2A(\tau)}{d\tau^2}\exp(-Y^2/4) - 2A(\tau)\exp(-Y^2/4) + 2A(\tau)B^2(\tau)\exp(-3Y^2/4)\left(\frac{Y^2}{8} - \frac{Y^4}{16}\right). \quad (4.99)$$

Next, in order to make all the terms on the left hand side of (4.99) vanish, we multiply (4.99) by the eigenfunction $\exp(-Y^2/4)$ and integrate between $y = \pm\infty$. Using

$$\int_{-\infty}^{\infty}\exp(-ax^2)dx = \sqrt{\frac{\pi}{a}}$$

and integrating by parts we find

$$\int_{-\infty}^{\infty}\exp(-Y^2/2)dY = \sqrt{2\pi}, \quad \int_{-\infty}^{\infty}\frac{Y^2}{8}\exp(-Y^2)dY = \frac{\sqrt{\pi}}{16}, \quad (4.100)$$

and

$$\int_{-\infty}^{\infty}\frac{Y^4}{16}\exp(-Y^2)dY = \frac{3\sqrt{\pi}}{64}. \quad (4.101)$$

Substituting (4.100) and (4.101) into (4.99) we find our amplitude equation is

$$\frac{d^2A}{d\tau^2} = A - \frac{AB^2}{64\sqrt{2}}. \quad (4.102)$$

This can be written as a system of ODEs given by

$$A_\tau = C, \quad B_\tau = A, \quad C_\tau = A - \frac{AB^2}{64\sqrt{2}}. \tag{4.103}$$

The system of ODEs (4.103) are directly comparable to (4.63) - (4.61) where $\alpha \neq 0.5$. Immediately obvious is the fact that the linear term in each system has not changed, hence, in a very weakly nonlinear regime the behavior will be very similar. The first difference to note is in the nonlinear terms: when $\alpha \neq 0.5$ the nonlinear terms are proportional to AB whereas when $\alpha = 0.5$ they are proportional to AB^2. The other difference between the two ODEs is in the nonlinear coefficient which for the $\alpha \neq 0.5$ case depends on α, whereas here when $\alpha = 0.5$ the nonlinear coefficient is fixed. We will not solve this case in detail since this case only arises in the very unusual choice of $\alpha = 0.5$, however a brief description of one type of behaviour of the ODE system (4.103) is given in figure 4.33.

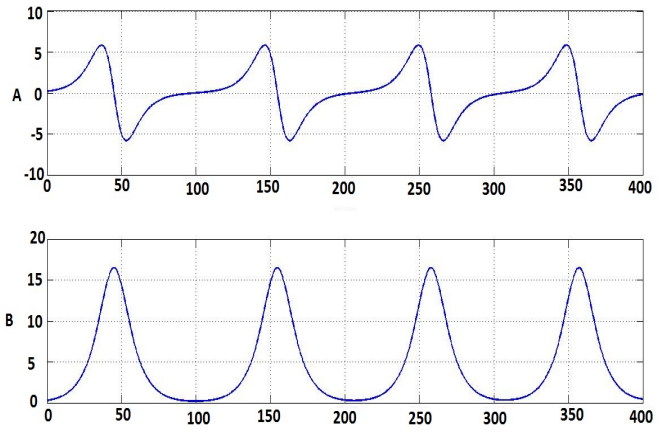

Figure 4.33: *The weakly nonlinear ODEs (4.103) solved numerically with* $A(0) = 0.2$, $B = g^{-1/4}A$ *and* $C = g^{1/4}A$, *which is the linear solution to (4.103). Here* $g^{1/2} = 0.5$.

4.6.2 Comparison to the analysis by Zhao and Ghil

We now make a comparison with a related study of weakly nonlinear inertial instability on the equatorial β-plane, which is that of Zhao and Ghil (1991). With low frequency ($20 - 30$ day) oscillations of the troposphere and stratosphere in mind, they studied the instability of a flow of the form $U = \gamma y + 1/2\delta y^2$, with standard linear (Rayleigh) friction for the flow and Newtonian cooling (i.e., linear damping of temperature perturbations). In contrast to our model, Zhao and Ghil used a primitive equation model in pressure coordinates, with a somewhat ad-hoc two-layer reduction (as described in section 4.6.3).

For weakly nonlinear disturbances and weak damping, Zhao and Ghil derive a fourth-order (in-time) set of amplitude equations

$$\frac{\partial^2 V_s}{\partial t^2} + \frac{\partial 2RV_s}{\partial t} - \alpha V_s + \nu\alpha V_s U_m = 0, \tag{4.104}$$

$$\frac{\partial U_s}{\partial t} + RU_s - V_s = 0, \tag{4.105}$$

$$\frac{\partial U_m}{\partial t} + RU_m - \nu U s V_s = 0. \tag{4.106}$$

Here R is the rescaled damping, whilst ν, α and a (which controls the growth rate) are fixed parameters. However, in the limit of no damping, (4.105), (4.106) together imply $\partial U_m/\partial t = \nu U_s \partial U_s/\partial t \Rightarrow U_m = \nu U_s^2/2$ (settling the constant of integration term to be zero), so that (4.104) can be rewritten as

$$\frac{\partial^2 V_s}{\partial t^2} = aV_s - \frac{\alpha\nu^2}{2} V_s U_s^2. \tag{4.107}$$

Writing $A = V_s$, $B = U_s$, $C = \partial V_s/\partial t$, this and (4.105) become

$$A_t = C, \quad B_t = A, \quad C_t = aA - \frac{\alpha\nu^2}{2} AB^2. \tag{4.108}$$

There is clearly a direct analogue to (4.103) (i.e., our amplitude equation for the special

case $\alpha = 0.5$), with $a = 1$ and $\alpha\nu^2 = -1/64\sqrt{2}$.

In many ways, it is a remarkable coincidence that Zhao and Ghil's primitive equation model should be equivalent to one of our two-layer shallow-water models. In an attempt to understand this coincidence, in the next few sections we rederive their results.

4.6.3 The Zhao and Ghil model

The equations of motion in pressure coordinates (e.g., Salmon (1998)) with $d/dx = 0$ are given by

$$\frac{Du}{Dt} - fv = 0, \quad \frac{Dv}{Dt} + fu = -\frac{\partial\phi}{\partial y}, \tag{4.109}$$

$$\frac{\partial v}{\partial y} + \frac{\partial\omega}{\partial p} = 0. \tag{4.110}$$

where ω is the vertical "velocity" in pressure coordinates (i.e., $\omega = Dp/Dt$). There is also a temperature equation and hydrostatic equation given by

$$\frac{\partial T}{\partial t} + v\frac{\partial T}{\partial y} - S\omega = 0, \quad \frac{\partial\phi}{\partial p} = -\frac{RT}{p}. \tag{4.111}$$

where S is the buoyancy frequency and R is the ideal gas constant. Here, we are taking the frictionless limit. Zhao and Ghil (1991) apply these in a two-layer setting in a somewhat non-standard manner. They use a subscript to denote the upper $(i = 3)$ and lower layer $(i = 1)$ as well as a subscript $i = 0, 2, 4$ to denote the upper lid, interface and bottom lid respectively. In the two-layers they take

$$\frac{D_1 u_1}{Dt} - fv_1 = 0, \quad \frac{D_3 u_3}{Dt} - fv_3 = 0, \tag{4.112}$$

$$\frac{D_1 v_1}{Dt} + fu_1 = -\frac{\partial\phi_1}{\partial y}, \quad \frac{D_3 v_3}{Dt} + fu_3 = -\frac{\partial\phi_3}{\partial y}, \tag{4.113}$$

$$\frac{\partial v_1}{\partial y} + \frac{\partial\omega_1}{\partial p} = 0, \quad \frac{\partial v_3}{\partial y} + \frac{\partial\omega_3}{\partial p} = 0, \tag{4.114}$$

here, u_i and v_i represent the horizontal depth averaged velocity in the x-direction and y-direction respectively. The material derivative in pressure coordinates is given by $D_i/Dt = \partial/\partial t + v_i\partial/\partial y + \omega_i\partial/\partial p$ and $\phi = gz$ independent of p. Some subtlety is needed to turn these equations into depth averaged formula; the pressure derivatives and vertical velocity can estimated using a finite difference approach, hence

$$\omega_1\frac{\partial u_1}{\partial p} = \left(\frac{\omega_2+\omega_0}{2}\right)\left(\frac{u_1-u_3}{p_1-p_3}\right) = -\frac{\omega_2(u_3-u_1)}{2\Delta p}, \tag{4.115}$$

$$\omega_3\frac{\partial u_3}{\partial p} = \left(\frac{\omega_4+\omega_2}{2}\right)\left(\frac{u_3-u_1}{p_3-p_1}\right) = -\frac{\omega_2(u_3-u_1)}{2\Delta p}, \tag{4.116}$$

$$\frac{\partial\omega_1}{\partial p} = \frac{\omega_2-\omega_0}{p_2-p_0} = \frac{\omega_2}{\Delta p}, \quad \frac{\partial\omega_3}{\partial p} = \frac{\omega_4-\omega_2}{p_4-p_2} = -\frac{\omega_2}{\Delta p}. \tag{4.117}$$

where $p_1-p_3 = \Delta p$, $p_4-p_2 = \Delta p$ and $p_0-p_2 = \Delta p$. A boundary condition in pressure, $\omega_0 = \omega_4 = 0$ has been applied which does not correspond to $w = 0$ at a fixed height. The temperature equation can then be neatly expressed at the interface, since ω_2 is the only relevant flow. Hence

$$\frac{\partial T_2}{\partial t} + v_2\frac{\partial T_2}{\partial y} - S\omega_2 = 0. \tag{4.118}$$

Finally, given T_2 appears in the hydrostatic equation it is natural to apply the hydrostatic equation at the interface, hence

$$\frac{\partial\phi_2}{\partial p} = -\frac{RT_2}{p_2}. \tag{4.119}$$

Likewise we take

$$\frac{\partial\phi_2}{\partial p} = \frac{\phi_1-\phi_3}{p_1-p_3} = \frac{\phi_1-\phi_3}{\Delta p} = -\frac{RT_2}{p_2}. \tag{4.120}$$

The Zhao and Ghil model assumes the pressure at the interface is also equal to the maximum pressure variation in the top and bottom layers, therefore $p_2 = \Delta p$ and we have $\phi_1-\phi_3 = RT_2$. Substituting this into (4.118) we have

$$\frac{\partial}{\partial t}(\phi_1-\phi_3) + v_2\frac{\partial}{\partial y}(\phi_1-\phi_3) - SR\omega_2 = 0. \tag{4.121}$$

Note also using (4.115) and (4.116) equations (4.112) - (4.114) can be written

$$\frac{\partial u_1}{\partial t} + v_1\frac{\partial u_1}{\partial y} + \frac{\omega_2}{2\Delta p}(u_3 - u_1) - \Big(\beta y - \Lambda\Big)v_1 = 0, \tag{4.122}$$

$$\frac{\partial u_3}{\partial t} + v_3\frac{\partial u_3}{\partial y} + \frac{\omega_2}{2\Delta p}(u_3 - u_1) - \Big(\beta y - \Lambda\Big)v_3 = 0, \tag{4.123}$$

$$\frac{\partial v_1}{\partial t} + v_1\frac{\partial v_1}{\partial y} + \frac{\omega_2}{2\Delta p}(v_3 - v_1) + \beta y u_1 = -\frac{\partial \phi_1}{\partial y}, \tag{4.124}$$

$$\frac{\partial v_3}{\partial t} + v_3\frac{\partial v_3}{\partial y} + \frac{\omega_2}{2\Delta p}(v_3 - v_1) + \beta y u_3 = -\frac{\partial \phi_3}{\partial y}, \tag{4.125}$$

$$\frac{\partial v_1}{\partial y} + \frac{\omega_2}{\Delta p} = 0, \quad \frac{\partial v_3}{\partial y} - \frac{\omega_2}{\Delta p} = 0, \tag{4.126}$$

$$\frac{\partial}{\partial}(\phi_1 - \phi_3) + v_2\frac{\partial}{\partial y}(\phi_1 - \phi_3) - \Delta p S\omega_2 = 0. \tag{4.127}$$

Note, there are two discrepancies between (4.122) - (4.127) and those stated by Zhao and Ghil (1991): the sign of the β term in (4.124) and (4.125) is different, their second term in both equations of (4.126) differs by a factor of $1/2$. Equations quoted in the next step by Zhao and Ghil can only be reproduced once these corrections have been made.

Our chosen basic shear flow has been introduced into the above, where $u_1 = u_3 = \Lambda y$, however Zhao and Ghil also included a vertical shear.

It follows directly from (4.126) that $\partial(v_1 + v_3)/\partial y = 0$ and hence $v_1 + v_3 = a(t)$. With rigid walls, we thus have $a(t) = 0 \Rightarrow v_1 + v_3 = 0$. For convenience we introduce new variables namely, $(f_1 + f_3)/2 = f_m$ and $(f_1 - f_3)/2 = f_s$, for $f = u, v$ and ϕ. Note now we have $v_m = 0$ since $v_1 + v_3 = 0$ and with the introduction of these new variables equations (4.122) - (4.127) become

$$\frac{\partial u_m}{\partial t} + \frac{\partial v_s u_s}{\partial y} = 0, \tag{4.128}$$

$$\frac{\partial (v_s v_s)}{\partial y} + \beta y u_m = -\frac{\partial \phi_m}{\partial y}, \tag{4.129}$$

$$\frac{\partial u_s}{\partial t} + v_s \frac{\partial u_m}{\partial y} - \Big(\beta y - \Lambda\Big) v_s = 0, \tag{4.130}$$

$$\frac{\partial v_s}{\partial t} + \beta y u_s = -\frac{\partial \phi_s}{\partial y}, \tag{4.131}$$

$$\frac{\phi_s}{\partial t} + c^2 \frac{\partial v_s}{\partial y} = 0, \tag{4.132}$$

where $c^2 = (\Delta p)^2 S/2$.

Next we nondimensionalise using the following

$$(u_m, v_s, u_s) = U(u'_m, v'_s, u'_s), \quad (\phi_s, \phi_m) = cU(\phi'_s, \phi'_m), \quad y = ly', \quad t = \tau t, \tag{4.133}$$

$$\tau = \frac{l}{c}, \quad \nu = \frac{U}{c} \quad l^2 = \frac{c}{\beta}, \quad \xi_0 = \frac{\Lambda}{2l\beta}. \tag{4.134}$$

Applying (4.133) and (4.134) to (4.128) - (4.132) we have

$$\frac{\partial u_m}{\partial t} + \nu \frac{\partial (v_s u_s)}{\partial y} = 0, \tag{4.135}$$

$$\nu \frac{\partial (v_s v_s)}{\partial y} + y u_m = -\frac{\partial \phi_m}{\partial y}, \tag{4.136}$$

$$\frac{\partial u_s}{\partial t} + \nu v_s \frac{\partial u_s}{\partial y} - (y - 2\xi_0) v_s = 0, \tag{4.137}$$

$$\frac{\partial v_s}{\partial t} + y u_s = -\frac{\partial \phi_s}{\partial y}, \tag{4.138}$$

$$\frac{\partial \phi_s}{\partial t} + \frac{\partial v_s}{\partial y} = 0, \tag{4.139}$$

where we have dropped the "′" notation. The above equations can be comparable to the equations of section 4.6, here equation (4.135) is comparable to (4.80), equation (4.137) comparable to (4.77), (4.138) comparable to (4.78) and lastly (4.139) to (4.79). Equation (4.136) would be comparable to an equation for the mean flow in the y-direction, however was not derived. We can also form an equation which is linear in v_s which is comparable

to (4.81) by taking $\partial/\partial t$ (4.138) and substituting for $\partial u_s/\partial t$ from (4.137) and $\partial \phi_s/\partial t$ from (4.139) to obtain

$$\frac{\partial^2 v_s}{\partial y^2} - \frac{\partial^2 v_s}{\partial t^2} - y(y - 2\xi_0)v_s = \nu y v_s \frac{\partial u_m}{\partial y}. \tag{4.140}$$

Linear analysis

Following previous analysis and as found in Zhao and Ghil we perform a linear analysis of equation (4.140), note that linearly we have

$$\frac{\partial^2 v_s}{\partial y^2} - \frac{\partial^2 v_s}{\partial t^2} - y(y - 2\xi_0)v_s = 0. \tag{4.141}$$

We assume solutions of the form $v_s = V(y)\exp(st)$ and substitute into (4.141) to obtain

$$\frac{d^2 v_s}{dy^2} + \Big(- s^2 - y(y - 2\xi_0)\Big)v_s = 0. \tag{4.142}$$

After completing the square this becomes

$$\frac{d^2 v_s}{dy^2} + \Big(- s^2 - (y - \xi_0)^2 + \xi_0^2\Big)v_s = 0. \tag{4.143}$$

We use a transform of variables and write $y - \xi_0 = Y/L$, where $L = \sqrt{2}$ and find

$$\frac{d^2 v_s}{dy^2} + \left(\mu - \frac{Y^2}{4} + \frac{1}{2}\right)v_s = 0, \tag{4.144}$$

where $\mu = (-s^2 + \xi_0^2)$. Equation (4.144) is the form of the parabolic cylinder equation as described by Bender and Orszag (1999). Applying the boundary conditions $v_s = 0$ at $Y = \pm\infty$ we find μ equal to any integer n, hence we have the dispersion relation

$$s^2 = \xi_0^2 - (2n + 1), \tag{4.145}$$

with $n = 0$ gives the most unstable node with marginal stability when $\xi_0^2 = \xi_{0c} = 1$. Note that this result is comparable to (4.82) with $\xi_0^2 = 1/4$ and $g^{1/2} = 1$.

Weakly nonlinear analysis

Here we will derive the weakly nonlinear amplitude equations which we shall be comparing directly to (4.102). In section 4.6 we controlled the instability through varying g from criticality by taking $g^{1/2} = 1/4 - \delta^2$; here we take $\xi_0 = \xi_{0c} + \epsilon\xi_0^1 + \ldots$. Firstly for convenience we will write equations (4.135) - (4.140) in terms of the new variable Y, recall $Y = \sqrt{2}(y - \xi_0)$, substituting into (4.135) - (4.140) we have

$$\frac{\partial u_m}{\partial t} + \sqrt{2}\nu\frac{\partial(v_s u_s)}{\partial Y} = 0, \quad \sqrt{2}\nu\frac{\partial(v_s v_s)}{\partial Y} + \left(\frac{Y}{\sqrt{2}} + 1\right)u_m = -\sqrt{2}\frac{\partial \phi_m}{\partial Y}, \tag{4.146}$$

$$\frac{\partial u_s}{\partial t} + \sqrt{2}\nu v_s\frac{\partial u_m}{\partial Y} - \left(\frac{Y}{\sqrt{2}} + 1 - 2\xi_0\right)v_s = 0, \tag{4.147}$$

$$\frac{\partial v_s}{\partial t} + \left(\frac{Y}{\sqrt{2}} + 1\right)u_s = -\sqrt{2}\frac{\partial \phi_s}{\partial Y}, \quad \frac{\partial \phi_s}{\partial t} + \sqrt{2}\frac{\partial v_s}{\partial Y} = 0, \tag{4.148}$$

$$2\frac{\partial^2 v_s}{\partial Y^2} - \frac{\partial^2 v_s}{\partial t^2} - \left(\frac{Y}{\sqrt{2}} + 1\right)\left(\frac{Y}{\sqrt{2}} + 1 - 2\xi_0\right)v_s = -\nu\sqrt{2}\left(\frac{Y}{\sqrt{2}} + 1\right)v_s\frac{\partial u_m}{\partial Y}. \tag{4.149}$$

Next we expand our variables in terms of our small variable ϵ, the scalings of choice used by Zhao and Ghil are as follows:

$$\xi_0 = 1 + \epsilon\xi_0^1, \quad v_s = \epsilon(v_s^{(1)} + \epsilon v_s^{(2)} + \ldots), \tag{4.150}$$

$$u_s = \epsilon^{1/2}(u_s^{(1)} + \epsilon u_s^{(2)} + \ldots), \quad \phi_s = \epsilon^{1/2}(\phi_s^{(1)} + \epsilon\phi_s^{(2)} + \ldots), \tag{4.151}$$

$$\phi_m = \epsilon(\phi_m^{(1)} + \epsilon\phi_m^{(2)} + \ldots), \quad u_m = \epsilon(u_m^{(1)} + \epsilon u_m^{(2)} + \ldots), \quad t = \epsilon^{1/2}\tau. \tag{4.152}$$

Substituting (4.150) - (4.152) into (4.146) - (4.149) we have

$$\frac{\partial}{\partial t}(u_m^{(2)} + \epsilon u_m^{(2)} + \ldots) + \sqrt{2}\nu\epsilon^{3/2}\frac{\partial}{\partial Y}(v_s^{(1)}u_s^{(1)} + \epsilon v_s^{(1)}u_s^{(2)} + v_s^{(2)}u_s^{(1)} + \ldots) = 0, \quad (4.153)$$

$$\sqrt{2}\nu\epsilon^2\frac{\partial}{\partial Y}(v_s^{(1)}v_s^{(1)} + 2\epsilon v_s^{(1)}v_s^{(2)} + \ldots) + \epsilon\left(\frac{Y}{\sqrt{2}} + 1\right)(u_m^{(1)} + \epsilon u_m^{(2)} + \ldots) = -\epsilon\sqrt{2}\frac{\partial}{\partial Y}(\phi_m^1 + \epsilon\phi_m^2 + \ldots), \quad (4.154)$$

$$\epsilon\frac{\partial}{\partial \tau}(u_s^{(1)} + \epsilon u_s^{(2)} + \ldots) + \epsilon^2\sqrt{2}\nu(v_s^{(1)} + \epsilon v_s^{(2)} + \ldots)\frac{\partial}{\partial Y}(u_m^{(1)} + \epsilon u_m^{(2)} + \ldots) - \epsilon\left(\frac{Y}{\sqrt{2}} + 1 - 2(1 + \epsilon\xi_0^{(1)})\right)(v_s^{(1)} + \epsilon v_s^{(2)} + \ldots) = 0, \quad (4.155)$$

$$\epsilon^{3/2}\frac{\partial}{\partial \tau}(v_s^{(1)} + \epsilon v_s^{(2)} + \ldots) + \epsilon^{1/2}\left(\frac{Y}{\sqrt{2}} + 1\right)(u_s^{(1)} + \epsilon u_s^{(2)} + \ldots) = -\epsilon^{1/2}\sqrt{2}\frac{\partial}{\partial Y}(\phi_s^{(1)} + \epsilon\phi_s^{(2)} + \ldots) \quad (4.156)$$

$$\epsilon\frac{\partial}{\partial \tau}(\phi_s^{(1)} + \epsilon\phi_s^{(2)} + \ldots) + \epsilon\sqrt{2}\frac{\partial}{\partial Y}(v_s^{(1)} + \epsilon v_s^{(2)} + \ldots) = 0, \quad (4.157)$$

$$2\epsilon\frac{\partial^2}{\partial Y^2}(v_s^{(1)} + \epsilon v_s^{(2)} + \ldots) - \epsilon^2\frac{\partial^2}{\partial \tau^2}(v_s^{(1)} + \epsilon v_s^{(2)} + \ldots) - \epsilon\left(\frac{Y}{\sqrt{2}} + 1\right)\left(\frac{Y}{\sqrt{2}} + 1 - 2(1 + \xi_0^{(1)})\right)(v_s^{(1)} + \epsilon v_s^{(2)} + \ldots) = -\epsilon^2\nu\sqrt{2}\left(\frac{Y}{\sqrt{2}} + 1\right)(v_s^{(1)} + \epsilon v_s^{(2)} + \ldots)\frac{\partial}{\partial Y}(u_m^{(1)} + \epsilon u_m^{(2)} + \ldots). \quad (4.158)$$

It remains to equate powers of ϵ. Starting with ϵ^1 from (4.158) we have

$$2\frac{\partial^2 v_s^{(1)}}{\partial Y^2} - \left(\frac{Y^2}{2} - 1\right) v_s^{(1)} = 0, \tag{4.159}$$

and we take a solution to be of the form $v_s^{(1)} = A(\tau)\exp(-Y^2/4)$. Next from (4.155) we have

$$\frac{\partial u_s^{(1)}}{\partial \tau} = \left(\frac{Y}{\sqrt{2}} - 1\right) A(\tau)\exp(-Y^2/4), \tag{4.160}$$

solving for $u_s^{(1)}$ we have $u_s^{(1)} = B(\tau)(Y/\sqrt{2}-1)\exp(-Y^2/4)$, where $dB(\tau)/d\tau = A(\tau)$. From (4.153) we have

$$\frac{\partial u_m^{(1)}}{\partial \tau} = -\sqrt{2}\nu A(\tau)B(\tau)\frac{\partial}{\partial Y}\left(\left(\frac{Y}{\sqrt{2}} - 1\right)\exp(-Y^2/2)\right), \tag{4.161}$$

hence

$$u_m^{(1)} = -\frac{\sqrt{2}\nu B^2(\tau)}{2}\left(\frac{1}{\sqrt{2}} - \frac{Y^2}{\sqrt{2}} + Y\right)\exp(-Y^2/2). \tag{4.162}$$

We can solve for ϕ_m and ϕ_s. However, as we shall see, the solutions to these are not needed for the derivation of the amplitude equation. At order ϵ^2 from (4.158) we have

$$2\frac{\partial^2 v_s^{(2)}}{\partial Y^2} - \frac{\partial^2 v_s^{(1)}}{\partial \tau^2} - \left(\frac{Y}{\sqrt{2}} + 1\right)\left(\frac{Y}{\sqrt{2}} + 1\right)v_2^{(2)} + 2\xi_0^1\left(\frac{Y}{\sqrt{2}} + 1\right)v_s^{(1)} = \\ -\nu\sqrt{2}\left(\frac{Y}{\sqrt{2}} + 1\right)v_s^{(1)}\frac{\partial u_m^{(1)}}{\partial Y}. \tag{4.163}$$

Substituting $v_s^{(1)} = A(\tau)\exp(-Y^2/4)$ and $u_m^{(1)}$ from (4.162) we have

$$2\frac{\partial^2 v_2^{(2)}}{\partial Y^2} - \left(\frac{Y}{\sqrt{2}}+1\right)\left(\frac{Y}{\sqrt{2}}-1\right)v_2^{(2)} + \exp(-Y^2/4)\frac{d^2A(\tau)}{d\tau^2} = 2\xi_0^{(1)}\left(\frac{Y}{\sqrt{2}}+1\right)\exp(-Y^2/4)A(\tau) + A(\tau)B^2(\tau)\nu^2\exp(-Y^2/4)\left(\frac{Y}{\sqrt{2}}+1\right)\frac{\partial}{\partial Y}\left(\left(\frac{1}{\sqrt{2}}-\frac{Y^2}{\sqrt{2}}+Y\right)\exp(-Y^2/2)\right). \tag{4.164}$$

Next we multiply (4.164) by the eigenfunction $\exp(-Y^2/4)$ so terms in v_2 disappear, then integrate between $Y = \pm\infty$, after some manipulation we have

$$\frac{d^2A(\tau)}{d\tau^2} = 2\xi_0^{(1)}A(\tau) - A(\tau)B^2(\tau)\nu^2\frac{1}{8\sqrt{2}}. \tag{4.165}$$

Equation (4.165) is the final amplitude equation and is analogous to the equations given earlier in this section. The first thing to note about (4.165) is that this equation is the same as (4.102), our $\alpha = 0.5$ case when $2\xi_0^{(1)} = 1$ and $\nu^2 = 1/8$.

Discussion of comparison

There are many differences to the model adopted by Zhao and Ghil and the one adopted in this thesis. Zhao and Ghil approach the problem using pressure coordinates. While both pressure coordinates and Cartesian coordinates adequately describe a two-layer model, differences become obvious when applying a zero vertical velocity rigid lid boundary condition. Assuming a zero vertical velocity at a constant layer depth is very different physically to applying the same boundary condition at constant pressure. Unless a constant pressure corresponds to a surface of constant height which is rarely ever the case these two boundary conditions are very different. There is also the role of thermodynamics in the Zhao and Ghil's model which is absent in the shallow water model adopted in this thesis.

Zhao and Ghil have a fixed layer depth with both layer depths being equal size, therefore their analysis should be compared with the special case $\alpha = 0.5$ as discussed in section 4.6. Zhao and Ghil have taken a crude model of taking an average constant pressure across each layer depth with the variation in pressure between the top and bottom of each layer being equal in both layers. This variation also happens to be equal to the pressure at the interface of the two-layers. This differs from our model which does allow for pressure variations in each layer.

4.7 Discussion

In this chapter we have analysed inertial instability in a two-layer system with a shear flow basic state on the equatorial β-plane, this set-up being the simplest model that could be adopted. The equations we use are the shallow water equations adapted to a two-layer model as derived in the previous chapter. For convenience we nondimensionalised the equations before performing any analysis.

We started our analysis with linear theory concentrating on the frictionless case, deriving a dispersion relation. We found the growth rate was controlled by only one parameter $\tilde{g}$ being a component of: reduced gravity, total layer depth, layer depth of the top and bottom layer and the shear of the basic state. Moreover, there was found to be a transition from stability to instability as $\tilde{g}$ decreases. We therefore found that the flow is most unstable for large shear, small reduced gravity, small overall layer depth and when one layer of fluid is smaller than the other.

However, to understand the nature of this transition we need to understand the nonlinear evolution and its effect on the mean flow. The simplest and most natural thing to do is to apply weakly nonlinear theory. Weakly nonlinear theory allows the derivation of an amplitude equation which can give a comprehensive understanding of the flow in this weakly nonlinear state. We analysed the amplitude equation and found the flow could

follow one of two types of behaviour: cyclical or follow a trajectory that grows to infinity with the latter being of most interest. A trajectory that grows to infinity is not practicable since we have applied a rigid lid to our model.

The natural next step was to investigate the fully nonlinear regime, which can only be done numerically. The first thing we did was to compare these numerics to the weakly nonlinear theory; the results agreed which gave confidence in the numerics and the weakly nonlinear theory. We are interested to understand how the flow was evolving, in particular what was happening to the mean flow. The system is initially unstable, which causes the horizontal velocities to grow and in turn the displaced fluid causes the interface to lift and dip away from its equilibrium position. This process causes a reduction in the mean flow which, in turn decreases the negativity of the absolute vorticity Q until the flow is stabilised. This momentarily stable state is however short lived; the instability is no longer driving the flow and the horizontal velocities start to decay to zero, the stability overshoots and now the meridional horizontal velocity is reversed; ultimately the flow becomes unstable again. The horizontal velocities reach their peak in amplitude and again decay to zero, the system is back to its initial state and the cycle is ready to repeat again. We have clearly shown that when the system is momentarily stable there is a reduction in the shear.

We extended our analysis to the fully nonlinear regime. Although the nonlinear behaviour had diverged from following the same trajectory of the weakly nonlinear analysis the behaviour was still cyclical. However, the system now spent less time in the state where amplitudes were small bringing the cycles closer together. The model restricted us to a moderately nonlinear regime rather than a strongly nonlinear regime, this was due to the interface between the two-layers growing too large and breaking through the rigid lid of the model. In these circumstances a breakdown of the model has occurred, in reality other physics would come in to play or a change to the numerical scheme could be applied. For example, physically we have assumed hydrostatic balance and assumed that no over turning in the fluid can occur (no z dependence) which is perhaps too crude

and here we have may have paid the price for simplicity. Another alternative would be to apply the frictional terms we have neglected which may offer some resistance as the flow approaches the boundary. A numerical way to overcome the problem could perhaps be to use a 2-layer, 1-layer, 2-layer split where the interface touches the upper and lower boundary. Although these workable ideas they are very complex to apply especially in the latter case.

This work complements other work on inertial instability with a two-layer model. Zeitlin et al. (2014) looked at strongly nonlinear asymmetric instabilities, looking at the competition between inertial instability and barotropic instability. They applied a Gaussian jet basic state. Interestingly they found that inertial instability out-competes barotropic instability to become the dominant instability. The behaviour of the system however is not cyclical, rather the nonlinear terms saturate the instability. Interestingly Zhao and Ghil (1991) is comparable to the special case where $\alpha = 0.5$, although there are many differences in the models used the resulting ODE equations under certain fixed parameters were the same. Both Zhao and Ghill and Zeitlin et al found similar properties of the behaviour of the inertial instability. Both confirmed stability was achieved through a reduction in the shear resulting in a reduction in the negativity of the potential vorticity.

Nonlinear analysis of inertial instability on the equatorial β-plane is not restricted to two-layer flows. For example Kloosterziel et al (2015) looked at inertial instability on the equatorial β-plane with continuous stratification with both a Gaussian jet and uniform shear applied. They looked at the system in the strongly nonlinear regime numerically and also found a saturation of the instability resulting from a reduction in the shear and thus a reduction in the negativity of the potential vorticity. It should be noted that interestingly Kloosterziel et al (2014) used linear theory to predict the change to mean flow as a result of the instability which was confirmed numerically. Griffiths (2003b) also confirmed process of achieving stability through changes to the mean flow using strongly nonlinear numerics with a uniform shear flow. We can therefore conclude that both the two-layer

model and continuously stratified system display similar dynamics and therefore the two-layer model is relevant as a simplistic model for the prediction of flows in the atmosphere and ocean.

In the frictional case there were found to be two parameters $\tilde{g}$ and nondimensional friction ϵ. The effects of small friction were looked at by fixing $\tilde{g}$ and finding the growth rate as a series expansion in ϵ. We looked at this series expansion solution for varying cases of $\tilde{g}$. It was found that in most cases the small amount of friction acted to stabilise the flow, with the opposite being true for a small parameter range of $\tilde{g}$. This result was a surprising one. We could have extended the work in this chapter by applying weakly nonlinear analysis and analysing the fully nonlinear regime.

Chapter 5

Nonlinear instabilities on the f-plane

5.1 Introduction

In the previous chapter we studied zonally symmetric ($\partial/\partial x = 0$) inertial instability for a two-layer uniform shear flow on the equatorial β-plane. We now focus our analysis on the two-layer system on the f-plane with a localised shear flow basic state. In this chapter, we study zonally symmetric inertial instability for a two-layer localised shear layer on a midlatitude f-plane. Recall that for the flow to be inertially unstable we must have $fQ < 0$, where $Q = f - du/dy$ is the absolute vorticity, and with $f = f_0$ we thus need

$$f_0(f_0 - du/dy) < 0. \tag{5.1}$$

Inertial instability thus requires $du/dy > f_0$ somewhere. For a shear layer with characteristic speed U and lengthscale L, we require $U/L > f_0$, or equivalently that the Rossby number $R_o = U/fL > 1$. This condition is of course not widely satisfied for large-scale atmospheric and ocean flows, which are well-known to favour small R_o. However, the possibility and existence of inertial instability at mid-latitudes has been discussed by Stevens and Ciesielski (1986) and Shen and Evans (2002), amongst others.

Much theoretical work on inertial instability in continuous stratified systems applies to both the equatorial β-plane and f-plane, such as the general theory of Griffiths (2008). Other work is specific to instabilities on the f-plane alone, such as the study of vertical scale selection at arbitrary Prandtl number by Kloosterziel et al. (2013). In terms of numerical simulations of nonlinear inertial instability on the f-plane for two-layer flows, Bouchut et al. (2011) perform a nonlinear analysis of a two-layer flow on the f-plane with a Bickley jet basic state.

In section 5.2 we nondimensionalise the full nonlinear frictional PDEs and conservation laws. In section 5.3 we derive the linear dispersion relation without friction. In section 5.4 we perform weakly nonlinear analysis deriving an amplitude equation where behaviour is anaylsed in depth in section 5.4.7. In section 5.6 we solve the full nonlinear PDEs numerically and compare the results with the weakly nonlinear results. In section 5.6.4 we discuss the limitations of the weakly nonlinear theory. Analysis of changes to the mean flow and the dynamics of the system are discussed in section 5.8 before finally concluding with a discussion of our findings in section 5.9.

5.2 Nondimensional equations of motion

Here we will look at a two-layer system as in chapter 4; however instead of the equatorial β-plane approximation $f = \beta y$, we will now use the f-plane approximation $f = f_0$, where f_0 is a constant. To begin, we will use the equations derived in section 3.2, that is equations (3.26) - (3.29),

$$\frac{\partial \hat{u}}{\partial t} + \frac{(H_1 - h)}{H}\hat{v}\frac{\partial}{\partial y}\left(\bar{u} + \frac{(H_1 - h)\hat{u}}{H}\right) + \frac{(H_2 + h)\hat{v}}{H}\frac{\partial}{\partial y}\left(\bar{u} - \frac{(H_2 + h)\hat{u}}{H}\right) - f\hat{v} = -\frac{\epsilon H \hat{u}}{(H_2 + h)(H_1 - h)}. \quad (5.2)$$

$$\frac{\partial \hat{v}}{\partial t} + \frac{1}{2}\frac{\partial}{\partial y}\left(\frac{(H_1 - h)\hat{v}}{H}\right)^2 - \frac{1}{2}\frac{\partial}{\partial y}\left(\frac{(H_2 + h)\hat{v}}{H}\right)^2 + f\hat{u} = -g'\frac{\partial h}{\partial y} - \frac{\epsilon \hat{v} H}{(H_1 - h)(H_2 + h)}, \quad (5.3)$$

$$\frac{\partial h}{\partial t} + \frac{\partial}{\partial y}\left(\frac{(H_2 + h)(H_1 - h)\hat{v}}{H}\right) = 0, \quad (5.4)$$

$$\frac{\partial \bar{u}}{\partial t} = -\frac{1}{H^2}\frac{\partial}{\partial y}\Big((H_2 + h)(H_1 - h)\hat{u}\hat{v}\Big). \quad (5.5)$$

On the f-plane these equations require a different nondimensionalisation than on the equatorial β-plane. To start, as before we use

$$\tilde{u} = \hat{u}/U, \quad \tilde{v} = \hat{v}/U, \quad \tilde{\bar{u}} = \bar{u}/U, \quad \tilde{h} = h/H_e, \quad \tilde{t} = t/T, \quad \tilde{y} = y/L, \quad (5.6)$$

where U, L, T are characteristic velocity, length and time scales respectively, and $H_e = H_1 H_2/H$ where $H_1 + H_2 = H$. Writing $H_1 = \alpha H$ and $H_2 = (1-\alpha)H$, equations (3.26) - (3.29) become

$$\frac{\partial \tilde{u}}{\partial \tilde{t}} + \left(\frac{UT}{L}\right)(\alpha - \alpha(1-\alpha)\tilde{h})\tilde{v}\frac{\partial}{\partial \tilde{y}}\Big(\tilde{\bar{u}} + (\alpha - \alpha(1-\alpha)\tilde{h})\tilde{u}\Big) + \left(\frac{UT}{L}\right)((1-\alpha) + \alpha(1-\alpha)\tilde{h})\tilde{v}\frac{\partial}{\partial \tilde{y}}\Big(\tilde{\bar{u}} - (((1-\alpha) + \alpha(1-\alpha)\tilde{h}))\tilde{u}\Big) - f_0 T\tilde{v} = -\frac{T\epsilon\tilde{u}}{H(1-\alpha)\alpha(1+\alpha\tilde{h})(1-(1-\alpha)\tilde{h})}, \quad (5.7)$$

$$\frac{\partial \tilde{v}}{\partial \tilde{t}} + \left(\frac{UT}{2L}\right)\frac{\partial}{\partial \tilde{y}}\Big((\alpha - \alpha(1-\alpha)\tilde{h})\tilde{v}\Big)^2 - \left(\frac{UT}{2L}\right)\frac{\partial}{\partial \tilde{y}}\Big(((1-\alpha) + \alpha(1-\alpha)\tilde{h}))\tilde{v}\Big)^2 + f_0 T\tilde{u} = -g'\frac{\alpha(1-\alpha)HT}{LU}\frac{\partial \tilde{h}}{\partial \tilde{y}} - \frac{T\epsilon\tilde{v}}{H(1-\alpha)\alpha(1+\alpha\tilde{h})(1-(1-\alpha)\tilde{h})}, \quad (5.8)$$

$$\frac{\partial \tilde{h}}{\partial \tilde{t}} + \left(\frac{UT}{L\alpha(1-\alpha)}\right)\frac{\partial}{\partial \tilde{y}}\Big(\alpha(1-\alpha)(1+\alpha\tilde{h})(1-(1-\alpha)\tilde{h})\tilde{v}\Big) = 0, \quad (5.9)$$

$$\frac{\partial \tilde{\bar{u}}}{\partial \tilde{t}} = -\left(\frac{UT}{L}\right)\frac{\partial}{\partial \tilde{y}}\left(\alpha(1-\alpha)(1+\alpha\tilde{h})(1-(1-\alpha)\tilde{h})\tilde{u}\tilde{v}\right). \tag{5.10}$$

If we choose the following scalings

$$\frac{UT}{L} = \frac{U}{f_0 L} = R_o, \qquad \tilde{g} = gH\alpha(1-\alpha)R_o/U^2, \qquad \tilde{\epsilon} = \frac{\epsilon T}{H},$$

where R_o is the nondimensional Rossby number, we have a complete set of nondimensional equations

$$\frac{\partial u}{\partial t} + R_o v\frac{\partial}{\partial y}(\bar{u}-u) + 2R_o v D_1\frac{\partial u}{\partial y} + R_o uv\frac{\partial D_1}{\partial y} - v = -\frac{\epsilon u}{D_1 D_2}, \tag{5.11}$$

$$\frac{\partial v}{\partial t} - R_o v\frac{\partial v}{\partial y} + 2R_o D_1 v\frac{\partial v}{\partial y} + R_o v^2\frac{\partial D_1}{\partial y} + u = -g\frac{\partial h}{\partial y} - \frac{\epsilon v}{D_1 D_2}, \tag{5.12}$$

$$\frac{\partial h}{\partial t} + \frac{R_o}{\alpha(1-\alpha)}\frac{\partial}{\partial y}\left(D_1 D_2 v\right) = 0, \tag{5.13}$$

$$\frac{\partial \bar{u}}{\partial t} + R_o\frac{\partial}{\partial y}\left(D_1 D_2 uv\right) = 0. \tag{5.14}$$

Note, we have dropped the tilde notation. Going forward our analysis of these equations will be concentrated on a localised basic state flow of the form $\bar{u} = R_o\tanh(y)$, Writing $\bar{u} = R_o\tanh(y) + \bar{u}_{non}$, equation (5.11) can be rewritten as

$$\frac{\partial u}{\partial t} + R_o v\frac{\partial}{\partial y}(\bar{u}_{non}-u) + 2R_o v D_1\frac{\partial u}{\partial y} + R_o uv\frac{\partial D_1}{\partial y} - Qv = -\frac{\epsilon u}{D_1 D_2}, \tag{5.15}$$

where $\bar{u}_{non}$ represents the nonlinear part of $\bar{u}$ and $Q = 1 - R_o\,\mathrm{sech}^2(y)$.

5.2.1 Conservation Laws

Since the conservation of energy derived in chapter 4 is independent of the Coriolis force f this conservation law will be identical for the equatorial β-plane and the f-plane. Hence

$$\frac{\rho}{2}\frac{\partial}{\partial t}\int_{-\infty}^{\infty}\left(\bar{u}^2+D_1D_2(\hat{u}^2+\hat{v}^2)-g\alpha(1-\alpha)h^2\right)dy=-\rho\int_{\infty}^{\infty}\epsilon(\hat{u^2}+\hat{v}^2)dy=0. \quad (5.16)$$

The same is also true for conservation of momentum and conservation of mass

$$\int_{-\infty}^{\infty}-R_o\frac{\partial}{\partial y}\left(D_1D_2uv\right)dy=0, \quad (5.17)$$

$$\frac{\partial}{\partial t}\int_{-\infty}^{\infty}hdy=0. \quad (5.18)$$

The conservation of potential vorticity is also the same, however with the appropriate change to f,

$$\frac{\partial}{\partial t}P_1-D_2\hat{v}\frac{\partial}{\partial y}P_1=0, \quad (5.19)$$

where

$$P_1=\left(\frac{1+R_0\frac{\partial}{\partial y}(D_2\hat{u}-\bar{u})}{D_1}\right). \quad (5.20)$$

Following this same derivation as the top layer, we have

$$\frac{\partial}{\partial t}P_2+D_1\hat{v}\frac{\partial}{\partial y}P_2=0, \quad (5.21)$$

where

$$P_2=\left(\frac{1-R_0\frac{\partial}{\partial y}(D_1\hat{u}+\bar{u})}{D_2}\right). \quad (5.22)$$

5.2.2 Frictionless limit

We focus on the frictionless limit $\epsilon = 0$ from hereon, in which case the nondimensional governing equations become

$$\frac{\partial u}{\partial t} + R_o v \frac{\partial}{\partial y}(\bar{u}_{non} - u) + 2R_o v D_1 \frac{\partial u}{\partial y} + R_o u v \frac{\partial D_1}{\partial y} - Qv = 0, \tag{5.23}$$

$$\frac{\partial v}{\partial t} - R_o v \frac{\partial v}{\partial y} + 2R_o D_1 v \frac{\partial v}{\partial y} + R_o v^2 \frac{\partial D_1}{\partial y} + u = -g\frac{\partial h}{\partial y}, \tag{5.24}$$

$$\frac{\partial h}{\partial t} + \frac{R_o}{\alpha(1-\alpha)} \frac{\partial}{\partial y}\Big(D_1 D_2 v \Big) = 0, \tag{5.25}$$

$$\frac{\partial \bar{u}_{non}}{\partial t} + R_o \frac{\partial}{\partial y}\Big(D_1 D_2 u v \Big) = 0. \tag{5.26}$$

Here $D_1 = \alpha - \alpha(1-\alpha)h$ and $D_2 = 1 - \alpha + \alpha(1-\alpha)h$, where α is the fractional depth of the lower layer.

5.3 Linear analysis with no friction

We start by linearising equations (5.23) - (5.25),

$$\frac{\partial u}{\partial t} - Qv = 0, \tag{5.27}$$

$$\frac{\partial v}{\partial t} + u = -g\frac{\partial h}{\partial y}, \tag{5.28}$$

$$\frac{\partial h}{\partial t} = -R_o \frac{\partial v}{\partial y}. \tag{5.29}$$

These equations can be combined into a single equation for v by taking $\partial/\partial t$ of (5.28) and substituting for u and h from (5.27) and (5.29) respectively,

$$\frac{\partial^2 v}{\partial y^2} - \frac{Q}{gR_o} v - \frac{1}{gR_o}\frac{\partial^2 v}{\partial t} = 0. \tag{5.30}$$

We assume the solution to (5.30) is of the form $v = \exp(st)v'(y)$ and therefore obtain

$$\frac{d^2v'}{dy^2} + \Big(E + \nu\,\mathrm{sech}^2(y)\Big)v' = 0, \tag{5.31}$$

where $E = -(1+s^2)/gR_o$ and $\nu = 1/g$. If we impose boundary conditions $v \to 0$ as $|y| \to \infty$, this becomes an eigenvalue problem for s^2 in terms of g and R_o.

5.3.1 General solution to the eigenvalue problem

We consider the eigenvalue problem (5.31) in terms of E and ν. This solution can be found in the research literature (e.g., Bender and Orszag (1999); Griffiths (2008)), but it is interesting to derive this in detail.

First we show that $E < 0$. Let us consider the limit, $|y| \to \infty$, here $\mathrm{sech}^2(y) \to 0$ and we have

$$\frac{d^2v}{dy^2} + Ev = 0, \tag{5.32}$$

where we have dropped the " $'$ " notation. The complete solution is

$$v = A\exp(\sqrt{-E}y) + B\exp(-\sqrt{-E}y), \tag{5.33}$$

where A and B are constants. Clearly we can see that if $E > 0$ we have imaginary indices in the exponential and hence oscillatory solutions. These do not decay as $|y| \to \infty$ and hence the boundary conditions are not satisfied. We therefore require $E < 0$.

Second, we show there is a similar restriction on ν. To do this, we multiply (5.31) by v and integrate over the domain

$$\int_{-\infty}^{\infty}\left(\left(\frac{d^2v}{dy^2}\right)v + Ev^2 + \nu\,\mathrm{sech}^2(y)v^2\right)dy = 0. \tag{5.34}$$

Integrating the first term by parts,

$$\left[\frac{dv}{dy}v\right]_{-\infty}^{\infty} - \int_{\infty}^{-\infty}\left(\frac{d^2v}{dy^2}\right)^2 dy + E\int_{-\infty}^{\infty} v^2 dy + \nu\int_{-\infty}^{\infty}\mathrm{sech}^2(y)v^2 dy = 0. \tag{5.35}$$

The first term is zero since $v \to 0$ as $|y| \to \infty$. The second term is negative, as is the third term, since the integral is positive and $E < 0$, hence we must have $\nu > 0$ since the integral in the final term is also positive. (Note: in our case we have $\nu = 1/g$, so this constraint is satisfied).

In summary, for non-oscillatory decaying solutions which satisfy the boundary conditions we must have

$$E < 0 \quad \text{and} \quad \nu > 0. \tag{5.36}$$

To solve (5.31) we first perform a transfer of variables using the identity

$$\mathrm{sech}^2(y) = 1 - \tanh^2(y). \tag{5.37}$$

We write $\tanh(y) = \eta$, so that y in $\mathbb{R}$ maps to η in (-1,1), and since

$$\frac{d}{dy} = (1-\eta^2)\frac{d}{d\eta} \qquad \text{and} \qquad \frac{d^2}{dy^2} = (1-\eta^2)\frac{d^2}{d\eta^2} - 2\eta(1-\eta^2)\frac{d}{d\eta}, \tag{5.38}$$

we can write (5.30) as

$$(1-\eta^2)^2\frac{d^2v}{d\eta^2} - 2\eta(1-\eta^2)\frac{dv}{d\eta} + \Big(E + \nu(1-\eta^2)\Big)v = 0. \tag{5.39}$$

We write v in the form

$$v(\eta) = (1-\eta^2)^{\frac{\theta}{2}}\phi(\eta), \tag{5.40}$$

where θ is of our choosing. We find

$$v_\eta = (1-\eta^2)^{\frac{\theta}{2}}\phi_\eta - \theta\eta(1-\eta^2)^{(\frac{\theta}{2}-1)}\phi \tag{5.41}$$

and

$$v_{\eta\eta} = (1-\eta^2)^{\frac{\theta}{2}}\phi_{\eta\eta} - 2\theta\eta(1-\eta^2)^{(\frac{\theta}{2}-1)}\phi_\eta - \theta[(1-\eta^2)^{(\frac{\theta}{2}-1)} - (\theta-2)\eta^2(1-\eta^2)^{(\frac{\theta}{2}-2)}]\phi. \tag{5.42}$$

Substituting (5.40) - (5.42) into (5.39) we have

$$(1-\eta^2)^2\phi_{\eta\eta} - (2\theta+2)\eta(1-\eta^2)\phi_\eta + \Big[\theta^2\eta^2 + E + (\nu-\theta)(1-\eta^2)\Big]\phi = 0. \tag{5.43}$$

Dividing through by $1-\eta^2$ would simplify the problem and this is most effective when we take $\theta^2 = -E$, since θ is left to our choice. Precisely, we take $\theta = +\sqrt{(}-E)$; then θ is real and positive, since we know $E < 0$, and from (5.40) we are imposing $v \to 0$ as $\eta \to \pm 1$ (i.e., $y \to \pm\infty$) provided ϕ remains bounded. Then (5.43) becomes

$$(1-\eta^2)\phi_{\eta\eta} - (2\sqrt{-E}+2)\eta\phi_\eta + (E+\nu-\sqrt{-E})\phi = 0. \tag{5.44}$$

Following Teeluck (2013), we proceed by looking for a power series solution of the form

$$\phi_n = \sum_{j=0}^{n} C_j\eta^j, \tag{5.45}$$

$$(\phi_n)_\eta = \sum_{j=0}^{n} jC_j\eta^{j-1}, \tag{5.46}$$

$$(\phi_n)_{\eta\eta} = \sum_{j=0}^{n} j(j-1)C_j\eta^{j-2}. \tag{5.47}$$

Substituting into (5.44)

$$\sum_{j=-2=0}^{n}(j+1)(j+2)C_{j+2}\eta^j - \sum_{j=0}^{n} j(j+1)C_j\eta^j - (4(\sqrt{-E}/2)+2)\sum_{j=0}^{n} jC_j\eta^j + (E+\nu-\sqrt{-E})\sum_{j=0}^{n} C_j\eta^j, \tag{5.48}$$

where we have shifted the index in the first term. We therefore have a relationship between the coefficients C_j and C_{j+2},

$$(j+1)(j+2)C_{j+2} = \left(j(j-1) + (4(\sqrt{-E}/2)+2)j - (E+\nu-\sqrt{-E})\right)C_j. \quad (5.49)$$

Note that this series terminates when $j = n$; then ϕ is guaranteed to be bounded, and we automatically satisfy $v \to 0$ as $\eta \to \pm 1$ (i.e., $y \to \pm\infty$). This termination condition is

$$n(n+1+2\sqrt{-E}) - (E+\nu-\sqrt{-E}) = 0. \quad (5.50)$$

This is our eigenvalue condition. We can rearrange to obtain a polynomial in $\sqrt{(}-E) = a$,

$$a^2 + (2n+1)a + n(n+1) - \nu = 0;$$

solving for a we find

$$\sqrt{-E} = \frac{1}{2}\left(\sqrt{1+4\nu} - (2n+1)\right). \quad (5.51)$$

We have taken the positive root of $\sqrt{1+4\nu}$ since to satisfy the boundary conditions we require $\theta > 0$. We therefore find

$$E = -\frac{1}{4}(2n+1-\sqrt{(1+4\nu)})^2. \quad (5.52)$$

We require $\theta = \sqrt{E} > 0$, therefore for fixed ν, from (5.51) we must have

$$n \leq \frac{\sqrt{1+4\nu}-1}{2}. \quad (5.53)$$

The complete set of finite eigenvalues are therefore given by

$$E = -\frac{1}{4}(2n+1-\sqrt{(1+4\nu)})^2, \quad \text{where} \quad 0 \leq n \leq \frac{\sqrt{1+4\nu}-1}{2}. \quad (5.54)$$

Note that with $n = 0$ we have

$$E = -\frac{1}{4}(1 - \sqrt{(1+4\nu)})^2, \quad \text{where} \quad 0 \leq \frac{\sqrt{1+4\nu}-1}{2}. \tag{5.55}$$

5.3.2 The dispersion relation

We can now find the dispersion relation for the growth rate s in terms of the parameters g and R_o for our instability problem (5.31). Since we have $E = -(1+s^2)/gR_o$ and $\nu = 1/g$, from (5.55) we thus have

$$s^2 = R_o - 1 + \frac{gR_o}{2}\left(1 - \sqrt{1+\frac{4}{g}}\right). \tag{5.56}$$

We show s^2 in terms of g, at $R_o = 1.5$, in figure 5.1. In general, we find $s^2 \to R_o - 1$ as $g \to 0$ and $s^2 \to -1$ as $g \to \infty$. Hence there exists a critical $g = g_c$ where $s^2 = 0$. To find this we set $s = 0$ in (5.56) and rearrange as follows

$$1 - \frac{2(1-R_o)}{R_0 g_c} = \sqrt{1+\frac{4}{g_c}}. \tag{5.57}$$

Squaring both sides we find a quadratic and after rearranging we have

$$g_c = \frac{(1-R_o)^2}{R_o}. \tag{5.58}$$

Note that to satisfy the left hand side of (5.57), the right hand side must be positive and assuming $g > 0$ this can only be the case when $R_o > 1$.

The local behaviour for $g \approx g_c$ can be found by making a Taylor expansion of s^2 about $g = g_c$:

$$s^2 \sim s^2(g = g_c) + (g - g_c)\frac{\partial s^2}{\partial g}\bigg|_{g_c} + \ldots, \tag{5.59}$$

giving

$$s^2 \sim +(g - g_c)\frac{R_o}{2}\left(1 - \frac{R_o^2 + 1}{(1 + R_o) \mid 1 - R_o \mid}\right) + \dots . \tag{5.60}$$

It is clear that since $R_o > 1$ for instability we require $g < g_c$. This will become important when considering the scalings when applying weakly nonlinear theory. As an example, if we set $R_o = 1.5$ we have

$$s^2 \sim -(g - g_c)\frac{6}{5}. \tag{5.61}$$

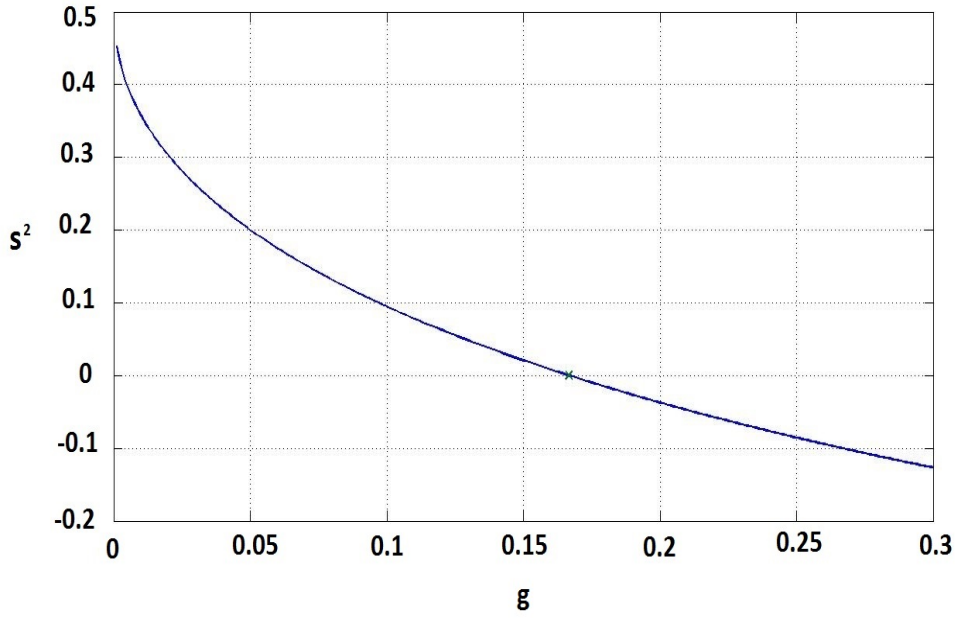

Figure 5.1: *Figure showing dispersion relation (5.56) when $R_o = 1.5$.*

5.4 Weakly nonlinear analysis

Now we have derived a system of PDEs that govern a two-layer system on the f-plane we can ask ourselves, how does the system behave when disturbed? Will any instabilities

grow indefinitely or will they dissipate and the system settle into an equilibrium state and how much of an influence do the initial conditions have on the system? There are two approaches which will be compared here, firstly applying weakly nonlinear theory to produce a system of ODEs and secondly solving the PDEs directly using a numerical scheme.

Weakly nonlinear theory can only be applied to disturbances of small growth rate, that is looking at the behaviour of the system where s from (5.56) is small. One way to do this is to fix the Rossby number R_o, which fixes g_c and choose our parameter g to deviate only slightly from g_c. We shall choose a small parameter δ to represent small deviations from criticality and write

$$g = g_c(1 - \delta^2). \tag{5.62}$$

5.4.1 Choice of scalings

We need to choose a suitable scaling for our variables, u, v, h, $\bar{u}$ and t. The scalings were justified as follows: we find if $g = g_c(1 - \delta^2)$ then from (5.56), $s \sim \delta$ and since $s \sim T^{-1}$ we have $T \sim \delta^{-1}$ and we write $\tau = \delta t$. We then look at the leading order terms of equations (5.23) - (5.26)

$$\delta\frac{\partial u}{\partial \tau} - Qv = 0, \tag{5.63}$$

$$u = -g\frac{\partial h}{\partial y}, \tag{5.64}$$

$$\delta\frac{\partial h}{\partial \tau} + \frac{R_o}{\alpha(1-\alpha)}\frac{\partial}{\partial y}\Big(D_1 D_2 v\Big) = 0, \tag{5.65}$$

$$\delta\frac{\partial \bar{u}_{non}}{\partial \tau} + R_o\frac{\partial}{\partial y}\Big(\alpha(1-\alpha)uv\Big) = 0. \tag{5.66}$$

It is necessary to introduce scalings for $\hat{u}$, $\hat{v}$, $\hat{h}$ and $\bar{u}_{non}$. Presumably they will all remain small, and thus each scale like some power of δ. However, it is not clear what those

powers should be. In (5.63) and (5.65) the leading order balance will be linear, with $\partial u/\partial t \sim v$ and $\partial h/\partial t \sim v$, implying $\delta u \sim v$ and $\delta h \sim v$. So, if $v \sim \delta^n$, we know $u \sim h \sim \delta^{(n-1)}$. Then, from (5.66), we have $\delta \bar{u}_{non} \sim uv \sim \delta^{(2n-1)}$, so $\bar{u}_{non} \sim \delta^{(2n-2)}$. However, this process does not determine n uniquely. We find from consideration of the nonlinear terms (below) that we should take $n = 2$ to get interesting dynamics.

$$v = \delta^2 \hat{v}, \quad u = \delta \hat{u}, \quad h = \delta \hat{h}, \quad \bar{u}_{non} = \delta^2 \hat{\bar{u}}_{non}, \tag{5.67}$$

are suitable scalings.

5.4.2 Scaled equations

Now we have the scalings in place we can perform a weakly nonlinear analysis. To start, we use equations (5.23) - (5.26) rearranged into a slightly different form,

$$\frac{\partial u}{\partial t} - Qv = -R_o v\left(\frac{\partial \bar{u}_{non}}{\partial y} + (2\alpha - 1)\frac{\partial u}{\partial y} - 2\alpha(1-\alpha)h\frac{\partial u}{\partial y} - \alpha(1-\alpha)u\frac{\partial h}{\partial y}\right), \tag{5.68}$$

$$\frac{\partial v}{\partial t} + u + g\frac{\partial h}{\partial y} = -R_o v\left((2\alpha - 1)\frac{\partial v}{\partial y} - 2\alpha(1-\alpha)h\frac{\partial v}{\partial y} - \alpha(1-\alpha)v\frac{\partial h}{\partial y}\right), \tag{5.69}$$

$$\frac{\partial h}{\partial t} + R_o\frac{\partial v}{\partial y} = -R_o\frac{\partial}{\partial y}\left((2\alpha - 1)hv - \alpha(1-\alpha)h^2 v\right), \tag{5.70}$$

$$\frac{\partial \bar{u}_{non}}{\partial t} = -R_o\frac{\partial}{\partial y}\left((\alpha - \alpha(1-\alpha)h)(1 - \alpha + \alpha(1-\alpha)h)uv\right). \tag{5.71}$$

Next substituting into these equations our scalings from (5.67) we have

$$\frac{\partial \hat{u}}{\partial \tau} - Q\hat{v} = -R_o\hat{v}\left(\delta^2\frac{\partial \hat{\bar{u}}_{non}}{\partial y} + (2\alpha-1)\delta\frac{\partial \hat{u}}{\partial y} - 2\alpha(1-\alpha)\delta^2\hat{h}\frac{\partial \hat{u}}{\partial y} - \alpha(1-\alpha)\delta^2\hat{u}\frac{\partial \hat{h}}{\partial y}\right) = \mathcal{N}_1, \tag{5.72}$$

$$\hat{u} + g\frac{\partial \hat{h}}{\partial y} = -\delta^2\frac{\partial \hat{v}}{\partial \tau} - R_o\delta\hat{v}\left((2\alpha-1)\delta^2\frac{\partial \hat{v}}{\partial y} - 2\alpha(1-\alpha)\delta^3\hat{h}\frac{\partial \hat{v}}{\partial y} - \alpha(1-\alpha)\delta^3\hat{v}\frac{\partial \hat{h}}{\partial y}\right) = \mathcal{N}_2, \tag{5.73}$$

$$\frac{\partial \hat{h}}{\partial \tau} + R_o \frac{\partial \hat{v}}{\partial y} = -R_o \frac{\partial}{\partial y}\left((2\alpha - 1)\delta \hat{h}\hat{v} - \alpha(1-\alpha)\delta^2 \hat{h}^2 \hat{v} \right) = \mathcal{N}_3, \tag{5.74}$$

$$\frac{\partial \hat{\bar{u}}_{non}}{\partial \tau} = -R_o \frac{\partial}{\partial y}\left((\alpha - \alpha(1-\alpha)\delta \hat{h})(1 - \alpha + \alpha(1-\alpha)\delta \hat{h})\hat{u}\hat{v} \right) = \mathcal{N}_4. \tag{5.75}$$

A single equation for $\hat{v}$ can be found by taking $\partial/\partial\tau$ of (5.73) and substituting for $\hat{u}$ and $\hat{h}$ from (5.72) and (5.74) respectively,

$$\left(\frac{\partial^2}{\partial y^2} - \frac{1}{gR_o} Q \right) \hat{v} = -\frac{1}{gR_o} \frac{\partial \mathcal{N}_2}{\partial \tau} + \frac{1}{gR_o} \mathcal{N}_1 + \frac{1}{R_o} \frac{\partial \mathcal{N}_3}{\partial y}. \tag{5.76}$$

The next step is to expand the variables, $\hat{v}$, $\hat{u}$, $\hat{h}$ and $\hat{\bar{u}}$ in terms of δ;

$$\hat{v} = \hat{v}_1 + \delta \hat{v}_2 + \delta^2 \hat{v}_3, \ldots \qquad \hat{u} = \hat{u}_1 + \delta \hat{u}_2 + \delta^2 \hat{u}_3 + \ldots, \tag{5.77}$$

$$\hat{h} = \hat{h}_1 + \delta \hat{h}_2 + \delta^2 \hat{h}_3, \ldots \qquad \hat{\bar{u}}_{non} = \hat{\bar{u}}_1 + \delta \hat{\bar{u}}_2 + \delta^2 \hat{\bar{u}}_3 + \ldots. \tag{5.78}$$

Substituting into equation (5.76) and also writing $g = g_c(1 - \delta^2)$ we have

$$\mathcal{L}_0 \hat{v} = \delta \frac{1}{g_c} \hat{v}_1 (2\alpha - 1) \frac{\partial \hat{u}}{\partial y} - \delta \frac{\partial^2}{\partial y^2}\left((2\alpha - 1)\hat{h}_1 \hat{v}_1 \right) + \mathcal{O}(\delta^2) + \ldots, \tag{5.79}$$

where

$$\mathcal{L}_0 = \frac{\partial^2}{\partial y^2} - \frac{1}{g_c R_o} Q. \tag{5.80}$$

Recall, $Q = 1 - R_o \operatorname{sech}^2(y)$.

This is the master equation. Similarly from (5.72), (5.74) and (5.75) we have

$$\frac{\partial \hat{u}}{\partial \tau} - Q\hat{v} = -\delta R_o \hat{v}_1 \left((2\alpha - 1) \frac{\partial \hat{u}_1}{\partial y} \right) + \mathcal{O}(\delta^2) + \ldots, \tag{5.81}$$

$$\frac{\partial \hat{h}}{\partial \tau} + R_o \frac{\partial \hat{v}}{\partial y} = -\delta R_o \frac{\partial}{\partial y}\left((2\alpha - 1)\hat{h}_1 \hat{v}_1 \right) + \mathcal{O}(\delta^2) + \ldots, \tag{5.82}$$

$$\frac{\partial \bar{u}_{non}}{\partial \tau} = -R_o \frac{\partial}{\partial y}\Bigg(\alpha(1-\alpha)\hat{u}_1\hat{v}_1 - \delta\alpha(2\alpha^2 - 3\alpha + 1)\hat{h}_1\hat{u}_1\hat{v}_1 + \delta\alpha(1-\alpha)(\hat{u}_1\hat{v}_2 + \hat{u}_2\hat{v}_1)\Bigg) + \mathcal{O}(\delta^2) + \ldots. \quad (5.83)$$

5.4.3 Leading-order equations

We can now equate powers of δ. Firstly from equation (5.79) at first order we have,

$$\mathcal{L}_0\hat{v}_1 = 0. \quad (5.84)$$

The solution is $\hat{v}_1 = A(\tau)\,\mathrm{sech}^{\theta}(y)$, where, using (5.51), $\theta = -1/2(1-\sqrt{1+4/g_c})$, with $n = 0$. From equations (5.81) , (5.82) and (5.83), at first order we obtain solutions for $\hat{u}_1$, $\hat{h}_1$ and $\hat{\bar{u}}_1$ given by

$$\hat{u}_1 = B(\tau)Q\,\mathrm{sech}^{\theta}(y), \quad \hat{h}_1 = -R_oB(\tau)\frac{\partial}{\partial y}\,\mathrm{sech}^{\theta}(y), \quad (5.85)$$

$$\hat{\bar{u}}_1 = -\frac{R_oB^2(\tau)}{2}\alpha(1-\alpha)\frac{\partial}{\partial y}(Q\,\mathrm{sech}^{2\theta}(y)), \quad (5.86)$$

where $A(\tau) = dB(\tau)/d\tau$ and we have used (5.73).

5.4.4 First-order equations

At order δ, we have from equation (5.79)

$$\mathcal{L}_0 v_2 = -g_c^{-1}\hat{v}_1(2\alpha-1)\frac{\partial \hat{u}_1}{\partial y} - \frac{\partial^2}{\partial y^2}\Bigg((2\alpha-1)\hat{h}_1\hat{v}_1\Bigg). \quad (5.87)$$

Substituting for $\hat{u}_1$, $\hat{v}_1$ and $\hat{h}_1$ from (5.85) into (5.87) we have

$$\mathcal{L}_0 v_2 = (2\alpha-1)\theta A(\tau)B(\tau)\bigg(g_c^{-1} - 4R_o\alpha\theta\bigg)\operatorname{sech}^{2\theta}(y)\tanh(y) + \\ (2\alpha-1)R_o A(\tau)B(\tau)\bigg(\alpha(2\theta+1)(2\theta+2) - g_c^{-1}(\theta+2)\bigg)\operatorname{sech}^{2\theta+2}(y)\tanh(y). \quad (5.88)$$

In order to make progress a solution for v_2 is requires; this is achieved numerically. First we write $v_2 = A(\tau)B(\tau)\tilde{v}_2$ and seek a numerical solution for $\tilde{v}_2$. We write (5.88) in matrix form creating an inverse matrix problem we then use Matlab's inbuilt software to solve (5.88). It therefore follows from (5.81) - (5.82)

$$\frac{\partial u_2}{\partial \tau} = Qv_2 - R_o v_1(2\alpha-1)\frac{\partial u_1}{\partial y}, \quad (5.89)$$

$$\frac{\partial h_2}{\partial \tau} = -R_o\frac{\partial v_2}{\partial y} - R_o(2\alpha-1)\frac{\partial}{\partial y}(h_1 v_1). \quad (5.90)$$

Substituting from (5.85) into the above we have

$$u_2 = \frac{B^2(\tau)}{2}\tilde{u}_2 = \frac{QB^2(\tau)}{2}\tilde{v}_2 - \frac{R_o B^2(\tau)}{2}(2\alpha-1)\operatorname{sech}^{\theta}(y)\frac{\partial}{\partial y}\bigg(Q\operatorname{sech}^{\theta}(y)\bigg), \quad (5.91)$$

$$h_2 = \frac{B^2(\tau)}{2}\tilde{h}_2 = -\frac{R_o B^2(\tau)}{2}\frac{\partial \tilde{v}_2}{\partial y} \\ + \frac{B^2(\tau)}{2}R_o^2(2\alpha-1)\frac{\partial}{\partial y}\bigg(\operatorname{sech}^{\theta}(y)\frac{\partial}{\partial y}(\operatorname{sech}^{\theta}(y))\bigg). \quad (5.92)$$

5.4.5 Second-order equations

At order δ^2 from (5.79) we have

$$\mathcal{L}_0 v_3 + \mathcal{L}_1 v_1 = \frac{\partial \hat{v}_3}{\partial y} - g_c^{-1} R_o^{-1} Q \hat{v}_3 - g_c^{-1} R_o^{-1} Q \hat{v}_1 = g_c^{-1} \hat{v}_1 \Bigg(\frac{\partial \hat{\bar{u}}_1}{\partial y} + (2\alpha - 1) \frac{\partial \hat{u}_2}{\partial y} - 2\alpha(1-\alpha)\hat{h}_1 \frac{\partial \hat{u}_1}{\partial y} - \alpha(1-\alpha)\hat{u}_1 \frac{\partial \hat{h}_1}{\partial y} \Bigg) - g_c^{-1}(2\alpha - 1)\hat{v}_2 \frac{\partial \hat{u}_1}{\partial y} - \frac{\partial^2}{\partial y^2} \Bigg((2\alpha - 1)(\hat{h}_1 \hat{v}_2 + \hat{v}_1 \hat{h}_2) - \alpha(1-\alpha)(\hat{h}_1^2 \hat{v}_1) \Bigg) + g_c^{-1} R_o^{-1} \frac{\partial^2 \hat{v}_1}{\partial \tau^2}, \quad (5.93)$$

where $\mathcal{L}_1 = -g_c^{-1} R_o^{-1} Q$. We substitute for $\hat{u}_1$, $\hat{v}_1$, $\hat{h}_1$, $\hat{\bar{u}}_1$, $\hat{v}_2$, $\hat{u}_2$ and $\hat{h}_2$ and then multiplying by the eigenfunction $\mathrm{sech}^{\theta}(y)$, so that the v_3 terms disappear when (5.93) is integrated between $y \pm \infty$. After some rearranging we find

$$\frac{d^2 A(\tau)}{d\tau^2} = \tilde{Q} A(\tau) - \tilde{R} A(\tau) B^2(\tau), \quad (5.94)$$

where the expressions for $\tilde{Q}$ and $\tilde{R}$ are complex and will be discussed in the next section. This is the required amplitude equation, which we can easily rewrite as a system of first-order ODEs:

$$\frac{dA(\tau)}{d\tau} = C(\tau), \quad (5.95a)$$

$$\frac{dB(\tau)}{d\tau} = A(\tau), \quad (5.95b)$$

$$\frac{dC(\tau)}{d\tau} = \tilde{Q} A(\tau) - \tilde{R} A(\tau) B^2(\tau). \quad (5.95c)$$

5.4.6 Coefficients in the amplitude equation

In (5.95c) the coefficient $\tilde{Q}$ is defined as

$$\tilde{Q} = \int_{-\infty}^{\infty} Q\,\mathrm{sech}^{2\theta}(y)dy\bigg(\int_{-\infty}^{\infty}\mathrm{sech}^{2\theta}(y)\bigg)^{-1}. \tag{5.96}$$

We can use the following identity to simplify $\tilde{Q}$

$$\int \mathrm{sech}^{2\theta+2}(y)dy = \frac{\mathrm{sech}^{2\theta}(y)\tanh(y)}{2\theta+1} + \frac{2\theta}{2\theta+1}\int \mathrm{sech}^{2\theta}(y)dy \tag{5.97}$$

and find

$$\tilde{Q} = \bigg(1 - \frac{2R_o\theta}{2\theta+1}\bigg), \tag{5.98}$$

where $\mathrm{sech}^{2\theta}(y)\tanh(y)$ has vanished upon integration since it is an odd function.

The remaining coefficient $\tilde{R}$ is defined as

$$\begin{aligned}
\tilde{R} = -\frac{R_o^2\alpha(1-\alpha)}{2}\bigg(\theta - 2\theta\int_{\infty}^{\infty} Q\,\mathrm{sech}^{3\theta}(y)\frac{\partial}{\partial y}\bigg(\mathrm{sech}^{\theta}(y)\tanh(y)\bigg)dy - \\
4\theta\int_{-\infty}^{\infty}\mathrm{sech}^{3\theta}(y)\tanh(y)\frac{\partial}{\partial y}\bigg(Q\,\mathrm{sech}^{\theta}(y)\bigg)dy - \\
2g_cR_o\theta^2\int_{-\infty}^{\infty}\mathrm{sech}^{\theta}(y)\frac{\partial^2}{\partial y^2}\bigg(\mathrm{sech}^{3\theta}(y)\tanh^2(y)\bigg)dy\bigg) \\
+\frac{R_o^2(2\alpha-1)^2}{2}\bigg(-R_o(\theta+2)\int_{-\infty}^{\infty}\mathrm{sech}^{2\theta}(y)\frac{\partial}{\partial y}\bigg(\mathrm{sech}^{2\theta+2}(y)\tanh(y)\bigg)dy + \\
\theta\int_{-\infty}^{\infty}\mathrm{sech}^{2\theta}(y)\frac{\partial}{\partial y}\bigg(\mathrm{sech}^{2\theta}(y)\tanh(y)\bigg)dy + \\
g_cR_o\int_{-\infty}^{\infty}\mathrm{sech}^{\theta}(y)\frac{\partial^2}{\partial y^2}\bigg(\mathrm{sech}^{\theta}(y)\frac{\partial}{\partial y}\bigg(\mathrm{sech}^{\theta}(y)\frac{\partial}{\partial y}\bigg(\mathrm{sech}^{\theta}(y)\bigg)\bigg)\bigg)dy\bigg) + \\
\bigg(\int_{-\infty}^{\infty}\mathrm{sech}^{2\theta}(y)dy\bigg)^{-1}\bigg(R_o^2g_c(2\alpha-1)\int_{-\infty}^{\infty}\mathrm{sech}^{\theta}(y)\frac{\partial^2}{\partial y^2}\bigg(\tilde{v}_2\frac{\partial}{\partial y}\mathrm{sech}^{\theta}(y)\bigg)dy -
\end{aligned} \tag{5.99}$$

$$R_o(2\alpha-1)\int_{-\infty}^{\infty}\tilde{v}_2\,\mathrm{sech}^{\theta}(y)\frac{\partial}{\partial y}\Big(Q\,\mathrm{sech}^{\theta}(y)\Big)dy+$$
$$R_o(2\alpha-1)\int_{-\infty}^{\infty}\mathrm{sech}^{\theta}(y)\frac{\partial}{\partial y}\Big(\frac{Q\tilde{v}_2}{2}-R_o(2\alpha-1)\,\mathrm{sech}^{2\theta}(y)\frac{\partial}{\partial y}\Big(Q\,\mathrm{sech}^{\theta}(y)\Big)\Big)dy-$$
$$\int_{-\infty}^{\infty}\frac{\partial^2}{\partial y^2}\Big(\,\mathrm{sech}^{2\theta}(y)\Big(-\frac{R_o}{2}\frac{\partial\tilde{v}_2}{\partial y}+\frac{R_o^2}{2}(2\alpha-1)\frac{\partial}{\partial y}\Big(\,\mathrm{sech}^{\theta}(y)\frac{\partial}{\partial y}\,\mathrm{sech}^{\theta}(y)\Big)\Big)\Big)dy\Big) \tag{5.100}$$

We can make some progress with the evaluation of $\tilde{R}$ by using identity (5.97). We can also evaluate the remaining integrals by noting from Gradshteyn and Ryzhik (2014) that

$$\int_{-\infty}^{\infty}\mathrm{sech}^{2n}(y)dy=\int_{0}^{\frac{\pi}{2}}\sin^{2n-1}(x)dx=2^{n-2}B(n,n), \tag{5.101}$$

where B denotes the beta functions and we have used the identity $\mathrm{sech}^2(y)=1-\tanh^2(y)$.

For instability we require $\tilde{Q}>0$. It is hard to say anything of value about $\tilde{R}$ due to its complexity however it can be evaluated numerically. As we shall see in the parameters we have used in our analysis, $\tilde{R}$ was never seen to be negative, we therefore assume $\tilde{R}>0$.

5.4.7 Properties of the ODE system

Through the double integration of equation (5.95c) a quartic polynomial emerges describing the solution of A^2 with respect to B. Two invariant functions (κ_1 and κ_2), are found which do not change as the solution evolves with τ. These invariant functions along with the quartic equation can help in the understanding of the solution before doing any numerical schemes.

Firstly, note that equation (5.95c) can be written as

$$\frac{dC}{d\tau} = \tilde{Q}\frac{dB}{d\tau} - \tilde{R}B^2\frac{dB}{d\tau}. \tag{5.102}$$

After integrating with respect to τ we have

$$C = \tilde{Q}B - \frac{\tilde{R}B^3}{3} + \kappa_1, \tag{5.103}$$

where κ_1 is a constant of integration. We see that the first invariant can be written in terms of any given initial conditions

$$\kappa_1 = C(0) - \tilde{Q}B(0) + \frac{\tilde{R}B^3(0)}{3}. \tag{5.104}$$

The second invariant comes from the further integration of (5.103), since $C = d^2B/d\tau^2$, multiplying equation (5.103) by $dB/d\tau$ we have

$$\frac{dB}{d\tau}\frac{d^2B}{d\tau^2} = \tilde{Q}B\frac{dB}{d\tau} - \frac{\tilde{R}B^3}{3}\frac{dB}{d\tau} + \kappa_1\frac{dB}{d\tau}. \tag{5.105}$$

After integrating,

$$\frac{A^2}{2} = \frac{1}{2}\left(\frac{dB}{d\tau}\right)^2 = \frac{\tilde{Q}B^2}{2} - \frac{\tilde{R}B^4}{12} + \kappa_1 B + \kappa_2. \tag{5.106}$$

Eliminating κ_1 from (5.106) using equation (5.104), the second invariant can therefore be written again in terms of any specified initial conditions,

$$\kappa_2 = \frac{A(0)^2}{2} + \frac{\tilde{Q}B(0)^2}{2} - \frac{\tilde{R}B(0)^4}{4} - B(0)C(0). \tag{5.107}$$

It should be noted that equation (5.106) is a quartic describing A^2 as a function of B. The analysis of this quartic can give an insight into the types of solutions we might expect and moreover the behaviour of the ODEs.

5.4.8 Behaviour of the quartic equation

Assuming a fixed $\tilde{Q}$ and $\tilde{R}$, it is clear the quartic equation (5.106) is governed by the values κ_1 and κ_2. Particularly affected are the intercept, given by κ_2, and the gradient at $B \ll 1$ approximated by κ_1. We also find that as $B \to \pm\infty$, $A^2 \to -\infty$. We shall look at these invariants to understand what they can tell us about the solution.

Firstly it should be noted that changing the sign of κ_1 has a limited effect on the behaviour of the ODEs since substituting $\kappa_1 = -\kappa_1$ and $B = -B$ into (5.106) the equation remains unchanged. Therefore it can be concluded that changing the sign of κ_1 need only flip the solution in the A^2-axis. It shall be assumed $\kappa_1 > 0$ without loss of generality. When $B \ll 1$ the gradient is approximately κ_1, hence all solutions investigated below must have a positive gradient at the A^2-axis.

Other factors that can provide information about the form of the solution are the intercept of the quartic, which can give us some indication of the type of roots of the quartic (real or complex) and secondly the second derivation of the quartic, which can tell us if the gradient is increasing or decreasing with B.

Product of the roots of the quartic

The sign of intercept of the quartic (5.106) can tell us how many of those roots might be positive or negative or even how many are real and complex. For example, let us write (5.106) as

$$f(B) = -\frac{\tilde{R}}{6}(B-a)(B-b)(B-c)(B-d) = -\frac{\tilde{R}}{6}B^4 + \ldots - \frac{\tilde{R}}{6}abcd. \qquad (5.108)$$

We see that the product of the roots is equivalent to

$$abcd = -\frac{12\kappa_2}{\tilde{R}}. \tag{5.109}$$

As discussed we take $\tilde{R} > 0$, therefore the nature of the roots depends upon the sign of κ_2 only.

Case 1, $\kappa_2 > 0$

Here, $abcd < 0$ and therefore we can have the following

(i). 4 real roots, (3 negative, 1 positive),
(ii). 4 real roots, (1 negative, 3 positive),
(iii). 1 complex conjugate pair, 2 real roots, (1 negative, 1 positive).

Case 2, $\kappa_2 < 0$

Here, $abcd > 0$ and therefore we can have

(i). 4 real roots, (all positive),
(ii). 4 real roots, (all negative),
(iii). 4 real roots, (2 negative, 2 positive),
(iv). 1 complex conjugate pair, 2 real roots, (both positive),
(v). 1 complex conjugate pair, 2 real roots, (both negative),
(vi). 2 complex conjugative pairs.

Figure 5.2 displays all possible forms of the solution in case 1 ($\kappa_2 > 0$), whereas case 2 is shown in figure 5.3. An exception to this is solutions case 2 (ii), (case 2 (i) if $\kappa_1 < 0$) and (vi): (ii) cannot be drawn since when $B \ll 1$, the gradient is determined by κ_1, ($A \approx 2\kappa_1 B + 2\kappa_2$). This case can only be drawn when $\kappa_1 < 0$ (it is therefore case (i) that

is no longer valid for the same argument when $\kappa_1 < 0$). Case 2 (vi) is of no interest since there are no real solutions for A (A^2 positive).

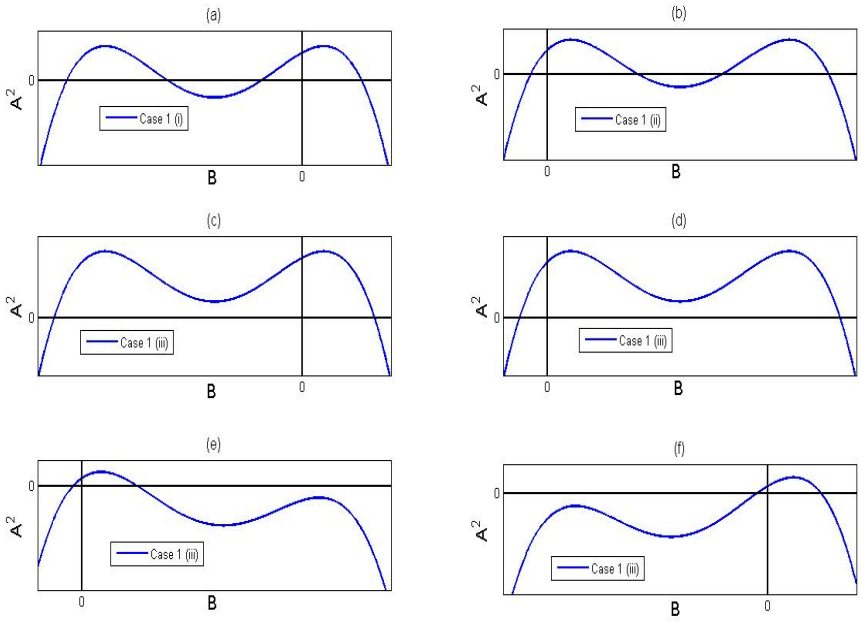

Figure 5.2: *Figure showing what the quartic solution may look like in Case 1, $\kappa_2 > 0$, ($\kappa_1 > 0$).*

Double derivative of the quartic

It is possible to discard a number of these solutions as drawn in figure 5.2 and figure 5.3 by looking at the second derivative,

$$f''(B) = -2\tilde{R}B^2 + 2\tilde{Q}, \tag{5.110}$$

which tells us if

$$-\sqrt{\frac{\tilde{Q}}{\tilde{R}}} < B < \sqrt{\frac{\tilde{Q}}{\tilde{R}}},$$

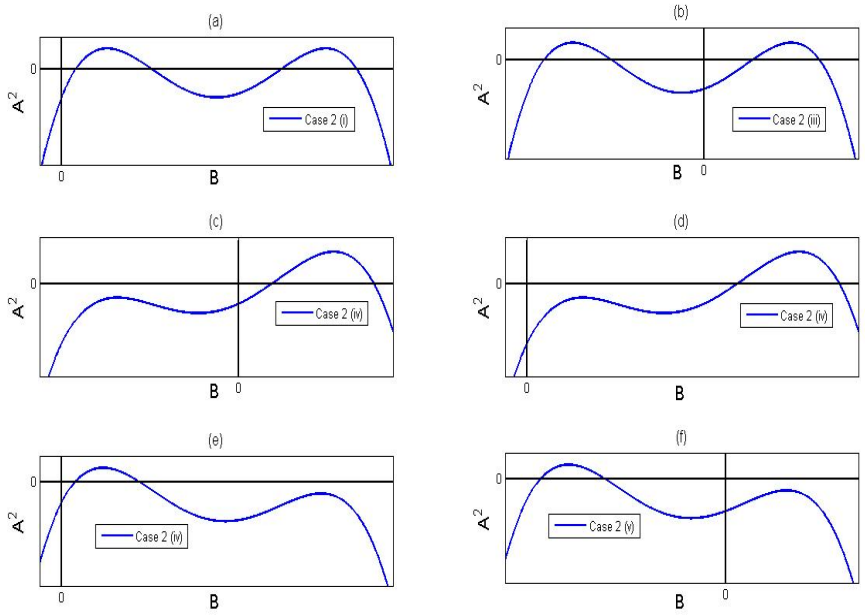

Figure 5.3: *Figure showing what the quartic solution may look like in Case 2, $\kappa_2 > 0$ ($\kappa_1 > 0$).*

we have $f''(B) > 0$ and therefore a local minimum. Hence, for

$$B < -\sqrt{\frac{\tilde{Q}}{\tilde{R}}} \qquad \text{or} \qquad B > \sqrt{\frac{\tilde{Q}}{\tilde{R}}}$$

we have $f''(B) < 0$ and a local maximum. Where we have a local minimum occurring to the right of the A^2-axis, ($0 < B < \sqrt{\tilde{Q}/\tilde{R}}$), we cannot have a local maximum occurring between this local minimum and the A^2-axis. For this reason solutions as drawn in figure 5.2(b), (d) and (e) cannot possibly occur. Similarly using the argument of $f''(B)$ as used when $\kappa_2 > 0$ we can also eliminate solutions as drawn in figure 5.3(a), (d) and (e).

The discriminant of the quartic

Lastly, it can be shown that solution (f) from figure 5.3 where $\kappa_2 < 0$ can also not occur. This solution occurs when the maximum on the right of the solution 5.3 (b) crosses the B-axis. For this to occur we must have

$$f(B) = -\frac{\tilde{R}}{6}B^4 + \tilde{Q}B^2 + 2\kappa_1 B + 2\kappa_2 = 0, \tag{5.111}$$

$$f'(B) = -\frac{2\tilde{R}}{3}B^3 + 2\tilde{Q}B + 2\kappa_1 = 0. \tag{5.112}$$

Now, to pass from (b) to (f) in figure 5.3 we must have the discriminant of (5.111) and (5.112) both equal to zero. From (5.112) we find

$$\kappa_1^2 = \frac{4\tilde{Q}^3}{9\tilde{R}}. \tag{5.113}$$

Substituting this into the discriminant of (5.111) to eliminate κ_1 we have

$$16\tilde{R}^3\kappa_2^3 + 24\tilde{R}^2\tilde{Q}^2\kappa_2^2 - 15\tilde{Q}^4\tilde{R}\kappa_2 + 2\tilde{Q}^6 = 0, \tag{5.114}$$

which is a cubic in κ_2. The discriminant of (5.114) is given by

$$\Delta = -414720\tilde{Q}^{12}\tilde{R}^6 < 0, \tag{5.115}$$

which tells us the roots of (5.114) consist of one complex conjugate pair and one real. The product of the roots must be equal to

$$\frac{64\tilde{Q}^6}{512\tilde{R}^3} > 0, \tag{5.116}$$

which tells us the real root must be positive, ($\kappa_2 > 0$). This contradicts our assumption that $\kappa_2 < 0$ and hence solution (f) does not exist.

In summary it is only solutions (a), (c) and (f) from figure 5.2 and solutions (b) and (c) from figure 5.3 that will ever been seen in the ODEs (when $\kappa_1 > 0$). Such cases will produce either one or two separate periodic orbits which can clearly be seen by plotting A against B.

5.5 Numerical solutions of the weakly nonlinear ODE system

We wish to solve the weakly nonlinear equations numerically. We use a 4th-order Runge-Kutta scheme, the details of which are given in Appendix C. We choose a 4th-order Runge-Kutta scheme because it is known to be highly accurate and has a large stability region.

We will look at the most unstable mode. This can be done by setting the initial conditions in our scheme to be the exact solution to the linear ODEs, namely

$$\frac{dC(\tau)}{d\tau} = \tilde{Q}A(\tau), \tag{5.117a}$$

$$\frac{dB(\tau)}{d\tau} = A(\tau), \tag{5.117b}$$

$$\frac{dA(\tau)}{d\tau} = C(\tau), \tag{5.117c}$$

which has solution

$$A^* = A_o \exp(\tilde{Q}^{1/2}\tau), \qquad B^* = A_o\tilde{Q}^{-1/2}\exp(\tilde{Q}^{1/2}\tau), \qquad C^* = A_o\tilde{Q}^{1/2}\exp(\tilde{Q}^{1/2}\tau), \tag{5.118}$$

where A_o is a constant of integration. We chose $\delta = 0.01$, $A_o = 0.1$ and also $R_o = 1.5$, which appears in $\tilde{R}$ and $\tilde{Q}$. Figure 5.4 shows the solution for this scheme, it is clear from (a) and (b) a periodic cycle exists. In (c) and (d) we can see the periodic orbit A and B

are following, and by looking closer at the origin in (e) and (f) we can identify what type of solution we have. Here $\kappa_1 = 0.0015$ and $\kappa_2 = -2.45 \times 10^{-4}$; it is therefore evident that here we have Case 2 (iii) as discussed above. By deviating away from the fastest

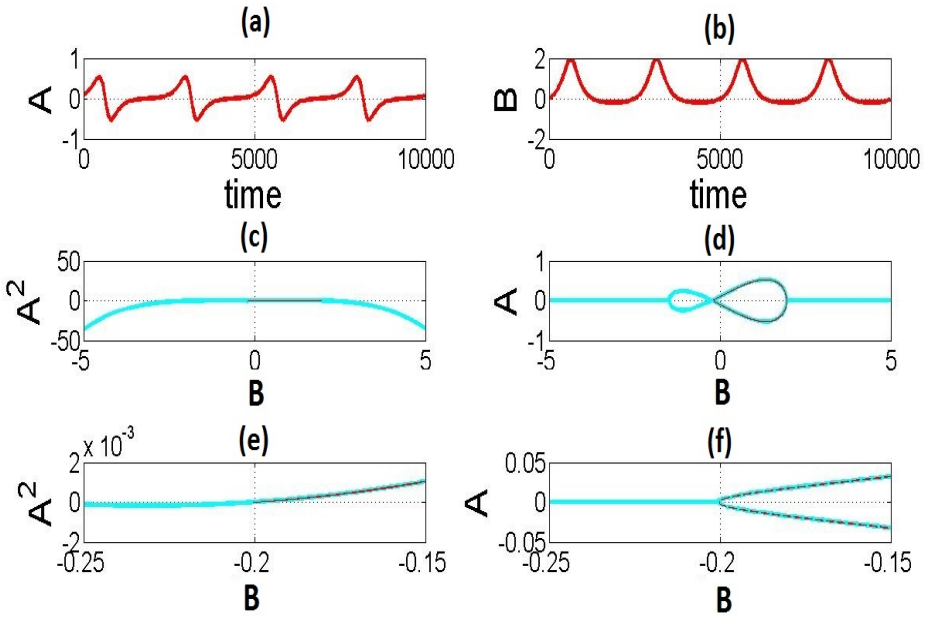

Figure 5.4: *The ODE (red) solution when initialised with the fastest growing mode and the quartic function (5.106) (cyan). (a) and (b) shows the solution of A and B against time, (c) and (d) shows the trajectory of these solutions. In (e) and (f) we can see a zoomed in version of (c) and (d). Here $\delta = 0.1$ and $A_o = 0.1$.*

growing mode we can manipulate the solution to demonstrate all cases shown in figure 5.2 and figure 5.3 that were shown to exist. Table 5.1 shows how the solution has deviated from the fastest growing mode where A^*, B^* and C^* (with $A_o = 1 \times 10^{-8}$) are the exact solution to the linear ODEs shown by (5.118). Also shown are the retrospective values for κ_1 and κ_2. Figures 5.5 - 5.9 shows these solutions.

Table 5.1: ODE Results

A	B	C	κ_1	κ_2	Case	Figure
500A*	-B*	1000C*	0.0448	0.0013	1(i)	5.5
1500A*	-B*	1800C*	0.0805	0.0013	1(iii)	5.6
1500A*	B*	500C*	0.0223	0.0012	1(iii)	5.7
A*	2000B*	2000C*	0.0117	-0.0239	2(iii)	5.8
A*	2000B*	3000C*	0.0564	-0.0439	2(iv)	5.9

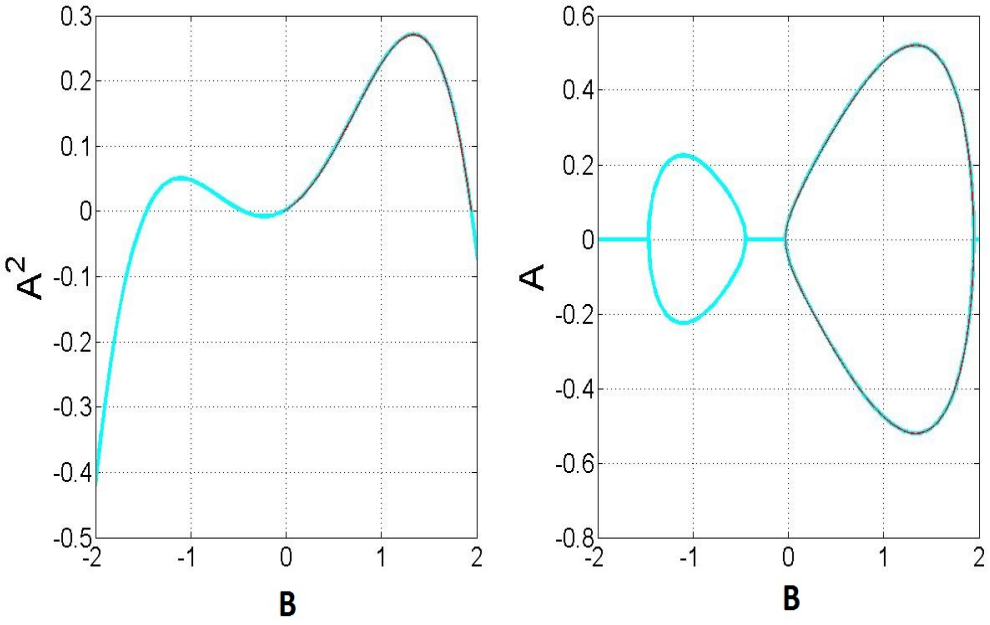

Figure 5.5: *The ODE solution (red) and quartic function (5.106) (cyan). Here we have case 1(i) as shown in figure 5.2,* $\delta = 0.01$, $\kappa_2 > 0$, $\kappa_1 > 0$.

5.6 Comparison between a numerical solution of the full nonlinear PDEs and the weakly nonlinear ODEs

The weakly nonlinear analysis has revealed the possibility of various types of cyclic orbits for weakly unstable conditions. We now ask if any of this behaviour actually occurs for small δ in the fully nonlinear PDEs. If so, this is a useful consistency check between the

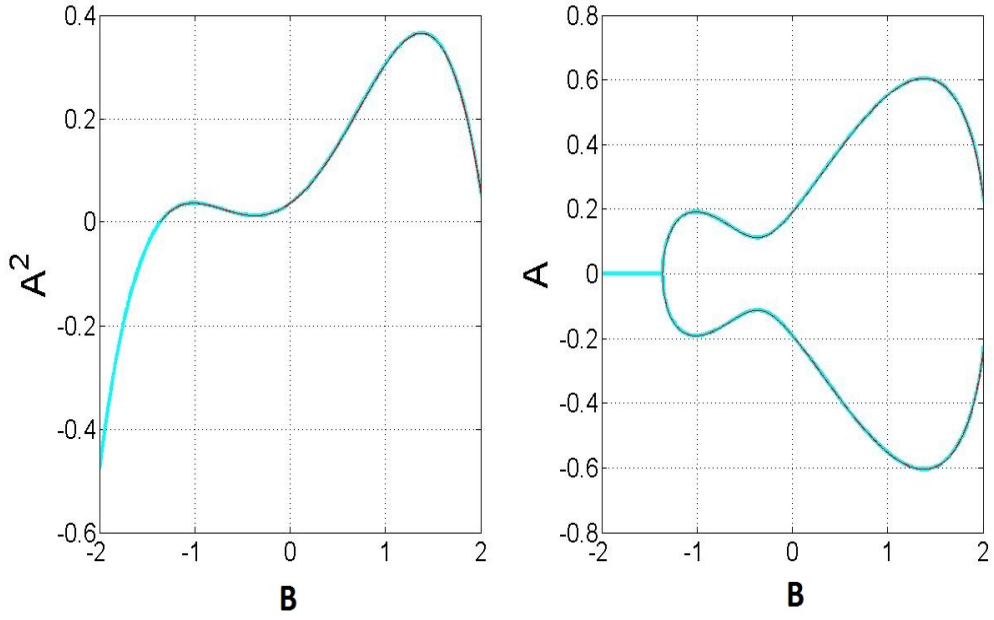

Figure 5.6: *The ODE solution (red) and quartic function (5.106) (cyan). Here we have case 1(iii) as shown in figure 5.2,* $\delta = 0.01$, $\kappa_2 > 0$, $\kappa_1 > 0$.

ODEs and PDEs. We might also ask how large can δ be made before the weakly nonlinear theory breaks down.

The equations to be solved are

$$\frac{\partial u}{\partial t} + R_o v \frac{\partial}{\partial y}(\bar{u}_{non} - u) + 2R_o v D_1 \frac{\partial u}{\partial y} + R_o uv \frac{\partial D_1}{\partial y} - Qv = 0, \tag{5.119}$$

$$\frac{\partial v}{\partial t} - R_o v \frac{\partial v}{\partial y} + 2R_o D_1 v \frac{\partial v}{\partial y} + R_o v^2 \frac{\partial D_1}{\partial y} + u = -g\frac{\partial h}{\partial y}, \tag{5.120}$$

$$\frac{\partial h}{\partial t} + \frac{R_o}{\alpha(1-\alpha)} \frac{\partial}{\partial y}\left(D_1 D_2 v \right) = 0, \tag{5.121}$$

$$\frac{\partial \bar{u}_{non}}{\partial t} + R_o \frac{\partial}{\partial y}\left(D_1 D_2 uv \right) = 0. \tag{5.122}$$

We use the same numerical scheme as for the simulations of section 4.5, and this following the scheme outlined in Appendix C. Equations (5.119) - (5.122) contain three parameters

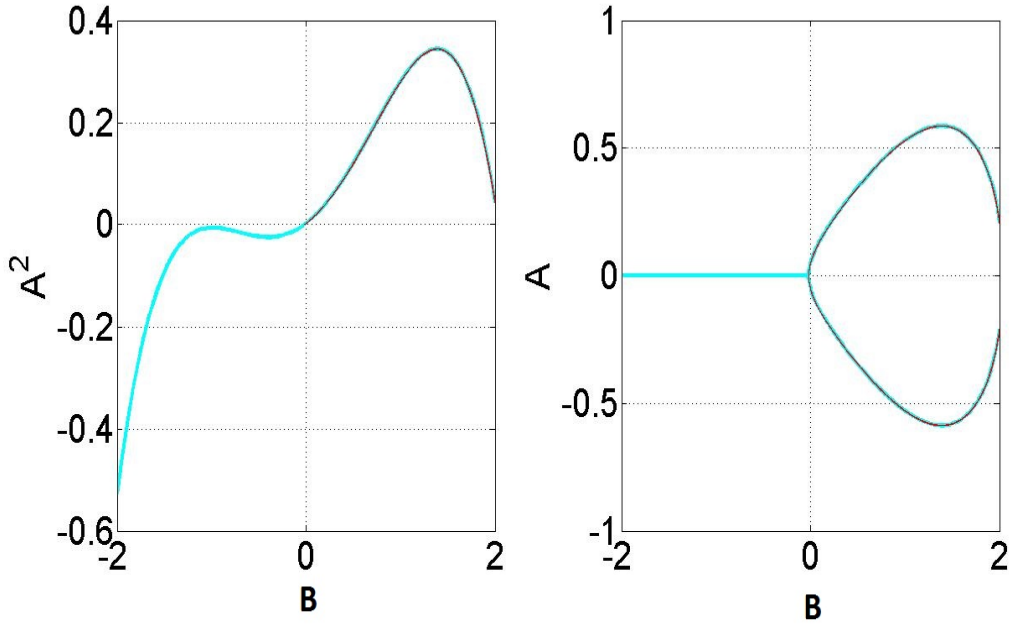

Figure 5.7: *The ODE solution (red) and quartic (5.106) (cyan). Here we have case 1(iii) as shown in figure 5.2,* $\delta = 0.01$, $\kappa_2 > 0$, $\kappa_1 > 0$.

α and R_o which are fixed and g which is variable. The PDEs are related to the ODEs through the relationship shown by (5.62) where $g = g_c(1 - \delta^2)$.

5.6.1 Experiment 1: $v(0) = 0$

As a precursor to looking at the fastest growing mode we shall set $v(0) = 0$ and keep other variables in this fastest growing mode state, namely

$$v(0) = 0 \tag{5.123a}$$

$$h(0) = \frac{v_m R_o \theta}{s} \operatorname{sech}^{\theta}(y) \tanh(y), \tag{5.123b}$$

$$u(0) = \frac{v_m Q}{s} \operatorname{sech}^{\theta}(y), \tag{5.123c}$$

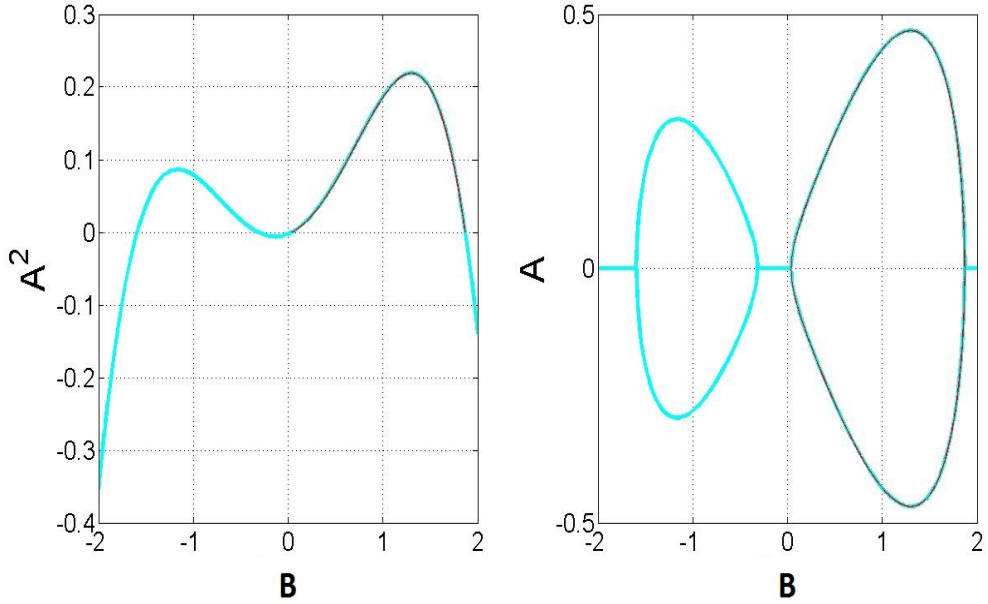

Figure 5.8: *The ODE solution (red) and quartic function (5.106) (cyan). Here we have case 2(iii) as shown in figure 5.3,* $\delta = 0.01$, $\kappa_2 < 0$, $\kappa_1 > 0$.

where s is the linear growth rate and θ is an eigenvalue given by the solution of (5.51). Various values of v_m were chosen each changing the behaviour of the solution and again we set $R_o = 1.5$.

The ODEs were initialised with the equivalent initial condition; we have $A \sim \delta^2 v$, $v = v_m \operatorname{sech}^{\theta}(y)$ and since $\operatorname{sech}^{\theta}(y)$ has a maximum of one we take $A(0) = v_m/\delta^2$. Lastly, $B(0)$ and $C(0)$ were then calculated using the solution to the linear ODEs written in terms of $A(0)$, namely

$$A(0) = v_m(0)/\delta^2, \tag{5.124a}$$

$$B(0) = A(0)/(\tilde{Q}^{1/2}), \tag{5.124b}$$

$$C(0) = \tilde{Q}^{1/2} A(0). \tag{5.124c}$$

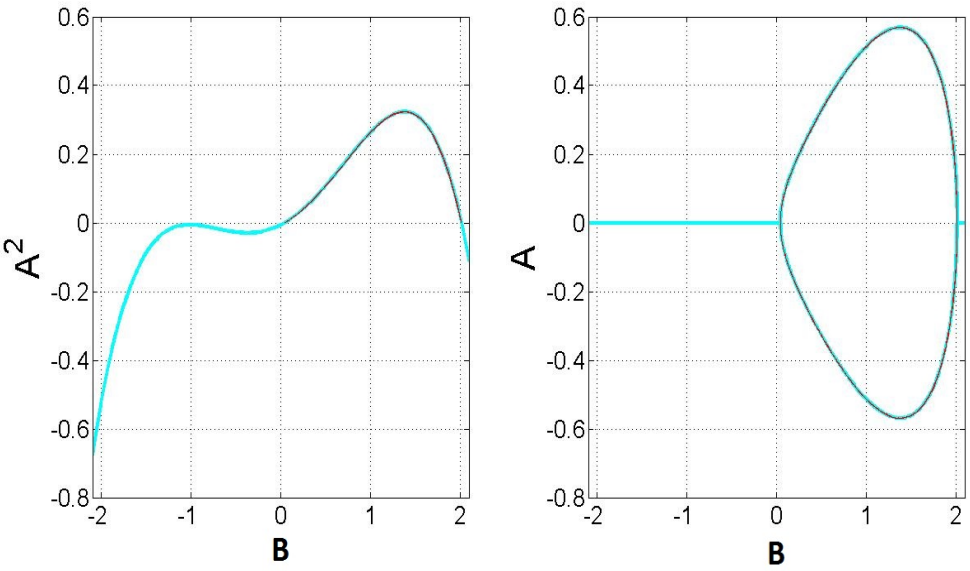

Figure 5.9: *The ODE solution (red) and quartic function (5.106)(cyan). Here we have case 2(iv) as shown in figure 5.3,* $\delta = 0.01$, $\kappa_2 < 0$, $\kappa_1 > 0$.

As with the PDEs, $A(0)$ was modified as follows

$$A(0) = 0; \tag{5.125}$$

however, $B(0)$ and $C(0)$ retain their values as if $A(0) = v_m(0)/\delta^2$. To compare the PDEs with the ODEs, v and u were projected onto A and B using the following,

$$A(\tau) = \frac{\int_{-\infty}^{\infty} \operatorname{sech}^{\theta}(y) v dy}{\int_{-\infty}^{\infty} \operatorname{sech}^{2\theta}(y) dy}, \qquad B(\tau) = \frac{\int_{-\infty}^{\infty} \tilde{Q} \operatorname{sech}^{\theta}(y) u dy}{\int_{-\infty}^{\infty} \tilde{Q}^2 \operatorname{sech}^{2\theta}(y) dy}. \tag{5.126}$$

To begin with, we choose $\delta = 0.01$, $v_m = 1 \times 10^{-8}$, which sets us in a weakly nonlinear regime. Figure 5.10 shows the solution; it is evident that this is equivalent to Case 2 (iii) with $\kappa_1 = 1.4592 \times 10^{-12}$ and $\kappa_2 = -5 \times 10^{-9}$. The ODE solution only represents one periodic orbit of two possible periodic orbits. The initial conditions themselves choose

which periodic orbit the solution will take. However we should apply caution; we cannot "choose" which of the two periodic orbits our ODEs will follow since choosing an initial condition that puts the solution in the other cycle then changes κ_1 and κ_2 itself and hence changes the periodic orbit. Figure 5.11 (a) shows the quartic function (5.106) (cyan)

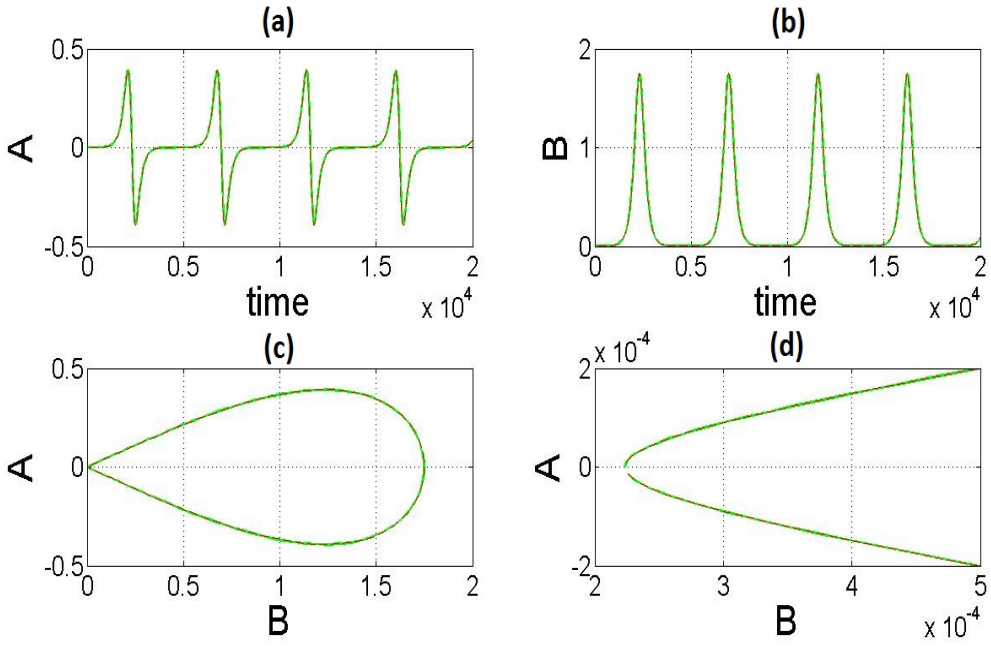

Figure 5.10: *The PDE (green) and ODE (red) solution with initial conditions (5.123a) - (5.123c) and (5.125),(5.124b) and (5.124c),* $v_m = 1 \times 10^{-8}$, $\delta = 0.01$, $\kappa_2 = -5 \times 10^{-9}$, $\kappa_1 = 1.4592 \times 10^{-12}$. *The solution enters a periodic orbit shown in (a) and (b).* A *is plotted against* B *in (c) and (d).*

plotted when $\kappa_1 = 1.4592 \times 10^{-12}$ and $\kappa_2 = -5 \times 10^{-9}$ as is the case when $v_m = 1 \times 10^{-8}$. The two periodic orbits are formed by taking the square root of this quartic to obtain A. A view of where the two periodic orbits are closest is shown in figure 5.11 (b) (cyan line), the PDE and ODE solutions are shown in green and red respectively. On a graphical view it appears the distance between these periodic orbits is approximately 5×10^{-4}.

In the next example $v_m = 5 \times 10^{-7}$, $\delta = 0.01$, shown in figure 5.12, the solution again takes the form of Case 2 (iii). Here $\kappa_1 = 1.824 \times 10^{-7}$ and $\kappa_2 = -1.2502 \times 10^{-5}$ and

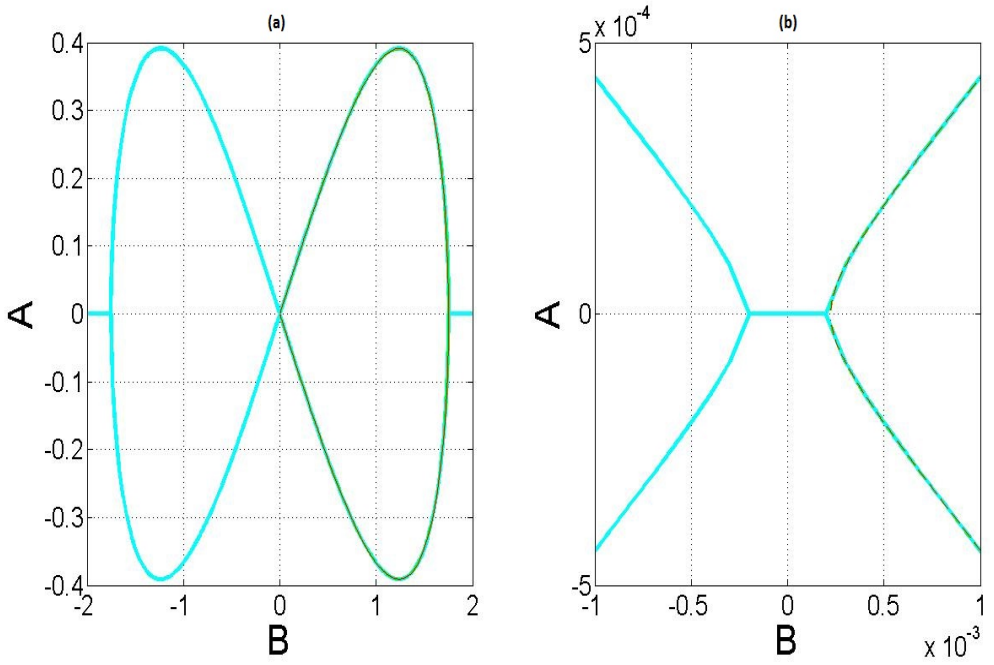

Figure 5.11: *The quartic function (5.106) (cyan) with the PDE (green) and ODE (red) solution with initial conditions (5.123a) - (5.123c) and (5.125),(5.124b) and (5.124c),* $v_m = 1 \times 10^{-8}$, $\delta = 0.01$, $\kappa_2 = -5 \times 10^{-9}$, $\kappa_1 = 1.4592 \times 10^{-12}$.

figure 5.13 shows the quartic (5.106) plotted with these values of κ_1 and κ_2. The distance between the two periodic orbits is growing and is now approximately 2.2×10^{-2}.

5.6.2 Experiment 2: effect of noise on the fastest growing mode

Something interesting happens when we set the initial conditions to the fastest growing mode ((5.127a) - (5.127c) and (5.128a) - (5.128c)), $v_m = 1 \times 10^{-12}$, $\delta = 0.01$ ($\kappa_2 = -5 \times 10^{-17}$,$\kappa_1 = 1.4592 \times 10^{-24}$). We would expect the PDEs and ODEs will agree, however this is not the case as shown in figure 5.14. Here, the two periodic orbits have become closer together than they were when $v_m = 1 \times 10^{-8}$. Since we have used a fourth order Runge-Kutta time stepping scheme, we incur unavoidable errors, "noise", which grow in magnitude with time. If any of the terms in our ODE system (5.95c)

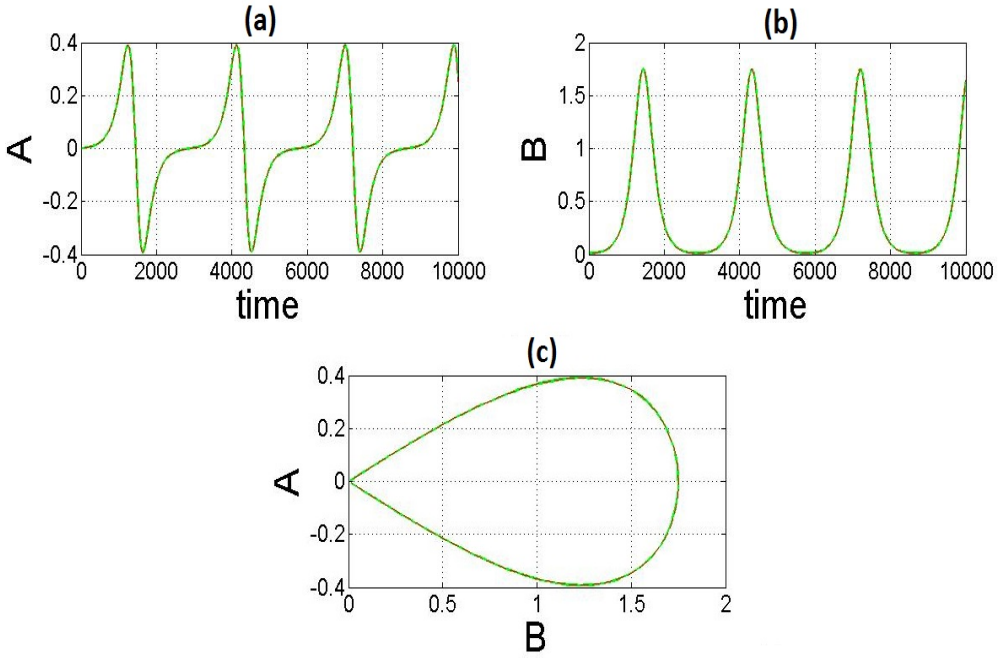

Figure 5.12: *The PDE (green) and ODE (red) solution with initial conditions (5.123a) - (5.123c) and (5.125),(5.124b) and (5.124c),* $v_m = 5 \times 10^{-7}$, $\delta = 0.01$, $\kappa_2 = -1.2502 \times 10^{-5}$, $\kappa_1 = 1.824 \times 10^{-7}$. *The solution enters a periodic orbit shown in (a) and (b). A plot of A against B is shown in (c).*

become small enough to be influenced by noise, this could "flip" the solution into the other periodic orbit. When looking at the fastest growing mode, we see that noise has a stronger influence on the solution. To obtain the fastest growing mode we initialise the PDEs with

$$v(0) = v_m \operatorname{sech}^{\theta}(y), \tag{5.127a}$$

$$h(0) = \frac{v_m R_o \theta}{s} \operatorname{sech}^{\theta}(y) \tanh(y), \tag{5.127b}$$

$$u(0) = \frac{v_m Q}{s} \operatorname{sech}^{\theta}(y), \tag{5.127c}$$

and the ODEs with

$$A(0) = v_m(0)/\delta^2, \tag{5.128a}$$

$$B(0) = A(0)/(\tilde{Q}^{1/2}), \tag{5.128b}$$

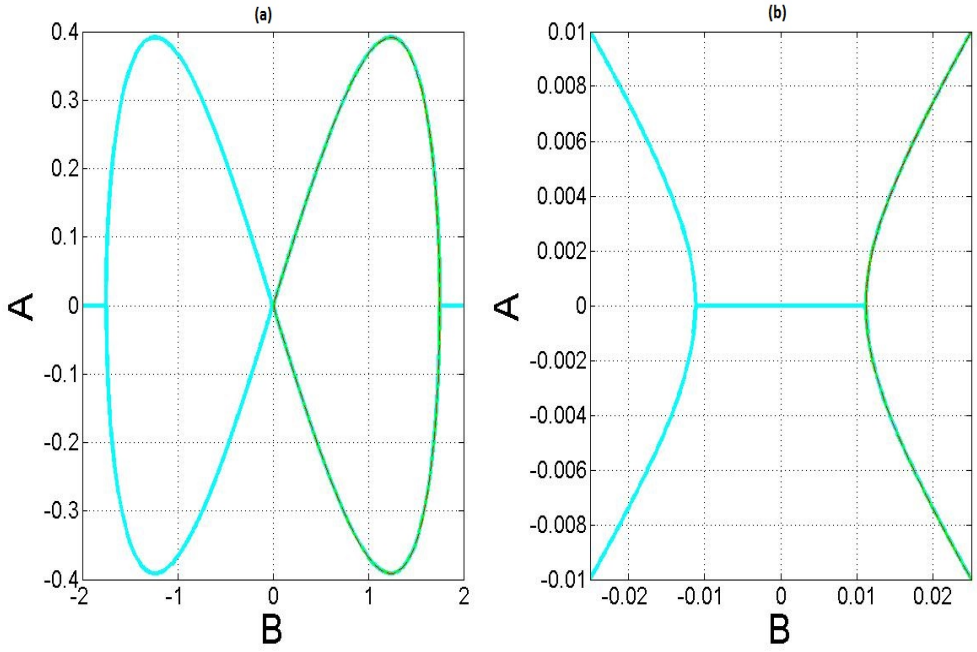

Figure 5.13: *The quartic function (cyan) with the PDE (green) and ODE (red) solution with initial conditions (5.123a) - (5.123c) and (5.125),(5.124b) and (5.124c),* $v_m = 5 \times 10^{-7}$, $\delta = 0.01$, $\kappa_2 = -1.2502 \times 10^{-5}$, $\kappa_1 = 1.824 \times 10^{-7}$.

$$C(0) = \tilde{Q}^{1/2} A(0), \tag{5.128c}$$

where $v_m(0)$ is the maximum of $v(0)$.

Starting again with $v_m = 1 \times 10^{-8}$ and $\delta = 0.01$, we can see in figure 5.16 even in a weakly nonlinear regime, the PDEs and the ODEs only agree for the initial cycle and deviate from each other as A (or v) and B (or u) become small. This is where we are likely to see noise interfering with the solution and in turn see a divergence in the PDE and ODE solutions. In this case $\kappa_1 = 1.459 \times 10^{-12}$ and $\kappa_2 = -2.45 \times 10^{-16}$ and the quartic plotted with these values can be seen in figure 5.17. Looking at (b) we can estimate that the distance between these two periodic orbits is 1.1×10^{-7}. The PDEs can not be seen in (b) since "noise" has flipped the solution over to the other periodic orbit before it gets close to the near meeting of these two periodic orbits. For similar reasons

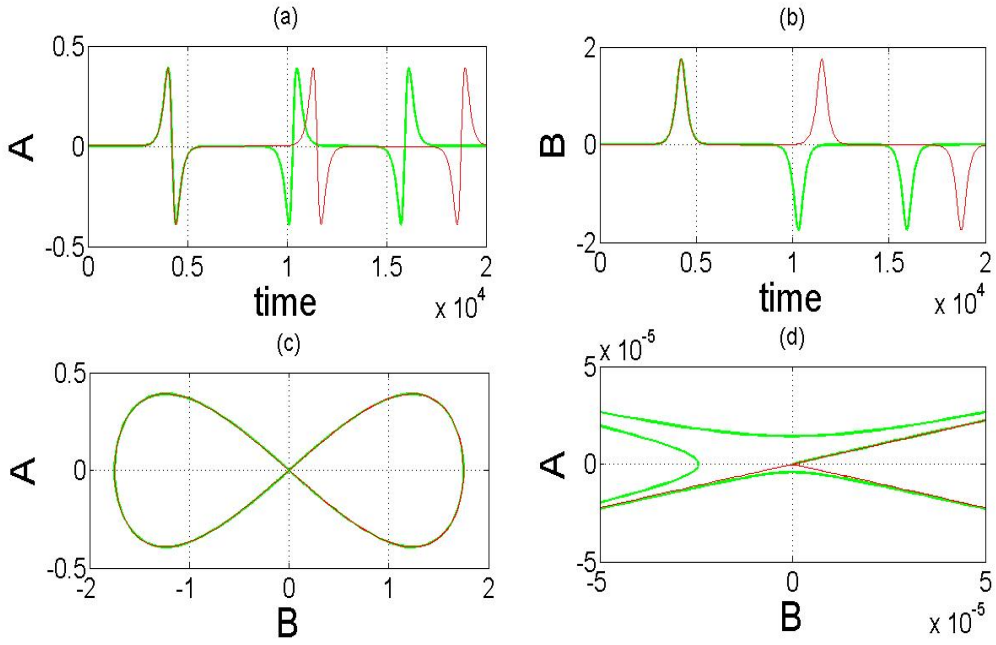

Figure 5.14: *The PDE (green) and ODE (red) solution with initial conditions (5.123a) - (5.123c) and (5.125) - (5.124c),* $v_m = 1 \times 10^{-12}$, $\delta = 0.01$, $\kappa_2 = -5 \times 10^{-17}$, $\kappa_1 = 1.4592 \times 10^{-24}$. *The solution enters a periodic orbit shown in (a) and (b). A closer look at where* A *and* B *are small is shown in (d). The PDEs are being "kicked" out of the orbit too soon as seen in (d),* A *and* B *are small enough to flip the PDEs and ODEs into the other periodic orbit.*

it is evident the ODEs have failed to closely follow the quartic function as it should. It is possible that noise, as well as pushing the solution in one direction into another periodic orbit it can also "kick" the solution in the other direction out of its orbit too soon.

We also looked at $v_m = 3 \times 10^{-6}$ and $\delta = 0.01$, here $\kappa_1 = 3.94 \times 10^{-5}$ and $\kappa_2 = -1.98 \times 10^{-6}$ and the solution can be seen in figure 5.18. Again the PDEs and ODEs agree for the first cycle, however the ODEs are displaying a shorter cycle than the PDEs. This time it appears that when A and B become closer to the invariant point (A and B small), noise is keeping the PDEs in a longer orbit. This can clearly be seen in figure 5.19 (b). It is clear that noise has an effect on the solution when A and B become small. If the two periodic orbits are close enough then any changes to the solution of A and B due to noise can flip the solution into the other periodic orbit. Alternatively noise may

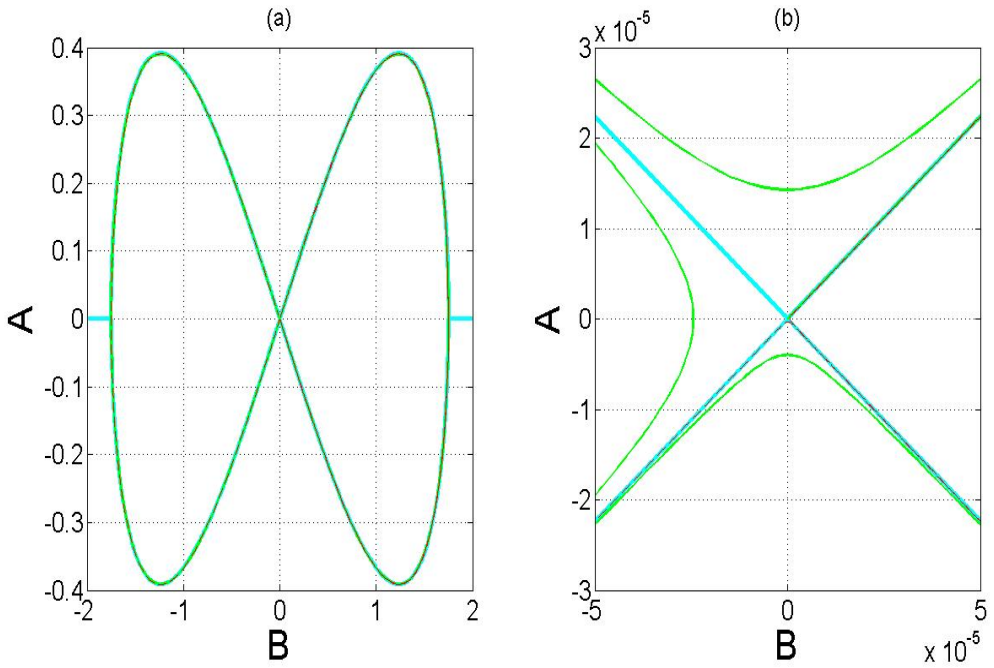

Figure 5.15: *The quartic function (cyan) with the PDE (green) and ODE (red) solution with initial conditions (5.123a) - (5.123c) and (5.125) - (5.124c),* $v_m = 1 \times 10^{-12}$, $\delta = 0.01$, $\kappa_2 = -5 \times 10^{-17}$, $\kappa_1 = 1.4592 \times 10^{-24}$. *The PDEs and ODEs are "flipping" over to the other periodic orbit.*

simply allow the ODEs or PDEs to "linger" near the invariant point for too long or kick them out too soon, adjusting the length of the period. One logical solution to this would be to increase our initial value of A so that the distance between the two periodic orbits is increased lessening the likelihood of an interference of noise. However, doing so may have consequences in that increasing $A(0)$ may violate the scalings; increasing $A(0)$ will in turn increase v_m at fixed δ, if A becomes too large subsequent terms in u, v and h may dwarf the leading order terms. It should also be noted that noise was never seen to have any affect on the maximum amplitude of the solution for A or B.

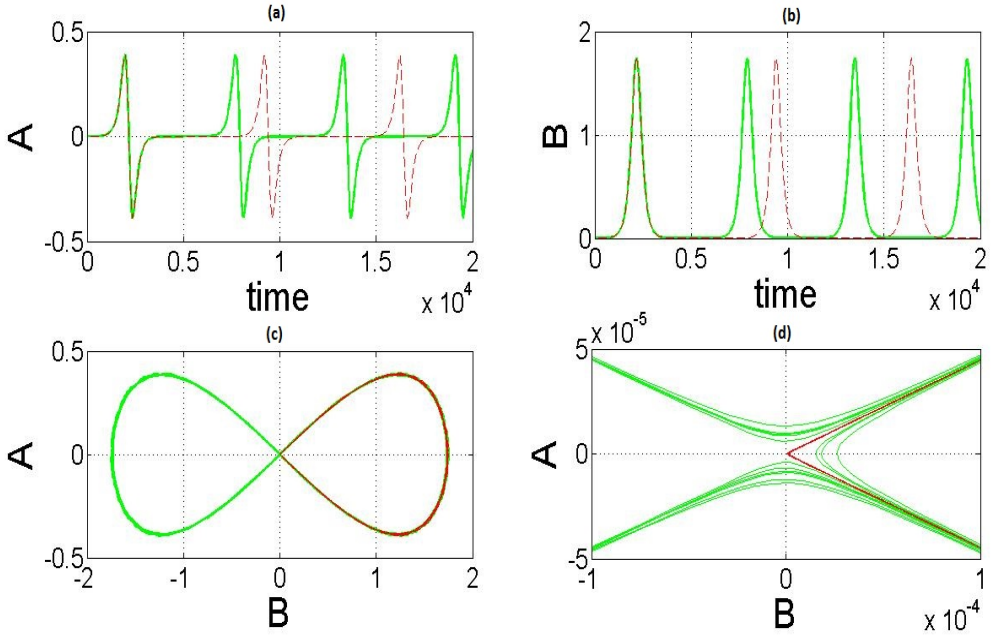

Figure 5.16: *The PDE (green) and ODE (red) solution with initial conditions (5.127a) - (5.127c) and (5.128a) - (5.128c),* $v_m = 1 \times 10^{-8}$, $\delta = 0.01$, $\kappa_2 = -2.45 \times 10^{-16}$, $\kappa_1 = 1.4592 \times 10^{-12}$. *The solution enters a periodic orbit shown in (a) and (b). A closer look at where* A *and* B *are small is shown in (d), the PDE solution is being "kicked" out of their orbit too soon and are "flipped" into the other periodic orbit as shown in (d).*

5.6.3 Experiment 3: starting off in the opposite periodic orbit

The final initial conditions we will look at are

$$v(0) = v_m \operatorname{sech}^{\theta}(y), \tag{5.129a}$$

$$h(0) = -\frac{v_m R_o \theta}{s} \operatorname{sech}^{\theta}(y) \tanh(y), \tag{5.129b}$$

$$u(0) = -\frac{v_m Q}{s} \operatorname{sech}^{\theta}(y), \tag{5.129c}$$

with corresponding initial conditions in the ODEs,

$$A(0) = v_m(0)/\delta^2, \tag{5.130a}$$

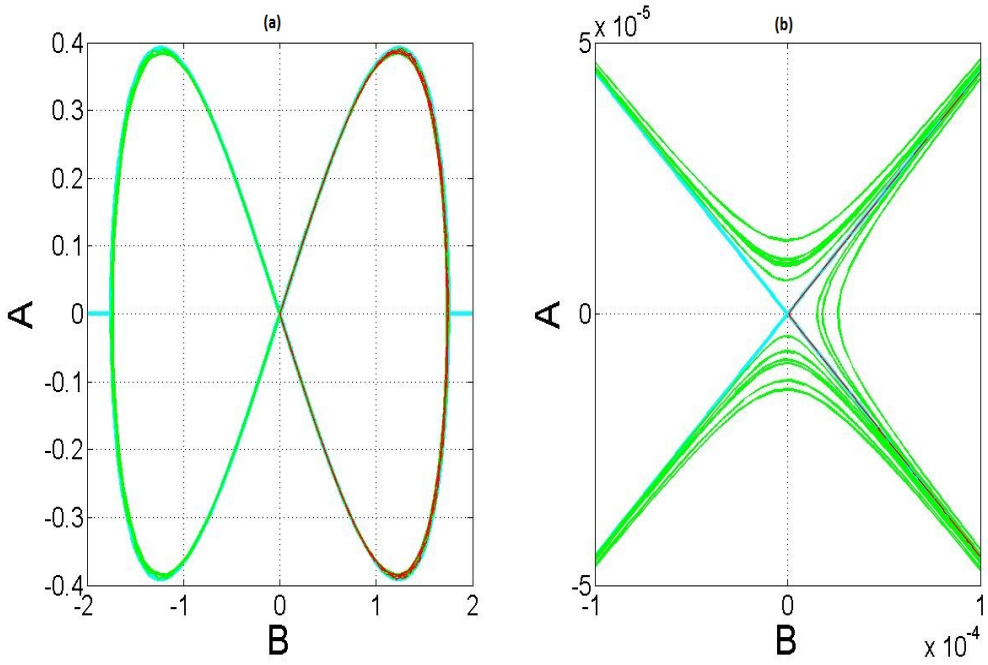

Figure 5.17: *The quartic function (cyan) with the PDE (green) and ODE (red) solution with initial conditions (5.127a) - (5.127c) and (5.128a) - (5.128c),* $v_m = 1 \times 10^{-8}$, $\delta = 0.01$, $\kappa_2 = -2.45 \times 10^{-16}$, $\kappa_1 = 1.4592 \times 10^{-12}$. *The PDE solution is flipping across periodic orbits.*

$$B(0) = -A(0)/(\tilde{Q}^{1/2}), \tag{5.130b}$$

$$C(0) = -\tilde{Q}^{1/2}A(0). \tag{5.130c}$$

The difference is a subtle change is the sign of B and C to those used in section 5.6.2, subsequently changing the sign of u and h.

Again we look at $v_m = 1 \times 10^{-8}$ and $\delta = 0.01$; we have $\kappa_2 = -2.45 \times 10^{-16}$ and $\kappa_1 = -1.46 \times 10^{-12}$. Both solutions begin a periodic cycle as seen in figure 5.20, up until $\tau = 10$ the PDEs and ODEs agree, with A decreasing and B increasing. Both A and B in the ODEs and PDEs then go through zero and it is here again we see the effects of noise. The ODEs initially stick to one periodic orbit for the first few cycles, however the PDEs repeatedly flip between the two. Eventually it can be seen from figure 5.20 (d) that noise has flipped the ODEs.

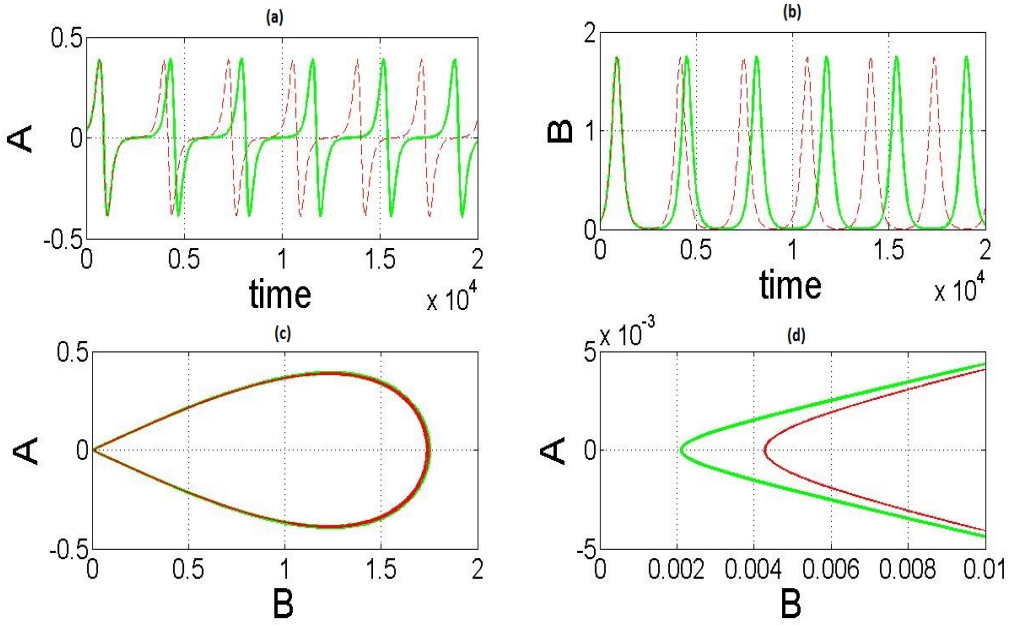

Figure 5.18: *The PDE (green) and ODE (red) solution with initial conditions (5.127a) - (5.127c) and (5.128a) - (5.128c),* $v_m = 3 \times 10^{-6}$, $\delta = 0.01$, $\kappa_2 = -1.98 \times 10^{-6}$, $\kappa_1 = 3.94 \times 10^{-5}$. *The solution enters a periodic orbit shown in (a) and (b). A closer look at where* A *and* B *are small is shown in (d), the PDE solution is spending too long in their orbit when* B *is small.*

Figure 5.21 shows the quartic plotted with these values of κ_1 and κ_2, it shows us how close the two periodic orbits are to each other. Lastly, with $v_m = 3 \times 10^{-6}$ and $\delta = 0.01$, we have $\kappa_1 = -3.94 \times 10^{-5}$ and $\kappa_2 = -1.98 \times 10^{-6}$ and the solution can be seen in figure 5.22. This initial decrease in A and increase in B can be clearly shown in the case as opposed to when $v_m = 1 \times 10^{-8}$. Both A and B pass through zero and again noise has pushed the PDEs towards the opposite periodic orbit. However, as shown in figure 5.23 (b) the periodic orbits are not close enough for the solution to flip to the other periodic orbit as they were when $v_m = 1 \times 10^{-8}$. Finally in figure 5.24 we have $v_m = 5 \times 10^{-5}$; the periodic cycle on this right hand side has almost vanished, shown in figure 5.25, and we are nearly at the stepping point from solutions (b) to (c) in figure 5.3.

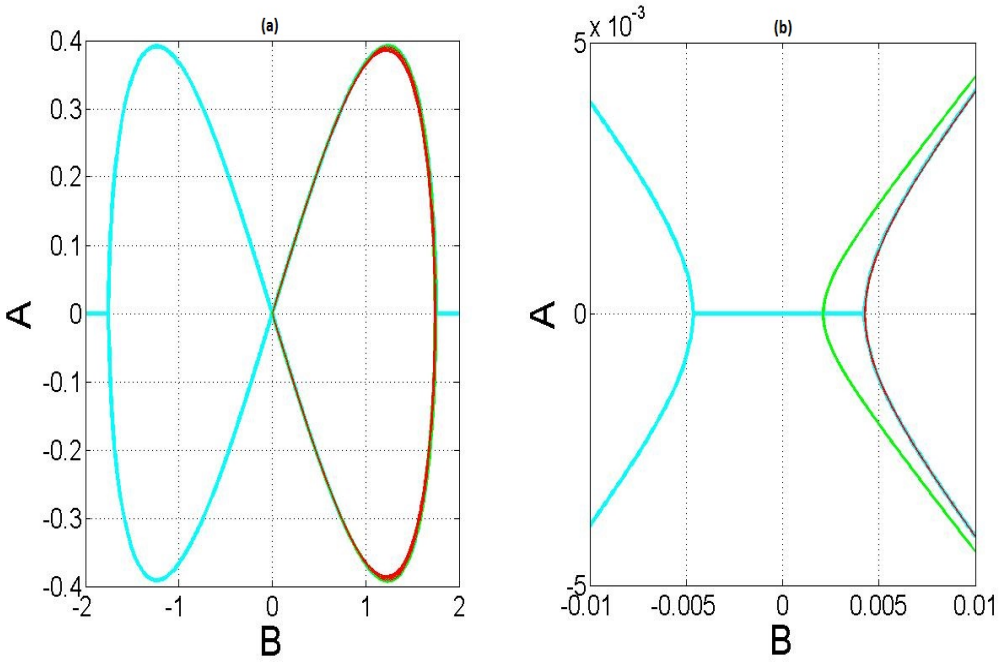

Figure 5.19: *The quartic function (cyan) with the PDE (green) and ODE (red) solution with initial conditions (5.127a) - (5.127c) and (5.128a) - (5.128c),* $v_m = 3 \times 10^{-6}$, $\delta = 0.01$, $\kappa_2 = -1.98 \times 10^{-6}$, $\kappa_1 = 3.94 \times 10^{-5}$.

5.6.4 Limitations of the weakly nonlinear theory

It is clear from figure 5.24 that the ODEs are beginning to break away from the PDE solution. Here we have reached a point where higher order terms discarded in the weakly nonlinear theory are no longer smaller than the terms that were retained. We can show this by looking at equation (5.72) with the variables expanded as they are in (5.77) and (5.78). Equating terms of order δ we have

$$\mathcal{O}(1): \qquad \frac{\partial \hat{u}_1}{\partial \tau} = Q\hat{v}_1, \tag{5.131}$$

$$\mathcal{O}(\delta): \qquad \frac{\partial \hat{u}_2}{\partial \tau} = Q\hat{v}_2 - R_o(2\alpha - 1)\hat{v}_1 \frac{\partial \hat{u}_1}{\partial y}, \tag{5.132}$$

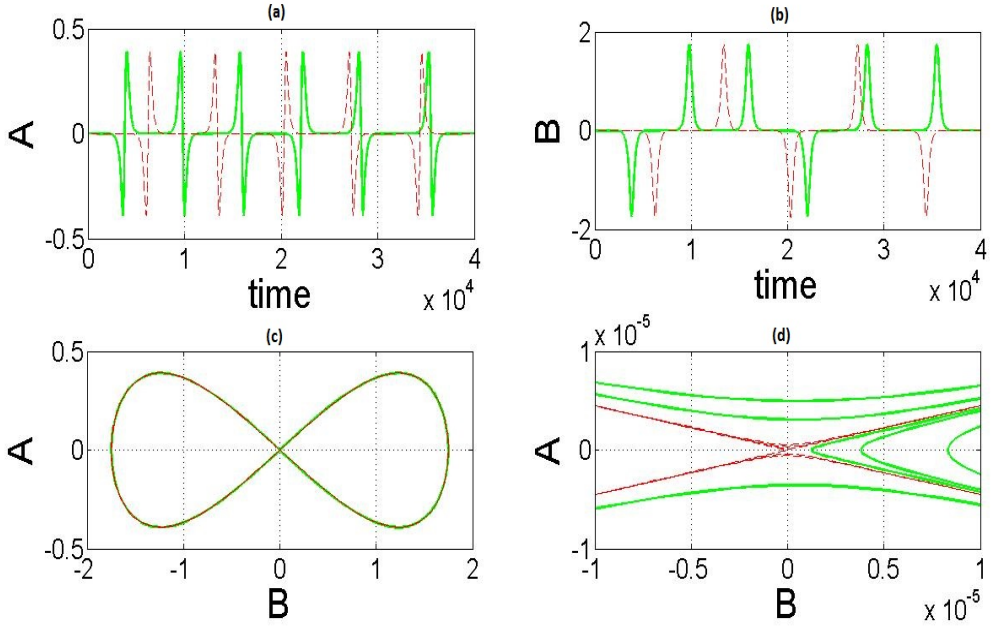

Figure 5.20: *The PDE (green) and ODE (red) solution with initial conditions (5.129a) - (5.129c) and (5.130a) - (5.130c),* $v_m = 1 \times 10^{-8}$, $\delta = 0.01$, $\kappa_2 = -2.45 \times 10^{-16}$, $\kappa_1 = -1.4592 \times 10^{-12}$. *The solution enters a periodic orbit shown in (a) and (b). A closer look at where* A *and* B *are small is shown in (d). The PDE solution is "kicked" out of its orbit too soon, and the PDE and ODE solutions are "flipping" between orbits.*

$$\mathcal{O}(\delta^2): \qquad \frac{\partial \hat{u}_3}{\partial \tau} = Q\hat{v}_3 - R_o(2\alpha-1)\hat{v}_2\frac{\partial \hat{u}_1}{\partial y} - R_o\hat{v}_1\bigg(\frac{\partial \hat{u}_1}{\partial y} + (2\alpha-1)\frac{\partial \hat{u}_2}{\partial y} - 2\alpha(1-\alpha)\hat{h}_1\frac{\partial \hat{u}_1}{\partial y} - \alpha(1-\alpha)\frac{\partial \hat{h}_1}{\partial y}\bigg). \quad (5.133)$$

We can approximate u_2, v_2, h_2 and $\bar{u}$ using the PDE solution and our ODE solution for u_1, v_1, h_1 and $\bar{u}_1$ together with (5.77) and (5.78), in other words

$$\hat{u}_2 \approx \frac{(\hat{u} - \delta\hat{u}_1)}{\delta^2}, \qquad \hat{v}_2 \approx \frac{(\hat{v} - \delta^2\hat{u}_1)}{\delta^3}, \quad (5.134)$$

$$\hat{h}_2 \approx \frac{(\hat{h} - \delta\hat{h}_1)}{\delta^2} \qquad \hat{\bar{u}}_2 \approx \frac{(\hat{\bar{u}} - \delta^2\hat{\bar{u}}_1)}{\delta^3}. \quad (5.135)$$

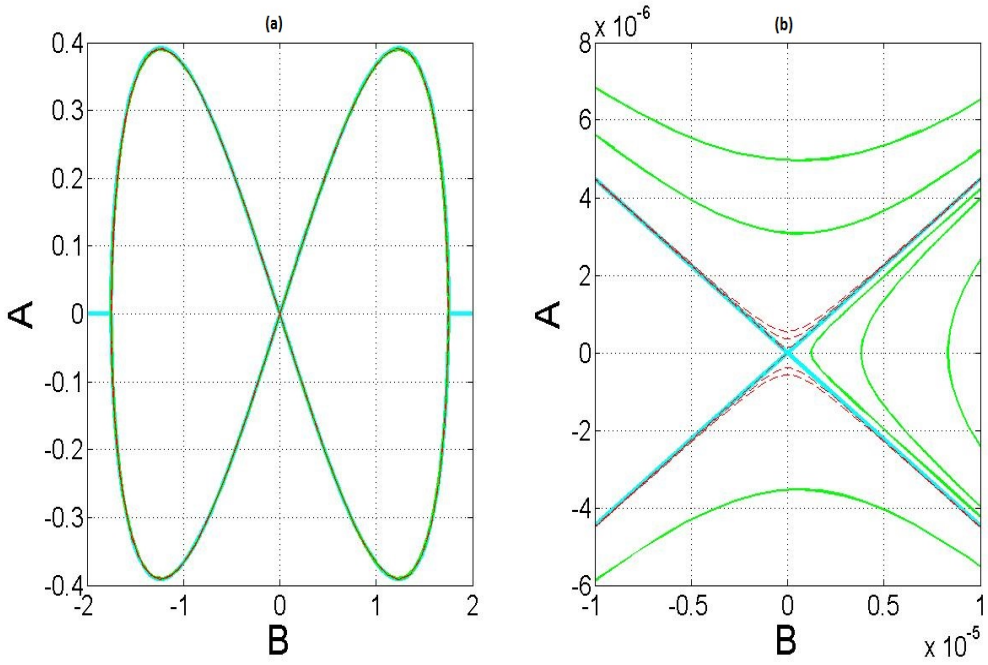

Figure 5.21: *The quartic function (cyan) with the PDE (blue) and ODE (red) solution with initial conditions (5.129a) - (5.129c) and (5.130a) - (5.130c),* $v_m = 1 \times 10^{-8}$, $\delta = 0.01$, $\kappa_2 = -2.45 \times 10^{-16}$, $\kappa_1 = -1.4592 \times 10^{-12}$.

The solution for $\hat{u}_1$, $\hat{u}_2$ and $\hat{u}_3$ is only valid when the terms at next order are smaller in magnitude. For example when $v_m = 5 \times 10^{-5}$ we have at order δ

$$-R_o(2\alpha - 1)\hat{v}_1 \frac{\partial \hat{u}_1}{\partial y} \sim 0.1, \tag{5.136}$$

whereas at order δ^2 we have

$$-R_o(2\alpha-1)\hat{v}_2\frac{\partial \hat{u}_1}{\partial y} - R_o\hat{v}_1\left(\frac{\partial \hat{u}_1}{\partial y} + (2\alpha-1)\frac{\partial \hat{u}_2}{\partial y} - 2\alpha(1-\alpha)\hat{h}_1\frac{\partial \hat{u}_1}{\partial y} - \alpha(1-\alpha)\frac{\partial \hat{h}_1}{\partial y}\right) \sim 10. \tag{5.137}$$

Multiplying (5.136) by δ and (5.137) by δ^2 we can see both terms are $\sim 10^{-3}$, hence terms ignored at order δ which were of order δ^2 were of the same order of magnitude. We can clearly see that this will lead to problems in our master equation, (5.79), since $\tilde{R}$ involved the solutions $\hat{u}_2$ and $\hat{v}_2$.

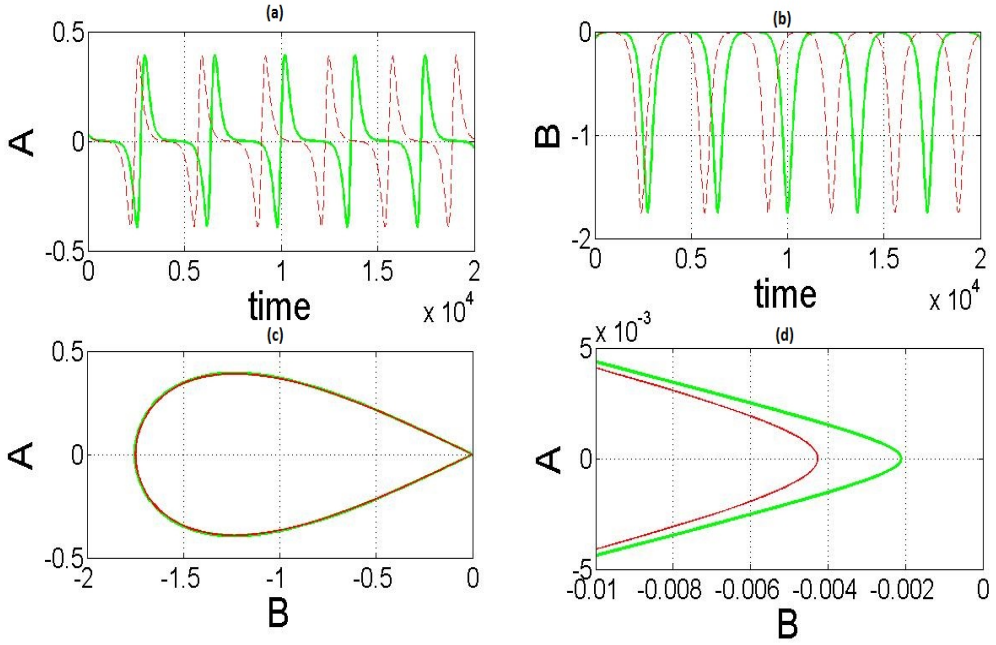

Figure 5.22: *The PDE (green) and ODE (red) solution with initial conditions (5.129a) - (5.129c) and (5.130a) - (5.130c),* $v_m = 3 \times 10^{-6}$, $\delta = 0.01$, $\kappa_2 = -1.98 \times 10^{-6}$, $\kappa_1 = -3.94 \times 10^{-5}$. *The solution enters a periodic orbit shown in (a) and (b). A closer look at where* A *and* B *are small is shown in (d). The PDE solution is spending longer in each periodic orbit than the ODE solution.*

5.7 The PDEs in the strongly nonlinear regime

We now wish to push the numerics to achieve the maximum growth rate that is permissible by our model. The strength of the nonlinearity can be adjusted through maximizing δ which in turn decreases $\tilde{g}$ and increases the growth rate. Small $\tilde{g}$ is also achieved through small α. This would mean making one layer depth much smaller than the other. However there becomes a fine balancing act between reducing $\tilde{g}$ through small α but not making α too small such that the interface becomes larger than one of the layer depths. Here we experiment with two choices of α ($\alpha = 0.25$ and $\alpha = 0.45$). We will push the PDE numerics to their most nonlinear behavior through increasing δ until the absolute maximum for h has been reached.

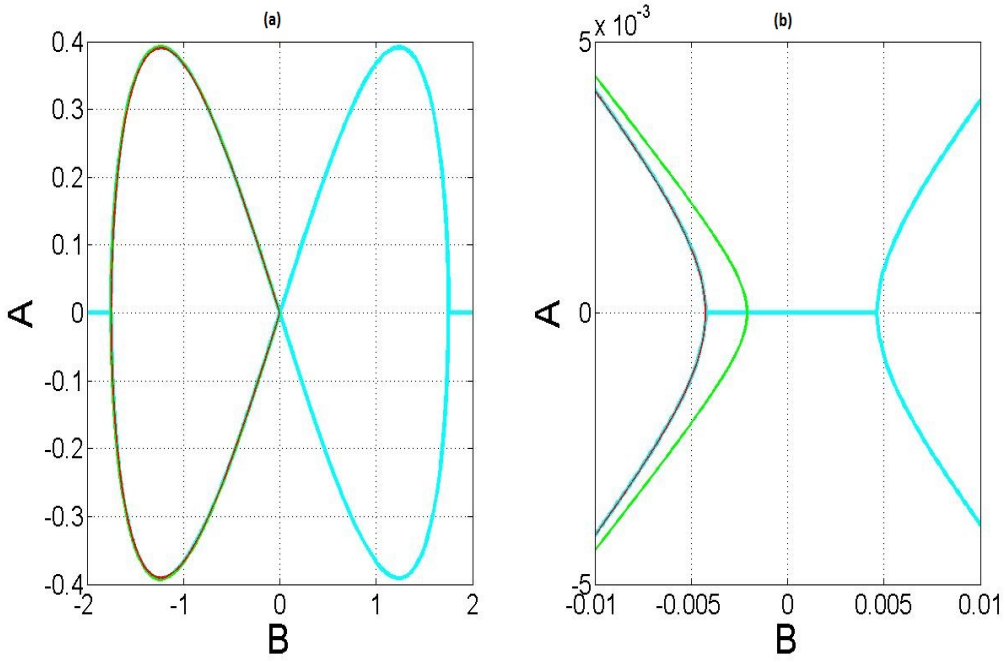

Figure 5.23: *The quartic function (cyan) with the PDE (green) and ODE (red) solution with initial conditions (5.129a) - (5.129c) and (5.130a) - (5.130c),* $v_m = 3 \times 10^{-6}$, $\delta = 0.01$, $\kappa_2 = -1.98 \times 10^{-6}$, $\kappa_1 = -3.94 \times 10^{-5}$. *The PDE solution is spending longer in each periodic orbit than the ODE solution.*

Firstly we look at $\alpha = 0.25$ and fix $v_m = 1 \times 10^{-4}$; we increased δ from 0.05 and noted the minimum interface height reached for each run. The results are shown in figure 5.26. Here, δ is plotted against the minimum interface height, h. Clearly the limits of the model have been reached when $min(h) \geq -0.25$ and this was where the experiment was stopped. A more accurate figure for δ can be obtain through linearly interpolating the results and it was found that $min(h) = 0.25$ when $\delta = 0.1257$. We also plotted the solutions in two cases when $\alpha = 0.25$, one when $\delta = 0.05$ when the layer depth is not a concern for the solution of the PDEs (figure 5.27) and another case when $\delta = 0.12$ where the limits of the model are closely met (figure 5.28).

Secondly we look at $\alpha = 0.45$ and fix $v_m = 1 \times 10^{-4}$, again we increased δ from 0.05 and noted the minimum interface height reached for each run. The results are shown in figure

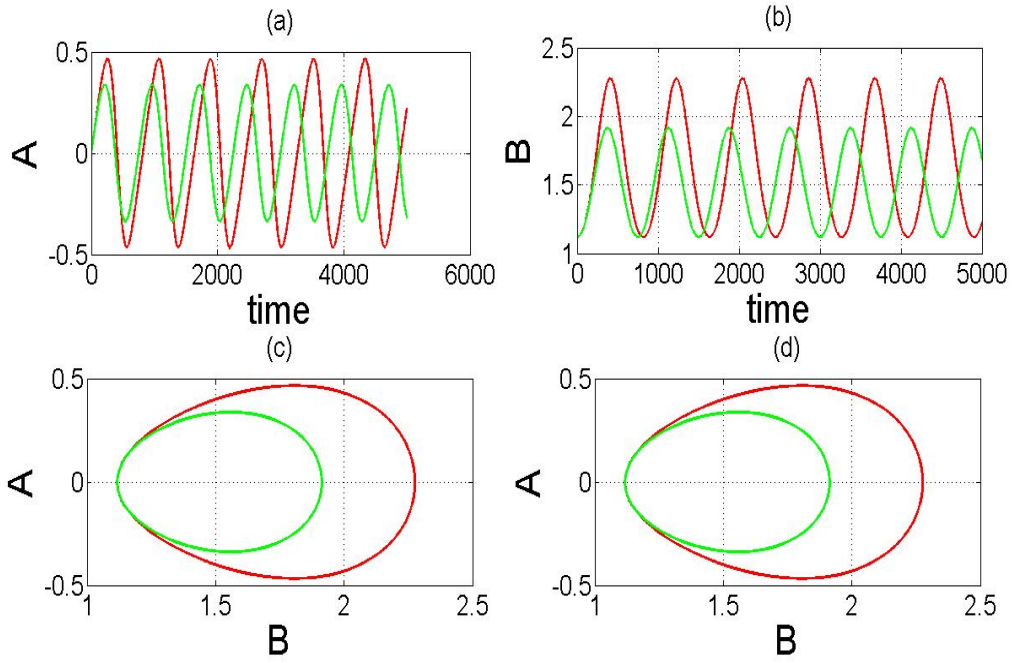

Figure 5.24: *The PDE (green) and ODE (red) solution with initial conditions (5.129a) - (5.129c) and (5.130a) - (5.130c),* $v_m = 5 \times 10^{-5}$, $\delta = 0.01$.

5.29, as before δ is plotted against the minimum interface height, h. This time the limits of the model have been reached when $min(h) \geq -0.45$. Through linear interpolation a more accurate figure for δ can be obtain and it was found that $min(h) = 0.45$ when $\delta = 0.2163$. We also plotted the solutions in two cases when $\alpha = 0.45$, one when $\delta = 0.05$ when the layer depth is not a concern for the solution of the PDEs (figure 5.30) and another case when $\delta = 0.12$ where the limits of the model are closely met (figure 5.31).

5.8 Changes to the mean flow

At the beginning of this chapter we asked the question: How does the instability grow? Will it grow indefinitely or settle into to new equilibrium state that is stable? We have already shown that the system is unstable and grows entering a periodic cycle where it

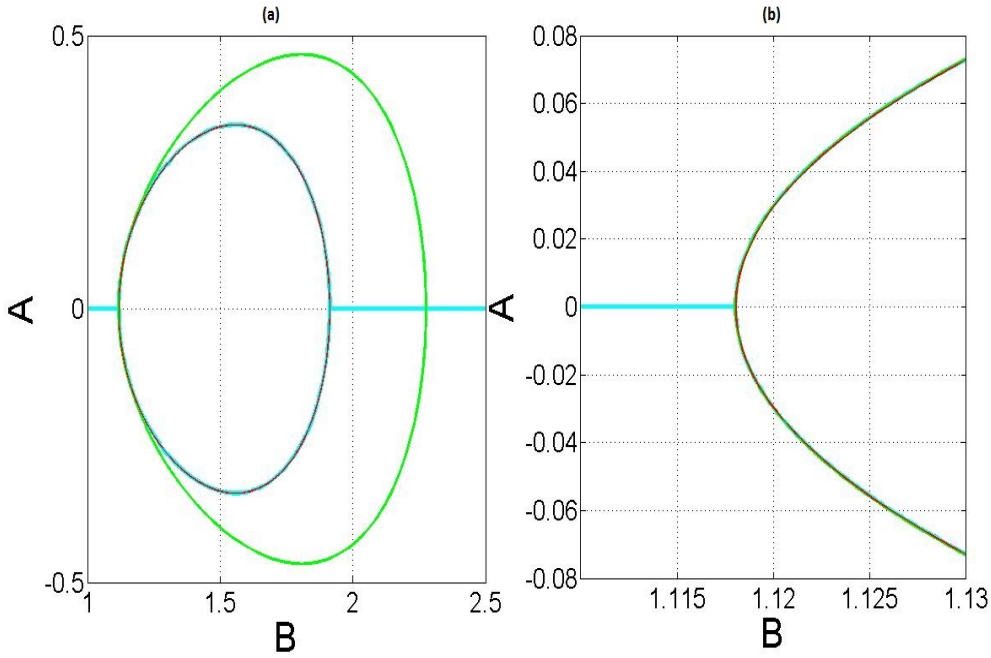

Figure 5.25: *The quartic function (cyan) shown in (a) with (b) showing the PDE (green) and ODE (red) solution with initial conditions (5.129a) - (5.129c) and (5.130a) - (5.130c),* $v_m = 5 \times 10^{-5}$, $\delta = 0.01$.

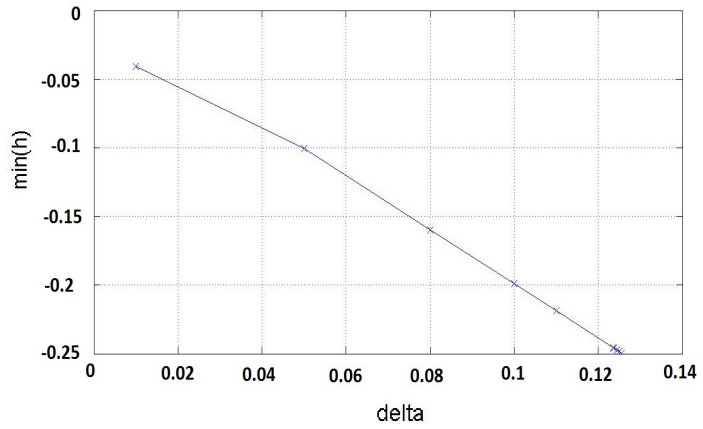

Figure 5.26: *The interface height plotted against* δ *when the interface is at its minimum. In this case* $\alpha = 0.25$ *and* $v_m = 1 \times 10^{-4}$.

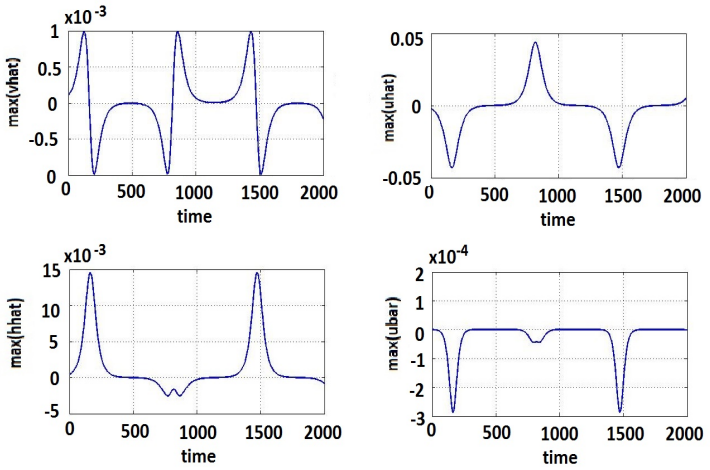

Figure 5.27: *The nonlinear solution of the PDEs when* $\alpha = 0.25$, $\delta = 0.05$ *and* $v_m = 1 \times 10^{-4}$.

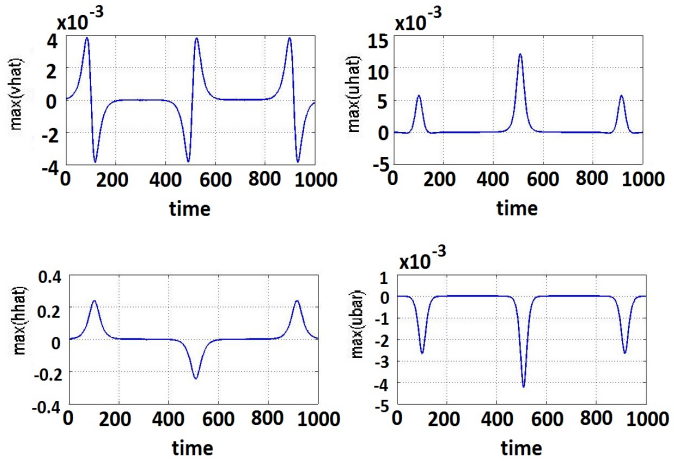

Figure 5.28: *The nonlinear solution of the PDEs when* $\alpha = 0.25$, $\delta = 0.12$ *and* $v_m = 1 \times 10^{-4}$.

decays again returning to its initial state. However our ultimate goal is to understand what is happening in a physical sense. In other words what is happening to the fluid system as it enters this periodic process, or moreover what is happening to the mean flow.

To begin with the flow is unstable causing growth in u, v, h and $\bar{u}$. Since this growth is periodic these variables reach a maximum before decaying again. The spatial profiles of u, v, h and $\bar{u}$ at their maximum are shown in figure 5.32 for the case where $R_o = 3$, $\alpha = 0.45$,

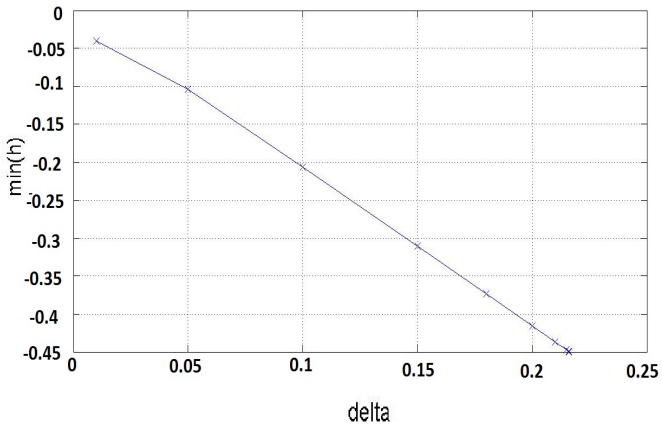

Figure 5.29: *The minimum interface height plotted against δ when the interface is at its minimum. In this case $\alpha = 0.45$ and $v_m = 1 \times 10^{-4}$.*

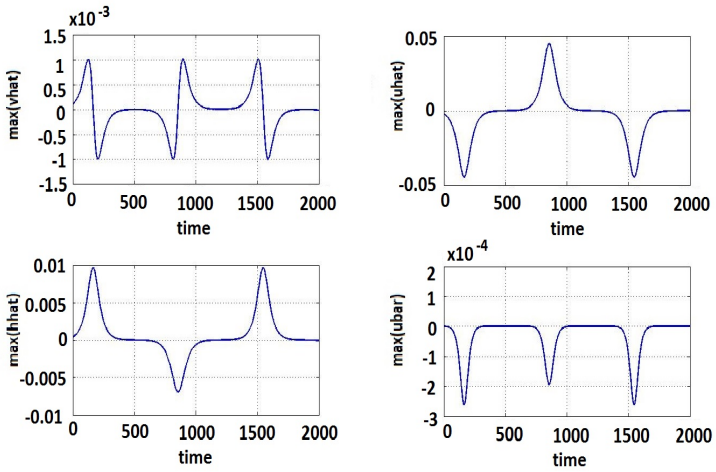

Figure 5.30: *The nonlinear solution of the PDEs when $\alpha = 0.45$, $\delta = 0.05$ and $v_m = 1 \times 10^{-4}$.*

$\delta = 0.2$ and with initial conditions as in (5.123a) - (5.123c) where $v_m = 3 \times 10^{-6}$. We can see in figure 5.32 (a) that the flow of v is strongest around $y = 0$, decaying exponentially towards the boundaries. The flow is positive and the shape of v is to be expected since the solution to the linear form of equations is the eigenfunction $v = v_m \operatorname{sech}^{\theta}(y)$, where θ is the corresponding eigenvalue. Since $v = v_2 - v_1 > 0$ in this case (where v_2 and v_1 are the horizontal flows in the y-direction or the bottom and upper layer respectively), we

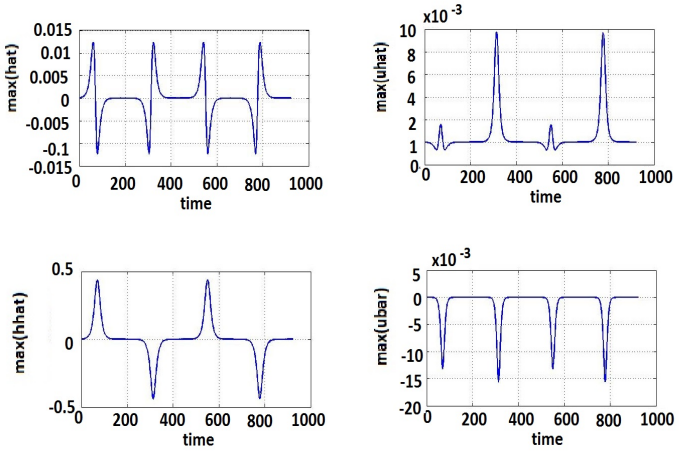

Figure 5.31: *The nonlinear solution of the PDEs when* $\alpha = 0.45$, $\delta = 0.21$ *and* $v_m = 1 \times 10^{-4}$.

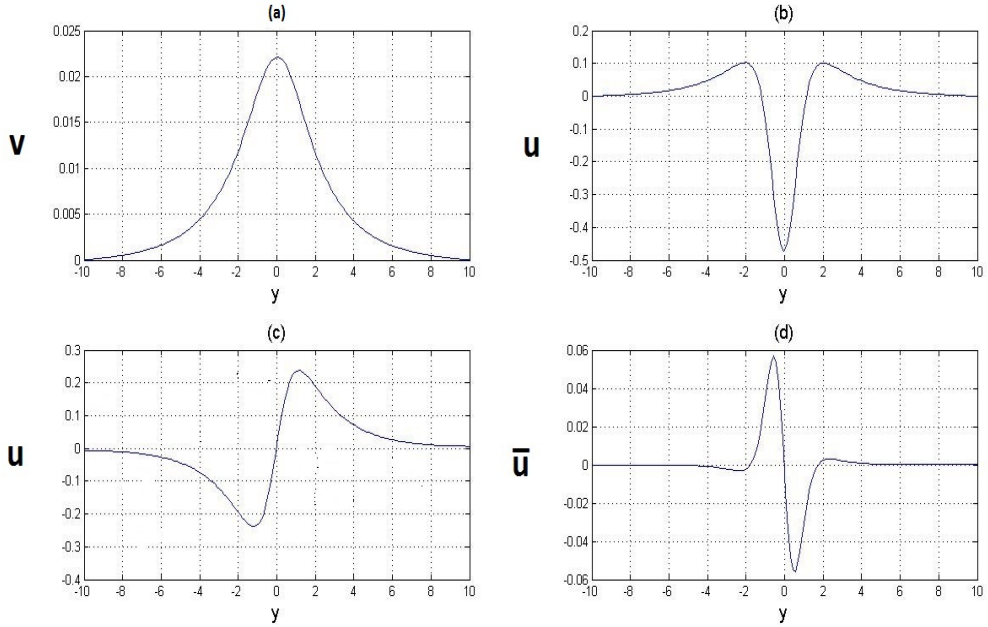

Figure 5.32: *The spatial profiles of (a)* v*, (b)* u*, (c)* h *and (d)* $\bar{u}$ *at their maximum growth, with* $R_o = 3$, $\alpha = 0.45$, $\delta = 0.2$ *and initial conditions (5.123a) - (5.123c) where* $v_m = 3 \times 10^{-6}$*, taken at* $t = 72$.

have one of two scenarios, we have either $v_2 > 0$ and $v_1 < 0$ with flow to the right in the bottom layer, or $v_2 < 0$ and $v_1 > 0$ with flow to the right in the top layer. Either case will

have the same effect on the interface just reflected in the $y = 0$ axis and therefore without loss of generality we will assume $v_2 > 0$ and $v_1 < 0$. This in turn causes the interface h to lift upwards to the right of $y = 0$. It can be shown using (5.25) that the interface height h is conserved by integrating over the fluid layer in y,

$$\int_{-L}^{L} \frac{\partial h}{\partial t} dy = -\frac{R_o}{\alpha(1-\alpha)} \int_{-L}^{L} \frac{\partial}{\partial y}\Big(D_1 D_2 v\Big) dy = \\ -\frac{R_o}{\alpha(1-\alpha)}(D_1(L)D_2(L)v(L) - D_1(-L)D_2(-L)v(-L)) = 0, \quad (5.138)$$

since $v = 0$ at the boundaries. This conservation of h shows the interface must become negative to the left of the origin which is indeed the case in figure 5.32.

The system then needs to complete its cycle and this is done by reversing the flow in v which returns this displaced fluid back across the origin. The direction of flow is reversed almost instantaneously, as shown in figure 5.33. When the system is ready to go through the next cycle the dynamics are repeated. An interesting case to look at when considering the dynamics of the flow is one where the noise has the influence of flipping the solution into a different periodic orbit as seen in figure 5.14 where the initial conditions are as in (5.123a) - (5.123c) with $R_o = 1.5$, $\alpha = 0.25$, $\delta = 0.01$ and $v_m = 1 \times 10^{-12}$. Here noise flips the system into the opposite periodic orbit on the third cycle which lifts the interface to the left of the origin rather than the right as shown in figure 5.34(c). This is a result of v growing negatively in the third cycle rather than growing in the positive. Since $v = v_2 - v_1 < 0$ we have flow to the right now in the top layer and to the left in the bottom layer. This displaced fluid causes the interface to fall to the right and rise to the left, the exact opposite to when v grows with $v > 0$ initially.

It is of interest to understand what is happening to the growth rate s and the potential vorticity Q in the mean flow as the flow goes through a cycle. Recall that a necessary but not sufficient condition for instability is $Q = 1 - \partial\bar{u}/\partial y < 0$, hence since it is shear, $(\partial\bar{u}/\partial y)$, that drives the flow, here $\bar{u} = R_o \tanh(y) + \bar{u}_{non}$. Therefore we will look at how

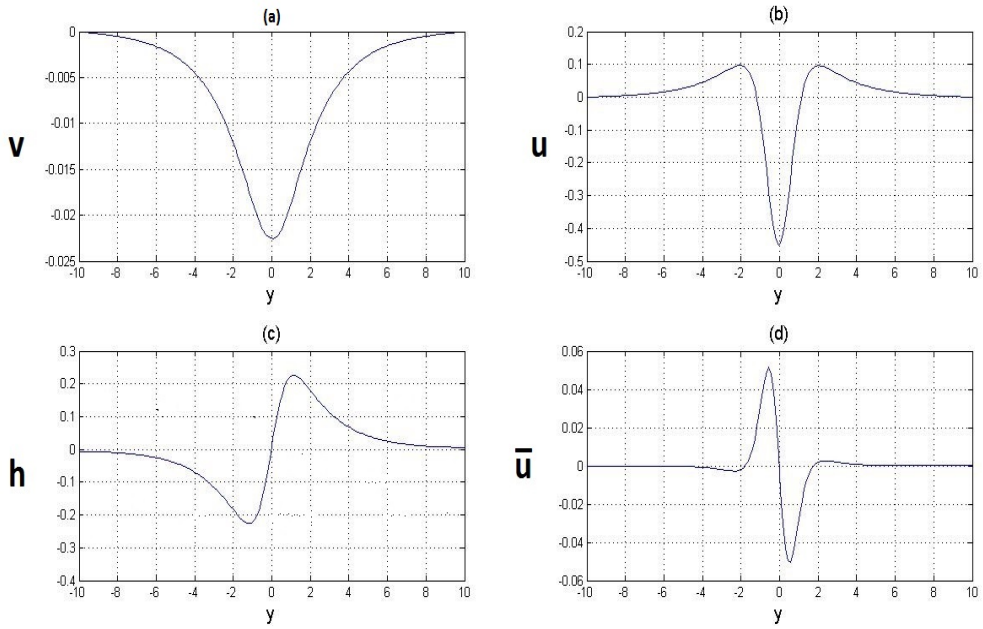

Figure 5.33: *The spatial profiles of (a) v, (b) u, (c) h and (d) $\bar{u}$ at their maximum growth, with $R_o = 3$, $\alpha = 0.45$, $\delta = 0.2$ and initial conditions (5.123a) - (5.123c) where $v_m = 3 \times 10^{-6}$, taken at $t = 83$. The arrows in (c) show the flow v which is the driving force behind the displacement of the interface, flow is strongest around the origin before decaying at the boundaries, the flow is also stronger in the bottom layer.*

this shear changes as the flow evolves.

The mean flow is constantly evolving and we can calculate the growth rate of a frozen mean flow, this will produce a growth rate as a function of time. Although the physical meaning of this is unclear we can use this to evaluate how stable the flow is at any given time. The evolving growth rate s was found using a boundary value solver for ordinary differential equations (BVP4C). Taking (5.30)

$$\frac{\partial^2 v}{\partial y^2} - \frac{Q}{gR_o} v - \frac{1}{gR_o} \frac{\partial^2 v}{\partial t} = 0. \tag{5.139}$$

We again assume the solution is of the form $v = \exp(st)v'(y)$, however now we have

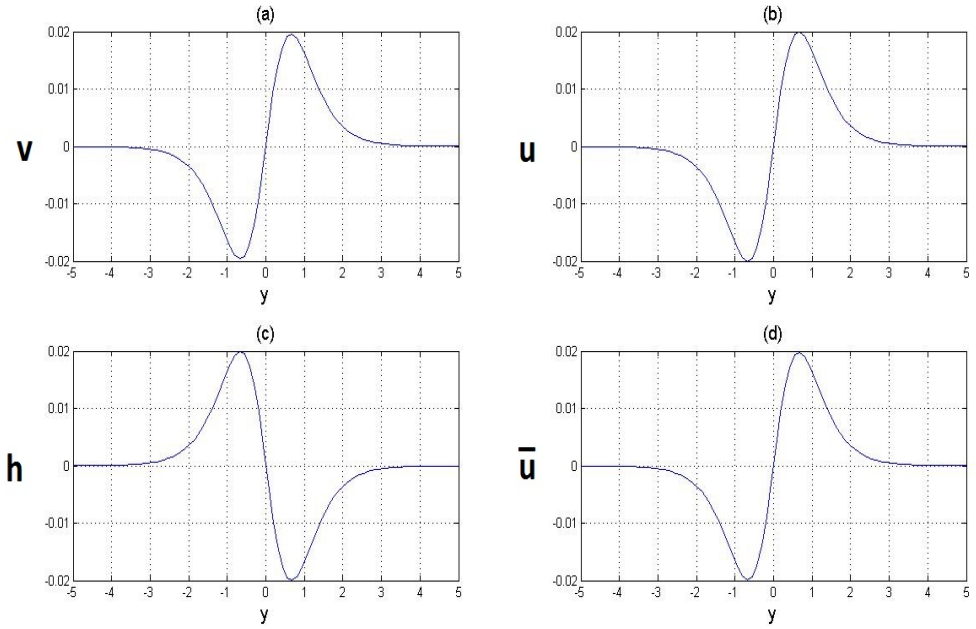

Figure 5.34: *The maximum spatial profiles of h at (a) 1st cycle, (b) 2nd cycle, (c) 3rd cycle and (d) 4th cycle, with $R_o = 1.5$, $\alpha = 0.25$, $\delta = 0.01$ and initial conditions (5.123a) - (5.123c) where $v_m = 1 \times 10^{-12}$. Noise has flipped the solution over to the opposite periodic orbit resulting in the interface lift reversing in (c) and (d).*

$Q = 1 - R_o \operatorname{sech}^2(y) - \partial \bar{u}_{non}/\partial y$ and therefore obtain the eigenvalue problem

$$\frac{d^2 v'}{dy^2} + \left(E + \nu \left(\operatorname{sech}^2(y) + \frac{1}{R_o} \frac{\partial \bar{u}_{non}}{\partial y} \right) \right) v' = 0. \tag{5.140}$$

Here $E = -(1 + s^2)/gR_o$ is the eigenvalue and $\nu = 1/g$, from E we have $s^2 = -gR_oE - 1$. Here, $\bar{u}_{non}$ is found through the numerical solutions of the PDEs. The BVP4C solver outputs an eigenvalue and an eigenfunctions, note, there are an infinite number of solutions to (5.140). However BVP4C requires an initial guess for the eigenvalue and this allows the user to guide the solution to the first eigenfunction. The initial guess was found from (5.55) using $n = 0$ which is the most unstable mode.

It would be expected that the growth rate s decreases as v, u and h grow reaching $s = 0$ when these variables peak, this is because at this point there is no growth in the system.

As these variables begin to decay again the growth rate is expected to build back up again reaching its most unstable point when the cycle is complete. To see this the results of BVP4C can be seen in figure 5.35; (a) shows s^2 plotted against time, it is clear that s^2 decreases to zero where in fact for a short time it does become negative, $s^2 = -7.4\times10^{-4}$. This coincides exactly where the maximum of (c) u and (d) h over y reach their peak at around $t = 75$ and v instantaneously flips direction. It is at this point we should turn

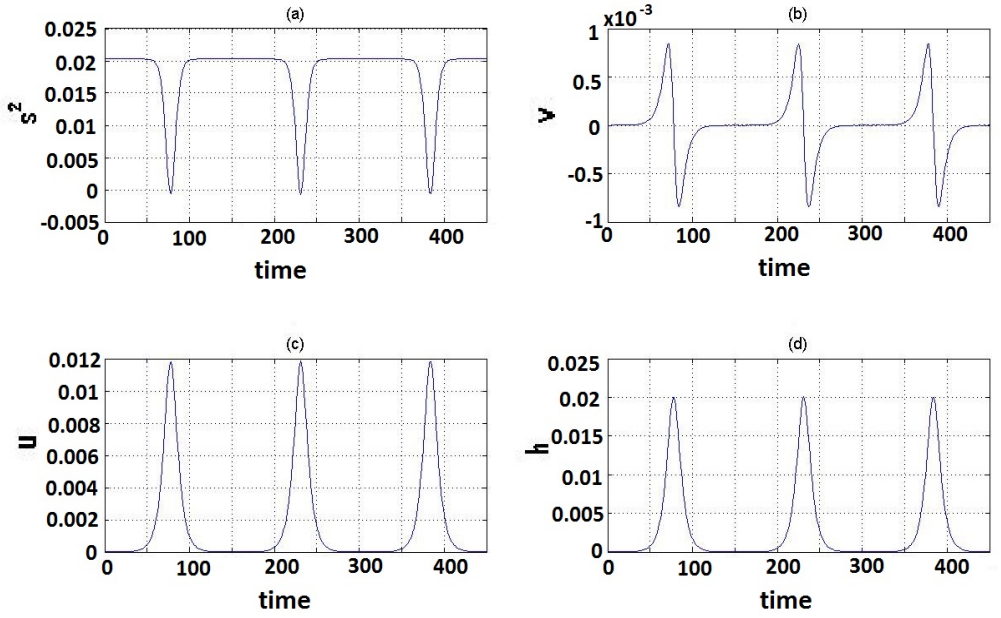

Figure 5.35: *The square of the growth rate (a) s^2 and the maximum of (b) v, (c) u and (d) h plotted against time, with $R_o = 3$, $\alpha = 0.45$, $\delta = 0.2$ and initial conditions (5.123a) - (5.123c) where $v_m = 3 \times 10^{-6}$. The minimum in s^2 coincides with the maximum in u and h and the reversal of the flow in v. The square of the growth rate s^2 does for a short time become negative, however the stability is short lived as it returns to its starting value.*

our attention to the mean flow $\bar{u} = R_0 \tanh(y) = \bar{u}_{non}$ since this is the driving force of the instability. It is the gradient of $\bar{u}$ that works to reduce the potential vorticity Q. We compared these in figure 5.36 at $t = 0$ and $t = 75$ where the maximum growth has been obtained. It is clear that the gradient of the mean flow has reduced around $y = 0$, (shown more clearly in figure 5.37). This in turn has caused a reduction in $Q = 1 - \partial\bar{u}/\partial y$ which

in turn causes a reduction in the instability. As with the interface h is can be shown $\bar{u}$ is conserved, this is done by integrating (5.26) over y and since $v = 0$ at the boundaries we have

$$\frac{\partial}{\partial t}\int_{-L}^{L} \bar{u}dy = -R_o \int_{-L}^{L} D_1 D_2 uv dy = 0. \tag{5.141}$$

Hence, $\bar{u}$ is conserved over y and since it can be seen from figure 5.36 the mean flow from $t = 0$ to $t = 75$ increases on the left it therefore must decrease on the right.

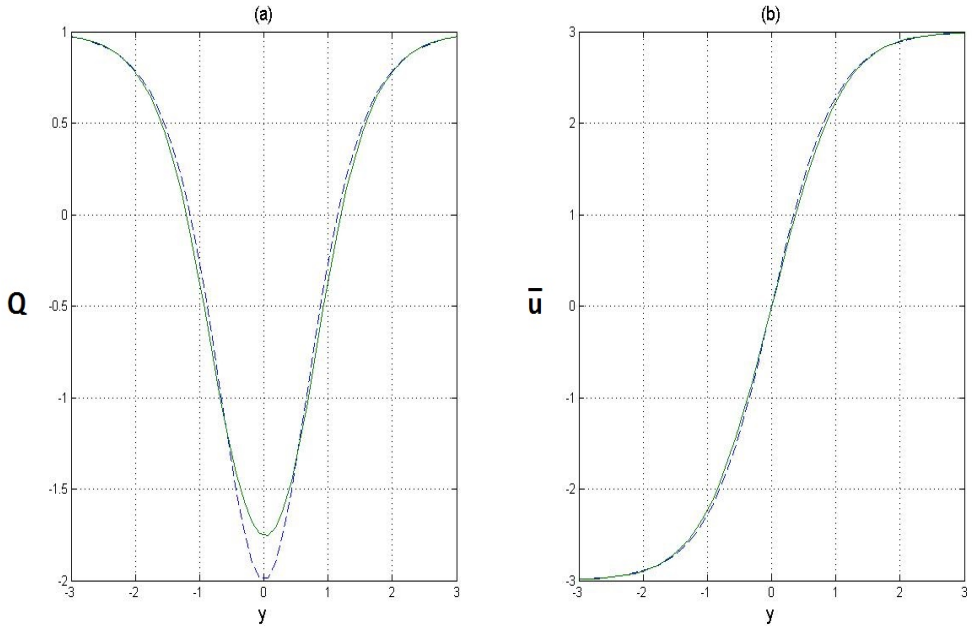

Figure 5.36: *(a) The potential vorticity Q at time $t = 0$, (dashed line), and $t = 75$ (solid line). The potential vorticity has clearly been reduced as the system tries to stabilize. (b) the mean flow $\bar{u}$ at $t = 0$, (dashed line) and $t = 75$, (solid line), the shear given by the gradient has been reduced around $y = 0$, this can be seen more evidently in figure 5.37. It can be shown that the mean flow, $\bar{u}$ is conserved and hence since the mean flow falls below the original shear, (at $t = 0$), to the right, it must therefore rise above the original shear by an equal amount on the left.*

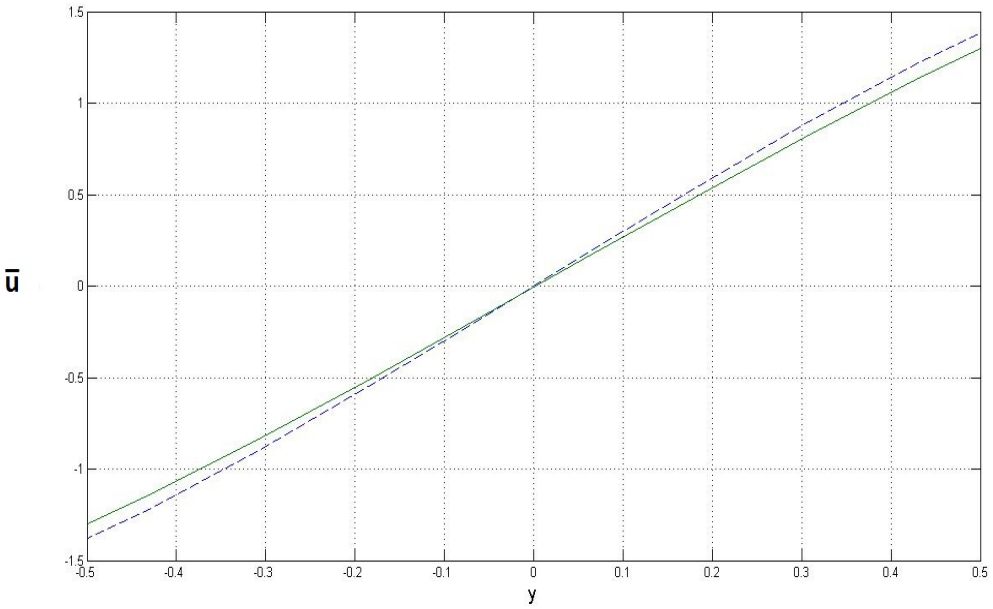

Figure 5.37: *A close up of the mean flow $\bar{u}$ around $y = 0$ at $t = 0$ (dashed line), and $t = 75$ (solid line): it can be seen more clearly here how the system has reduced the shear in turn reducing the potential vorticity Q and making the system less unstable than at $t = 0$.*

5.9 Discussion

In this chapter we have analysed inertial instability in a two-layer system with a localized shear flow basic state on the f-plane. The equations we use are the shallow water equations adapted to a two-layer model, as derived in chapter 3. For convenience we nondimensionalised the equations before performing any analysis.

We started our analysis with linear theory concentrating on the frictionless case, deriving a dispersion relation. We found the growth rate was controlled by two parameters $\tilde{g}$ and Rossby number R_0. The parameter $\tilde{g}$ being a combination of reduced gravity, total layer depth, layer depth of the top and bottom layer and the shear of the basic state. Moreover, the critical $\tilde{g}$ was found as a function of R_0 and there was found to be a transition from stability to instability as $\tilde{g}$ decreases with R_0 fixed. We found that the flow is most unstable

for large shear, small reduced gravity, small overall layer depth and when one layer of fluid is smaller than the other.

To understand the nature of this transition we need to understand the nonlinear evolution and its effect on the mean flow. The simplest and most natural thing to do is to apply weakly nonlinear theory. Weakly nonlinear theory allows for the derivation of an amplitude equation which can give a comprehensive understanding of the flow in this weakly nonlinear state. We analysed the amplitude equation and found the flow was periodic. Unlike its equatorial β-plane counterpart there is no trajectory here that can take the flow on a path to infinity. The solution in this case involves two or one enclosed periodic orbit.

The natural next step was to investigate the fully nonlinear regime, which can only be done numerically. The first thing we did was to compare these numerics to the weakly nonlinear theory. While for solutions initialised with larger amplitudes the weakly nonlinear theory agreed with the numerical solution to the PDEs we found that for smaller initial amplitudes noise had an effect on both the PDEs and ODEs. Noise had the effect of either causing the PDEs or ODEs to have a longer period or kicked them out of their periodic orbit sooner than they would have done had they not been affected by noise. Alternatively noise may also kick the PDEs and ODEs from one periodic orbit into another periodic orbit; this being possible due to the close proximity of both periodic orbits. While the equatorial β-plane was found not to be influenced by noise it is apparent that the f-plane solution is very sensitive to noise. The chaotic behavour found in our system due to noise flipping the sign of some velocities was an unexpected development. Although unrelated to inertial instability it is worth introducing work by Pedlosky (1980). Pedlosky looked at weak baroclinic instability in a continuously stratified system. Cyclical behavour similar to that observed in this chapter was found. More interestingly Pedlosky found the flipping of the solution between opposite cycles as was found in this chapter. He remarks on the unpredictability and chaotic nature of the solution as a result of this behavour.

We are interested in understanding how the flow was evolving, in particular what was happening to the mean flow. The system is initially unstable, which causes the horizontal velocities to grow and in turn the displaced fluid causes the interface to lift and dip away from its equilibrium position. This process causes a reduction in the mean flow which in turn decreases the negativity of the potential vorticity until the flow is stabilised. This momentarily stable state is however short lived; the instability is no longer driving the flow and the horizontal velocities start to decay to zero, the stability overshoots and now the meridional horizontal velocity is reversed; ultimately the flow becomes unstable again. The horizontal velocities reach their peak in amplitude and again decay to zero, the system is back to its initial state and the cycle is ready to repeat again. We have clearly shown that when the system is momentarily stable there is a reduction in the shear.

We extended our analysis to the fully nonlinear regime. Although the nonlinear behaviour had diverged from following the same trajectory of the weakly nonlinear analysis the behaviour was still periodic. It is important to note that in this regime noise does not affect the nonlinear numerical solution. The system now spent less time in the state where amplitudes were small, shortening the period length. The numerical method adopted restricted us to a moderately nonlinear regime rather than a strongly nonlinear regime, this was due to the interface between the two-layers growing too large and breaking through the rigid lid of the model. In these circumstances a breakdown of the model has occurred, in reality other physics would come in to play or a change to the numerical scheme could be applied. For example physically we have assumed hydrostatic balance and assumed that no over turning in the fluid can occur (no z dependence) which is perhaps too crude and here we have may have paid the price for simplicity. Another alternative would be to apply the frictional terms we have neglected which may offer some resistance as the flow approaches the boundary. A numerical way to overcome the problem could perhaps be to use a 2-layer, 1-layer, 2-layer split where the interface touches the upper and lower boundary. Although these are workable ideas, they are very complex to apply especially in the latter case.

The most closely related work to the work involved in this chapter is Zeitlin et al (2011), who considered inertial instablity in a two-layer flow on the f-plane with a Bickley jet shear flow basic state. It should be noted also that as well as the difference in the basic state flow, Zeitlin et al also used an upper free surface in their model. They looked at asymmetric instabilities and found competing inertial and barotropic instability with inertial instability dominating for large R_0. Baroclinic and barotropic instabilities become the dominating instabilities as R_0 diminishes. This is consistent with our findings that for inertial instability to be present we must have $R_0 > 1$. As consistent with our findings, Zetlin et al find that stability is achieved through the reduction of the shear, causing a reduction in the negativity of the potential vorticity. Kloosterziel et al (2013) looked at nonlinear instability on the f-plane in a continuously stratified system with a Guassian Jet basic state. Kloosterziel found instability when $R_0 > 1.165$ which is a similar result found in our two-layer system. Kloosterziel showed the flow stabilised through a reduction in the shear flow which in turn causes a reduction in the negativity of the potential vorticity. Moreover Kloosterziel et al used linear theory to predict the final mean flow as a result of the reduction in shear; this was confirmed numerically.

In the frictional case there were found to be three parameters: $\tilde{g}$, friction, ϵ and Rossby number R_0. We could have extended the work in this chapter by applying weakly nonlinear analysis and analysing the fully nonlinear regime. Although Pedlosky (1980) looked at barotopic instability in a continuously stratified system with dissipation we could extrapolate his results and make a prediction to our weakly nonlinear frictional system. Pedlosky found periodic behavour in his system, however dissipation produced a limit cycle.

Chapter 6

Conclusion

We have previously discussed the idea of inertial instability being an extension of centrifugal instability, the inviscid case being analysed by Rayleigh (1916). Rayleigh derived instability criteria for inviscid flow between two rotating cylinders. The flow was symmetric which as we have seen is a characteristic of inertial instability. Taylor (1923) developed Rayleigh's work by introducing viscosity in the flow, experimentally he found horizontally stacked disks forming between the two cylinders. We consider inertial instability to be an extension of the above when considering parallel flows with cross-stream shears that are typical of zonal jets in the atmosphere and ocean. What strongly connects the work of Rayleigh and Taylor with inertial instability is that in all cases the instability involves overturning circulations with along stream symmetry.

When considering inertial instability we found that for instability we must have $fQ < 0$, where f is the Coriolis parameter and Q is the vertical component of the absolute vorticity, $Q = f - \partial u/\partial y$. We can see that the case for inertial instability is strongest at the equator where $f = 0$, any shear is therefore unstable. This however does not mean there is not a strong case for inertial instability at mid-latitudes.

Observations of these vertically stacked structures in the atmosphere have been found

in observational data by Hayashi and Shiotani (1998). The case for inertial instability here is made by comparing these observed structures with the structures described by the linear theory of Dunkerton (1981). Dunkerton found in a continuously stratified flow on the equatorial β-plane with a shear flow basic state and $Pr = 1$, vertically stacked structures of alternating temperature. Likewise Hayashi and Shiotani (1998) also observed stacked structures of alternating temperature. Moreover, both showed structures of small vertical length scales compared to horizontal length scales, a characteristic akin to inertial instability.

The argument for inertial instability being responsible for the observable interleaving of saltier and fresher water in the ocean was made by Richards and Edwards (2003). The appearance of these structures are not as striking in their resemblance to the structures of the linear theory of Dunkerton (1981) but nonetheless Richards and Edwards made a strong case for inertial instability being at least partially responsible. It should be noted that the structures in the ocean had a much larger vertical to horizontal scale ratio than those observed in the atmosphere.

In chapter 2 we started our analysis of inertial instability by looking at linear theory in a continuously stratified system. We looked at inertial instability on the equatorial β-plane with uniform N and a uniform shear flow basic state. We first recapped the work of Dunkerton (1981) by using Prandt number unity, $Pr = 1$. We found through the dispersion relation the instability was strongest at a specific wavenumber. Moreover, we found as found in Dunkerton a critical wavenumber and critical shear flow as a function of the viscosity and stratification. As to be expected it was found viscosity and stratification stabalise the flow.

The next case we looked at was as found in Dunkerton (1982). We changed the Prandtl number from unity to $Pr = \infty$. Where Dunkerton solved the dispersion relation numerically to find the critical case for instability, we solved the dispersion relation obtaining an analytic result. The $Pr = \infty$ case is most relevant for molecular and

turbulent diffusivities; however, the mismatch between the vertical scales selected by the linear theory and the vertical scales found in observational data still remains. We must therefore conclude that there are other mechanisms at play and further work has been done nonlinearly to establish the disconnection.

Further nonlinear work includes variations from the most common 3D, continuously stratified system on the equatorial β-plane such as 2D models, f-plane models (Kloosterziel et al., 2007), and asymmetric models (Clark and Haynes (1996)) and two layer models with a free surface approximation (Bouchut et al., 2011; Zeitlin et al., 2014).

There is a simpler approach when looking at inertial instability: we can consider two-layer models and in chapter 3 we showed that there is an analogy between a two-layer system with a rigid lid approximation and a continuously stratified model. The two-layer model was derived using the shallow water equations, this resulted in there being no z-dependence within each layer which in turn simplifies the analysis. As we have previously discussed, the two-layer model has not been used as extensively as the continuously stratified model when looking at inertial instability. Moreover, all such analysis has used a free surface approximation rather than a rigid lid approximation as we used.

The limited examples of nonlinear analysis of inertial instability using a two-layer model includes Zeitlin and Plougonven (2009) and Zeitlin et al. (2014), using f-plane and equatorial β-plane approximations respectively with free surface approximations. There analysis contained within some preliminary linear analysis. The only weakly nonlinear analysis was made by Zhao and Ghil (1991) on the equatorial β-plane in pressure coordinates. Zhao and Ghil (1991) found cyclical behaviour in their ODEs.

In chapter 3 we derived the governing equations of the two-layer model with a rigid lid approximation. Introduced in the equations was a special form of momentum conserving friction in an attempt to mimic the vertical diffusivity of the atmosphere which is known to be important for vertical scale selection. We then discussed the linear problem deriving an eigenvalue problem, the formal analogy with the continuously stratified system with $Pr =$

1 was then discussed. As with the continuously stratified system we found oscillatory instabilities.

With the two-layer system we had to choose a particular layer depth by fixing H_1 and H_2, whereas for the continuously stratified model there was an extra freedom through the variance of the vertical wavenumber. This suggests the two-layer model is somehow like the continuously stratified model with $Pr = \infty$, however constrained to a particular wavenumber. Griffiths (2003a) discussed how nonlinear effects cause an upscale in the vertical scale selection of the instability, effectively constraining the vertical wavenumber. This makes a strong case for the two-layer model being a good approximation for a continuously stratified model in the nonlinear phase.

The most natural thing we did once we derived the governing equations of our two-layer model was to perform weakly nonlinear analysis. We did this first on the equatorial β-plane because this is where the instability is mostly observed. We looked at the inviscid (frictionless) case around marginal stability. We fixed the layer depths H_1 and H_2 and controlled the strength of the instability by decreasing the density difference between the two layers slightly from critical. The result was to produce a third order ordinary differential equation, which we analysed analytically.

Depending on the initial conditions of the ordinary differential equations (ODEs) different behaviours were displayed. Firstly there was cyclic behaviour where as the instability grew, horizontal velocities u, v and interface height h grew with it. Then as the flow was momentarily stabilised, the velocities and interface height started to decay. The system overshot its stability and oscillated between instability and stability always returning to its initial starting state. The other behaviour that was observed in the ODEs was non-cyclic behaviour, the horizontal velocities and interface height grew in amplitude but continued to grow indefinitely. Of course such behaviour could not physically be seen in our model due to the rigid lid approximation we used, in other words the interface height at some point would become larger than the smallest layer depth. There was a third behaviour that

was observed in the ODEs more as a result of the merging of the two previous behaviours already described. The cyclic trajectory merged with the infinite trajectory such that after one cycle was completed the velocities and interface height then grew indefinitely. This type of cyclic behaviour is typical of inviscid instabilities, for example Pedlosky (1970), and dissipative instabilities (Pedlosky and Frenzen (1980)).

The weakly nonlinear analysis was verified through numerical analysis of the fully nonlinear PDEs and shown to be consistent with each other. Furthermore, we extended the analysis of the fully nonlinear PDEs to a moderately nonlinear regime. However, interestingly we could not extend this further. The reason for this was that as the instability became stronger the interface would grow larger than the smallest layer depth.

Our next step was to look at the weakly nonlinear regime using an f-plane approximation. We chose to look at a shear flow of the form $u = \tanh(y)$, since the problem can be solved analytically. This has not been done before with a two-layer system, however Griffiths (2003b) has applied it to the continuously stratified model. Unexpectedly there was a different scaling involved when deriving the amplitude equation. However, like on the equatorial β-plane the resulting ODE was third order. The subtle difference was in the coefficient of the linear and nonlinear terms but also the nonlinear terms were a higher order than on the equatorial β-plane. The resulting behaviour was more complex, however unlike the equatorial β-plane it was always cyclic.

The first type of behaviour was a single cycle where the structure of u or h did not change but always remained of the same composition but with a change in amplitude. Only v changed direction half way through the cycle, growing in one direction and then reversing to a flow in the opposite direction. The cycle was set to repeat indefinitely. The other behaviour which was observed was as above, however each second cycle the flow in u and h would be as the previous cycle but reflected in the $y = 0$ axis, v would also flow first in the opposite direction to the cycle before.

On top of these two distinct behaviours that were observed there was an extra phenomenon

affecting the behaviour of the ODEs, (noise), however it was rather a symptom of the numerics than a unique behaviour of the ODE system. The ODE system was very sensitive to noise when the variables became very small. This had various effects on the solution, firstly noise kicked the solution out of its orbit too soon such that the period of the cycle would be shortened. On the other hand noise kicked the solution into a completely different cyclic orbit all together. This accounted for the discrepancy between the ODEs and fully nonlinear PDEs. However, it could clearly be seen the two solutions diverged when the variables became small amplitude.

While the two ODE equations show cyclical behaviour we showed they can behave very differently. On the equatorial β-plane the system in some instances grew indefinitely, although from a model point of view this was not a valid solution. Also we found the full nonlinear PDEs and ODEs from the weakly nonlinear analysis on the equatorial β-plane both agreed, whereas on the f-plane we showed a system which was very sensitive to noise when the system was initialised in a certain way. More investigation is required to understand the true behaviour of the ODEs and PDEs. In both systems we attempted to show there to be a mean flow change such that $\partial u/\partial y$ is reduced which in turn reduced the negativity of fQ. While we unable to show this for the β-plane we were successful on the f-plane: in the f-plane case we saw the growth rate becomes momentarily stabilised at the point when the minimum of fQ is at its least negative point. The stability however was short lived and the growth rate started to increase again. Further analysis needs to be undertaken on the β-plane.

There are limitations to the weakly nonlinear analysis. We have already discussed how noise interfered with the solution, however, another limitation with our analysis was the neglect of dissipation. We would expect the introduction of dissipation to lead to a steady state, presumably where the instability has been neutralised. We would expect this to be achieved through the mixing of momentum, this has been discussed by many such as Griffiths (2003a) and Kloosterziel et al. (2007). This would naturally be the next step in

our analysis.

Other extensions to this work would possibly be to look at the zonally asymmetric system as found in Zeitlin et al. (2014). Recall this was discussed as another possible mechanism for the upscaling of the vertical scale of the observed structures in the atmosphere and ocean. We could also look into models involving extra layers, the first being a three-layer model. We can view the addition of more layers as getting closer to the continuously stratified model and therefore worth doing.

Appendix A

The Boussinesq Approximation

A.1 Governing equations

We start by giving the standard equations of motion for a viscous, compressible, density-stratified fluid, (Gill, 1982). The momentum equation and continuity equation are given by

$$\rho\left(\frac{D\mathbf{u}}{Dt} + 2\boldsymbol{\Omega}\times\mathbf{u}\right) = -\nabla p - g\rho\mathbf{k} + \mu\nabla^2\mathbf{u} + \frac{\mu}{3}\nabla(\nabla\cdot\mathbf{u}), \tag{A.1a}$$

$$\frac{D\rho}{Dt} + \rho(\nabla\cdot\mathbf{u}) = 0. \tag{A.1b}$$

Here we are using a local Cartesian coordinate system (x, y, z), with x representing the longitude direction, y representing latitude and z representing height. The corresponding flow is $\mathbf{u} = (u, v, w)$, with density ρ, pressure p, g is the gravitational acceleration, μ is the dynamic viscosity and $\mathbf{k}$ is the unit vector in the vertical. Here $\boldsymbol{\Omega} = (0, \Omega\cos\theta, \Omega\sin\theta)$ is the rotation vector, ($\Omega = 7.2921 \times 10^{-5}$ radians per second).

We also require an equation of state; we use the simplest such equation, which is that for an ideal gas. However, there also exists an equation of state for the ocean, which

can be shown to reproduce the same results with the Boussinesq approximation. Such an equation of state for the Ocean is complex but can be found in the Appendix of Gill (1982). The equation of state for an ideal gas is

$$p = \rho R T, \tag{A.2}$$

where R is the gas constant (typically $8314.36\text{Jkmol}^{-1}\text{K}^{-1}$ for dry air) and T is the temperature.

We finally require an entropy equation. We start with the equation of Gill (1982) for the internal energy E given by

$$\frac{\partial \rho E}{\partial t} + \nabla \cdot (\rho E \mathbf{u}) \equiv \rho \frac{DE}{Dt} = -p(\nabla \cdot \mathbf{u}) + K \nabla^2 T, \tag{A.3}$$

where K is the thermal conductivity (typically $0.6\text{Wm}^{-1}\text{K}^{-1}$ for air or $0.023\text{Wm}^{-1}\text{K}^{-1}$ for water). This can be interpreted as the rate of change of energy of a fixed volume which can change due to advection across the sides (the $\rho E \mathbf{u}$ term), or by compression and expansion of the fluid in the volume ($p \nabla \cdot \mathbf{u}$ term). In addition to this we can also have a change in energy due to the heat exchange by molecular conduction which is proportional to the temperature gradient (the $K \nabla^2 T$ term). There are viscous terms in (A.3) which have been omitted; Spiegel and Veronis (1960) show that these terms contribute negligibly to the energy balance.

To summarise, the complete set of equations is given by

$$\rho \left(\frac{D\mathbf{u}}{Dt} + 2\boldsymbol{\Omega} \times \mathbf{u} \right) = -\nabla p - g\rho \mathbf{k} + \mu \nabla^2 \mathbf{u} + \frac{\mu}{3} \nabla (\nabla \cdot \mathbf{u}), \tag{A.4a}$$

$$\frac{D\rho}{Dt} + \rho (\nabla \cdot \mathbf{u}) = 0, \tag{A.4b}$$

$$p = \rho R T, \tag{A.4c}$$

$$\rho C_v \frac{DT}{Dt} = -p(\nabla \cdot \mathbf{u}) + K\nabla^2 T, \tag{A.4d}$$

where we have used $E = C_v T$ for an ideal gas and C_v is the specific heat at a constant volume (typically $C_v = 0.718$ kJ(kgK)$^{-1}$ for dry air).

A.2 The Boussinesq approximation

The Boussinesq approximation is used widely to model atmospheric and oceanic flows, and will be the foundation of our analysis of a continuously stratified flow. There are two key steps to make. Firstly we analyse a depth of the fluid layer that is small enough such that perturbations in background density are small in magnitude compared to that of the vertically averaged density of a static flow. We also extend this to the background pressure and potential temperature of the flow. Clearly the density in the atmosphere and ocean varies with height. However, by selecting a layer of fluid small enough in the vertical, we can restrict density perturbations to be much smaller than the background averaged density.

The Boussinesq approximation assumes that once the flow has been perturbed and motion introduced, the dynamic density perturbation resulting from this motion is small compared to the vertically averaged density. To implement this assumption and derive the equations of the Boussinesq approximation let us first define three scale heights which set a restriction on the vertical depth of our fluid.

We follow the steps of Spiegel and Veronis (1960) and partition the density, pressure and temperature three ways, firstly into a reference density, pressure or temperature ρ_s, p_s and T_s respectively which are calculated from the density, pressure or temperature averaged across the fluid layer. Secondly a density, pressure or temperature variation, $\rho_o(z)$, $p_o(z)$ or $T_o(z)$ respectively descriptive of how the density, pressure or temperature will vary with height when at rest and finally a density, pressure or temperature perturbation as a

result of motion $\rho'(x,y,z,t)$, $p'(x,y,z,t)$ or $T'(x,y,z,t)$ respectively, i.e.

$$\rho(x,y,z,t) = \rho_s + \rho_o(z) + \rho'(x,y,z,t), \tag{A.5a}$$

$$p(x,y,z,t) = p_s + p_o(z) + p'(x,y,z,t), \tag{A.5b}$$

$$T(x,y,z,t) = T_s + T_o(z) + T'(x,y,z,t). \tag{A.5c}$$

Now we introduce scale heights for the variables ρ and p, namely

$$D_\rho = \left|\frac{1}{\rho_s}\frac{d\rho_o}{dz}\right|^{-1}, \qquad D_p = \left|\frac{1}{p_s}\frac{dp_o}{dz}\right|^{-1}, \qquad D_T = \left|\frac{1}{T_s}\frac{dT_o}{dz}\right|^{-1}. \tag{A.6}$$

These height scales are going to set a bound on the layer depth of fluid and therefore it is important to understand them. If we think of two different density profiles that vary as a function of height, $\rho_1(z)$ and $\rho_2(z)$ say, with ρ_1 changing faster with height than ρ_2, ($d\rho_1/dz > d\rho_2/dz$), we would be required to select a fluid with smaller layer depth for fluid with a ρ_1 profile. This is because a smaller layer depth will be required to satisfy the first assumption; that density variations in the absence of motion are small when compared to a background averaged density ($\rho_o(z) \ll \rho_s$). Hence a smaller density gradient allows us to increase our layer depth without compromising this first assumption.

The first step is therefore to define the thickness of our fluid layer d as satisfying

$$d \ll D, \qquad \text{where} \qquad D = min(D_\rho, D_p, D_T). \tag{A.7}$$

In other words, d is much smaller than the smallest height scale, thus ensuring that when the fluid is at rest, perturbations in density ρ_o, pressure p_o and temperature T_o are much smaller in comparison to their vertically averaged values, ρ_s, p_s and T_s. We conclude that

$$\Delta\rho_o/\rho_s \equiv \epsilon \ll 1, \tag{A.8}$$

where $\Delta\rho_o$ is the maximum variation in ρ_o across the fluid layer.

The second assumption is to assume that when the fluid is perturbed and no longer at rest, the perturbation in density $\rho'(x, y, z, t)$ is much smaller than the vertically averaged density ρ_s, in other words

$$\mid \rho'/\rho_s \mid \leq O(\epsilon). \tag{A.9}$$

To justify this, consider values as stated by Salmon (1998); for the ocean we typically have

$$\rho_s \approx 1.04\text{g cm}^{-3}, \qquad \rho_o \approx 0.03\text{g cm}^{-3}, \qquad \rho' \approx 0.003\text{g cm}^{-3}. \tag{A.10}$$

It will become useful to note that from our equation of state at rest we have (A.4c)

$$p_s + p_o(z) = R(\rho_s T_s + \rho_s T_o(z) + \rho_o(z) T_s + \rho_o(z) T_o(z)). \tag{A.11}$$

Hence at leading order we have

$$\frac{p_o}{p_s} = \frac{T_o}{T_s} + \frac{\rho_o}{\rho_s}. \tag{A.12}$$

Next introducing motion and using (A.11) to cancel terms

$$p' = R(\rho_s T' + \rho_o T' + \rho' T' + \rho' T_s + \rho' T_o). \tag{A.13}$$

Dividing (A.13) by $P_s = R\rho_s T_s$, and using (A.8) and (A.9) we have

$$\frac{p'}{p_s} = \frac{T'}{T_s} + \frac{\rho'}{\rho_s} \tag{A.14}$$

after retaining terms in the highest order of ϵ.

We start with modifying the continuity equation, (A.1b). Substituting from (A.5a) into (A.4b) we have

$$\frac{D}{Dt}(\rho_o + \rho') + (\rho_s + \rho_o + \rho')(\nabla \cdot \mathbf{u}) = 0. \tag{A.15}$$

Diving through by ρ_s and using (A.8) we have

$$\frac{D}{Dt}\left(\epsilon\frac{\rho_o}{\Delta\rho_o}+\epsilon\frac{\rho'}{\Delta\rho_o}\right)+\left(1+\epsilon\frac{\rho_o}{\Delta\rho_o}+\epsilon\frac{\rho'}{\Delta\rho_o}\right)(\nabla\cdot\mathbf{u})=0. \tag{A.16}$$

At leading order we find

$$\nabla\cdot\mathbf{u}=0 \tag{A.17}$$

and we are left with

$$\frac{D\rho'}{Dt}+w\frac{d\rho_o}{dz}=0. \tag{A.18}$$

We will now look at the adaptation of the momentum equations under the Boussinesq approximation. First we use (A.17) which eliminates the second diffusive term in (A.16), then in the absence of motion we have

$$\frac{dp_o}{dz}=-g(\rho_s+\rho_o(z)). \tag{A.19}$$

Next using (A.8) and (A.9) and using (A.19) to cancel terms, at leading order we have

$$\frac{D\mathbf{u}}{Dt}+2\Omega\times\mathbf{u}=-\frac{1}{\rho_s}\nabla p'-g\frac{\rho'}{\rho_s}\mathbf{k}+\nu\nabla^2\mathbf{u}, \tag{A.20}$$

where ν is the kinematic viscosity. Note that even though the term $g\rho'/\rho_s$ is of order ϵ or less, we choose to retain it here. It is important to retain the bouyancy term when considering instability in stratified systems. Finally note, using (A.14) we can write

$$-\frac{1}{\rho_s}\frac{\partial p'}{\partial z}-g\frac{\rho'}{\rho_s}=-\frac{1}{\rho_s}\left(\frac{\partial p'}{\partial z}+\frac{p'}{H}\right)+g\frac{T'}{T_s}, \tag{A.21}$$

where $H=p_s/(g\rho_s)$ represents the thickness of a layer where ρ_s is a uniform density across the layer, and where p_s is the pressure at the top of the layer. Using (A.19) and the definition of D_p from (A.6) we can write $H=D_p+\bigcirc(\epsilon)$. Therefore since $dp'/dz\sim p'/d$ and $d\ll D_p$ we conclude that p'/H is negligible compared to $\partial p'/\partial z$. Hence (A.20) can

be written as

$$\frac{D\mathbf{u}}{Dt} + 2\boldsymbol{\Omega}\times\mathbf{u} = -\frac{1}{\rho_s}\nabla p' + g\frac{T'}{T_s}\mathbf{k} + \nu\nabla^2\mathbf{u}. \tag{A.22}$$

As a consequence to neglecting p'/H in (A.21) we can re-write (A.14) as

$$\frac{\rho'}{\rho_s} = -\frac{T'}{T_s}. \tag{A.23}$$

Finally we consider the entropy equation (A.4d). First note that at rest we have $K\nabla^2 T = 0$; therefore inducing motion at leading order we can write

$$\rho_s C_v\left(\frac{DT'}{Dt} + w\frac{dT_o}{dz}\right) = -p_s(\nabla\cdot\mathbf{u}) + K\nabla^2 T'. \tag{A.24}$$

Next note that from (A.16) we have

$$p_s(\nabla\cdot\mathbf{u}) = p_s\left(\frac{\partial}{\partial t} + \mathbf{u}\cdot\nabla\right)\left(\frac{\rho_o}{\rho_s} + \frac{\rho'}{\rho_s}\right) \tag{A.25}$$

Then note that from (A.11) we have $\rho_o/\rho_s = T_o/T_s - p_o/p_s$ and from (A.23) we have $p'/p_s = T'/T_s$, hence we have

$$p_s(\nabla\cdot\mathbf{u}) = p_s\left(\frac{\partial}{\partial t} + \mathbf{u}\cdot\nabla\right)\left(\frac{T_o + T'}{T_s} - \frac{p_o}{p_s}\right). \tag{A.26}$$

From (A.19) at leading order we have $dp_o/dz = -g\rho_s$, therefore (A.24) becomes

$$\frac{Db}{Dt} + N^2(z)w = \kappa\nabla^2 b, \tag{A.27}$$

where we have used $C_p = C_v + p_s/(\rho_s T_S)$ (C_p is the specific heat at constant pressure) and $\kappa = K/\rho_s C_v$. Here,

$$N^2(z) = \frac{g}{T_s}\left(\frac{dT_o}{dz} + \frac{g}{C_p\rho_s}(\rho_s + \rho_o)\right) \tag{A.28}$$

and $b = gT'/T_s$.

It is worth noting that using (A.12) and $c^2 = C_p R T_s / C_v$, where c^2 is the speed of sound, we can show that

$$N^2(z) = -\frac{g}{\rho_s}\left(\frac{d\rho_o}{dz} + \frac{g}{c^2}(\rho_s + \rho')\right), \tag{A.29}$$

which is an alternative definition of the buoyancy frequency.

To summarize, the set of Boussinesq equations we shall hereafter use is given by

$$\frac{D\mathbf{u}}{Dt} + 2\Omega\times\mathbf{u} = -\nabla\phi' + b\mathbf{k} + \nu\nabla^2\mathbf{u}, \tag{A.30a}$$

$$\nabla\cdot\mathbf{u} = 0, \tag{A.30b}$$

$$\frac{g}{\rho_s p_s}\frac{\partial\phi}{\partial z} = b, \tag{A.30c}$$

$$\frac{Db}{Dt} + N^2(z)w = \kappa\nabla^2 b, \tag{A.30d}$$

where $\phi = p'/\rho_s$.

Appendix B

A note on boundary conditions

The boundary conditions applied to equation (2.45) were $\hat{v} \to 0$ as $Y = L(y - \Lambda/2\beta) \to \pm\infty$ and we have found solutions which are only valid provided $\mid arg(Y) \mid < \pi/4$ or equivalently $\mid arg(L) \mid < \pi/4$ (Bender & Orszag). Since $Y \to \infty$ we must have $\mid arg(L(y - \Lambda/2\beta)) \mid < \pi/4$ since $(y - \Lambda/2\beta)$ is strictly real and does not affect the argument. Recall that we have

$$L^4 = \frac{4|m|^2\beta^2}{N^2}\left(\frac{s}{s + \nu|m|^2}\right) \tag{B.1}$$

and hence L can become complex with complex s. However we can show that the condition $\mid arg(L) \mid < \pi/4$ is not broken and the solution is still valid for complex and negative s. There are three cases to look at.

Case one: s real and positive

When s is real and positive we have L^4 is also real and positive and hence the fourth root can be chosen such that L is also real and positive. This tells us that the $\mid arg(L) \mid < \pi/4$ since L is restricted to lie on the real axis in the real imaginary plane.

Case two: s complex

Complex s will result in L^4 also being complex, however we can show that we can still satisfy $\mid arg(L) \mid < \pi/4$. Suppose we have

$$\frac{4|m|^2\beta^2}{N^2}\left(\frac{s}{s+\nu|m|^2}\right) = A\exp(i\theta + 2n\pi), \qquad \text{with} \qquad -\pi < \theta < \pi, \tag{B.2}$$

then taking the fourth root of this

$$L = \left(\frac{4|m|^2\beta^2}{N^2}\left(\frac{s}{s+\nu|m|^2}\right)\right)^{1/4} = \exp(i\theta/4), \quad \exp(i\theta/4 + \pi/2), \tag{B.3a}$$

$$\exp(i\theta/4 + \pi), \quad \exp(i\theta/4 + 3\pi/2).$$

Since $= -\pi < \theta < \pi$ we have at least one root such that $\mid arg(L) \mid < \pi/4$ and hence the solution and dispersion relation remain valid provided this root is used.

Case three: s real and negative

Provided $\mid s \mid > \mid \nu|m|^2 \mid$ the results is as per case one. However if $\mid s \mid < \mid \nu|m|^2 \mid$ we have $\mid arg(L) \mid = \pi/4$, the solution changes and hence so does the dispersion relation. However since we are interested in looking at unstable solutions we do not need to consider this case.

Appendix C

Numerical Schemes

There are two things to consider when approaching the problem of solving a system of PDEs such as (4.6) - (4.9) in chapter 4 or (5.11) - (5.122) in chapter 5; firstly how do we evaluate the differentials numerically with accuracy and secondly how do we march the PDEs forward in time. Many differential matrices exist, each more suitable to their own niche of functions and the same can be said for various time stepping schemes. Here I will outline two differential matrices I compared: a fourth order finite difference differential matrix and a Chebyshev differential matrix. I will then discuss the 4th order Runge Kutta time stepping scheme and why it was chosen.

Differentiation Matrices

Although many differentiation schemes exist, the principle behind them is the same: we choose a discretization of the domain, (i.e. equispaced grid points), to form a discrete set of grid points. Given a data set of values evaluated at these grid points we then interpolate to form a polynomial; how the polynomial is interpolated is unique to each scheme. This unique polynomial is then differentiated to obtain coefficients used to construct the elements of the differential matrix such that

$$D_N u_i \approx \dot{u}(x) \qquad \text{for} \quad i = 1, \ldots, N+1 \tag{C.1}$$

Note that we use D_N to denote an $(N+1) \times (N+1)$ matrix; this notation is common when describing differentiation matrices, as seen in Trefethen 2000.

One obvious requirement is that $D_N u_i \rightarrow \dot{u}(x)$ as $N \rightarrow \infty$. This convergence requirement is not necessarily guaranteed and is much dependent on the form of the solution (periodic or non-periodic). This is discussed further in this next section.

Equispaced or Chebyshev Discretization

Two methods of discretization will be discussed here, these are equispaced grid points spread evenly over the domain and Chebyshev grid points spread unevenly.

Equispaced grid points

Equispaced grid points are the more simplistic of the two; given a domain of $[-L, L]$ to obtain $N+1$ equally space grid points we define our grid spacing as

$$h = 2L/N,$$

then our grid points are defined as follows

$$x_j = -L + h(j-1), \qquad \text{for} \quad j = 1, \ldots, N+1. \tag{C.2}$$

Now, although equally spaced grid points do not come recommended for non-periodic solutions one can overcome this by "assuming" the solution is periodic. However when these solutions are extended periodically there may be discontinuities in the solution which play havoc in the numerics with fatal consequences. The error in the interpolant is of $O(1)$ and in the derivative is $O(N)$. We can bend this rule slightly for solutions

such as those that decay exponentially to zero at the boundaries, these discontinuities are minimised. Since in my PDEs I have used initial conditions and basic states involving functions such as $\mathrm{sech}(y)$ etc. which decay exponentially to zero in a large enough domain, I will persevere with this type of discretization. My main reason for doing so is computational; finite difference matrices involve a sparse matrix which require less storage.

Chebyshev grid points

A choice of unevenly spaced grid points were chosen to compare with evenly spaced grid points. The non-periodicity of the solution itself calls for uneven-grid spacing (Fornberg and Sloan, 1994), a widely used choice being Chebyshev grid spacing resulting in a Chebyshev differentiation matrix. The Chebyshev points create an uneven grid spacing with points clustered around the boundaries.

One of the advantages of using a Chebyshev method is that the errors typically decay at an exponential rate rather than a much slower polynomial rate as with the finite difference method (Fornberg and Sloan (1994)). The grid points are calculated as follows: given a domain $[-1, 1]$ our $N + 1$ grid points are given by

$$x_j = \cos(j\pi/N), \qquad for \quad j = 0, \ldots, N. \tag{C.3}$$

Our domain is not limited to $[-1, 1]$ since we can simply multiply the grid points by L. When using the finite difference differential matrix the differential at the end points is calculated using information that is one-sided (i.e. a one sided backward difference); this one-sidedness can limit the accuracy of the solution. Hence, it makes sense to increase the density of the grid points at the boundaries as is done in the Cebyshev case. Another explanation for why Chebyshev nodes are more suited for non-periodic functions is complex and involves potential theory, the reader is asked to refer to Trefethen (2000),

Chapter 5 for more detail.

Construction of differentiation matrices

A 4th order finite difference differentiation matrix

A 4th order finite difference differentiation matrix was constructed using a combination of central, forward and backward difference formulas of 4th order. Let us show how the central difference around a point x_i is derived as an example. We interpolate the corresponding date points u_i locally. For a central difference this involves the two data points either side of and inclusive of x_i to obtain a polynomial p_i such that $p_i(x_{i\pm1}) = u_{i\pm1}$, $p_i(x_{i\pm2}) = u_{i\pm2}$ and $p_i(x_i) = u_i$. This polynomial is defined as follows

$$p_j(x) = a_{-2}u_{j-2} + a_{-1}u_{j-1} + a_0u_j + a_1u_{j+1} + a_2u_{j+2}, \tag{C.4}$$

where

$$a_{-2} = \frac{(x - x_{j-1})(x - x_j)(x - x_{j+1})(x - x_{j+2})}{24h^4}, \tag{C.5}$$

$$a_{-1} = -\frac{(x - x_{j-2})(x - x_j)(x - x_{j+1})(x - x_{j+2})}{6h^4}, \tag{C.6}$$

$$a_0 = \frac{(x - x_{j-2})(x - x_{j-1})(x - x_{j+1})(x - x_{j+2})}{4h^4}, \tag{C.7}$$

$$a_1 = -\frac{(x - x_{j-2})(x - x_{j-1})(x - x_j)(x - x_{j+2})}{6h^4}, \tag{C.8}$$

$$a_2 = \frac{(x - x_{j-2})(x - x_{j-1})(x - x_j)(x - x_{j+1})}{24h^4}. \tag{C.9}$$

This polynomial is then differentiated and evaluated at x_i to obtain the central difference formula

$$w_i = p_i'(x_i) = \frac{1}{h}\left(\frac{1}{12}u_{i-2} - \frac{2}{3}u_{i-1} + \frac{2}{3}u_{i+1} - \frac{1}{12}u_{i+2}\right), \tag{C.10}$$

where w_i is an approximation of the derivative of $u(x)$ at x_i. These coefficients form the elements of the differentiation matrix so that

$$w_i = \sum_{j=1}^{N+1} D_{i,j}(u')_j = \frac{1}{h}\left(\frac{1}{2}u_{i-2} - \frac{2}{3}u_{i-1} + \frac{2}{3}u_{i+1} - \frac{1}{12}u_{i+2}\right) \quad for \quad i = 3, \ldots, N-1. \tag{C.11}$$

It is clear we have missed rows $i = 1, 2, N$ and $N + 1$; clearly here a central difference scheme is not possible since we would hit the boundaries either side. Here we adopt a forward and backward difference for $i = 1$ and $i = N + 1$ respectively. Where $i = 2$ we interpolate using one element to the left and three to the right of x_2 and use a reverse approach to $i = N$. The coefficients for the four rows are given in full by

$$i = 1: \qquad w_1 = \sum_{N+1}^{j=1} D_{1,j}(u)_j' = \frac{1}{h}\left(-\frac{25}{12}u_1 + 4u_2 - 3u_3 + \frac{4}{3}u_4 - \frac{1}{4}u_5\right), \tag{C.12}$$

$$i = 2: \qquad w_2 = \sum_{N+1}^{j=1} D_{2,j}(u)_j' = \frac{1}{h}\left(-\frac{1}{4}u_1 - \frac{5}{6}u_2 - \frac{3}{2}u_3 - \frac{1}{2}u_4 + \frac{1}{12}u_5\right), \tag{C.13}$$

$$i = N: \qquad w_N = \sum_{N+1}^{j=1} D_{N,j}(u)'_j = \frac{1}{h}\left(-\frac{1}{12}u_{N-3} + \frac{1}{2}u_{N-2} - \frac{3}{2}u_{N-1} + \frac{5}{6}u_N + \frac{1}{4}u_{N+1}\right), \quad \text{(C.14)}$$

$$i = N+1: \qquad w_{N+1} = \sum_{N+1}^{j=1} D_{N+1,j}(u)'_j = \frac{1}{h}\left(\frac{1}{4}u_{N-3} - \frac{4}{3}u_{N-2} + 3u_{N-1} - 4u_N + \frac{25}{12}u_{N+1}\right). \quad \text{(C.15)}$$

It is worth mentioning out of interest that in those cases where the solution is periodic the the solution "wraps" around so that in (C.10) when $i = 1$ we can use $u_0 \equiv u_{N+1}$ and $u_{-1} \equiv u_N$ and therefore we can "wrap" around the coefficients in the differential matrix. Therefore, an alternative approach for the end rows is to use a finite central difference at the two end rows.

By considering Taylor series it can be shown this scheme converges at a rate of $O(h^4)$ as $h \to 0$.

Chebyshev Differentiation Matrix

A Chebyshev differentiation matrix is constructed in a very similar way to the 4th order finite difference method. However, the discretization of the grid is as per (C.3) with points clustering around the boundaries. The Chebyshev differentiation matrix is formed on the domain $[-1, 1]$; however, this does not mean we are limited the problems on this domain; we can stretch our domain to a length $2L$ by multiplying the domain by L, the

corresponding adjustment to the differentiation matrix is to divide all elements by L.

As with the finite difference method we interpolate the discrete set of data values u_j, but with one crucial difference. In the finite difference case we used a local interpolation, i.e. using four points either side of u_j to calculate the j-th row of the differentiation matrix. In the Chebyshev case we use a global interpolation by using the complete set of discrete data points u_j to interpolate at any point j. The local interpolation in the finite difference case produces a sparse matrix which has computational benefits; these matrices are easier to manipulate and require less storage, the same cannot be said for the Cherbyshev differentiation matrix. However the Chebyshev method has its own strengths; it is better suited to non-periodic functions and, as discussed, Chebyshev differentiation matrix has a much faster convergence of the error as N is increased.

The exact Chebyshev differentiation matrix is defined as follows: let p be the unique polynomial of degree $\leq N$ with $p(x_j) = u_j$, $0 \leq j \leq N$, we set $w_j = p'(x_j)$. We therefore have

$$w = D_N u.$$

A pattern emerges with the entries of the differentiation matrix and the following formula are produced

$$(D_N)_{00} = \frac{2N^2+1}{6}, \qquad (D_N)_{NN} = -\frac{2N^2+1}{6}, \tag{C.16}$$

$$(D_N)_{jj} = -\frac{x_j}{2(1-x_j^2)}, \qquad j = 1, \ldots, N-1, \tag{C.17}$$

$$(D_N)_{ij} = \frac{c_i}{c_j}\frac{(-1)^{i+j}}{(x_i - x_j)}, \qquad i \neq j, \quad i, j, 0 =, \ldots, N, \tag{C.18}$$

where

$$c_i = \begin{cases} 2 & i = 0 \quad \text{or} \quad N, \\ 1 & \text{otherwise.} \end{cases}$$

Figure C.1 shows the error for the fourth order finite difference method and the Chebyshev differentiation method when differentiating the function $u(x) = \exp(-x^2)$.

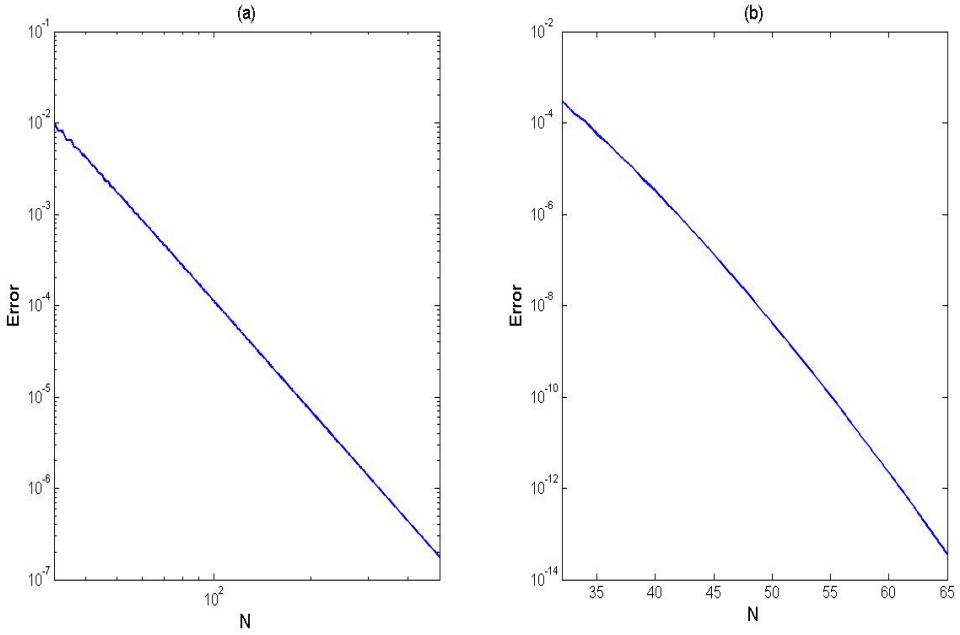

Figure C.1: *The differentiation error in the fourth order finite difference method (a) and Chebyshev method (b), when* $u(x) = \exp(-x^2)$.

4th order Runge-Kutta time stepping scheme

We have shown two methods for evaluating the differentials in our PDEs. Now we we will show how we march our PDEs forward in time. Note that we also used this method to solve the ODEs found using weakly-non-linear theory. Our method of choice is a 4th order Runge-Kutta scheme and our reason for doing so is the large stability region of the scheme which will be discussed in more detail. Firstly let us define the scheme for a single PDE: given a PDE of the form

$$\frac{\partial u}{\partial t} = f(u,t), \qquad u(t_0) = u_0, \tag{C.19}$$

we define a time step size h such that $t_{n+1} - t_n = dt$. Then our $n+1$-th step is given by

$$u_{n+1} = u_n + \frac{dt}{6}(k_1 + 2k_2 + 2k_3 + k_4), \tag{C.20}$$

where

$$k_1 = f(u_n, t_n), \qquad k_2 = f(t_n + \frac{dt}{2}, u_n + \frac{dt}{2}k_1), \tag{C.21}$$

$$k_3 = f(t_n + \frac{dt}{2}, u_n + \frac{dt}{2}k_2), \qquad k_4 = f(t_n + dt, u_n + dtk_3). \tag{C.22}$$

We can therefore see that the 4th order Runge-Kutta scheme involves an evaluation at four intermediate points, k_1, k_2, k_3 and k_4. The error is fourth order, i.e. $O(dt^4)$. This can very easily be applied to a system of PDEs with each PDE using information from variables calculated at the intermediate steps from the other PDE equations.

Stability

We can calculate the stability of the 4th order Runge-Kutta scheme by taking the simplest PDE problem, which is the linear problem

$$\frac{\partial u}{\partial t} = f(t_n, u_n) = \lambda u. \tag{C.23}$$

Using a time step dt our 4th order Runge Kutta scheme is given by

$$u_{n+1} = (1 + dt\lambda t + \frac{1}{2}(dt\lambda)^2 + \frac{1}{6}(dt\lambda)^3 + \frac{1}{24}(dt\lambda)^4)u_n \tag{C.24}$$

where we have used

$$k_1 = dt\lambda, \qquad k_2 = dt\lambda(1 + \frac{dt\lambda}{2}), \tag{C.25}$$

$$k_3 = dt\lambda(1 + \frac{dt\lambda}{2}(1 + \frac{dt\lambda}{2})), \qquad k_4 = dt\lambda(1 + dt\lambda(1 + \frac{dt\lambda}{2}(1 + \frac{dt\lambda}{2}))). \tag{C.26}$$

We now define a function $g = u_{n+1}/u_n$ and hence for convergence we require $|g| < 1$,

$$|g| = |1 + dt\lambda t + \frac{1}{2}(dt\lambda)^2 + \frac{1}{6}(dt\lambda)^3 + \frac{1}{24}(dt\lambda)^4| < 1. \tag{C.27}$$

Figure C.2 is a sketch of this stability region assuming $dt\lambda$ is complex and plotting real and imaginary parts. Assuming $dt\lambda$ is purely real we find the stability is bounded by 0 and -2.7853, whereas purely imaginary $dt\lambda$ is bounded by ± 2.8284.

Boundary conditions

We require to apply the boundary conditions $v \to 0$ as $|y| \to \infty$. Clearly numerically it is not possible to apply these boundary conditions as we cannot solve numerically on an infinite domain. Therefore we apply boundary conditions over a finite domain, since we have only dealt with problems that decay at $|y| \to \infty$, provided we choose a domain that is sufficiently large this should be a good approximation for an infinite domain. Our amended boundary conditions are therefore $v = 0$ at $y = \pm L$ over the domain $y = [-L, L]$. We implement this into the Runge-Kutta scheme by setting $v(-L) = 0$ and $v(L) = 0$ at each time step but also at the intermediate time steps, therefore given the PDE

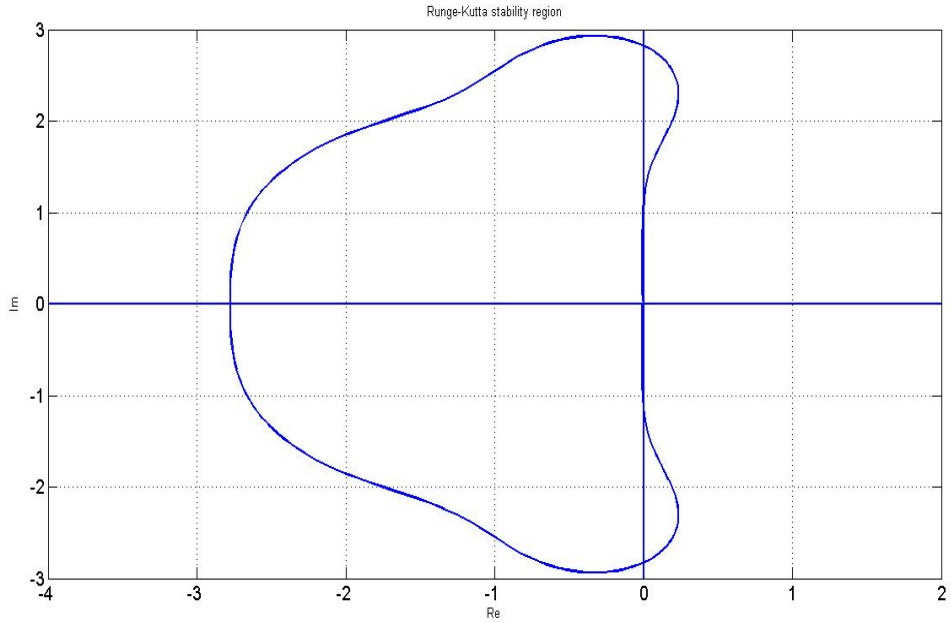

Figure C.2: *The 4th order Runge-kutta stability region, $|g| < 1$, the stable region is given inside the enclosed curve.*

$$\frac{\partial v}{\partial t} = f(t, v) \tag{C.28}$$

when calculating the $n + 1$ time step, splitting the domain into $N + 1$ points, we set

$$k_1(t_n, 1) = 0, \qquad k_1(t_n, N + 1) = 0, \tag{C.29}$$

and similarly for k_2, k_3 and k_4. Then finally when calculating v_{n+1} we set

$$v(t_{n+1}, 1) = v(t_{n+1}, N + 1) = 0. \tag{C.30}$$

Bibliography

Arakawa, H. (1951). *The criterion of dynamic stability of zonal motion including the vertical shear*, volume 20. Springer.

Bénard, H. (1900). Les tourbillons cellulaires dans une nappe liquide. *Rev. Gen. Sci. Pure Appl.*, 11:1261–1271.

Bender, C. M. and Orszag, S. A. (1999). *Advanced Mathematical Methods for Scientists and Engineers I*. Springer-Verlag, New York.

Bouchut, F., Ribstein, B., and Zeitlin, V. (2011). Inertial, barotropic, and baroclinic instabilities of the Bickley jet in two-layer rotating shallow water model. *Phys. Fluids*, 23(12):126601.

Boyd, J. P. and Christidis, Z. D. (1982). Low wavenumber instability on the equatorial beta-plane. *Geophysical research letters*, pages 769–772.

Clark, P. D. and Haynes, P. H. (1996). Inertial instability on an asymmetric low-latitude flow. *Q. J. R. Meteorol Soc.*, 122:151–182.

D'Orgeville, M. and Hua, B. L. (2005). Equatorial inertial-parametric instability of zonal symmetric oscillating shear flows. *J. Fluid Mech.*, 531:261–291.

Drazin, P. G. and Reid, W. H. (2004). *Hydrodynamic Stability*. Cambridge University Press.

Dunkerton, T. J. (1981). On the inertial stability of the equatorial middle atmosphere. *J. Atmos. Sci.*, 38:2354–2364.

Dunkerton, T. J. (1982). The double-diffusive modes of symmetric instability on the equatorial beta plane. *J. Atmos. Sci.*, 39:1653–1657.

Dunkerton, T. J. (1983). A non-symmetric inertial instability. *J. Atmos. Sci.*, 40:807–813.

Fornberg, B. and Sloan, D. (1994). *A review of pseudospectral methods for solving partial differential equations*. Cambridge University Press, Cambridge.

Gill, A. E. (1982). *Atmosphere-Ocean Dynamics*. Academic Press.

Gradshteyn, I. S. and Ryzhik, I. M. (2014). *Table of integrals, series, and products*. Academic press.

Griffiths, S. D. (2000). Inertial instability in the equatorial stratosphere. Ph.D. thesis, University of Cambridge.

Griffiths, S. D. (2003a). The nonlinear evolution of zonally symmetric equatorial inertial instability. *J. Fluid Mech.*, 474:245–273.

Griffiths, S. D. (2003b). Nonlinear vertical scale selection in equatorial inertial instability. *J. Atmos. Sci.*, 60:977–990.

Griffiths, S. D. (2008). The limiting form of inertial instability in geophysical flows. *J. Fluid Mech.*, 605:115–143.

Hayashi, H. and Shiotani, M. (1998). Vertically stacked temperature disturbances near the equatorial stratopause as seen in cyogenic limb array etalon spectrometer data. *J. Geophys. Res.*, 103:19,469–19,483.

Hobbs, P. V. and Wallace, J. M. (1977). *Atmospheric Science, an introductory survey*. Academic press.

Hua, B. L., Moore, D. W., and Le Gentil, S. (1997). Inertial nonlinear equilibration of equatorial flows. *J. Fluid Mech.*, 331:345–371.

Hurwitz, A. (1895). On the conditions under which an equation has only roots with negative real parts. *Mathematische Annelen*, pages 273–284.

Kloosterziel, R. C., Orlandi, P., and Carnevale, G. F. (2007). Saturation of inertial instability in rotating planar shear flows. *J. Fluid Mech.*, 583:413–422.

Kloosterziel, R. C., Orlandi, P., and Carnevale, G. F. (2013). Inertial and barotropic instabilities of a free current in a three-dimensional rotating flow. *J. Fluid Mech.*, 725:117–151.

Kloosterziel, R. C., Orlandi, P., and Carnevale, G. F. (2015). Saturation of equatorial inertial instability. *J. Fluid Mech.*, 767:562–594.

Laplace, P. S. (1776). Recherches sur plusieurs points du systme du monde. *Mem. Acad. Roy. Sci. Paris*, 89:177–264.

Natarov, A. and Richards, K. J. (2015). Persistent presence of small vertical scale velocity features during three-dimension equilibration of equatorial inertial instability. *Phys. Fluids*, 27 (8):84109.

Pedlosky, J. (1970). Finite amplitude baroclinic waves. *J. Atmos. Sci.*, 16:15–30.

Pedlosky, J. and Frenzen, C. (1980). Chaotic and periodic behaviour of finite-amplitude baroclinic waves. *J. Atmos. Sci.*, 38:1177–1196.

Rayleigh, L. (1916). On the dynamics of revolving fluids. *Proc. R. Soc. Lond. A*, 55:758–776.

Ribstein, B., Plougonven, R., and Zeitlin, V. (2014). Inertial versus baroclinic instability of the bickley jet in continuously stratified rotating fluid. *J. Fluid Mech.*, 743:1–31.

Richards, K. J. and Edwards, N. R. (2003). Lateral mixing in the equatorial pacific: The importance of inertial instability. *Geophysical research letters*, 30(17).

Salmon, R. (1998). *Geophysical Fluid Dynamics*. Oxford University Press.

Sawyer, J. S. (1949). The significance of dynamic instability in atmospheric motions. *Quarterly Journal of the Royal Meteorological Society*, 75(326):364–374.

Shen, C. Y. and Evans, T. E. (2002). Inertial instability and sea spirals. *Geophysical research letters*, 29(23).

Spiegel, E. and Veronis, G. (1960). On the boussinesq approximation for a compressible fluid. *The Astrophysical Journal*, 131:442–446.

Stevens, D. E. and Ciesielski, P. E. (1986). Inertial instability of horizontally sheared flow away from the equator. *Journal of the atmospheric sciences*, 43(23):2845–2856.

Taylor, G. I. (1923). Stability of a viscous liquid contained between two rotating cylinders. *Philosophical Transactions of the Royal Society of London. Series A, Containing Papers of a Mathematical or Physical Character*, 223:289–343.

Teeluck, V. (2013). Surface and internal tides above sea-floor topography. Ph.D. thesis, University of Leeds.

Vallis, G. K. (2006). *Atmospheric and Oceanic Fluid Dynamics: Fundamentals and Large-scale Circulation*. Cambridge University Press.

Zeitlin, V. and Plougonven, R. (2009). Nonlinear development of inertial instability in a barotropic shear. *Phys. Fluids*, 21:106601.

Zeitlin, V., Ribstein, B., and Tissier, A. (2014). Barotropic, baroclinic and inertial instabilities of the easterly gaussian jet on the equatorial beta plane in rotating shallow water model. *Phys. Fluids*, 26:056605.

Zhao, J. X. and Ghil, M. (1991). Nonlinear symmetric instability and intraseasonal oscillations in the tropical atmosphere. *J. Atmos. Sci.*, 48:2552–2568.